ADDIS ABABA INSTITUTE OF TECHNOLOGY

SCHOOL OF CIVIL AND ENVIRONMENTAL ENGINEERING

Effect of Dynamic Soil-Structure Interaction on Buildings in Selected Sites of Addis Ababa

By

Rediet Lemma

A Thesis Submitted to the School of Graduate Studies of Addis Ababa Institute of Technology in Partial Fulfillment of the Requirements for the Degree of Master of Science in Civil Engineering (Geotechnical Engineering)

Advisor

Professor Dr.-Ing. Asrat Worku

Addis Ababa, Ethiopia

Jan 2025

The undersigned have examined the thesis entitled **"Effect of Dynamic Soil-Structure Interaction on Buildings in Selected Sites of Addis Ababa"** prepared by **Rediet Lemma,** a candidate for the degree of **Master of Science** in geotechnical engineering and hereby certify that it is worthy acceptance.

Professor Dr.-Ing. Asrat Worku Advisor	Signature	30-01-2025 Date
Dr.-Henok Fikre Internal Examiner	Signature	23/01/2025 Date
Dr.-Ing. Tensay G/medhin External Examiner	Signature Abrham Gebreyohannes (Dr.) Dean, School of Civil & Environmental Engineering	28/01/25 Date
Chair Person	Signature	Date

Addis Ababa Institute of Technology
Addis Ababa University

DECLARATION

I hereby declare that the work presented in this thesis is my own work carried out under the supervision of Professor Dr.-Ing. Asrat Worku. Where information has been derived from other sources, I confirm that this has been duly acknowledged. This work has not been submitted for an academic degree award at any university.

Rediet Lemma

ABSTRACT

Currently, structural engineers typically design structures as fixed-base systems, neglecting soil-structure interaction (SSI). This practice is primarily due to the complexities associated with soil modeling and the absence of specific procedures for incorporating SSI effects in many seismic design codes including the Ethiopian code.

Both the European and Ethiopian building codes recommend dynamic SSI effects for slender structures or those with significant second-order (P-Δ) effects. However, they mandate the inclusion of SSI in design without providing explicit guidelines for its calculation. Structures founded on piles or massive foundations, such as offshore caissons, silos, and bridge piers, should account for SSI effects in their design (ES EN 1998-5:2015; ES EN 1998-5:2015).

In contrast to the European and Ethiopian building codes, international codes and standards, such as ASCE/SEI 7-10 (2010), ASCE/SEI 7-16 (2017), and ASCE/SEI 41-17 (2017), provide procedures for incorporating SSI into structural design.

This research delves into various studies and evidence, emphasizing the need for a nuanced understanding of SSI effects on building structures. Additionally, it explores the main approaches employed to evaluate seismic SSI problems, focusing on commonly used modeling techniques and computational methods. Notably, the thesis adopts the code approach outlined by NIST GCR 12-917-21 (2012) based on Pais and Kausel (1988), FEMA P-2082-1 (2020) and ASCE/SEI 7-16 (2017) to address and analyze SSI-related challenges in seismic analysis of buildings.

To ground the study in real-world scenarios, five specific sites in Addis Ababa were selected based on recent ground response analyses conducted by Getu (2023). Additionally, one idealized softer site was included. The selected sites from Getu (2023) correspond to two ground types, C and D, according to ASCE/SEI 7-16 (2017). The inclusion of the idealized soil condition was intended to more clearly observe soil flexibility, which is assumed to correspond to ground type E according to ASCE/SEI 7-16 (2017).

Five earthquake motions selected from the PEER ground motion database were matched to these ground types, and four building models, ranging from G+5 to G+30, were assumed. The analysis was conducted using ETABS 21.1.0 software.

The common perspective on Soil structure interaction (SSI) has long regarded it as a beneficial factor in structural response. However, contemporary research and insights gleaned from past

seismic events have revealed instances where consideration of SSI can exhibit detrimental effects under specific conditions.

In this study, it is observed that some structures with flexible base models show a smaller response compared to their fixed-base counterparts. However, in certain cases, a significant increase in response is observed. This increase is dependent on the predominant period of the earthquake motions and the fundamental period of the structure. Within the scope of the study conducted, as the number of stories increases, the SSI influence increases, particularly for storey displacement, storey drift ratio, and storey overturning moment. Additionally, SSI also leads to reduced base shear for shorter building models in most earthquake motions.

ACKNOWLEDGMENT

First and foremost, I would like to express my deepest gratitude to God Almighty for His unwavering guidance and blessings throughout my life.

I am deeply grateful to my advisor, Professor Dr.-Ing. Asrat Worku, Professor at the School of Civil and Environmental Engineering at Addis Ababa Institute of Technology, for his invaluable guidance and mentorship. His expertise and unwavering support have been instrumental in shaping my research journey and ensuring the success of this project.

I am deeply grateful to Betemariam Getu for generously sharing her primary data, which were crucial for my thesis. Her insights and collaboration have been invaluable.

Additionally, I would like to thank Tewodros Temam, a structural engineer, for his expertise in building design. His contributions have significantly enhanced the quality of my research.

Finally, I extend my heartfelt thanks to my family, my husband and my friends, including Selamihun Berihe, Tesfaeshet Mulugeta, and Brikt Solomon, for their support, encouragement, and understanding throughout this process.

Table of Contents

List of Tables

List of Figures

CHAPTER ONE
INTRODUCTION

1.1. Background

In the realm of structural engineering, the intricate interplay between soil and structures holds profound significance, particularly in regions susceptible to seismic activity. Understanding and effectively incorporating the principles of Soil structure interaction (SSI) into design practices are imperative for ensuring the resilience and stability of structures subjected to dynamic forces.

As urbanization continues to expand, seismic resilience becomes a critical consideration in engineering practices. In regions like Addis Ababa, Ethiopia, where seismic activity is a pertinent concern, the understanding of SSI assumes heightened importance. This study seeks to contribute to the existing body of knowledge by scrutinizing the effects of SSI on different building categories within this urban context.

One pivotal aspect of this investigation is the reliance on established code provisions that guide seismic design practices. Codes and standards serve as the bedrock of structural engineering, providing a structured framework to ensure the safety and integrity of buildings. In the context of SSI, adherence to relevant codes becomes paramount. For this study, particular attention is given to the code provisions outlined in renowned standards and reports, such as ASCE/SEI 7-16 (2017), NIST GCR 12-917-21 (2012), and ASCE/SEI 41-17 (2017).

ASCE/SEI 7-16, (2017), NIST GCR 12-917-21 (2012) and ASCE/SEI 41-17 (2017) are widely recognized in the United States and offer seismic provisions integral to ensuring structural resilience. These codes provide a systematic approach to consider the dynamic interaction between soil and structures, offering methodologies, criteria, and performance objectives.

This research aims to bridge theoretical insights with practical implications by employing these established code provisions to assess the SSI effects on various building categories. The study utilizes data obtained from recent site characterization studies in Addis Ababa, enhancing the relevance and specificity of the findings to the local context. By aligning with recognized standards, the research endeavors to provide actionable insights that contribute to improved seismic design practices in regions vulnerable to soil-structure interaction effects.

1.2. Objective

1.2.1 General objective

The general objective of the study is to investigate the effect of SSI on the response of selected buildings in selected sites of Addis Ababa subjected to scaled recorded earthquake ground motions.

1.2.2 Specific objective

The specific objectives of the study are listed below:

- Check the SSI effect by code approach
- Analyze the impact of varying ground types on the SSI response of different building categories.
- Evaluate the influence of building height (G+5 to G+30) on the interaction dynamics between the structures and the underlying soil.
- Show the effect of different recorded ground motions on selected buildings and sites.

1.3. Scope of the study

This study investigates the influence of soil-structure interaction on four distinct building categories (G+5, G+10, G+20, and G+30) across different sites in Addis Ababa. These sites have recently undergone geophysical investigations by Getu (2023) to study site effect on earthquake ground motions. An additional idealized softer soil formation is also included to widen the range of site condition. By analyzing the varying ground conditions, the research aims to provide a comprehensive understanding of how soil properties affect the interaction between different building types and the underlying soil.

1.4. Methodology

The information and data regarding soil conditions are obtained from the recent site characterization study conducted by Getu (2023) with an additional idealized site condition.

1.4.1. Building Selection and Modeling

Four distinct building categories are chosen, ranging from short rise to high-rise buildings (i.e., G+5, G+10, G+20, and G+30). This enables an analysis of how building height and stiffness affect SSI behavior. To avoid the influence of torsional effects on the analysis, the buildings are assumed to be symmetrical.

The appropriate foundation type (mat foundation) for each building at each site is selected based on the specific building load demands and the soil conditions identified in Getu (2023). This ensures that the foundation choice reflects the real condition at each location.

1.4.2. Input Ground Motion Selection

To capture a realistic representation of seismic events, the input ground motions for the SSI analysis are selected from PEER ground motion database. This ensures that the chosen ground motions align with the seismic characteristics relevant to the tectonic regime under consideration, which is characterized by shallow-depth earthquakes.

1.4.3. Soil-Structure Interaction Modeling

The code approach, which is the substructure method, together with Pais and Kausel (1988) suggestions for spring and dashpot coefficients is employed for this study. This method allows for the incorporation of soil flexibility into structural analysis. Spring coefficients, representing the stiffness of the foundation and its interaction with the underlying soil, and dashpot coefficients, which represent the damping in the soil-structure interaction, are computed based on the data and information provided in Getu (2023) regarding the soil properties at each site. These spring and dashpot coefficients play a crucial role in simulating the SSI.

1.4.4. Software Selection and Analysis

ETABS, a widely used industry-standard commercial software, is selected to account for the influence of SSI. This software allows for the integration of the specified building models, foundation types, spring constants, and relevant loading conditions. The analysis is conducted to generate results such as storey displacements, storey shear forces, storey drift ratios, storey overturning moments, and base shears.

1.5. Organization of the study

This thesis is organized in seven chapters. Chapter 1 introduces the subject matter in general and the objective and scope of the thesis with methodology followed.

Chapter 2-Literature Review: This chapter provides a comprehensive review of existing literature on SSI. It delves into various SSI analysis methods, the different types of interaction mechanisms, and relevant engineering codes that address SSI considerations.

Chapter 3-Selected sites and their descriptions: This chapter focuses on the selected study sites. It provides detailed descriptions of each site's location, soil conditions, geological characteristics, and seismic hazard levels.

Chapter 4-Building models: This chapter outlines the selection process for the buildings analyzed in the study. It also details the assumptions made regarding the building characteristics and their selection criteria.

Chapter 5-Input Ground Motions: This chapter discusses the selection of ground motions used for the analysis. It elaborates on the criteria employed in choosing these ground motions to effectively represent the potential seismic activity at the study sites.

Chapter 6-Results and Discussion: This chapter presents the key findings obtained from the SSI analysis. It discusses the results in detail, providing insights into the impact of various factors on the structural response.

Chapter 7-Conclusions and Recommendations: This chapter summarizes the main conclusions derived from the analysis. It also offers recommendations for future research endeavors that could expand upon the present study's findings or investigate other aspects of SSI.

CHAPTER TWO
LITERATURE REVIEW

2.1. Meaning of Soil structure interaction

Seismic soil-structure interaction (SSI) analysis emerges as a critical tool for understanding the dynamic behavior of structures during earthquakes. It delves into the collective response of a building, its foundation, and the surrounding soil layers to free-field ground motions which is uninfluenced by the structure itself. This analysis, as outlined in NIST GCR 12-917-21 (2012), highlights the difference between the actual response of a structure and its theoretical response under a rigid base assumption, where SSI effects are negligible.

Understanding this distinction is crucial, particularly when considering structures on different foundation types. While structures on rock (exceptionally stiff) can often be treated as having a fixed base, softer soil deposits introduce complexities. In such cases, the foundation's inability to perfectly follow free-field motions and the structure's dynamic response influencing soil deformation create an interplay known as SSI. This two-way interaction, where the structure and soil influence each other's behavior, necessitates careful consideration for designing seismic-resistant structures on various foundations (Kramer, 1996).

2.2. Effect of soil- structure interaction

According to Wolf (1985), when a structure is located on soft soil, the motion of the base at point O (Figure 2.1a) deviates from the control motion observed at point A due to the interaction between the structure and the soil system. To better understand how the soil influences the dynamic response of the structure, it is helpful to differentiate among the three effects.

The effects are as follows.

I. The motion of the site in the absence of the structure and any of excavation, what is called the free- field response is modified, Figure 2.1c.
II. Excavating and inserting the rigid base into the site will modify the motion, Figure 2.1d. The rigid base will experience some average horizontal displacement and a rocking component. This rigid body motion will result in accelerations which will vary over the height of the structure, in contrast to the applied accelerations in the case of a structure founded on rock.
III. The inertial loads applied to the structure will lead to an overturning moment and a transverse shear acting at point O, Figure 2.1e. These will cause deformations in the

soil and thus, once again, modify the motion as the base. This part of the interplay is referred to as inertial interaction.

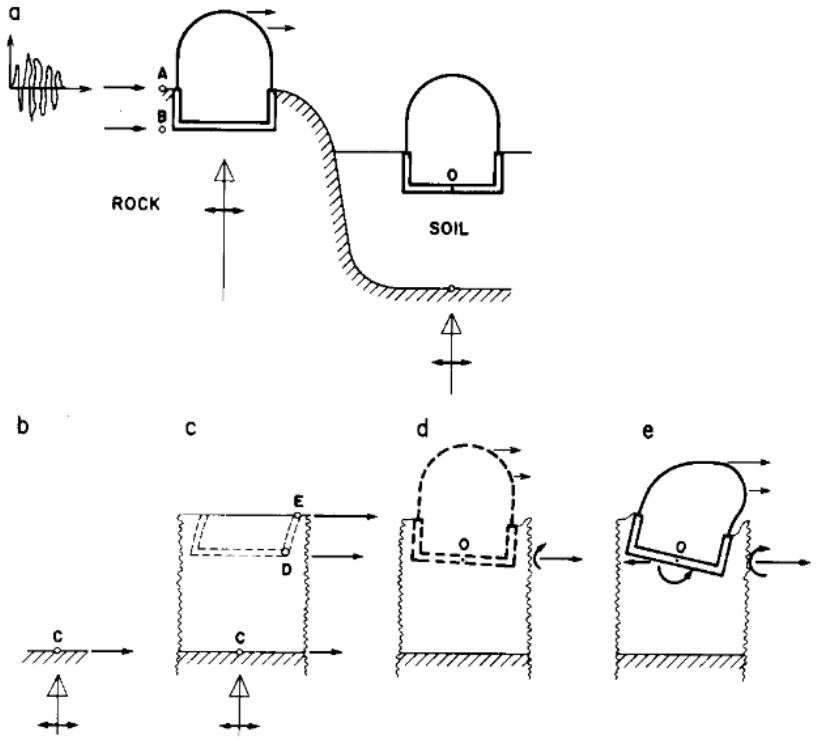

Figure 2.1: Seismic response of structure founded on rock and soil a) sites; b) outcropping rock; c) free field; d) kinematic interaction; e) inertial interaction (Wolf, 1985)

Horizontal motion can be applied straight to the base of the rock-based structure. Over the height of the structure, the applied horizontal inertial load will have a constant input acceleration. During the earthquake, a transverse shear acting at the base and an overturning moment will emerge. These two stress results will not cause further deformation at the base since the rock is exceedingly rigid. As a result, there is no base rocking because the base's horizontal displacement is equal to the control motion. The structure's seismic response for a specific control motion is solely dependent on the structure's characteristics (Wolf, 1985).

2.3. Types of SSI

As clearly stated in NIST GCR 12-917-21 (2012), the complex phenomenon of SSI can be further categorized into three distinct effects as described in section 2.3.1 through 2.3.3:

2.3.1. Inertial interaction

When a structure vibrates, its inertia generates resultant forces like base shear, moment, and torsion at its foundation. These forces, in turn, cause displacements and rotations at the point where the structure meets the soil. The flexibility of the soil-foundation system allows for these movements, which contribute to the overall flexibility of the structure and consequently increase its natural period of vibration. Furthermore, these displacements lead to energy dissipation through mechanisms like radiation damping and hysteretic soil damping, significantly impacting the overall damping of the entire system. Since these effects are directly linked to the structure's inertia, they are collectively termed inertial interaction effects (NIST GCR 12-917-21, 2012).

2.3.2. Kinematic interaction

Kinematic interaction arises from the alteration of seismic wave propagation due to the presence of a structure's foundation. The foundation's distinct density and elasticity compared to the surrounding soil act as a barrier, causing changes in wave velocity, reflection, and refraction (scattering) at the soil-foundation interface. This phenomenon manifests as the difference between the structural response calculated using the free-field ground motion (uninfluenced by the structure) and the response obtained using the actual ground motion at the foundation base, which considers the structure's presence. Notably, kinematic interaction occurs independently of the structure's mass and is influenced by factors like foundation geometry, embedment depth, incoming wave type (shear or surface), and wave incidence angle. It's important to note that shallow foundations subjected to vertically propagating shear waves do not experience kinematic interaction (Villaverde,2009).

2.3.3. Soil-foundation flexibility

Soil-foundation flexibility significantly impacts the seismic demands on foundation elements. While structures exert forces and displacements, the flexibility of the soil and foundation influences how these forces are distributed. Flexural, axial, and shear deformations within the foundation, representing the seismic demands, are influenced by this flexibility. Rigid foundations experience higher concentrated demands, while flexible foundations like rafts and piles distribute loads more evenly, often leading to lower peak demands (NIST GCR 12-917-21, 2012).

2.4. Methods of analysis

Two popular methods are used to describe the interactions between a structure, its foundation, and the soil that supports it, as well as the soil's flexibility and damping.

2.4.1. Substructure method

The substructure method, a widely used technique for analyzing SSI, simplifies the complex interaction between a structure and its supporting soil. This method employs a spring-based model, where the soil is represented by a series of interconnected springs. These springs effectively capture the stiffness and damping properties of the soil, allowing for an efficient and practical approach to SSI analysis (NIST GCR 12-917-21, 2012; FEMA P-2091, 2020). Figure 2.2 shows the schematic representation of Substructure method.

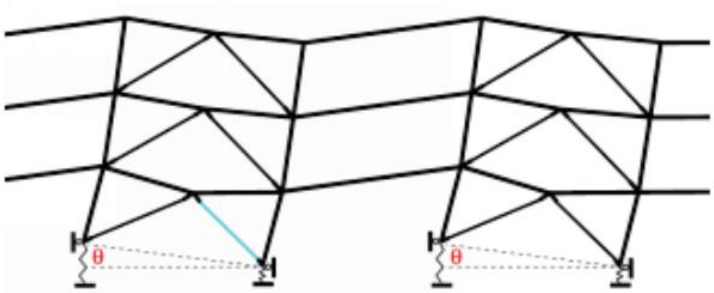

Figure 2.2: Substructure method of SSI (NIST GCR 12-917-21, 2012; FEMA P-2091, 2020)

2.4.2. Direct method

The direct method involves the modeling and analysis of the soil and structure system as a unified entity subjected to ground motion specified at the free field. The method is illustrated schematically in Figure 2.3 for a foundation soil that can be idealized as a horizontally layered system underlain by bedrock and excited by vertically propagating shear waves. To address the kinematic and inertial interaction between the soil and the structure, the method follows a series of steps. In the initial step, the ground motion at the bedrock level is defined using the prescribed surface motion in the free field, often termed the control motion. This is achieved through an inverse amplification process known as deconvolution. Subsequently, assuming that the ground motion at the bedrock directly beneath the building mirrors the bedrock motion determined in the first step, this motion serves as input for a dynamic analysis of the soil-structure system. The characteristics of the ground motion at the base of the structure and the response of the structure at any desired point can then be derived from this dynamic analysis (Villaverde, 2009).

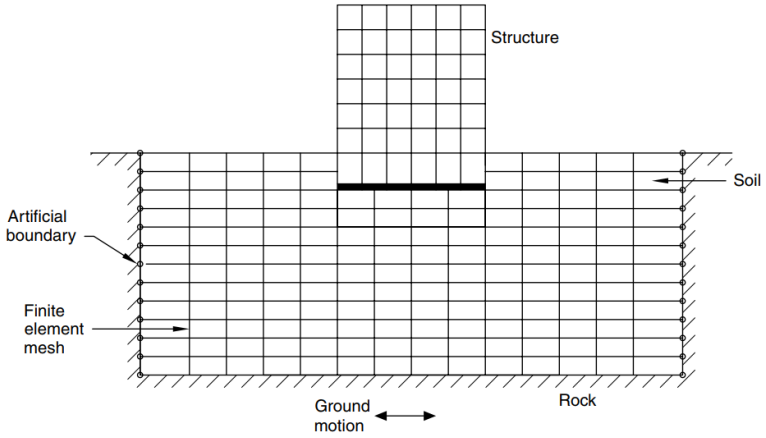

Figure 2.3: Direct method of SSI (Villaverde, 2009)

2.5. Code provisions for SSI

2.5.1 Eurocode 8 and Ethiopian building code

Eurocode 8 (EN 1998-5, 2004) and Ethiopian building code (ES EN 1998-5:2015) highlight the following situations where dynamic soil-structure interaction becomes significant:

I. structures where P-**Δ** (2^{nd} order) effects play a significant role;
II. structures with massive or deep-seated foundations, such as bridge piers, offshore caissons, and silos;
III. slender tall structures, such as towers and chimneys,
IV. structures supported on very soft soils, with average shear wave velocity less than 100 m/s, such as those soils in ground type S_1.

While EN 1998-5 (2004) and ES EN 1998-5:2015 identify situations where SSI assessment is crucial, they lack provisions for specific analysis details. This suggests that solely relying on these codes and standards might be insufficient for real-world engineering applications.

2.5.2. ASCE/SEI 7-16

ASCE/SEI 7-16 (2017) permits the inclusion of SSI effects in determining design earthquake forces and associated displacements for structures. This allowance applies when employing the equivalent lateral force procedure, linear dynamic analysis methods, or the nonlinear response history procedure, specifically for structures located on Site Class C, D, E, or F. In cases where SSI effects are considered, the analytical model of the structure must encompass horizontal, vertical, and rotational foundation and soil flexibility. Section 19 of ASCE/SEI 7-16 (2017) emphasizes the importance of considering both upper and lower bound estimates for foundation

and soil stiffness. The design process should favor the case resulting in lesser reduction or greater amplification in response parameters.

2.5.3. ASCE/SEI 41-17

This provision details three methods for simulating soil behavior in substructure analysis using spring constants:

I. Rigid foundations (Method 1): Uncoupled springs represent the soil for foundations deemed rigid compared to the surrounding soil (Figure 2.4). Equations of translational spring constants of this method are stated in Equations 2.1 through 2.9.

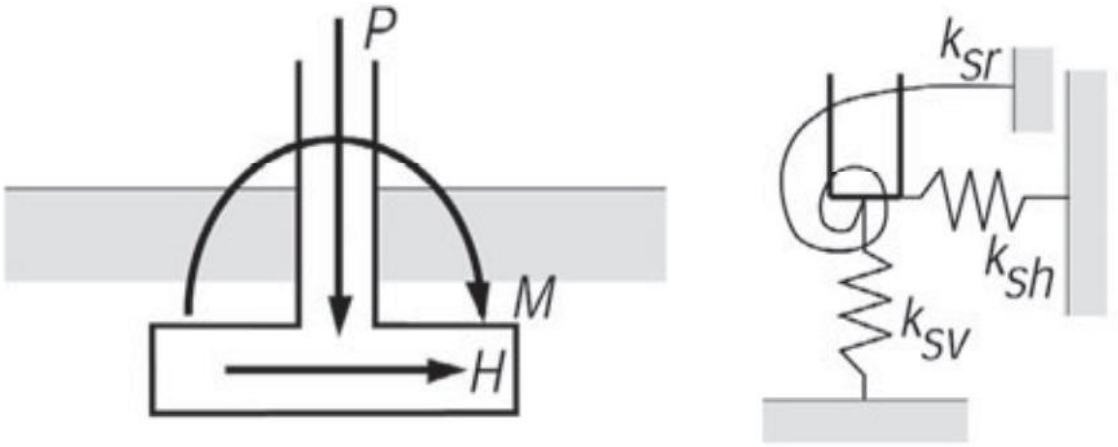

(a) Foundation load (b) Uncoupled spring model

Figure 2.4: Uncoupled spring model for rigid foundation

$$K_{x,sur} = \frac{GB}{2-v}\left[3.4\left(\frac{L}{B}\right)^{0.65} + 1.2\right] \tag{2.1}$$

$$K_{y,sur} = \frac{GB}{2-v}\left[3.4\left(\frac{L}{B}\right)^{0.65} + 0.4\frac{L}{B} + 0.8\right] \tag{2.2}$$

$$K_{z,sur} = \frac{GB}{1-v}\left[1.55\left(\frac{L}{B}\right)^{0.75} + 0.8\right] \tag{2.3}$$

$$\beta_x = \left(1 + 0.21\sqrt{\frac{D}{B}}\right) * \left[1 + 1.6\left(\frac{hd(B+L)}{BL^2}\right)^{0.4}\right] \tag{2.4}$$

$$\beta_y = \beta_x \tag{2.5}$$

$$\beta_z = \left[1 + \frac{D}{21B}\left(2 + 2.6\frac{B}{L}\right)\right] * \left[1 + 0.32\left(\frac{d(B+L)}{BL}\right)^{\frac{2}{3}}\right] \quad (2.6)$$

$$K_{x,emb} = \beta_x K_{x,sur} \quad (2.7)$$

$$K_{y,emb} = \beta_y K_{y,sur} \quad (2.8)$$

$$K_{z,emb} = \beta_z K_{z,sur} \quad (2.9)$$

Where;

$K_{x,sur}$, $K_{y,sur}$, $K_{z,sur}$ = stiffness of foundation at surface for translation along X, Y and Z axes, respectively

$\beta_x, \beta_y, \beta_z$ = correction factor for embedment for translation along X, Y and Z axes, respectively

$K_{x,emb}$, $K_{y,emb}$, $K_{z,emb}$ = Stiffness of foundation at embedded depth for translation along X, Y and Z axes, respectively

B = width of foundation

L =length of foundation

D =foundation depth (Figure 2.5)

d = height of effective sidewall contact, which may be less than total foundation height (Figure 2.5)

h = depth to centroid of effective sidewall contact (Figure 2.5)

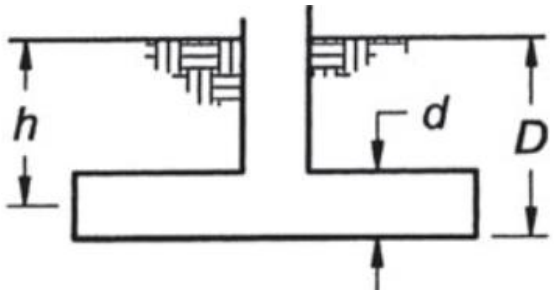

Figure 2.5: Foundation depth measurements h, d and D

II. Shallow foundation not rigid with respect to the supporting soil (Method 2):

In this method, a finite element representation of nonlinear foundation behavior using Winkler models will be employed to represent the vertical and rotational stiffness provided by the soil

reaction. To adjust the Winkler model to approximately match both the vertical and rotational stiffnesses from the elastic solutions in Equations 2.1 through 2.9, stiffer vertical springs are placed at the end regions of the footing (with a length of L_{end} = B/6), as illustrated in Figure 2.6.

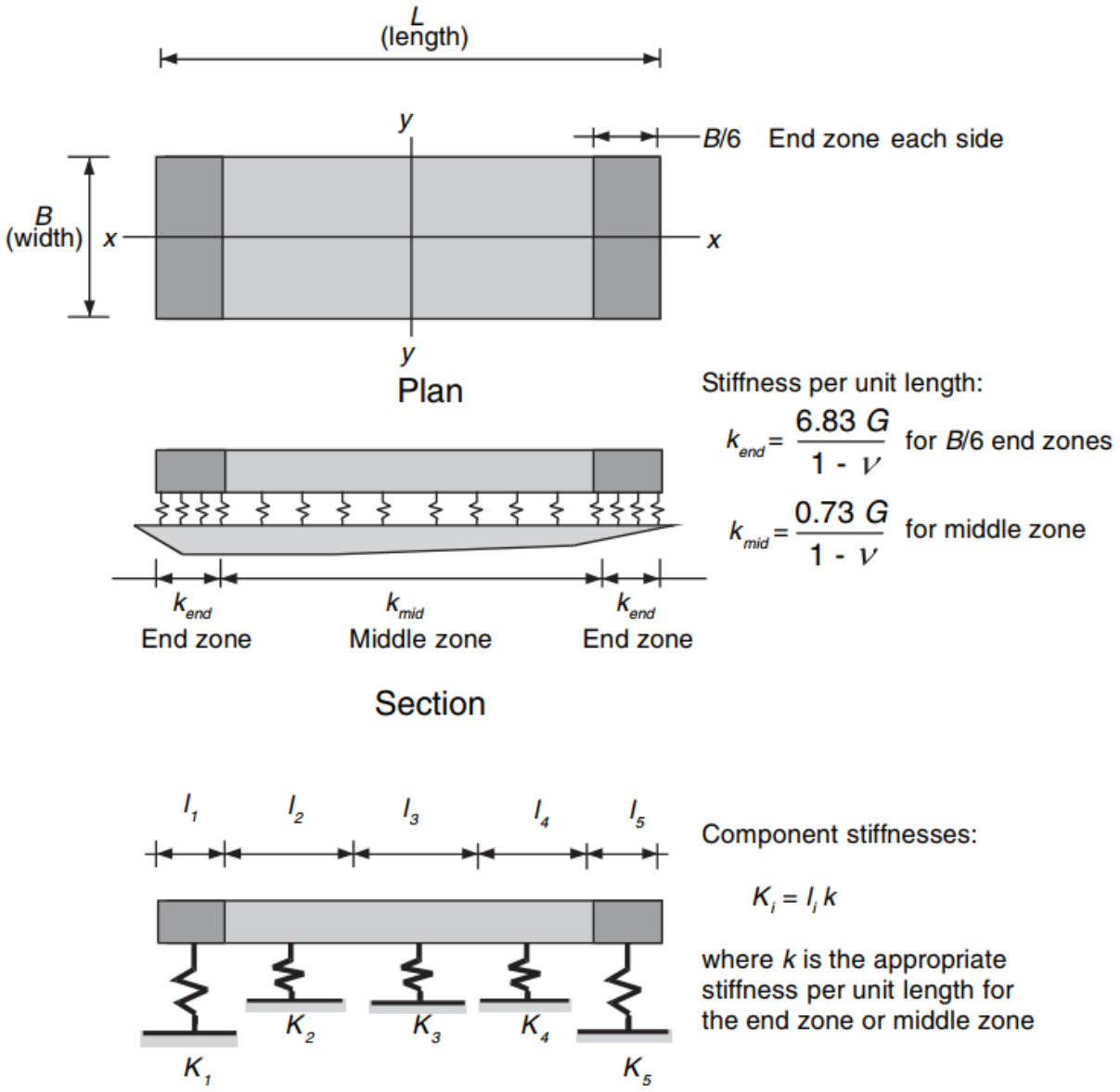

Figure 2.6: Vertical stiffness modelling for shallow footings (Method 2)

III. Shallow foundations that are flexible with respect to the supporting soils (Method 3):

For flexible shallow foundations, approved theoretical solutions for beams or plates on elastic supports can be used to calculate foundation stiffness. This method employs a decoupled Winkler model with a unit subgrade spring coefficient. This approach simplifies the analysis while still capturing the essential aspects of soil-foundation interaction for flexible foundations.

$$k_{sv} = \frac{1.3G}{B_f(1-v)} \tag{2.10}$$

Where:

G = Shear modulus

B = Width of footing

v = Poisson's ratio

2.5.4. FEMA P-2082-1

FEMA P-2082-1 (2020) contains a provision that addresses the impact of SSI on both foundation damping and soil damping. In seismic analysis and design, it is crucial to account for the complex interaction between the structure and the supporting soil, as this interaction significantly influences the overall dynamic response of the system. The provision acknowledges that the damping characteristics, both foundation and the surrounding soil, play a key role in dissipating energy during seismic events.

Foundation damping refers to the dissipation of vibrational energy within the structural foundation itself, while soil damping pertains to the energy dissipation within the underlying and surrounding soil layers. The consideration of SSI effects on damping in FEMA P-2082-1 (2020) implies that the standard recognizes the need to accurately model and incorporate the dynamic characteristics of the foundation and soil in seismic analyses. This helps ensure a more realistic representation of the structure's behavior under seismic loading conditions and contributes to a comprehensive and effective approach to earthquake-resistant design. By addressing SSI effects on damping, FEMA P-2082-1 (2020) aims to enhance the precision of seismic assessments, ultimately promoting the safety and resilience of structures in earthquake prone regions. It suggests the following equation to calculate effective damping ratio of SSI. Equations 2.12 and 2.13 are equations used to calculate parameters in the computation of effective damping ratio (Equation 2.11).

$$\beta_o = \beta_f + \frac{\beta}{\left(\tilde{T}/T\right)_{eff}^{\ 2}} \tag{2.11}$$

$$\left(\tilde{T}/T\right)_{eff} = \left\{1 + \frac{1}{\mu}\left[\left(\tilde{T}/T\right)^2 - 1\right]\right\}^{0.5} \tag{2.12}$$

$$\beta_f = \left[\frac{\left(\tilde{T}/_T\right)^2 - 1}{\left(\tilde{T}/_T\right)^2}\right]\beta_s + \beta_{rd} \tag{2.13}$$

where; β_o= effective damping ratio of the soil–structure system

β_f= effective viscous damping ratio relating to foundation–soil interaction

β= effective viscous damping ratio of the structure, taken as 5%

β_s= soil hysteretic damping ratio

β_{rd}= radiation damping ratio

$\left(\tilde{T}/_T\right)_{eff}$= effective period lengthening ratio

μ= expected ductility demand

2.5.5. Foundation Impedance functions suggested by NIST GCR 12-917-21

Impedance functions, influenced by factors like soil properties, vibration frequency, and foundation type, describe the frequency-dependent damping and stiffness characteristics of the interaction. Accurate prediction of structural response to dynamic loads, such as seismic events, relies on these functions. By quantifying the complex interplay between foundation and soil under dynamic conditions, impedance functions assist in designing foundations that are more resistant to vibration and minimize potential damage. In NIST GCR 12-917-21(2012) the formulations of impedance functions adopted by Gazetas (1991) and Pais and Kausel (1988) are discussed. As suggested by NIST GCR 12-917-21(2012), Pais and Kausel (1988) formulations are most often used in practice.

Table 2.1 presents the static stiffness formulas and embedment correction factors for the six degrees of freedom of a rigid surface foundation, while Tables 2.2 and 2.3 show the dynamic stiffness modifiers and radiation damping ratios. Tables 2.4 and 2.5 give radiation damping ratios for embedded foundation.

The equations of stiffness and dashpot coefficients recommended for the simulation of SSI used in the document NIST GCR 12-917-21(2012) are presented in Tables 2.1 through 2.5 and in Equations 2.14 through 2.16.

Table 2.1: Static stiffness of rigid footings at the ground surface (NIST GCR 12-917-21(2012) adopted from Pais and Kausel (1988))

Degree of Freedom	Static Stiffness	Embedment Correction Factors
Translation along z-axis	$K_{z,sur} = \frac{GB}{1-v}\left[3.1\left(\frac{L}{B}\right)^{0.75} + 1.6\right]$	$\eta_z = \left[1.0 + \left(0.25 + \frac{0.25}{L/B}\right)\left(\frac{D}{B}\right)^{0.8}\right]$
Translation along y-axis	$K_{y,sur} = \frac{GB}{2-v}\left[6.8\left(\frac{L}{B}\right)^{0.65} + 0.8\left(\frac{L}{B}\right) + 1.6\right]$	$\eta_y = \left[1.0 + \left(0.33 + \frac{1.34}{1+L/B}\right)\left(\frac{D}{B}\right)^{0.8}\right]$
Translation along x-axis	$K_{x,sur} = \frac{GB}{2-v}\left[6.8\left(\frac{L}{B}\right)^{0.65} + 2.4\right]$	$\eta_x = \left[1.0 + \left(0.33 + \frac{1.34}{1+L/B}\right)\left(\frac{D}{B}\right)^{0.8}\right]$
Torsion about z-axis	$K_{zz,sur} = GB^3\left[4.25\left(\frac{L}{B}\right)^{2.45} + 4.06\right]$	$\eta_{zz} = \left[1 + \left(1.3 + \frac{1.32}{L/B}\right)\left(\frac{D}{B}\right)^{0.9}\right]$
Rocking about y-axis	$K_{yy,sur} = \frac{GB^3}{1-V}\left[3.73\left(\frac{L}{B}\right)^{2.4} + 0.27\right]$	$\eta_{yy} = \left[1.0 + \frac{D}{B} + \left(\frac{1.6}{0.35 + (L/B)^4}\right)\left(\frac{D}{B}\right)^2\right]$
Rocking about x-axis	$K_{xx,sur} = \frac{GB^3}{1-V}\left[3.2\left(\frac{L}{B}\right) + 0.8\right]$	$\eta_{xx} = \left[1.0 + \frac{D}{B} + \left(\frac{1.6}{0.35 + L/B}\right)\left(\frac{D}{B}\right)^2\right]$

Table 2.2: Dynamic stiffness modifiers and radiation damping ratios for rigid footings (NIST GCR 12-917-21(2012) adopted from Pais and Kausel (1988))

Degree of Freedom	Surface Stiffness Modifiers	Radiation Damping
Translation along z-axis	$\alpha_z = 1.0 - \left[\frac{\left(0.4 + \frac{0.2}{L/B}\right){a_o}^2}{\left(\frac{10}{1+3(L/B-1)}\right) + {a_o}^2}\right]$	$\beta_z = \left[\frac{4\Psi(L/B)}{(K_{z,sur}/GB)}\right]\left[\frac{a_0}{2\alpha_z}\right]$
Translation along y-axis	$\alpha_y = 1.0$	$\beta_y = \left[\frac{4(L/B)}{(K_{y,sur}/GB)}\right]\left[\frac{a_0}{2\alpha_y}\right]$

Table 2 3: Dynamic stiffness modifiers and radiation damping ratios for rigid footings (NIST GCR 12-917-21 (2012) adopted from Pais and Kausel (1988))

Degree of Freedom	Surface Stiffness Modifiers	Radiation Damping
Translation along x-axis	$\alpha_x = 1.0$	$\beta_x = \left[\frac{4(L/B)}{(K_{x,sur}/GB)}\right]\left[\frac{a_0}{2\alpha_x}\right]$
Torsion about z-axis	$\alpha_{zz} = 1.0 - \left[\frac{\left(0.33 - 0.03\sqrt{L/B - 1}\right){a_o}^2}{\left(\frac{0.8}{1 + 0.33(L/B - 1)}\right) + {a_o}^2}\right]$	$\beta_{zz} = \left[\frac{(4/3)[(L/B)^3 + (L/B)]{a_0}^2}{(K_{zz,sur}/GB^3)\left[\left(\frac{1.4}{1 + 3(L/B - 1)^{0.7}}\right) + {a_0}^2\right]}\right]\left[\frac{a_0}{2\alpha_{zz}}\right]$
Rocking about y-axis	$\alpha_{yy} = 1.0 - \left[\frac{0.55{a_o}^2}{\left(0.6 + \frac{1.4}{(L/B)^3}\right) + {a_o}^2}\right]$	$\beta_{yy} = \left[\frac{(4\Psi/3)(L/B)^3{a_0}^2}{(K_{yy,sur}/GB^3)\left[\left(\frac{1.8}{1 + 1.75(L/B - 1)}\right) + {a_0}^2\right]}\right]\left[\frac{a_0}{2\alpha_{yy}}\right]$
Rocking about x-axis	$\alpha_{xx} = 1.0 - \left[\frac{\left(0.55 - 0.01\sqrt{L/B - 1}\right){a_o}^2}{\left(2.4 + \frac{0.4}{(L/B)^3}\right) + {a_o}^2}\right]$	$\beta_{xx} = \left[\frac{(4\Psi/3)(L/B){a_0}^2}{(K_{xx,sur}/GB^3)\left[\left(2.2 - \frac{0.4}{(L/B)^3}\right) + {a_0}^2\right]}\right]\left[\frac{a_0}{2\alpha_{yy}}\right]$

Table 2.4: Radiation damping ratios for embedded foundation (NIST GCR 12-917-21 (2012) adopted from Pais and Kausel (1988))

Degree of Freedom	Radiation Damping
Translation along z-axis	$\beta_z = \left[\frac{4[\Psi(L/B) + (D/B)(1 + L/B)]}{(K_{z,emb}/GB)}\right]\left[\frac{a_0}{2\alpha_z}\right]$
Translation along y-axis	$\beta_y = \left[\frac{4[L/B + (D/B)(1 + \Psi\, L/B)]}{(K_{y,emb}/GB)}\right]\left[\frac{a_0}{2\alpha_y}\right]$
Translation along x-axis	$\beta_x = \left[\frac{4[L/B + (D/B)(\Psi + L/B)]}{(K_{x,emb}/GB)}\right]\left[\frac{a_0}{2\alpha_x}\right]$

Note: Stiffness modifiers for embedded foundation is the same as surface stiffness modifiers (i.e., $\alpha_{emb} = \alpha_{sur}$)

Table 2.5: Radiation damping ratios for embedded foundation (NIST GCR 12-917-21 (2012) adopted from Pais and Kausel (1988))

Degree of Freedom	Radiation Damping
Torsion about z-axis	$\beta_{zz} = \left[\frac{(4/3)[3(L/B)(D/B) + \Psi(L/B)^3(D/B) + 3(L/B)^2(D/B) + \Psi(D/B) + (L/B)^3 + (L/B)]{a_0}^2}{\left(K_{zz,emb}/GB^3\right)\left[\left(\frac{1.4}{1+3(L/B-1)^{0.7}}\right) + {a_0}^2\right]}\right]\left[\frac{a_0}{2\alpha_{zz}}\right]$
Rocking about y-axis	$\beta_{yy} = \left[\frac{(4/3)[(L/B)^3(D/B) + \Psi(D/B)^3(L/B) + (D/B)^3 + 3(L/B)^2(D/B) + \Psi(L/B)^3]{a_0}^2}{\left(K_{yy,emb}/GB^3\right)\left[\left(\frac{1.8}{1+1.75(L/B-1)}\right) + {a_0}^2\right]} + \frac{\left(\frac{4}{3}\right)\left(\frac{L}{B}+\Psi\right)\left(\frac{D}{B}\right)^3}{\left(K_{yy,emb}/GB^3\right)}\right]\left[\frac{a_0}{2\alpha_{yy}}\right]$
Rocking about x-axis	$\beta_{xx} = \left[\frac{(4/3)[(D/B)^3 + (D/B) + \Psi(D/B)^3(L/B) + 3(L/B)(D/B) + \Psi(L/B)]{a_0}^2}{\left(K_{xx,emb}/GB^3\right)\left[\left(\frac{1.8}{1+1.75(L/B-1)}\right) + {a_0}^2\right]} + \frac{\left(\frac{4}{3}\right)\left(\Psi\frac{L}{B}+1\right)\left(\frac{D}{B}\right)^3}{\left(K_{xx,emb}/GB^3\right)}\right]\left[\frac{a_0}{2\alpha_{xx}}\right]$

$$a_0 = \frac{\omega B}{V_s} \tag{2.14}$$

$$\omega = 2\pi f \tag{2.15}$$

$$\Psi = \sqrt{\frac{2(1-v)}{1-2v}} \leq 2.5 \tag{2.16}$$

Where,

a_0= dimensionless frequency

B= half width

ω =angular frequency

V_s= shear wave velocity

v = Poisson's ratio of a soil

f=frequency of vibration (earthquake motion)

The stiffness equation for embedded foundation is computed using the surface stiffness and embedment correction factor (from Table 2.1) for each degree of freedom (Equation 2.14).

$$K_{emb} = \eta K_{sur} \tag{2.14}$$

As clearly stated in NIST GCR 12-917-21(2012) the dynamic stiffness modifier for embedded foundation is the same as surface stiffness modifiers.

Based on the formulas provided in Table 2.1 through 2.3 the dynamic stiffness and dashpot coefficients are computed by,

$$k_j = \eta_j \alpha_j K_j \tag{2.15}$$

$$c_j = \frac{2K_j \beta_j}{\omega} \tag{2.16}$$

Where, k_j= dynamic stiffness of each degree of freedom

c_j = dashpot coefficient

β_j=is the sum of soil hysteretic damping and foundation radiation damping

η_j= embedment correction factor

The impedance functions proposed by Pais and Kausel (1988) and Gazetas (1991) are commonly used in soil-structure interaction analysis, particularly for the foundations of buildings and bridges. These functions are based on a simplified homogeneous half-space soil model, which provides valuable insights but has significant limitations. The model assumes homogeneous and isotropic soil properties, which may not accurately represent real-world conditions characterized by soil layering, variations in stiffness, and anisotropy. Furthermore, the model relies on linear elastic soil behavior, neglecting the effects of nonlinearity that can occur at large strains. Additionally, the accuracy of these impedance functions is often limited to a specific frequency range, potentially reducing their applicability at certain frequencies. The stiffness equations suggested by ASCE/SEI 7-16 (2017) and ASCE/SEI 41-17 (2017) are derived from these impedance functions. To address these limitations, standards and reports such as ASCE/SEI 7-16, ASCE/SEI 41-17, and NIST GCR 12-917-21 (2012) incorporate adjustments or consider more complex soil profiles, such as averaging soil properties over a certain depth of influence, to account for variations in soil conditions with depth.

2.6. Previous works

2.6.1. A study on the effect of soil-structure interaction on Seismic response of reinforced concrete buildings supported on Pile foundations by Birhan Mequanenet

Mequanenet (2015) investigates the effects of soil-foundation-structure interaction (SFSI) on five reinforced concrete building models supported by pile foundations. The buildings are assumed to have regular geometry and stiffness to simplify the analysis, avoiding torsional effects. Using the substructure method, where the superstructure is supported by springs and dashpots representing foundation stiffness and damping, the study analyzes seismic responses of both flexible-base and fixed-base models. The dynamic impedance functions provide the spring and dashpot coefficients. The analysis, conducted with SAP software, compares parameters such as base shear, overturning moments, bending moments, shear forces, axial forces, and bending moments in shear walls to assess the influence of soil flexibility. The results show that soil-structure interaction generally reduces seismic responses, offering economic advantages, although in some cases, it can increase the responses.

2.6.2. A study on the effect of soil-structure interaction on the dynamic response of symmetrical reinforced concrete buildings by Abdulwasi Usmail

Usmail (2004) examines the impact of soil-structure interaction on the dynamic response of reinforced concrete buildings with regular and symmetrical geometry, embedded in

homogeneous soil formations underlain by stiff material or bedrock. The building-foundation-soil system is subjected to earthquake ground motions, with the superstructure modeled as lumped masses at floor levels, coupled with the substructure represented by springs and dashpots. The foundation's frequency-dependent impedances are incorporated into the model, and actual earthquake records are used for excitation. The modal superposition principle is applied, though the equations remain coupled due to differing damping mechanisms in the superstructure and soil. An iterative solution method is used to solve the coupled equations and obtain displacement responses. Parametric studies are conducted for structures of varying heights, foundation embedment depths, and soil conditions from three sites in Addis Ababa. Results show that flexible-base structures generally exhibit lower natural frequencies, base shears, and inter-story displacements compared to fixed-base structures, particularly when the soil is thick. However, for thinner soil layers, the response becomes less predictable due to the irregular impedance functions, making it difficult to determine whether the fixed-base approach provides conservative design forces.

The paper by Mequanenet (2015) is based on response spectrum analysis, while Usmail (2004) used time history analysis for single earthquake motion. In this thesis, five earthquake motions are selected for time history analysis. These earthquake motions were chosen based on criteria that aim to simulate real-world conditions. The response of the flexible base model is compared to the fixed base model based on base shear, overturning moments, bending moments, shear forces, axial forces in shear walls, and bending moments, as discussed in Mequanenet (2015). In contrast, Usmail (2004) compares parameters such as natural frequencies, base shears, base turning moments, and inter-story displacements. For this thesis, the parameters used for comparison include natural period, effective flexible base damping, storey displacement, storey drift ratio, storey shear force, storey overturning moment, base shear, and base overturning moment for the selected earthquake motions.

CHAPTER THREE

SELECTED SITES AND THEIR DESCRIPTIONS

3.1. Geology and Seismicity of the Study Area

3.1.1 Location and Topography

At an altitude of 2,355 meters, Addis Ababa is situated in the grassland biome at 9°1′48″N 38°44′24″E, at the base of Mount Entoto (https://en-us.topographic-map.com/map-ffms3l/Addis-Ababa/?center=-29.26723%2C-24.4064&zoom=4). It is part of the Awash River's watershed. From 2,326 meters (7,631 feet) at Bole International Airport in the south to over 3,000 meters in the Entoto Mountains in the north, the city's altitude varies.

3.1.2. Seismic Hazard of Addis Ababa

Mammo (2005) identified three seismogenic provinces or seismic source zones based on seismic activity, geological features, and tectonic processes: the Afar Depression, the Escarpment, and the Ethiopian Rift System. Each zone has unique tectonic, geological, and seismic characteristics, with earthquakes assumed to occur randomly within these areas. According to Mammo (2005), seismic activity in Addis Ababa is primarily influenced by the active Ethiopian Rift System, which extends in a northeast-southwest direction across the country. The seismicity map reveals clusters of small to moderate earthquakes in specific areas, with occasional activity elsewhere (Figure 3.1).

The Ethiopian Rift System, which connects the Red Sea and Gulf of Aden rifts to the East African Rift System through the Afar Depression, is a seismically active region that significantly influences Addis Ababa, located on the margin of the East African Rift System and affected by the Main Ethiopian Rift. The city and its surroundings have a history of notable earthquakes, including a 1906 event with a magnitude of 6.8, the largest ever recorded in Ethiopia. Other significant quakes include a 1960 magnitude 6.3 earthquake, a 1987 magnitude 6.2 event within the Ethiopian Rift System, and the 1961 Karakore Earthquake with a magnitude of 6.6, located 200 km from Addis Ababa. Additionally, in July 1997, a magnitude 4.0 earthquake occurred 22 km southwest of the city. The region also experienced smaller magnitude earthquakes in 1977, 1984, and 1985, which were felt in the upper stories of high-rise buildings. A particularly notable event was the Serdo earthquake near the eastern margin of the Tendaho Graben, recorded by seismic stations as far as Uppsala, Sweden, with a magnitude of 6.0, followed by approximately 250 aftershocks over two months, one of which

reached a magnitude of 6.2 (Williams 2016). Despite its strength, this aftershock caused minimal additional damage due to the extensive destruction from the initial earthquake, which is believed to have resulted from lateral movement along a fault aligned in a northeast-southwest direction, parallel to the seafloor spreading in the Red Sea and Gulf of Aden (Mammo 2005; Haile 2004; Williams 2016).

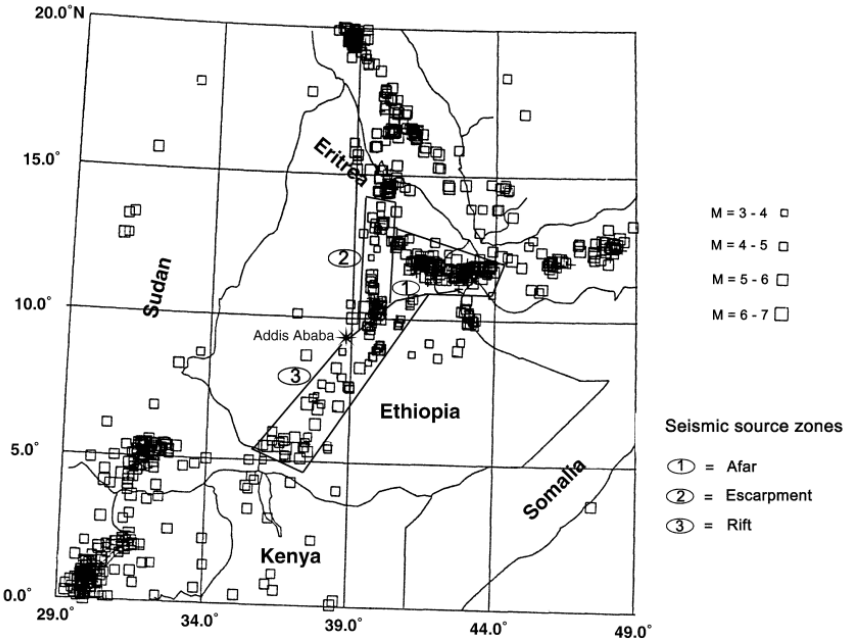

Figure 3.1: Seismicity of Ethiopia with the seismic source zones (Mammo 2005).

3.1.2.1 Ethiopian Building Code Standard, ES EN 1998:2015

ES EN 1998:2015 incorporating enhanced considerations for site effects and return periods, was formulated based on European standards. This code provides the bedrock acceleration ratio for a 475-year return period (with an exceedance rate of 10% within 50 years).

As per ES EN 1998:2015, the country is segmented into five distinct zones, designating zone 3 for Addis Ababa with a Peak Ground Acceleration (PGA) of 0.1 g (Table 3.1). This underscores a significant enhancement in the existing seismic provisions. However, notable disparities exist between the prescribed PGA values in the hazard maps and those listed in the accompanying tables.

Table 3.1: Bedrock Acceleration Ratio, α_0 (ES EN 1998:2015)

Zone	5	4	3	2	1
α_0	0.2	0.15	0.1	0.07	0.04

The PGA values obtained from the hazard maps in ES EN 1998:2015 and Table 3.1 for Addis Ababa show a significant discrepancy. The map-based estimate suggests a PGA of approximately 0.08g, which is considerably lower than the tabular value.

3.1.2.2. Global Seismic Hazard Assessment Program (GSHAP)

The Global Seismic Hazard Assessment Program (GSHAP), launched in 1992 by the International Lithosphere Program (ILP) with the support of the International Council of Scientific Unions (ICSU), gained recognition as a demonstration program under the United Nations International Decade for Natural Disaster Reduction (UN/IDNDR) (Giardini et al., 1999). This initiative established a foundational global framework for assessing seismic hazards. It aimed to provide a crucial resource for national and regional agencies to conduct further detailed studies tailored to their specific needs. One key output of GSHAP was a map depicting Peak Ground Acceleration (PGA) with a 10% chance of exceeding a certain level within 50 years, which corresponds to a return period of 475 years.

According to the Ethiopian building code (ES EN 1998:2015), the seismic hazard of many locations in the country are underestimated when compared to the GSHAP. The widely recognized GSHAP Seismic Hazard Map (Figure 3.2) indicates a PGA value for the city ranging from 1.0 to 1.3 m/s². Averaging this range yields a value of 1.15 m/s², which is approximately 0.12g. To ensure consistency and facilitate accurate comparisons within this study, the 0.12g PGA value from the GSHAP Seismic Hazard Map (Figure 3.2) is selected.

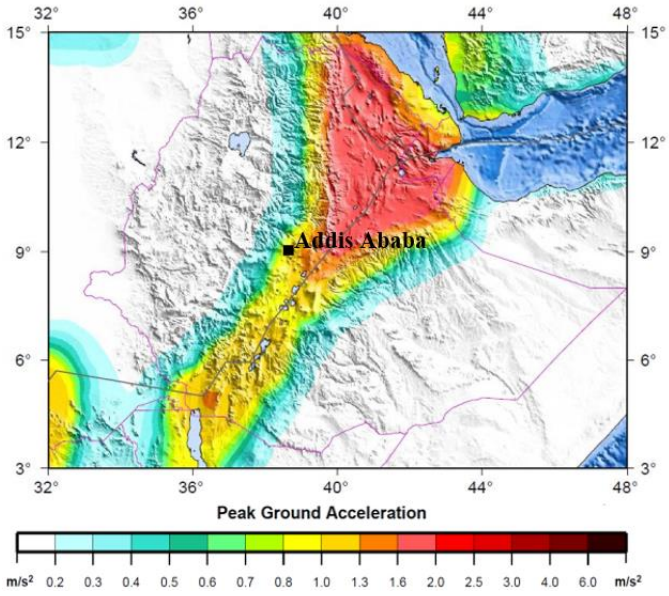

Figure 3.2: Seismic hazard map of Ethiopia based on the GSHAP data for a return period of 475years

3.2. Selected Sites

Five sites were carefully selected in Addis Ababa from a recent ground response study (Getu & Worku, 2024). The site characterization was done by geophysical tests. These sites were specifically chosen because their soil investigation had been conducted using both seismic refraction and MASW tests in addition to geotechnical studies, ensuring a comprehensive understanding of the underlying soil conditions. The sites are Ayat, CMC, Bole, Lebu, and Jemmo. Figure 3.3 shows the locations of these sites on the map and Table 3.2 presents the geographic coordinates of the selected sites.

Figure 3.3: Location of selected sites (Getu, 2023)

Table 3.2: Location of selected sites for the study (coordinates)

Profile	Northing	Easting
Bole	8.9844444	38.8008333
Ayat	9.0119444	38.8952778
CMC	9.0230556	38.8513889
Jemmo	8.9477778	38.7097222
Lebu	8.9530556	38.7333333

3.3. Soil data collected from geophysical testing

Getu's (2023) study builds on the efficiency of seismic refraction method and improves its shortcomings by integrating it with the Multi-Channel Analysis of Surface Waves (MASW) test.

Seismic refraction, widely used for assessing soil and rock properties, measures the travel time of seismic waves refracted at layer boundaries. This approach offers an advantage over

reflection methods by focusing on the arrival times of the first waves, regardless of their path. However, limitations arise from the inability to detect low-velocity layers buried within high-velocity layers and its limited sampling within thick soil sections (Ayolabi et al., 2009; Luna & Jadi, 2000).

To overcome these drawbacks, Getu (2023) incorporates the Multi-Channel Analysis of Surface Waves (MASW). This complementary technique excels at detecting low-velocity layers and provides detailed information on shear wave velocities within the shallow subsurface. By integrating both methods, the study aims to enhance the overall reliability of the subsurface assessment. This combined approach allows for a more accurate picture of the subsurface, encompassing both deeper structures (through refraction) and detailed information on the shallow layers (through MASW).

Table 3.3 through Table 3.5 summarize the primary and secondary wave velocities of the selected sites from Getu (2023).

3.4. Soil parameters used for study

3.4.1. Primary and secondary wave velocities

When an earthquake occurs, it generates different types of seismic waves: body waves and surface waves. Body waves, which travel through the Earth's interior, are classified into two types: P-waves and S-waves. P-waves, also known as primary, compressional, or longitudinal waves, cause successive compression and extension of the materials they pass through. These waves are similar to sound waves, with particle motion parallel to the direction of travel. P-waves can move through both solids and fluids. S-waves, or secondary, shear, or transverse waves, induce shearing deformations as they propagate. The particle motion for S-waves is perpendicular to their direction of travel (Kramer, 1996). In this study, S-waves and P-waves are obtained from the seismic refraction and MASAW tests conducted by Getu (2023). Figures 3.4 to 3.5 Show the graphical representation of shear wave velocity against depth for all sites obtained from geophysical tests. The shear wave velocities determined from geophysical tests are more reliable than those computed from the correlation of standard penetration test blow counts. Therefore, shear wave velocities from geophysical tests are used in this study.

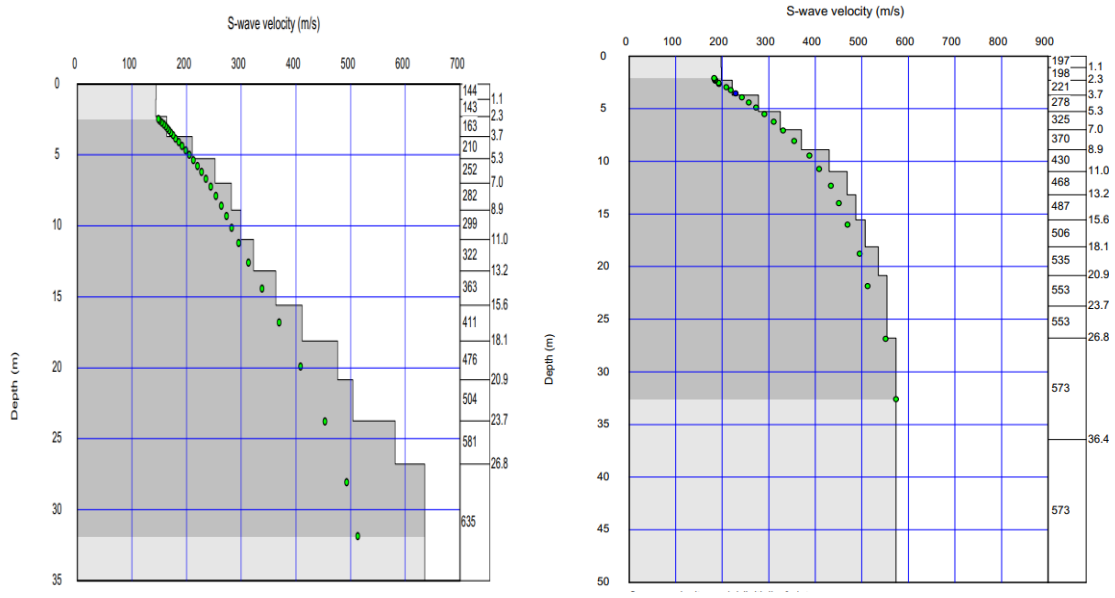

(a) Ayat

(b) CMC

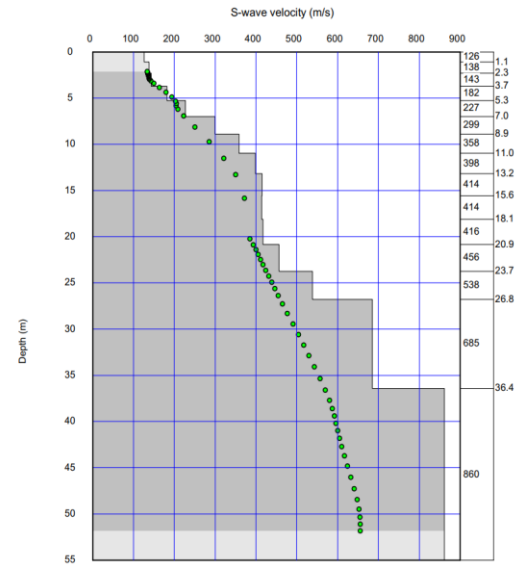

(c) Bole

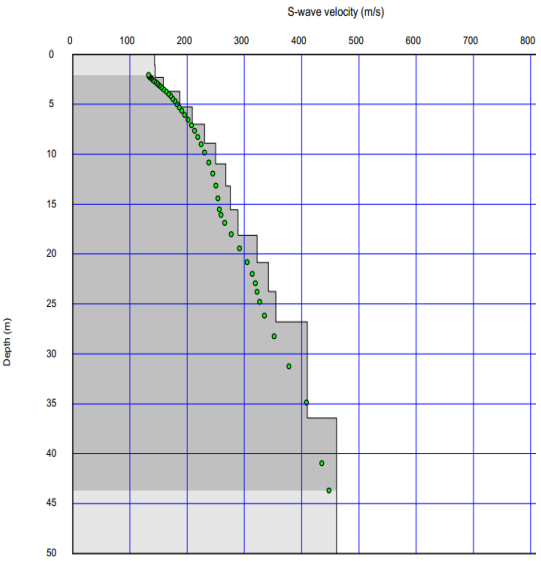

(d) Jemmo

Figure 3.4: Shear wave velocity profiles obtained from geophysical tests (Getu, 2023) for (a) Ayat site, (b) CMC site, (c) Bole site, and (d) Jemmo site

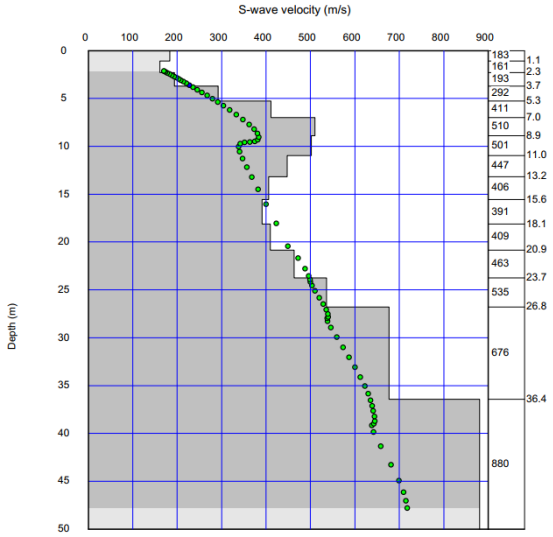

(e) Lebu

Figure 3.5: Shear wave velocity profiles obtained from geophysical tests (Getu, 2023) for (e) Lebu site

3.4.2. Poisson's ratio

Poisson's ratio is a fundamental mechanical constant that characterizes the relationship between transverse and longitudinal strains in elastic materials, unaffected by experimental conditions or deformation modes. It represents a change in shape while maintaining constant volume. Poisson's ratio can be calculated using primary and secondary wave velocities, which are obtained from geophysical tests. Equation 3.2 derives from the relationships between body wave velocities and elastic parameters, providing a method for calculating Poisson's ratio for soils using these wave velocities.

$$v = \frac{1 - a^2/2}{1 - a^2} \tag{3.2}$$

Where; $a = \frac{v_p}{v_s}$

v = Poisson's ratio

a = ratio of primary wave velocity to secondary wave velocity

v_p = primary wave velocity

v_s = secondary wave velocity

3.4.3. Unit weight of soil

The unit weight of soil refers to its weight per unit volume and is typically expressed in units of kN/m³. It is an essential parameter in geotechnical engineering, because it directly influences

various soil properties. In this specific study, it is used in the calculation of the shear modulus (Section 4.4.3).

Table 3.3 through 3.6 show the soil properties used in the study for the calculation of spring and dashpot coefficients suggested by Pais and Kausel (1988) (see section 2.5.5) and characterizing the soil beneath the foundation used for the study.

Table 3.3: Measured values of primary and secondary wave velocities and unit weight at Ayat and CMC sites (Getu, 2023)

Ayat				CMC			
Depth(m)	V_s (m/s)	V_p (m/s)	γ (kN/m^3)	Depth(m)	V_s (m/s)	V_p (m/s)	γ (kN/m^3)
0.0	144.3	291.7		0.0	197.3	394.6	
1.1	143.73	291.5	14.9	1.1	198.6	397.3	16.1
2.3	163.8	330.4	14.9	2.3	221.1	442.3	16.2
3.7	210.4	419.3	15.4	3.7	278.0	556.1	16.6
5.3	252.2	500.3	16.4	5.3	325.1	650.2	17.7
7.0	282.0	560.6	17.2	7.0	370.5	741.0	18.4
8.9	299.4	598.2	17.7	8.9	430.0	860.0	19
11.0	322.6	647.1	18	11.0	468.5	936.9	19.8
13.2	363.2	727.6	18.4	13.2	487.1	974.2	20.2
15.6	411.5	819.9	18.9	15.6	506.8	1013.6	20.5
18.1	476.5	942.8	19.6	18.1	535.1	1070.3	20.7
20.9	504.1	989.3	20.3	20.9	553.9	1107.7	21
23.7	581.7	1134.7	20.6	23.7	553.8	1107.7	21.2
26.8	635.4	1232.1	21.4	26.8	573.1	1146.2	21.2
36.4	654.5	1263.5	21.9	36.4	573.1	1146.2	21.3

Table 3.4: Measured values of primary and secondary wave velocities and unit weight at Bole and Jemmo sites (Getu, 2023)

Bole				Jemmo			
Depth(m)	V_s (m/s)	V_p (m/s)	γ(kN/m3)	Depth(m)	V_s (m/s)	V_p (m/s)	γ(kN/m3)
0.0	126.3	254.0		0.0	143.3	286.6	
1.1	138.1	275.9	16.1	1.1	144.1	288.2	14.8
2.3	143.3	288.3	16.2	2.3	158.4	316.8	14.9
3.7	182.2	367.6	16.6	3.7	187.1	374.2	15.2
5.3	227.5	454.6	17.7	5.3	209.3	418.6	15.9
7.0	299.2	588.7	18.4	7.0	230.4	460.7	16.4
8.9	358.015	697.9	19	8.9	249.6	499.2	16.8
11.0	398.6	776.5	19.8	11.0	267.6	535.3	17.2
13.2	414.4	812.4	20.2	13.2	275.5	551.1	17.5

Table 3.5: Measured values of primary and secondary wave velocities and unit weight at Bole and Jemmo sites (Getu, 2023)

Bole				Jemmo			
Depth(m)	V_s (m/s)	V_p (m/s)	γ(kN/m3)	Depth(m)	V_s (m/s)	V_p (m/s)	γ(kN/m3)
15.6	414.4	820.4	20.5	15.6	289.0	578.0	17.6
18.1	416.8	831.5	20.7	18.1	322.4	644.7	17.8
20.9	456.3	909.1	21	20.9	342.1	684.2	18.4
23.7	538.4	1062.2	21.2	23.7	354.8	709.5	18.6
26.8	685.2	1336.4	21.2	26.8	410.1	820.2	18.8
36.4	860.9	1660.4	21.3	36.4	461.3	922.5	19.5

Table 3.6: Measured values of primary and secondary wave velocities and unit weight at Lebu site (Getu, 2023)

Lebu			
Depth(m)	V_s (m/s)	V_p (m/s)	γ(kN/m3)
0.0	183.3	362.8	
1.1	161.4	324.3	15.8
2.3	193.7	388.6	15.3
3.7	292.3	583.0	16.1
5.3	411.2	815.1	17.9
7.0	510.3	1008.4	19.6
8.9	501.9	991.3	20.7
11.0	447.9	887.7	20.6
13.2	406.1	811.0	20
15.6	391.2	787.1	19.5
18.1	409.9	827.0	19.3
20.9	463.1	932.3	19.5
23.7	535.9	1074.8	20.2
26.8	676.5	1350.6	21
36.4	880.6	1748	22.3

3.4. Ground types of the selected sites

In EN 1998-1 (2004), ES EN 1998:2015, and ASCE/SEI 7-16 (2017), ground types are described based on stratigraphic profiles. These ground types are essential for accounting for the influence of local ground conditions on seismic action. The stratigraphic profiles provide information about the geological layers and characteristics of the soil at a specific site.

Referring to these codes, $V_{s,30}$ is a parameter representing the time-averaged shear-wave velocity in the upper 30 meters of the Earth's surface, used to classify ground types based on

their seismic response characteristics. In EN 1998-1, ground types are categorized into 7 soil types ranging from rock to soft soil formations. Similarly, ASCE/SEI 7-16 (2017) and ASCE /SEI 7-10 classify sites into six categories (Table 3.7)

The site classification in ASCE/SEI 7-16 (2017) and ASCE/SEI 7-10 (2010) are used in this study. This is because the Eurocode and the Ethiopian building code lack clear procedures for analyzing SSI.

Table 3.7: Ground types based on EN 1998-1 (2004), and ASCE/SEI 7-16 (2017),

EN 1998-1 (2004)			ASCE/SEI 7-16 (2017)		
Ground type	$V_{s,30}$ (m/s)	Description	Ground type	$V_{s,30}$ (m/s)	Description
A	>800	Rock	A	>1500	Hard rock
B	360-800	Very dense sand, gravel or very stiff clay	B	760 -1500	Rock
C	180-360	Dense or medium-dense sand, gravel or stiff clay	C	360-760	Very dense soil and soft soil
D	<180	Loose to medium cohesionless soil or soft to firm cohesive soil	D	180-360	Stiff soil
E		A soil profile consisting of surface alluvium layer with V_s values of type C or D and thickness varying between about 5m and 20m, underlain by stiffer material with V_s>180m/s	E	<180	Soft clay soil
S_1		Deposits consisting, or containing a layer at least 10 m thick, of soft clays/silts with a high plasticity index (PI > 40) and high water content	F		Soils requiring site response analysis
S_2		Deposits of liquefiable soils, of sensitive clays, or any other soil profile not in types A-E or S_1			

Equation 3.3 shows how to calculate $V_{s,30}$ and Table 3.8 shows the ground types of the selected sites based on EN 1998-1 (2004) and ASCE/SEI 7-16 (2017).

$$v_{s,30} = \frac{30}{\sum_{i=1}^{n} \frac{h_i}{v_{si}}} \tag{3.3}$$

Where,

$v_{s,30}$ = average shear wave velocity of upper most 30 meters

h_i , v_{si} = thickness (in metres) and shear-wave velocity (at a shear strain level of 10^{-5} or less) of the i-th formation or layer, in a total of N, existing in the top 30 m, respectively.

Table 3.8: Ground types of the selected sites according to EN 1998-1 (2004) and ASCE/SEI 7-16 (2017)

Sites	$V_{s,30}$	Ground type (EN 1998-1, 2004)	Ground type (ASCE/SEI 7-16, 2017)
Ayat	356.8	C	D
CMC	433.5	B	C
Bole	358.2	C	D
Lebu	426.2	B	C
Jemmo	278.4	C	D

3.5. Idealized soil

The selected sites fall under soil types C and D as per ASCE/SEI 7-16 (2017), as shown in Table 3.8. In theoretical analyses of SSI, it is generally assumed that SSI effects are more pronounced in softer soils. To better understand the impact of SSI in this study, an additional idealized site has been included with $V_{s,30}$ of 150m/s categorized under type E according to ASCE/SEI 7-16 (2017) and ASCE/SEI 7-10 (2010). This site represents softer soil conditions to observe how SSI influences the structural response.

CHAPTER FOUR
BUILDING MODELS

4.1. Building assumptions

The study focuses on four building categories, each with a floor plan dimension of 25m by 35m and a grid spacing of 5m. Building Model 1 is a five-storey residential building. Building Model 2 is a ten-story mixed-use building. Building Model 3 is a twenty-storey mixed-use building. Building Model 4 is a thirty-storey building.

To mitigate the undesired complications due to twisting forces (torsion) that can arise during earthquakes with the soil foundation interaction the selected buildings are intentionally selected to be symmetrical both geometrically and in terms of lateral rigidity.

Building models 1 and 2 share symmetrical geometry, staircase positioning, and elevator placement. The distinguishing factor lies in the dimension of the columns, as indicated in Tables 4.1 and 4.2. Similarly, building models 3 and 4 exhibit identical geometry, staircase, and shear wall locations, as well as elevator placements, but they differ in concrete grade and column sizes, as specified in Tables 4.2 and 4.3. All building plans and 3D views are shown in Figures 4.1 and 4.2.

The structural adequacy of the building structures is verified using ETABS 21.1.0 for the superstructure and SAFE 20 for the foundation. Structural adequacy involves ensuring that stresses and deflections remain within acceptable limits under various loads. The process includes modeling the structure's geometry, material properties, and loads in ETABS; modeling the foundation's soil properties and geometry in SAFE; conducting structural and foundation analyses; and checking for stress, deflection, and bearing capacity compliance with design codes.

Table 4.1: Selected buildings and their description

Building Model 1-G+5	Type		Dual system
	Conc. grade		C-30/37
	Steel grade		S-500
	Beam dimension		300mm*500mm
	Column dimension	Ground to G+2	650mm*650mm
		G+3 to roof	450mm*450mm
	Slab thickness		150mm
	Live load	G+1 to G+5	$3kN/m^2$ (Category A)

Table 4.2: Selected buildings and their description

Building Model 1-G+5	Live load	Roof and Roof top	$1kN/m^2$ (Category H)
	Partition load		$1.2\ kN/m^2$
	Floor finish and Screed plaster		$2\ kN/m^2$
	Shear wall thickness		300mm
Building Model 2-G+10	Type		Dual system
	Conc. grade		30/37
	Steel grade		S-500
	Beam dimension		300mm*500mm
	Column dimension	Ground to G+2	800mm*800mm
		G+3 to G+7	700mm*700mm
		G+8 to roof	400mm*400mm
	Slab thickness		150mm
	Shear wall thickness		300mm
	Live load	G+1 to G+2	$4kN/m^2$(Category D)
		G+3 to G+10	$3kN/m^2$(Category A)
		Roof and Roof top	$1kN/m^2$ (Category H)
	Partition		$1.2\ kN/m^2$
	Floor finish and Screed plaster		$2kN/m^2$
Building Model 3-G+20	Type		Dual system
	Conc. grade		30/37
	Steel grade		S-500
	Beam dimension		300mm*500mm
	Column dimension	Ground to G+3	700mm*700mm (composite column)
		G+4 to G+10	700mm*650mm (composite column)
		G+11 to G+15	600mm*600mm
		G+16 to roof	500mm*500mm
	Slab thickness		150mm
	Shear wall thickness		300mm
	Live load	G+1 to G+2	$4kN/m^2$(Category D)
		G+3 to G+20	$3kN/m^2$(Category A)
		Roof and Roof top	$1kN/m^2$ (Category H)
	Floor finish and Screed plaster		2 kN/m^2
Building Model 4-G+30	Type		Dual system
	Conc. grade		40/50
	Steel grade		S-500
	Beam dimension		300mm*600mm
	Column dimension	Ground to G+5	750mm*750mm (composite column)
		G+6 to G+15	700mm*700mm (composite column)

Table 4.3: Selected buildings and their description

Building Model 4-G+30	Column dimension	G+16 to G+25	700mm*650mm (composite column)
		G+26 to roof	700mm*600mm (composite column)
	Slab thickness		150mm
	Shear wall thickness		300mm
	Live load	G+1 to G+2	$4kN/m^2$(Category D)
		G+3 to G+40	$3kN/m^2$(Category A)
		Roof and Roof top	$1kN/m^2$ (Category H)
	Floor finish and Screed plaster		2 kN/m^2

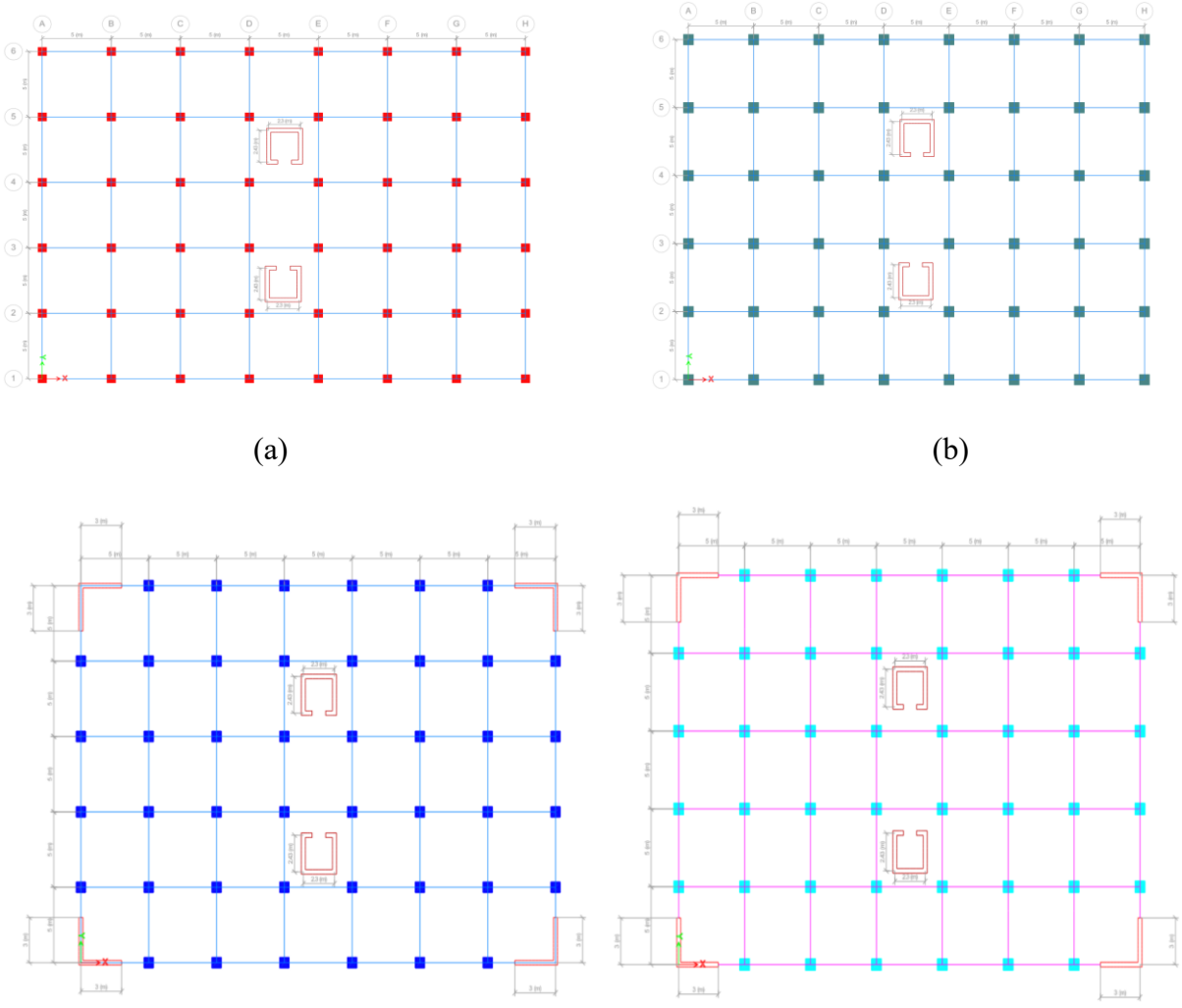

(a) (b)

(c) (d)

Figure 4.1: Ground floor plan; (a) Model 1, (b) Model 2, (c) model 3, (d) Model 4

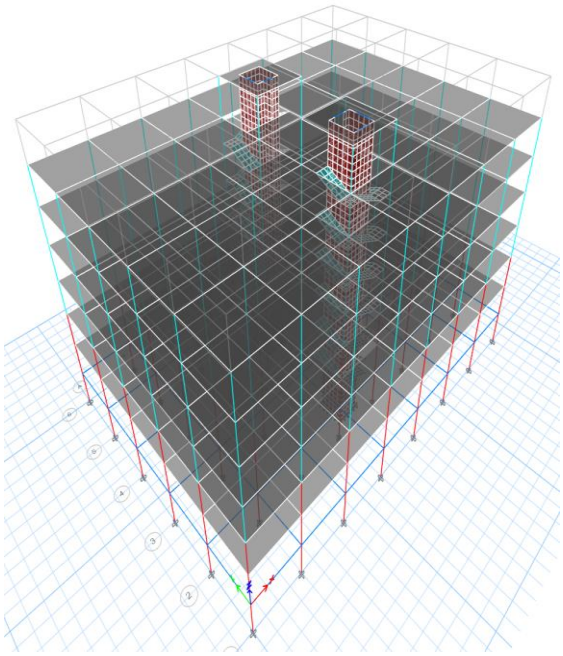

(f)

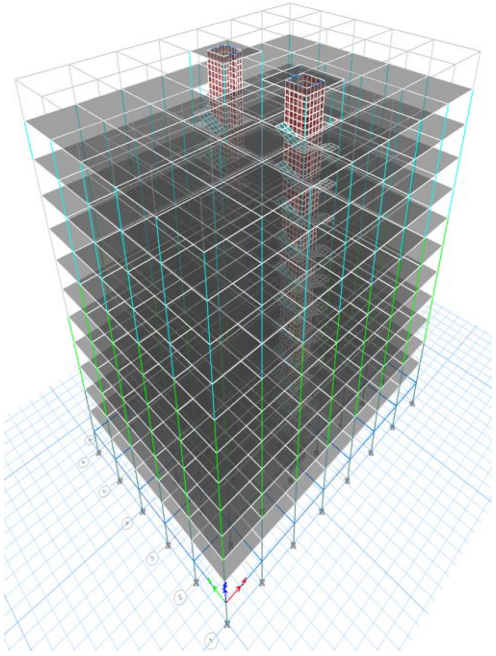

(g)

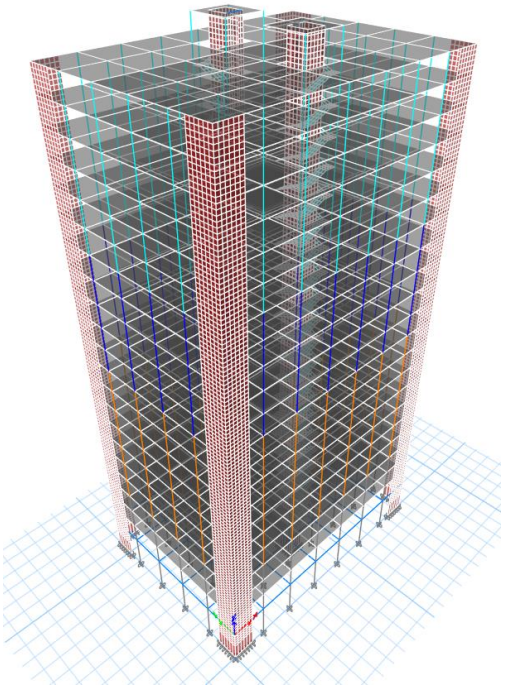

(h)

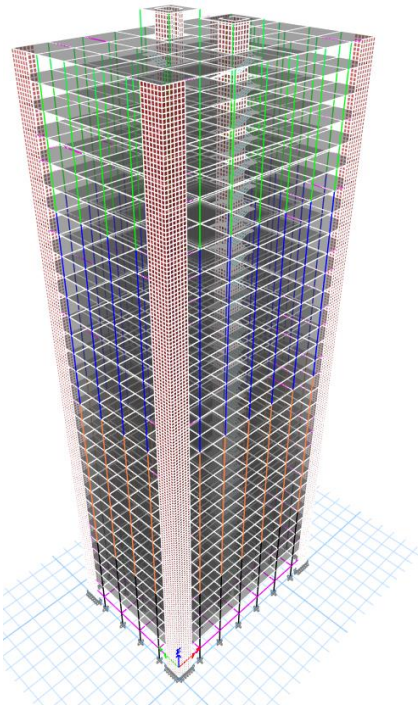

(i)

Figure 4.2: 3D view; (f) Model 1, (g) Model 2, (h) Model 3, (i) Model 4

4.2. Foundation used for the study

Foundations serve as the crucial connection between buildings and the ground they stand upon. Their primary function is to safely transfer the building's weight and other loads (dead, live, wind, etc.) to the underlying soil, ensuring the structure's stability and longevity (Das and Sivakugan, 2019). To achieve this critical role, foundations must meet two essential design criteria:

I. Bearing capacity: The foundation must be designed to prevent failure within the supporting soil. If the soil cannot withstand the imposed loads, it could lead to foundation collapse, risking the entire structure's integrity.

II. Settlement: The foundation's movement (settlement) under the building's weight must be kept within acceptable limits. Excessive settlement can cause cracks, uneven floors, including structural damage.

For all building models, mat foundation is used by applying the above criteria. The description of the foundation in each case is stated in Table 4.4.

Table 4.4: Foundations and their description

Building model	Dimension of mat foundation (m)	Thickness of mat foundation (m)	Total foundation depth (m)	Concrete grade
1	25.4*35.4	0.6	3.6	30/37
2	26.4*36.4	1.5	4.5	40/50
3	26.4*36.4	1.6	6.6	40/50
4	27.4*37.4	2.0	8.0	40/50

4.3. Selected method of analysis

There are two methods for the analysis of SSI (Section 2.4). These are: the substructure method, which simplifies the complex relationship between a structure and its supporting soil by employing a spring-based model, and the direct method, which involves modeling and analyzing the soil and structure as a unified system subjected to specified ground motion. According to FEMA P-2091 (2020), the direct method is typically reserved for large and important projects, such as nuclear power plants, massive bridges, tunnels, subway stations, tanks, and marine structures, due to its complexity and resource requirements. For this study, the substructure approach was selected, aligning with code-based modeling practices, to

investigate the significance of SSI considerations within the framework of existing design codes.

4.4. Spring and dashpot constants for simulation of SSI

In Sections 2.5.2 to 2.5.5, different simulation methods for SSI are discussed. For this study, the impedance functions suggested by NIST GCR 12-917-21(2012) are chosen, based on a formulation derived from the research by Pais and Kausel (1988). Tables 4.5 and 4.6 present the calculated spring and dashpot constants according to Section 2.5.5 (NIST GCR 12-917-21, 2012). These constants are computed as representatives of the influence depth (Equations 4.1 through 4.3).

4.4.1 Influence depth

Soil properties such as shear modulus, shear wave velocity, and Poisson's ratio used to calculate spring constants (foundation stiffness), can be averaged over the influence depth below the foundation level for different degrees of freedom, as defined in NIST GCR 12-917-21 (2012), as shown in Equations 4.1 through 4.3.

$$Horizontal\ (x\ and\ y): \mathrm{Z}_p = \sqrt{BL} \tag{4.1}$$

$$Rocking\ (xx): \mathrm{Z}_p = \sqrt[4]{B^3 L} \tag{4.2}$$

$$Rocking\ (yy): \mathrm{Z}_p = \sqrt[4]{B L^3} \tag{4.3}$$

Where;

Z_p = influence depth

B , L = half width and half length of foundation

4.4.2. Shear wave velocity at low strains (v_{so})

Neither ASCE/SEI 41-17 (2017) nor ASCE/SEI 7-16 (2017) explicitly address the calculation of shear wave velocity at low strains within the influence depth. However, FEMA P-2091 (2020) recommends using the average shear wave velocity equation over the influence depth for such calculations (Equation 4.4).

$$v_{so} = \frac{\sum_{i=1}^{n} d_i}{\sum_{i=1}^{n} \frac{d_i}{v_{si}}} \tag{4.4}$$

Where;

v_{so} = shear wave velocity at low strains, evaluated within the influence depth

d_i = the thickness of any layer within the influence depth

v_{si} = the shear wave velocity of each layer

4.4.3. Shear modulus

The initial shear modulus (G_0) according to Equation 4.5 is an important parameter for determining soil-structure interaction within the defined influence depth. However, for stiffness calculations, this initial value is not used directly. Instead, the effective shear modulus ratio (ASCE/SEI 41-17, 2017) adjusts the initial modulus to account for factors like strain level and loading conditions, ensuring a more accurate representation of the soil's behavior under the foundation's influence.

$$G_o = \frac{\gamma {v_{so}}^2}{g} \tag{4.5}$$

$$G = \left(\frac{G}{G_o}\right) G_o \tag{4.6}$$

Where;

G, G_o = shear modulus (strain dependent) and initial shear modulus respectively

$\frac{G}{G_o}$ = effective shear modulus ratio (strain dependent)

v_{so} = shear wave velocity at low strains, evaluated at the influence depth

g = gravity

Applying the formulas suggested by Pais and Kausel (1988), which are provided in Section 2.5.5 and Equations 4.1 to 4.6, the shear modulus, shear wave velocity, and Poisson's ratio are computed. These values are used to calculate spring coefficients (stiffness) and dashpot coefficients for soil types C, D, and E according to ASCE/SEI 7-16 (2017). The computed values are presented in Tables 4.5 and 4.6. As shown in these tables, stiffness decreases as soil flexibility increases. However, within the structural models used for building analysis, stiffness increases as the average shear wave velocity within the depth of influence increases.

Table 4.5: Spring and dashpot constants for Building model 1 and 2

Building model 1			Building model 2		
Soil type (ASCE/SEI 7-16, 2017)	Stiffness	Damping Coefficient	Soil type (ASCE/SEI 7-16, 2017)	Stiffness	Damping Coefficient
Type C	K_x =4.04*10^7 kN/m	C_x = 1.30*10^6 kN-s/m	Type C	K_x =3.90*10^7 kN/m	C_x = 1.45*10^6 kN-s/m
	K_y = 4.14*10^7 kN/m	C_y = 1.36*10^6 kN-s/m		K_y = 4.11*10^7 kN/m	C_y = 1.52*10^6 kN-s/m
	K_z = 4.02*10^7 kN/m	C_z = 2.12*10^6 kN-s/m		K_z = 4.00*10^7 kN/m	C_z = 2.30*10^6 kN-s/m
	K_{xx} = 6.42*10^9 kN-m	C_{xx} = 8.50*10^7 kN-m-s		K_{xx} = 6.81*10^9 kN-m	C_{xx} = 1.13*10^8 kN-m-s
	K_{yy} = 8.98*10^9 kN-m	C_{yy} = 2.31*10^8 kN-m-s		K_{yy} = 9.25*10^9 kN-m	C_{yy} = 3.07*10^8 kN-m-s
	K_{zz} = 1.40*10^{10} kN-m	C_{zz} = 2.23*10^8 kN-m-s		K_{zz} = 1.50*10^{10} kN-m	C_{zz} = 2.86*10^8 kN-m-s
Type D	K_x = 2.08*10^7 kN/m	C_x = 9.18*10^5 kN-s/m	Type D	K_x = 2.04*10^7 kN/m	C_x = 1.04*10^6 kN-s/m
	K_y = 2.26*10^7 kN/m	C_y = 9.61*10^5 kN-s/m		K_y = 2.3*10^7 kN/m	C_y = 1.09*10^6 kN-s/m
	K_z = 2.20*10^7 kN/m	C_z = 1.59*10^6 kN-s/m		K_z = 2.23*10^7 kN/m	C_z = 1.75*10^6 kN-s/m
	K_{xx} = 3.10*10^9 kN-m	C_{xx} = 8.08*10^7 kN-m-s		K_{xx} = 3.36*10^9 kN-m	C_{xx} =1.07*10^8 kN-m-s
	K_{yy} =4.27*10^9 kN-m	C_{yy} =2.52*10^8 kN-m-s		K_{yy} =4.52*10^9 kN-m	C_{yy} =3.27*10^8
	K_{zz} = 4.27*10^9 kN-m	C_{zz} = 1.89*10^8 kN-m-s		K_{zz} = 7.81*10^9 kN-m	C_{zz} = 2.41*10^8 kN-m-s
Type E	K_x =1.37*10^6 kN/m	C_x = 3.41*10^5 kN-s/m	Type E	K_x =1.43*10^6 kN/m	C_x = 3.94*10^5 kN-s/m
	K_y = 2.35*10^6 kN/m	C_y = 3.55*10^5 kN-s/m		K_y = 2.53*10^6 kN/m	C_y = 4.12*10^5 kN-s/m
	K_z = 2.28*10^6 kN/m	C_z = 8.60*10^5 kN-s/m		K_z = 2.46*10^6 kN/m	C_z = 9.69*10^5
	K_{xx} = 2.20*10^8 kN-m	C_{xx} = 6.48*10^7 kN-m-s		K_{xx} = 2.60*10^8 kN-m	C_{xx} = 8.30*10^7 kN-m-s
	K_{yy} = 3.33 *10^8 kN-m	C_{yy} =2.49*10^8 kN-m-s		K_{yy} = 3.85 *10^8 kN-m	C_{yy} =3.07*10^8 kN-m-s
	K_{zz} = 7.16*10^8 kN-m	C_{zz} =1.00*10^8 kN-m-s		K_{zz} = 8.51*10^8 kN-m	C_{zz} =1.27*10^8 kN-m-s

Table 4.6: Spring and dashpot constants for Building model 3 and 4

Building model 3			Building model 4		
Soil type (ASCE/SEI 7-16, 2017)	Stiffness	Damping Coefficient	Soil type (ASCE/SEI 7-16, 2017)	Stiffness	Damping Coefficient
Type C	$K_x = 3.31*10^7$ kN/m	$C_x = 1.58*10^6$ kN-s/m	Type C	$K_x = 3.12*10^7$ kN/m	$C_x = 1.76*10^6$ kN-s/m
	$K_y = 3.71*10^7$ kN/m	$C_y = 1.68*10^6$ kN-s/m		$K_y = 3.63*10^7$ kN/m	$C_y = 1.87*10^6$ kN-s/m
	$K_z = 3.61*10^7$ kN/m	$C_z = 2.35*10^6$ kN-s/m		$K_z = 3.53*10^7$ kN/m	$C_z = 2.55*10^6$ kN-s/m
	$K_{xx} = 6.33*10^9$ kN-m	$C_{xx} = 1.52*10^8$ kN-m-s		$K_{xx} = 6.70*10^9$ kN-m	$C_{xx} = 2.11*10^8$ kN-m-s
	$K_{yy} = 8.26*10^9$ kN-m	$C_{yy} = 4.05*10^8$ kN-m-s		$K_{yy} = 8.45*10^9$ kN-m	$C_{yy} = 5.55*10^8$ kN-m-s
	$K_{zz} = 1.42*10^{10}$ kN-m	$C_{zz} = 3.05*10^8$ kN-m-s		$K_{zz} = 1.50*10^{10}$ kN-m	$C_{zz} = 4.42*10^8$ kN-m-s
Type D	$K_x = 1.78*10^7$ kN/m	$C_x = 1.15*10^6$ kN-s/m	Type D	$K_x = 1.71*10^7$ kN/m	$C_x = 1.29*10^6$ kN-s/m
	$K_y = 2.13*10^7$ kN/m	$C_y = 1.22*10^6$ kN-s/m		$K_y = 2.13*10^7$ kN/m	$C_y = 1.38*10^6$ kN-s/m
	$K_z = 2.07*10^7$ kN/m	$C_z = 1.82*10^6$ kN-s/m		$K_z = 2.07*10^7$ kN/m	$C_z = 2.01*10^6$ kN-s/m
	$K_{xx} = 3.21*10^9$ kN-m	$C_{xx} = 1.40*10^8$ kN-m-s		$K_{xx} = 3.47*10^9$ kN-m	$C_{xx} = 1.92*10^8$ kN-m-s
	$K_{yy} = 4.17*10^9$ kN-m	$C_{yy} = 4.18*10^8$ kN-m-s		$K_{yy} = 4.39*10^9$ kN-m	$C_{yy} = 5.59*10^8$ kN-m-s
	$K_{zz} = 7.61*10^9$ kN-m	$C_{zz} = 2.92*10^8$ kN-m-s		$K_{zz} = 8.23*10^9$ kN-m	$C_{zz} = 3.66*10^8$ kN-m-s
Type E	$K_x = 1.51*10^6$ kN/m	$C_x = 4.47*10^5$ kN-s/m	Type E	$K_x = 1.59*10^6$ kN/m	$C_x = 5.52*10^5$ kN-s/m
	$K_y = 2.77*10^6$ kN/m	$C_y = 5.00*10^5$ kN-s/m		$K_y = 2.99*10^6$ kN/m	$C_y = 5.83*10^5$ kN-s/m
	$K_z = 2.70*10^6$ kN/m	$C_z = 1.08*10^6$ kN-s/m		$K_z = 2.91*10^6$ kN/m	$C_z = 1.22*10^6$ kN-s/m
	$K_{xx} = 3.10*10^8$ kN-m	$C_{xx} = 1.08*10^8$ kN-m-s		$K_{xx} = 3.75*10^8$ kN-m	$C_{xx} = 1.45*10^7$ kN-m-s
	$K_{yy} = 4.43*10^8$ kN-m	$C_{yy} = 3.80*10^8$ kN-m-s		$K_{yy} = 5.21*10^8$ kN-m	$C_{yy} = 4.86*10^8$ kN-m-s
	$K_{zz} = 1.01*10^9$ kN-m	$C_{zz} = 1.61*10^8$ kN-m-s		$K_{zz} = 1.20*10^9$ kN-m	$C_{zz} = 2.04*10^8$ kN-m-s

4.5. Selected Software for the study

The selected software for the study is ETABS 21.1.0. It is specialized engineering software tailored for the analysis and design of multi-storey buildings. For SSI using the substructure method, ETABS is a preferred structural analysis program for several strong reasons. Its easy-to-use graphical interface simplifies the process of defining and modeling structures. In addition, ETABS is remarkably adaptable, capable of analyzing a wide variety of structures,

including buildings, bridges, and retaining walls, with a particular emphasis on building structures (https://www.csiamerica.com/products/etabs).

CHAPTER FIVE
INPUT GROUND MOTIONS

Accurately analyzing soil-structure interaction (SSI) in dynamic assessments requires meticulously chosen ground motion data. Due to limited availability of such data in Ethiopia, this study turned to the Pacific Earthquake Engineering Research Center (PEER) database (https://ngawest2.berkeley.edu/) as a reliable source. Developed by PEER, this database is a comprehensive collection of processed ground motion records from shallow crustal earthquakes around the world. It offers valuable metadata, such as distance measures, site characterizations, and earthquake source information. Notably, the PEER database includes unscaled, as-recorded ground motions, providing a more fundamental representation of earthquake shaking. Additionally, for researchers focusing on specific regions, the NGA-East and NGA-West 2 databases offer extensive ground motion data tailored to Central and Eastern North America and active tectonic regions, respectively. The filtering criteria used to select ground motions for this study are detailed in sections 5.1 to 5.7.

5.1. Tectonic Regime

The initial step in choosing input motions from PEER databases involves selecting ground motion recordings from regions with a similar tectonic regime as the area under investigation. Within the PEER database, the NGA-West 2 ground motion database offers an extensive collection of ground movements stemming from shallow crustal earthquakes in active tectonic regimes globally. These recordings are particularly pertinent to the NGA-West 2 ground motion database. As highlighted by Kebede and van Eck (1997), earthquakes in the Middle Ethiopian Rift (MER) are characterized by shallow crustal origins. Consequently, for the case of Addis Ababa, the optimal choice of database is NGA-West 2.

5.2. Definition of Target Spectrum

After selecting the appropriate database, the next step is to establish the necessary filtering criteria to obtain the target spectrum. This spectrum represents the anticipated ground motion response at the reference site, typically expressed as pseudo-acceleration spectra. Since site exploration often concludes upon encountering rock formations, reference site conditions are frequently modeled using rock properties.

The first stage in defining the target spectrum involves assessing the seismic hazard of the region. As per ES EN 1998:2015, the reference return period for a design ground acceleration

(PGA) with a 10% probability of exceedance in 50 years is 475 years. For this analysis, the PGA value of 0.12g extracted from GSHAP is employed. Additionally, ground Type A (representing rock material) will be adopted to develop the target spectrum, considering the common practice of using rock conditions for reference sites.

For horizontal components of the seismic action, the elastic response spectrum Se (T) is defined by the following expressions for 5% damping (ES EN 1998:2015):

$$
\begin{aligned}
&0 \le T \le T_B: \quad S_e(T) = a_{\mathbf{g}}.S.\left[1 + \frac{T}{T_B}.(\eta.2.5 - 1)\right] \\
&T_B \le T \le T_{C:} \quad S_e(T) = a_{\mathbf{g}}.S.\eta.2.5 \\
&T_C \le T \le T_{D:} \quad S_e(T) = a_{\mathbf{g}}.S.\eta.2.5\left[\frac{T_C}{T}\right] \\
&T_D \le T \le 4s \quad S_e(T) = a_{\mathbf{g}}.S.\eta.2.5\left[\frac{T_C T_D}{T^2}\right]
\end{aligned}
\tag{5.1}
$$

where:

$S_e(T)$ is the elastic response spectrum

T is the vibration period of a linear single-degree-of-freedom system;

$a_{\mathbf{g}}$ is the design ground acceleration on type A ground;

T_B is the lower limit of the period of the constant spectral acceleration branch;

T_C is the upper limit of the period of the constant spectral acceleration branch;

T_D is the value defining the beginning of the constant displacement response range of the spectrum;

S is the soil factor

η is the damping correction factor with a reference value of η = 1 for 5% viscous damping

As per ES EN 1998:2015, two design spectra options exist: Type 1 and Type 2. Type 2 spectra are appropriate for areas with earthquakes producing surface wave magnitudes smaller than 5.5. Conversely, Type 1 spectra are applicable for surface waves exceeding 5.5 in magnitude.

Research by Kebede and van Eck (1997) indicates that surface wave magnitudes within the main Ethiopian rift fall between 5.5 and 6.5. Because the magnitude exceeds the 5.5 threshold, the Type 1 design spectrum is the suitable choice for this region.

Table 5.1 lists the parameters that define the response spectrum, and Figure 5.1 shows the plot of the response spectrum of Equation 5.1.

Table 5.1: Parameters that describe the response spectrum,

Ground type	S	$T_B\ (S)$	T_C (S)	$T_D\ (S)$
A	1	0.15	0.4	2

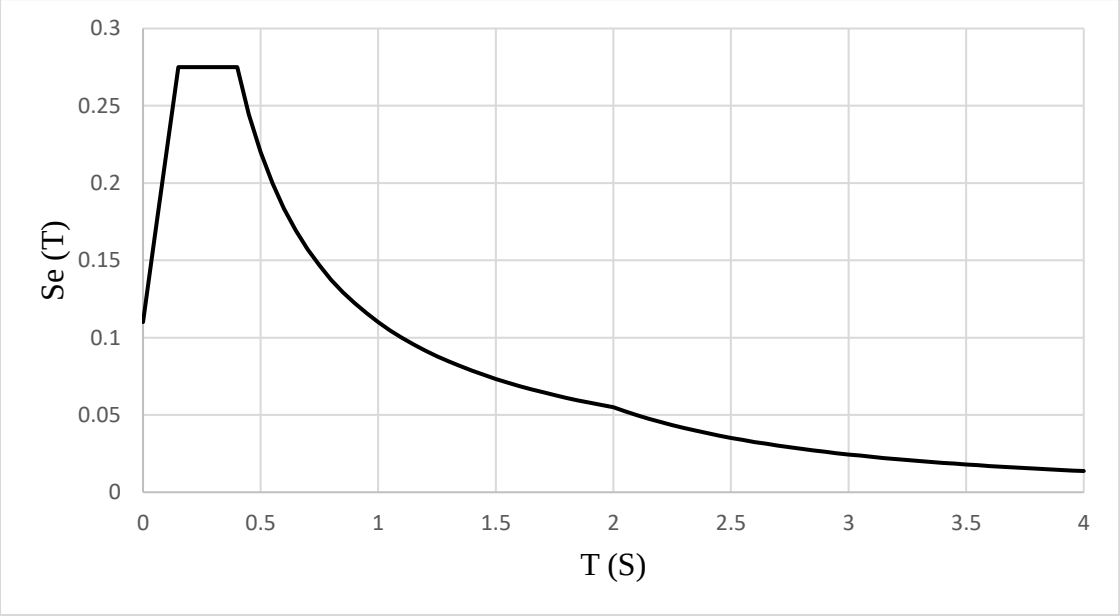

Figure 5.1 Recommended Type 1 elastic response spectrum for ground type A (ES EN 1998:2015)

5.3. Moment magnitude Range

Selecting relevant magnitude ranges for input ground motion is another selecting criterion. Kebede and van Eck (1997) offer a valuable study summarizing various seismic investigations in the Horn of Africa. Examining these studies, they identified eight distinct seismic source zones responsible for the region's damaging earthquakes. Zone 2 encompasses the crucial Main Ethiopian Rift (MER) system and even incorporates Ethiopia's southernmost rifts. Moreover, this zone includes the Wonji Fault Belt, located directly next to Addis Ababa.

The study conducted by Kebede and van Eck (1997) provides valuable insights into the seismic behavior of Zone 2, which encompasses the Main Ethiopian Rift system and adjacent regions.

According to Table 2 in their article, the lower bound moment magnitude (M_o) is 4.0, while the upper bound moment magnitude (M_{max}) is 7.0. Notably, this parameter is directly used in the selection of input motion by the PEER ground motion database.

5.4. Source to Site Distances

Two definitions of this crucial parameter for filtering ground motion data are rupture distance R_{rup} and Joyner-Boore distance R_{JB}. R_{rup} represents the shortest distance between the site and the actual fault rupture plane, while R_{JB} refers to the shortest distance to the surface projection of the fault. The PEER ground motion database allows for the use of both definitions, even though various interpretations exist regarding the distance between a site and the earthquake source (fault rupture).

The determination of source-to-site distances for Addis Ababa relies on significant earthquakes experienced in the city over the past century, as documented in Mammo (2005). However, this earthquake list lacks details on the source depth and provides no explicit information on fault type and geometry. Despite these limitations, shallow crustal earthquakes in the Ethiopian Rift System are generally characterized by an estimated average depth of 10 km (Ayele, 2017). Utilizing data from Mammo (2005) and Ayele (2017), Gashaye (2018) calculated both distances. The computed distances, as summarized in Table 5.2, reveal a range of 18.6 km to 266 km for R_{rup} and 15.7 km to 265.8 km for R_{JB}.

A wide range of rupture distances (R_{rup}) and Joyner-Boore distances (R_{JB}) in PEER ground motion database allows for a comprehensive understanding of ground motion across different scenarios. By including both near-field and far-field effects, the database helps to develop more accurate SSI models, leading to safer and more resilient structural designs.

Table 5.2: Earthquakes felt at Addis Ababa during the last century (Mammo, 2005; Gashaye, 2018) and the two distances.

Year	Month	Day	Time	Latitude (°N)	Longitude (°E)	Magnitude	Intensity (M.M*)	R_{JB}(km)	R_{rup}(Km)
1906	08	25	11:55	7.70	38.80	6.6	7	141.7	142.0
1906	08	25	13:47	7.70	38.80	6.8	8	141.7	142.0
1961	06	01	23:29:18	10.54	39.89	6.7	7	213.9	214.1
1961	08	25	21:43:49	10.65	40.10	4.5	4	237.7	237.9
1968	01	23	19:18:13	8.71	37.66	5.1	4	126.1	126.5
1973	03	08	AM	9.00	39.00	4.1	4	26.3	28.1
1974	02	25	16:05:40	9.90	39.7	4.5	3	146.0	146.3
1977	07	08	06:23:02	10.94	39.63	5.0	5	238.3	238.5
1979	07	28	19:22:16	8.85	38.70	4.1	6	15.7	18.6
1984	04	10	08:17:26	11.37	38.71	5.2	4	265.8	266.0
1985	10	28	12:08:45	9.47	39.61	4.8	5	108.7	109.2
1993	02	13	02:25:50	8.33	39.31	5.0	-	93.8	94.4

*M.M = Modified Mercalli Scale; AM=morning

5.5. Style of Faulting

Earth's crust can fracture in various ways, categorized as reverse, normal, and strike-slip faults. Notably, the Main Ethiopian Rift unfolds its dramatic landscapes primarily through normal faulting, where the hanging wall of the rift valley sinks relative to the foot wall (Kebede & van Eck, 1997). This dominant faulting style signifies the region's extension and thinning crust, shaping the rift's unique geological character.

5.6. Duration Range

The other important factor that should be considered in input ground motion selection is the duration of strong motion, as it significantly affects the amount of damage that could be sustained by structures.

All of the definitions of strong motion duration that are developed by different investigators are based upon the fact that the damage potential of an earthquake is a function of the energy of the earthquake and that the majority of the total energy associated with any earthquake is contained in portions of the earthquake time history which is much shorter in time than the total duration of the record (Salmon et al., 1992). Bommer et al. (2009) grouped all of the definitions introduced so far into three generic categories: bracketed, uniform, and significant duration.

Bommer et al. (2009) created relationships that can be used to calculate the range of strong motion duration required to select input ground motions with significant duration (Figure 5.2).

Their proposed relation has been used to estimate ground-motion durations of shallow crustal earthquakes with magnitudes, Mw, between 4.8 and 7.9 at distances of up to 100 km from the source. From this relationship, the significant duration for this study is estimated to be 17.5 seconds using shallow crustal earthquakes with a minimum magnitude, Mw, of 4.0 and a maximum magnitude, Mw, of 7.0 from the seismic area under consideration.

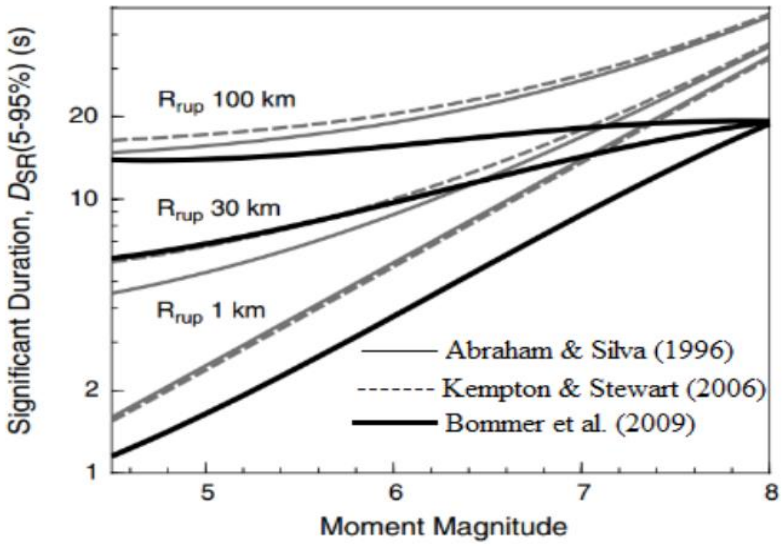

Figure 5.2: Comparison of empirical predictive models for significant duration (Bommer et al., 2009)

5.7. Shear-wave velocity of uppermost 30m ($V_{S,30}$)

Another parameter considered during the input ground motion selection procedure is the average shear wave velocity of the top 30 meters at the site of interest. According to Stewart et al. (2014), this shear wave velocity should align with the reference site condition. Specifically, it should correspond to the velocity associated with the reference site condition, which is the condition below the site profiles being analyzed in the SSI study.

The reference site condition is the site class used to develop the user-defined target response spectrum. Stewart et al. (2014) suggest that the reference site condition is typically rock which is classified as ground type A in EN 1998:2015 or types A and B in ASCE/SEI 7-16 and 7-10, the reference site condition is assumed to be where the ground motions are initially expected to occur.

To select the input motion, a filtering criterion is applied based on a $V_{S,30}$ range of 760-1500 m/s.

5.8. Input Ground Motion Matching

To analyze the selected input ground motion effectively, it is necessary to align it with the design response spectrum featuring 5% damping in the case of fixed base model and 6% to 10% damping in the case of flexible base models (these effective damping values are calculated as described in section 6.1.2). The matching process involves adjusting the ground motion to correspond with the target response spectra for ground types for each building model, which are found to be types C, D and E (for idealized site) according to ASCE/SEI 7-16 (2017). The software employed for this purpose is ETABS 21.1.0, a computer program designed to modify ground-motion records, ensuring their spectral acceleration response aligns with a specified target response spectrum.

For the matching process, ES EN 1998:2015 as well as ASCE/SEI 7-16 (2017) recommend utilizing a range of $0.2T_1$ to $2T_1$, where T_1 represents the fundamental period of vibration. Through modal analysis in ETABS 21.1.0, the fixed base model is utilized to determine the fundamental period of vibration (T_1). The corresponding maximum and minimum periods are detailed in Table 5.3.

Table 5.3: Period range used for matching of ground motions

Building model	Fundamental period of fixed base model (sec)	Minimum period (sec)	Maximum period (Sec)
Model 1	0.54	0.108	1.08
Model 2	0.78	0.156	1.56
Model 3	1.19	0.238	2.38
Model 4	1.55	0.31	3.1

Based on the criteria provided earlier, the subsequent input motions have been selected, Table 5.4 shows the pertinent input motion parameters.

Table 5.4: Ground motions selected from PEER ground motion database

RSN	5-95% Duration (sec)	Earthquake Name	Year	Station Name	Magnitude	R_{JB} (km)	R_{rup} (km)	$V_{s,30}$ (m/sec)
8209	15.3	Anza-02	2001	El Monte County Park	4.92	73.77	74.82	805
2508	17.2	Chi-Chi_ Taiwan-03	1999	CHY102	6.2	59.99	60.36	804.36
4438	12.5	Molise-02_ Italy	2002	Sannicandro	5.7	49.6	51.32	865
795	11.9	Loma Prieta	1989	SF - Pacific Heights	6.93	75.96	76.05	1249.86
59	10.4	San Fernando	1971	Cedar Springs_ Allen Ranch	6.61	89.37	89.72	813.48

Figures 5.3 and 5.4 show the unscaled ground motions selected from PEER database.

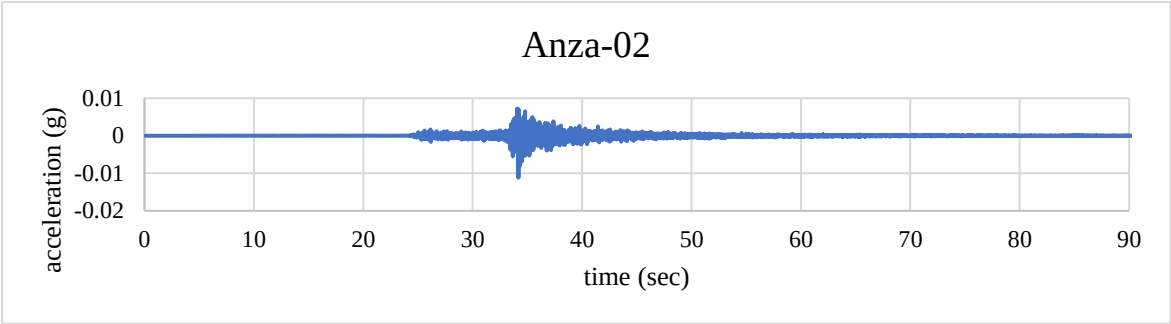

(a)

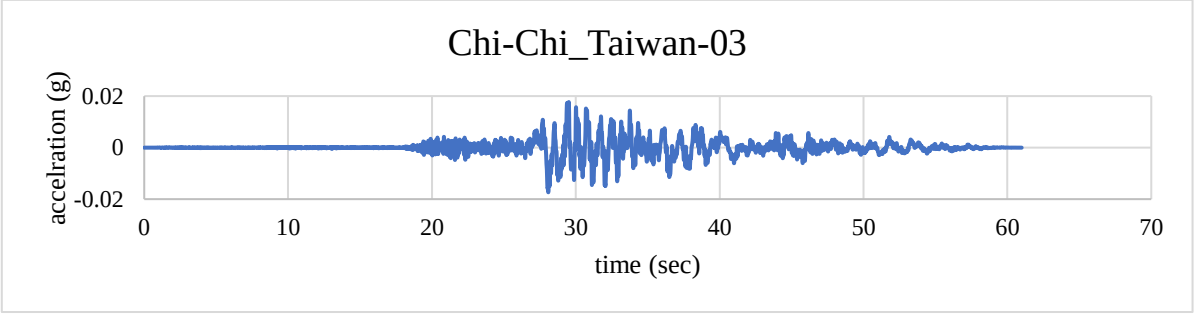

(b)

Figure 5.3: Selected input motions: (a) Anza-02, (b) Chi-Chi_Taiwan-03

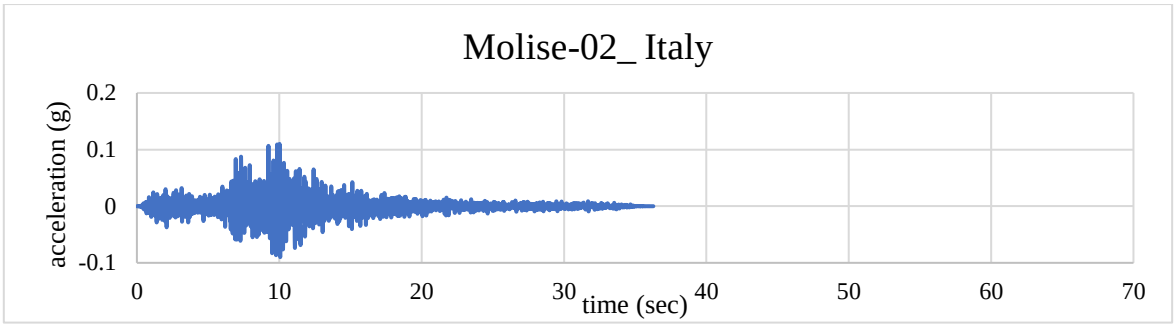

(c)

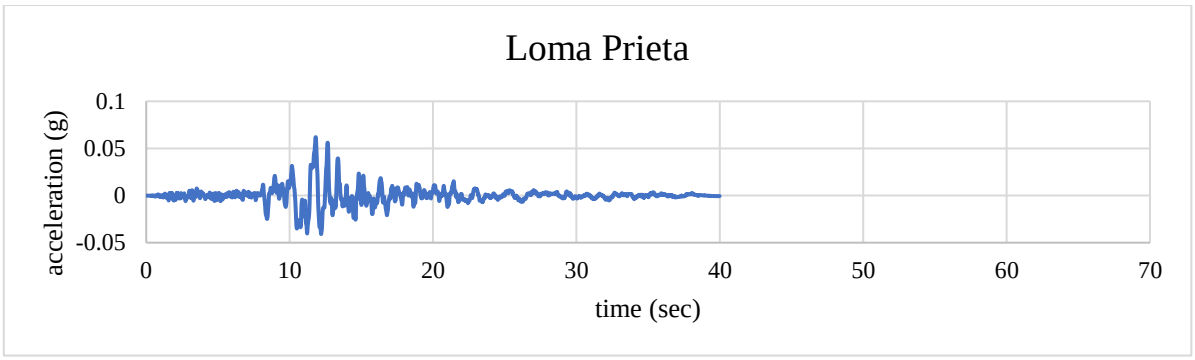

(d)

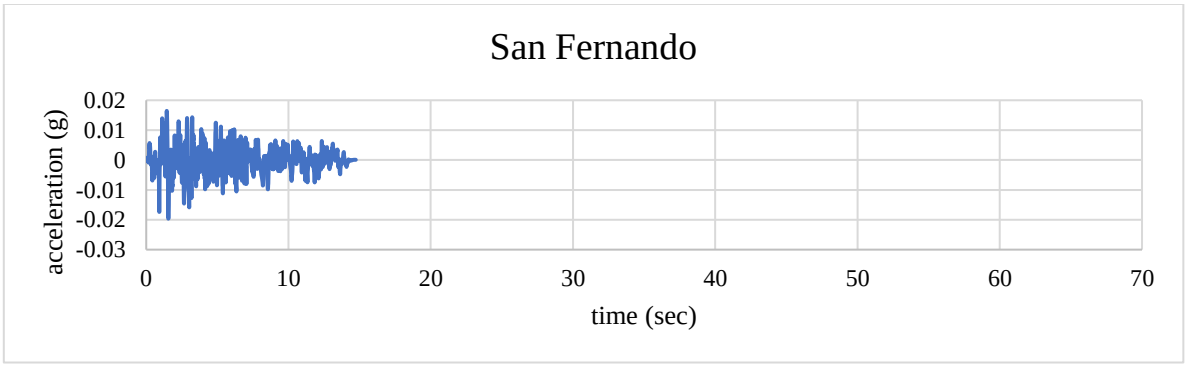

(e)

Figure 5.4: Selected input motions: (c) Molise-02_ Italy (d) Loma Prieta, (e) San Fernando

Figures 5.5 and 5.6 show the Fourier amplitude of selected earthquake motions matched to type C soil with 5 percent damping. And Figures 5.7 and 5.8 show the frequency domain spectral acceleration of selected earthquake motions matched to type C soil with 5 percent damping. The rest matched earthquake motions to type D and E as well as matched to different damping ratios are listed in Appendix A.

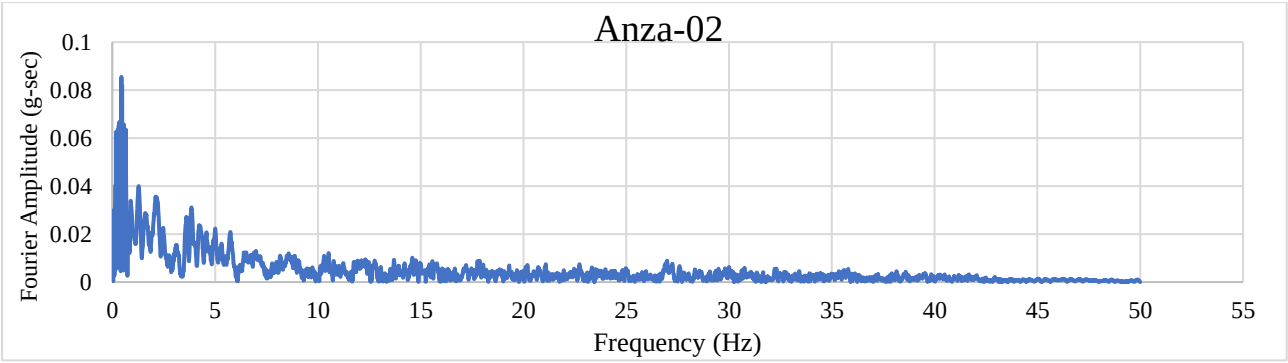

(a)

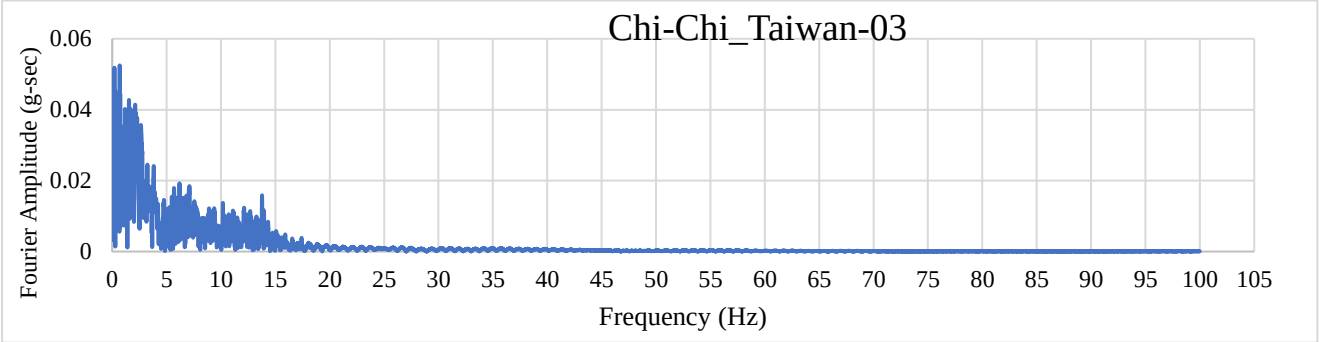

(b)

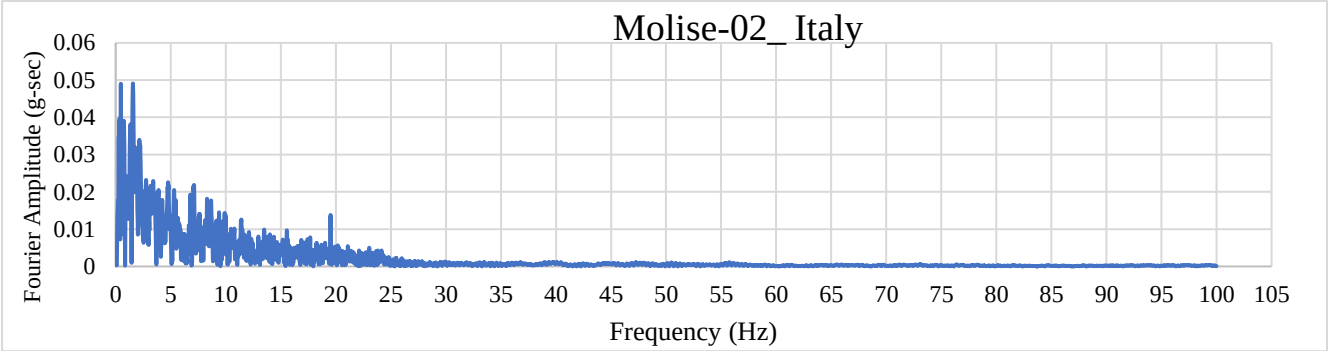

(c)

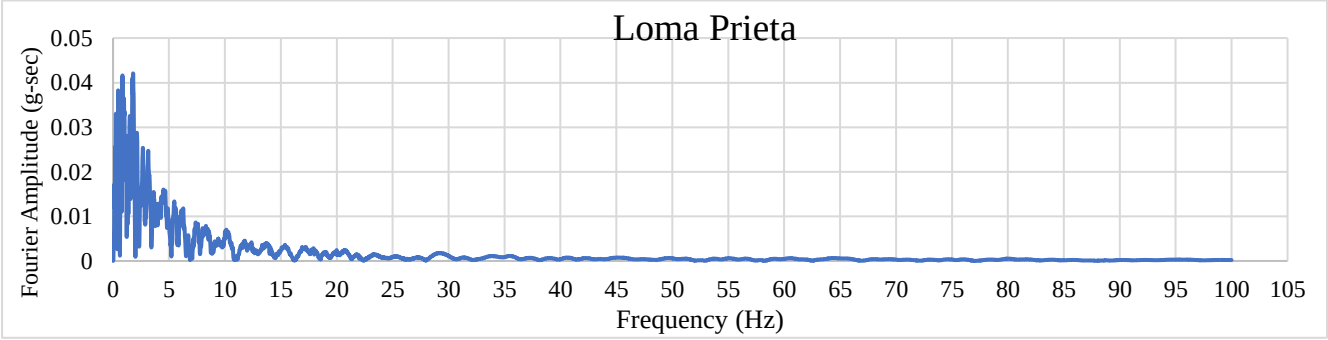

(d)

Figure 5.5: Fourier amplitude of: (a) Anza-02; (b) Chi-Chi_Taiwan-03; (c) Molise-02_ Italy; (d) Loma Prieta earthquakes matched to ground type C

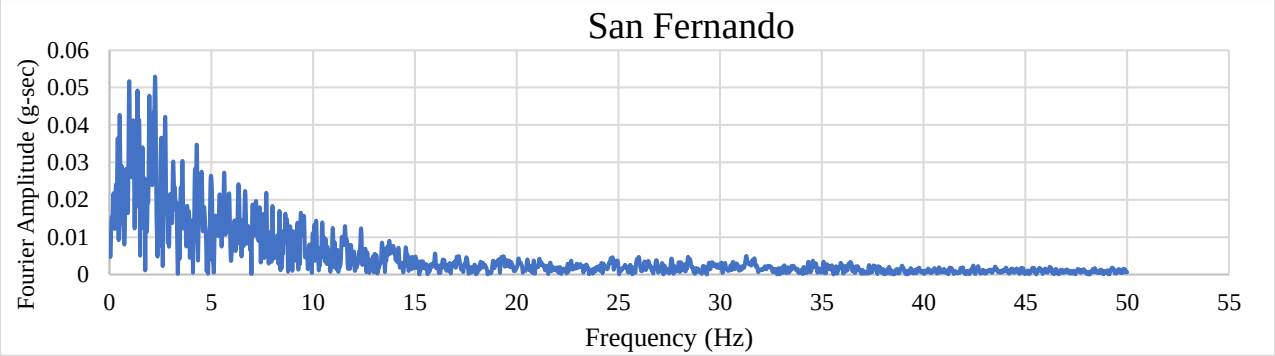

(e)

Figure 5.6: Fourier amplitude of: (e) San Fernando earthquake matched to ground type C

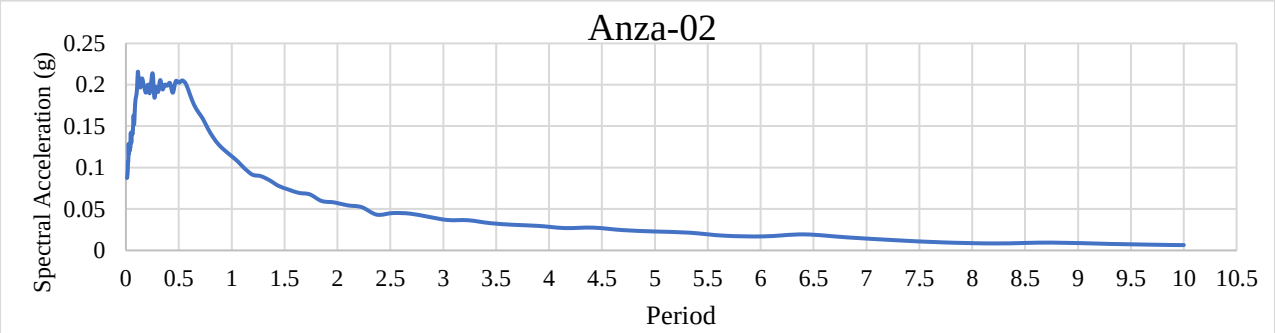

(a)

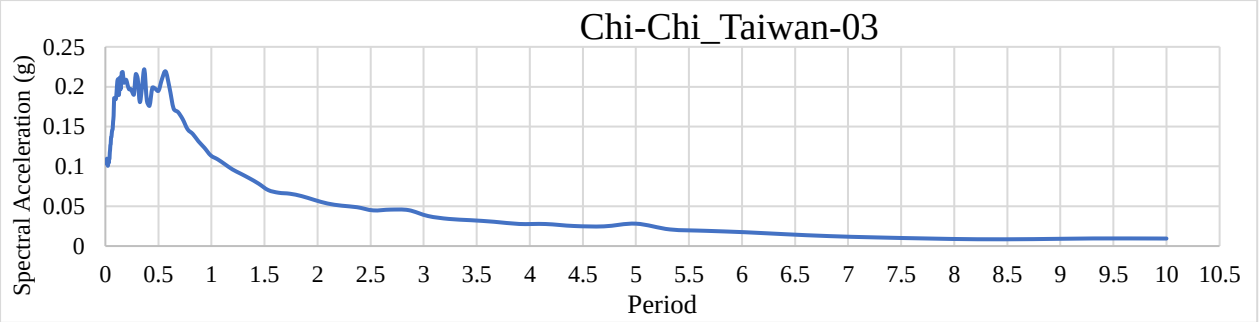

(b)

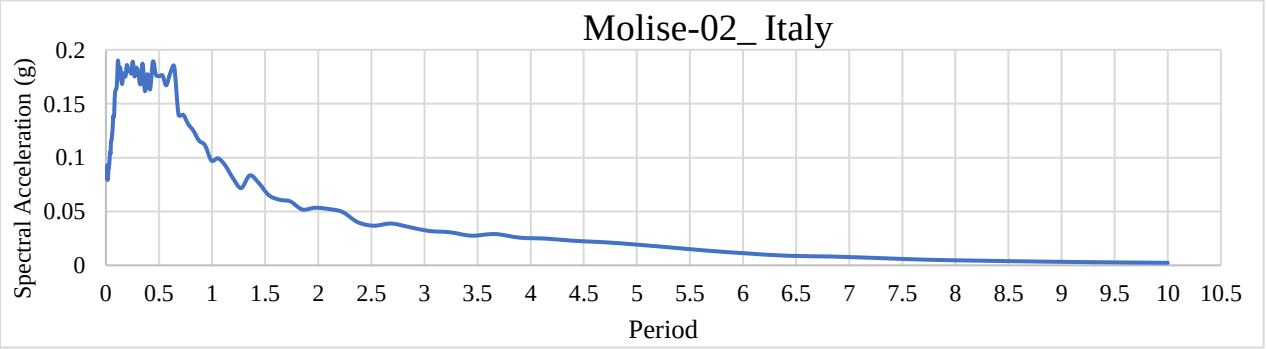

(c)

Figure 5.7: Frequency domain spectral acceleration of: a) Anza-02; (b) Chi-Chi_Taiwan-03; (c) Molise-02_ Italy earthquakes matched to ground type C

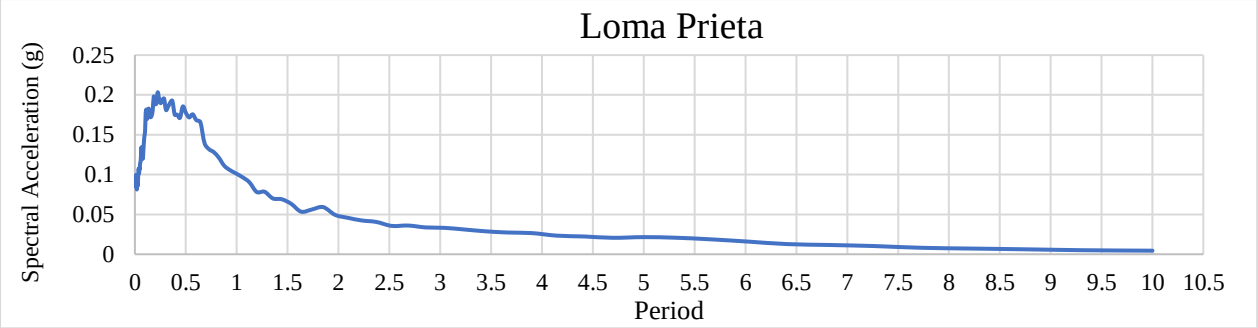

(d)

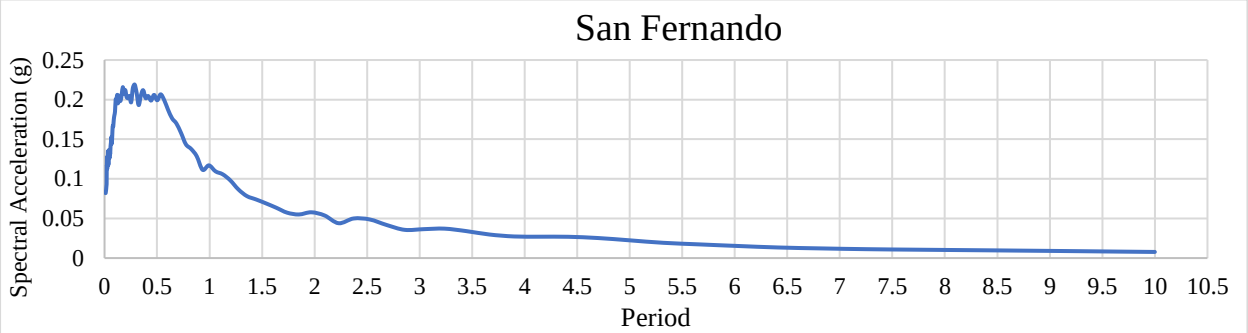

(e)

Figure 5.8: Frequency domain spectral acceleration of: (d) Loma Prieta; (e) San Fernando earthquakes matched to ground type C

CHAPTER SIX
RESULTS AND DISCUSSION

6.1. Analysis results

For this study, time-history analysis is used. Time-history analysis is a method used to determine the dynamic response of a structure to arbitrary loading. The dynamic equilibrium equations to be solved are given by (Computers & Structures, Inc. 2017.):

$$Ku(t) + C\dot{u}(t) + M\ddot{u}(t) = r(t) \tag{6.1}$$

where K = stiffness matrix

C = damping matrix

M = diagonal mass matrix

u, $\dot{u}$, and $\ddot{u}$ = displacements, velocities, and accelerations of the structure respectively

r = applied load. If the load includes ground acceleration, the displacements, velocities, and accelerations are relative to this ground motion.

The load, $r(t)$, applied in a given time-history case may be an arbitrary function of space and time.

$$r(t) = \sum_i f_i(t) P_i \tag{6.2}$$

Where: $f_i(t)$ = time functions (they are arbitrary functions of time or periodic functions)

P_i= spatial load vectors (ETABS software uses Acceleration loads to represent spatial load vectors, and the displacements, velocities, and accelerations are all measured relative to the ground).

The following sections present the response of buildings, as output from ETABS. This includes the fundamental period of the structure, storey displacement, storey drift ratio, storey shear force, storey overturning moment, and base shear.

6.1.1. Period lengthening

6.1.1.1. Fundamental period of the fixed base Structures

The fundamental period of a fixed-base model is the natural frequency at which the structure vibrates when subjected to a disturbance, assuming that the base of the structure is rigidly fixed.

The fundamental period of the structure (T) can be obtained from a computer model or by using the approximate fundamental period from ASCE/SEI 7-16 (2017); BSSC (2004).

$$T = T_a = C_t {h_n}^x \tag{6.3}$$

where:h_n = structure height as defined in ASCE/SEI 7-16 (2017) Section 11.2 plus depth of footing

C_t = coefficient from ASCE/SEI 7-16 (2017) Table 12.8-2 that depends on the structural system

x = coefficient from ASCE/SEI 7-16 (2017) Table 12.8-2 that depends on the structural system

6.1.1.2. Fundamental period of the flexible base Structure

The fundamental period of flexible-base model depends on the soil type (specifically, the shear wave velocity of the soil), the height of the structure, the weight of the structure, and the foundation dimensions. BSSC, (2004) and ASCE/SEI 7-10 (2010) provide an equation to calculate the fundamental period of a structure supported by a mat foundation (equation 6.4).

$$\tilde{T} = T\sqrt{1 + \frac{25\alpha r_a \bar{h}}{{v_s}^2 T^2}\left(1 + \frac{1.12 r_a \bar{h}^2}{\alpha_\theta {r_m}^3}\right)} \tag{6.4}$$

Where: α= relative effective weight of the structure and the soil, defined by equation 6.5

r_a and r_m= foundation characteristic lengths defined by equations 6.6 and 6.7

α_θ = dynamic foundation stiffness modifier for rocking as determined from Table 6.1

v_s = shear wave velocity within influence depth

T = Fundamental period of fixed base Structure (Equation 6.3)

$$\alpha = \frac{\bar{W}}{\gamma A_o \bar{h}} \tag{6.5}$$

$$r_a = \sqrt{\frac{A_o}{\pi}} \tag{6.6}$$

$$r_m = \sqrt[4]{\frac{4I_o}{\pi}} \tag{6.7}$$

where $\bar{W}$= the effective seismic weight of the structure, which shall be taken as $0.7W$, except for structures where the effective seismic weight is concentrated at a single level, it shall be taken as equal to W

$\bar{h}$ = the effective height of the structure, which shall be taken as 0.7 times the structural height, except for structures where the gravity load is effectively concentrated at a single level, the effective height of the structure shall be taken as the height to that level

A_o = the area of the load-carrying foundation

I_o = the static moment of inertia of the load-carrying foundation about a horizontal centroidal axis normal to the direction in which the structure is analyzed

Note: Seismic weight W includes the dead load and

- A minimum of 25% of the reduced floor live load in areas used for storage (floor live load in public garages and open parking structures need not be included)
- Actual partition weight or a minimum weight of 0.48 kN/m^2 of floor area, whichever is greater
- Weight of permanent equipment
- 20% of flat-roof snow load when the flat-roof snow load exceeds 1.44 kN/m^2, regardless of actual roof slope (ASCE/SEI 7-16, Villaverde, 2009)

Table 6.1 presents values suggested by BSSC (2004) and ASCE/SEI 7-10 (2010) for determining the α_θ modifier based on the fundamental period of a fixed base model, foundation characteristic lengths and soil shear wave velocity. These values range from 0.6 to 1.0.

Table 6.1: values of α_θ

$\frac{r_m}{v_s}T$	α_θ
< 0.05	1.0
0.15	0.85
0.35	0.7
0.5	0.6

As shown in Table 6.2, flexible base models exhibit longer fundamental periods than their fixed base counterparts. This difference varies depending on soil type. Soils with higher shear wave velocities generally show a smaller difference in fundamental period between flexible and fixed base models, while the opposite is true for soils with lower shear wave velocities.

Table 6.2: Fundamental period of fixed and flexible base models

Building Model	Fundamental period of Fixed Base Model (T (sec)) from equation 6.1	Fundamental period of Fixed Base Model (T (sec)) from ETABS output	Fundamental period of Flexible Base Model ($\tilde{T}$ (sec)) from ETABS output			Period ratio$\left(\frac{\tilde{T}}{T}\right)$		
			Ground type C	Ground type D	Ground type E	Ground type C	Ground type D	Ground type E
Model 1	0.54	0.837	0.838	0.841	0.846	1.001	1.005	1.011
Model 2	0.78	1.481	1.486	1.482	1.485	1.003	1.001	1.003
Model 3	1.19	2.714	2.743	2.723	2.866	1.011	1.003	1.056
Model 4	1.55	3.768	3.774	3.778	3.829	1.002	1.003	1.016

6.1.2. Effective flexible-base damping

An important factor affecting the dynamic behavior of a structure is flexible base damping, which results from the interaction between the structure and its underlying deformable foundation in addition to the fixed base damping, which is entirely structural. There are two main types of damping that make up this additional damping: radiation damping, which comes from stress waves spreading out from the foundation, and hysteretic damping or material, which comes from energy dissipating in the soil.

The effective damping factor for the soil structure interaction ($\tilde{\beta}$) shall be computed using Equation 6.8 (BSS,2004; ASCE/SEI 7-10, 2010; ASCE/SEI 7-05)

$$\tilde{\beta} = \beta_o + \frac{0.05}{\left(\tilde{T}/_T\right)^3} \tag{6.8}$$

where β_o = foundation damping factor as shown in Figure 6.1

The quantity r in Figure 6.1 is a characteristic foundation length that shall be determined as follows:

For $\frac{\bar{h}}{L_o} \leq 0.5, r = r_a$

For $\frac{\bar{h}}{L_o} \geq 1.0, r = r_m$

Note: L_o is the overall length of the side of the foundation in the direction being analyzed.

Note: For values of $\frac{S_{DS}}{2.5}$ between 0.10 and 0.20 the values of β_o shall be determined by linear interpolation between the solid lines and the dashed line of Figure 6.1 in each case. Similarly, for intermediate values of $\frac{\bar{h}}{L_o}, r$ shall be determined by linear interpolation.

S_{DS}= Design earthquake spectral response acceleration parameters at short periods it can be computed by Equation 6.9 (ASCE/SEI 7-16,2017)

$$S_{DS} = \frac{2}{3} S_{MS} \tag{6.9}$$

$$S_{MS} = F_a S_s \tag{6.10}$$

Where; S_{MS}= Risk-Targeted Maximum Considered Earthquake (MCE_R) spectral response acceleration parameters for short periods

S_s= the mapped MCE_R spectral response acceleration parameter at short periods

F_a= site coefficient

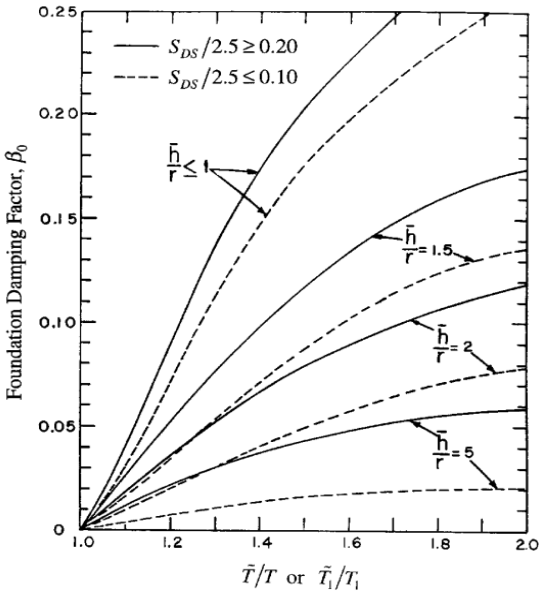

Figure 6.1: Foundation damping factor (BSSC,2004; ASCE/SEI 7-05, 2006)

The effective flexible base damping depends on soil type, fundamental period of fixed and flexible base model, height of structure and foundation area as described in this section. For smaller period ratio ($\tilde{T}/T$) and smaller values of $\frac{\bar{h}}{L_o}$ the effective damping becomes larger as shown Figure 6.1. The computed effective-damping values for each model and the different

types of sites are given in Table 6.3. Note that, the value in each case is larger than the superstructure damping of 0.05.

Table 6.3: Effective flexible-base damping

Building Model	Effective flexible-base damping		
	Type C	Type D	Type E
Model 1	0.07	0.07	0.08
Model 2	0.07	0.07	0.10
Model 3	0.07	0.07	0.06
Model 4	0.07	0.07	0.06

6.1.3. Building response

6.1.3.1. Storey displacement

Storey displacement in ETABS refers to the horizontal movement of a floor level due to applied loads like wind or seismic forces. It is a critical parameter in structural analysis and design, indicating how much a floor shifts from its original position under these forces.

6.1.3.1.1. Building model 1

Compared to its fixed base counterpart, the flexible base model of Building Model 1 shows a decrease in storey displacement across all soil types when exposed to the Anza-02, Chi-Chi Taiwan 03, and Molise-02 Italy earthquakes, except for ground type C, which shows a small increase at around the top of the building. A similar pattern is observed for the Loma Prieta earthquake, where ground type C also shows an increase. In the case of the San Fernando earthquake, storey displacement decreases for type C and D soils but shows an increase for type E soil (Figures 6.2 through 6.4).

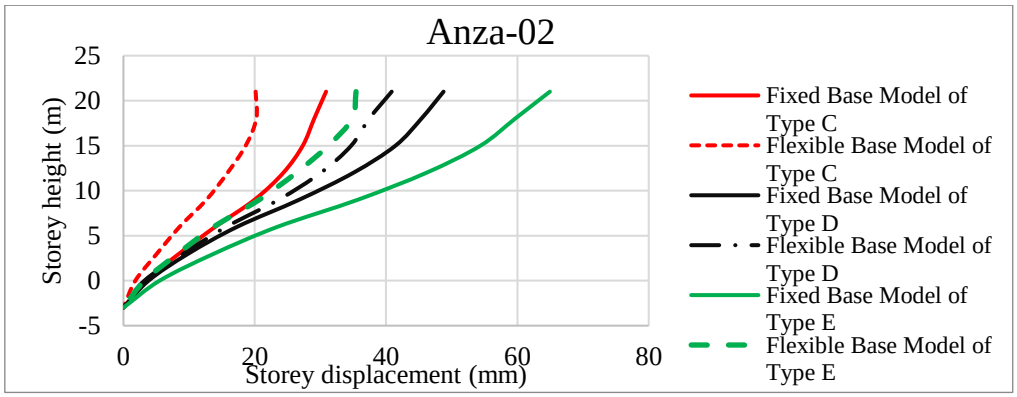

(a)

Figure 6.2: Storey displacement of Model 1 for (a) Anza-02

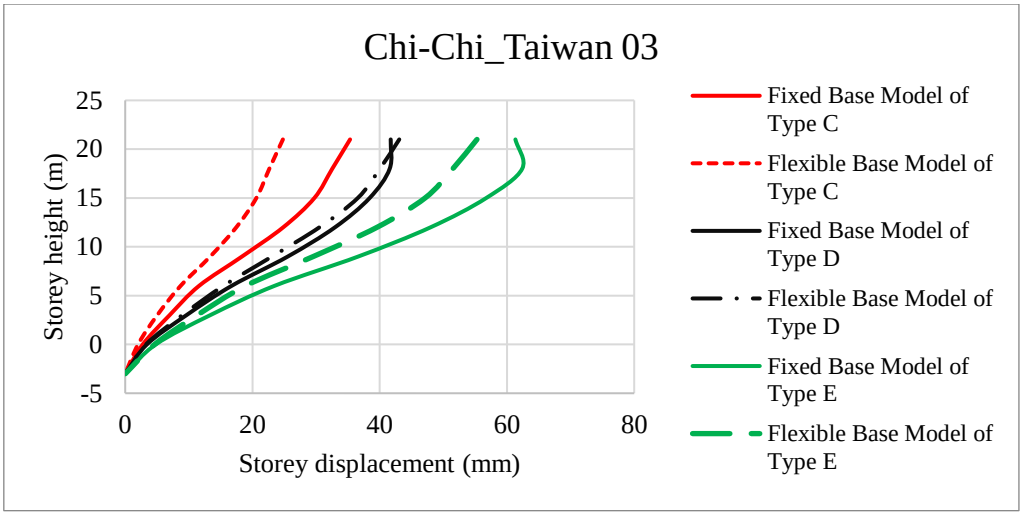

(b)

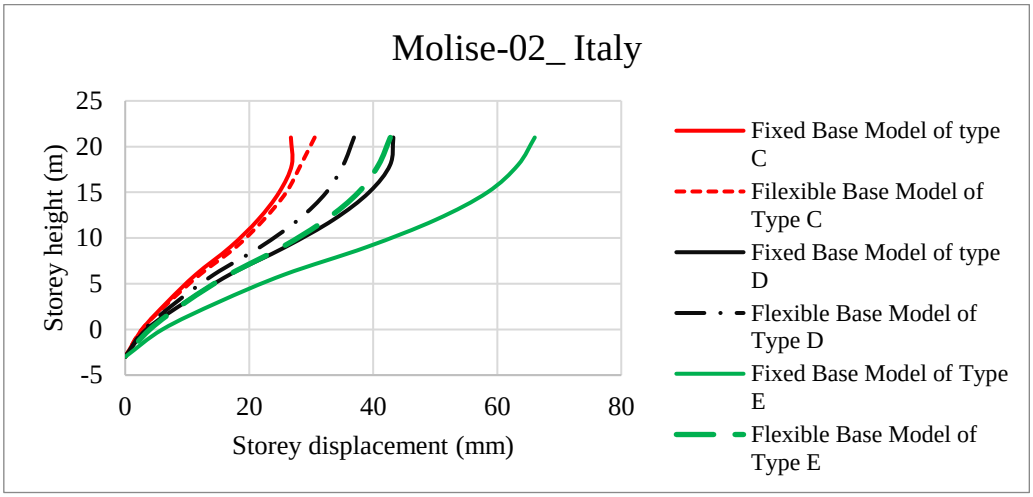

(c)

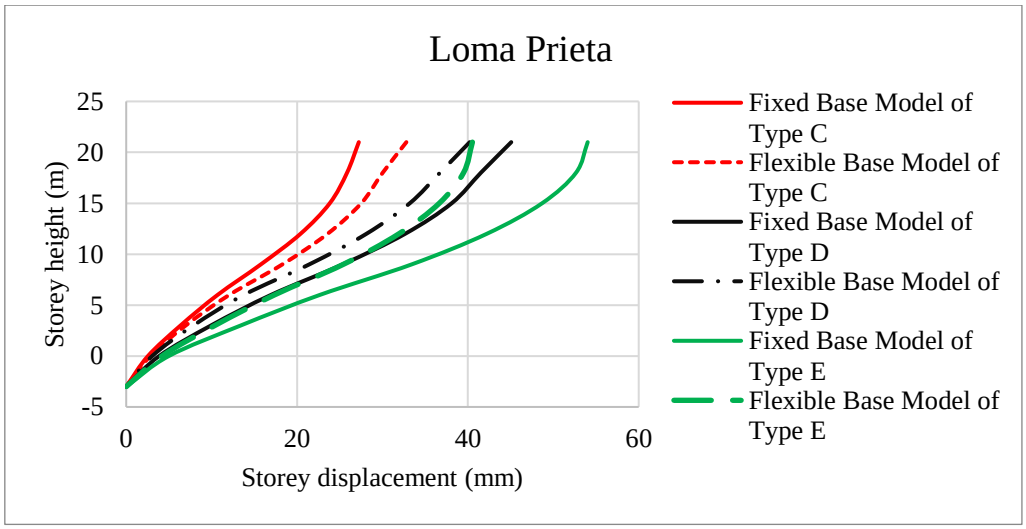

(d)

Figure 6.3: Storey displacement of Model 1 for (b) Chi-Chi_Taiwan 03, (c) Molise-02_ Italy, (d) Loma Prieta

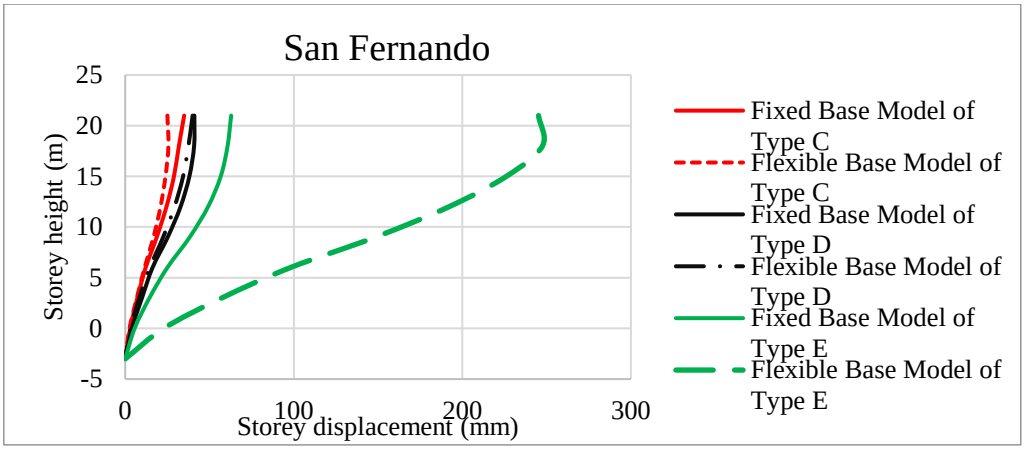

(e)

Figure 6.4: Storey displacement of Model 1 for (e) San Fernando

6.1.3.1.2. Building model 2

The storey displacement of the flexible-base building model 2 shows a decrement for type C soil when it exposed to the Anza-02, Chi-Chi Taiwan 03, and Molise-02 Italy earthquakes, but in Loma Prieta and San Fernando earthquakes it shows an increment. In the case of type D soil, it shows a decrement when the model is exposed to all earthquakes except Anza-02 earthquake which show an increment. For type E soil the flexible base model of building model 2 shows an increment when the model is exposed to Molise-02 Italy, Loma Prieta and San Fernando earthquakes, whereas a decrement is observed for Anza-02 and Chi-Chi Taiwan 03 earthquakes (Figures 6.5 through 6.7).

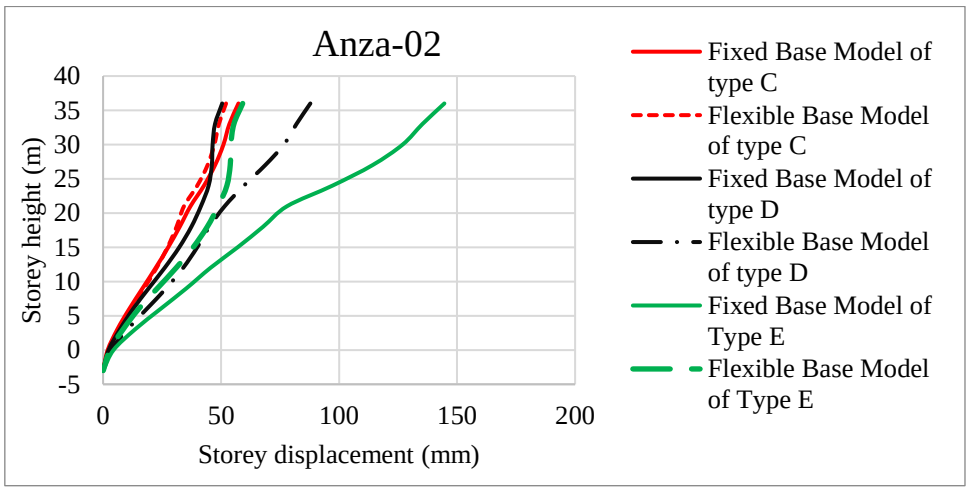

(a)

Figure 6.5: Storey displacement of Model 2 for (a) Anza-02

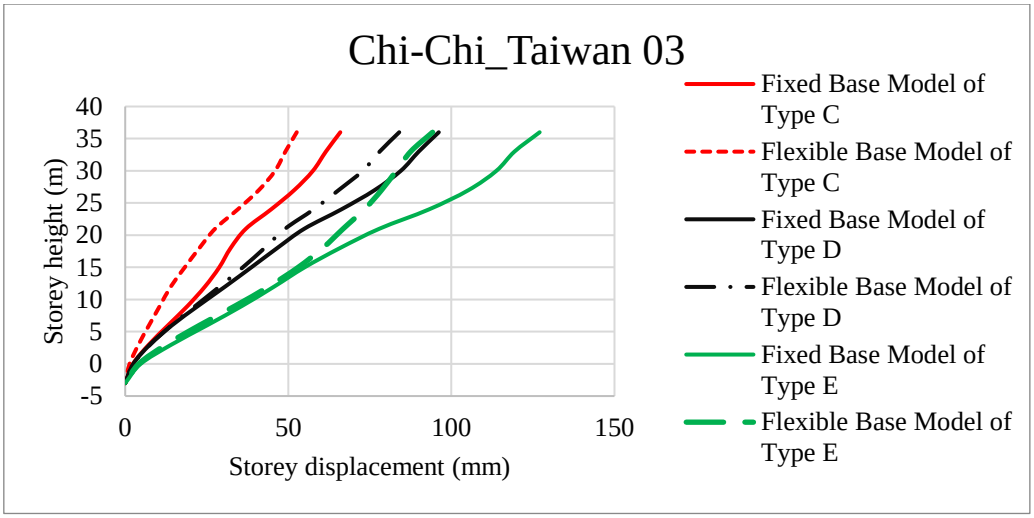

(b)

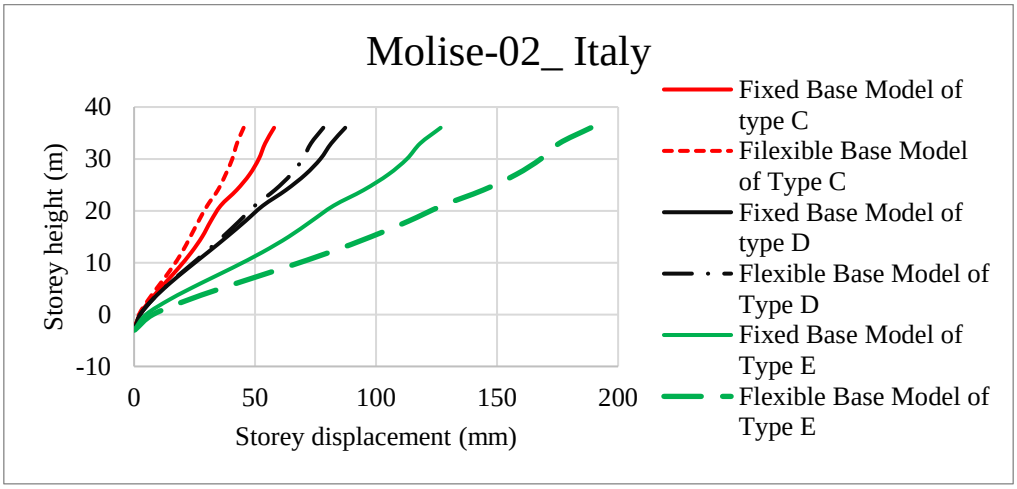

(c)

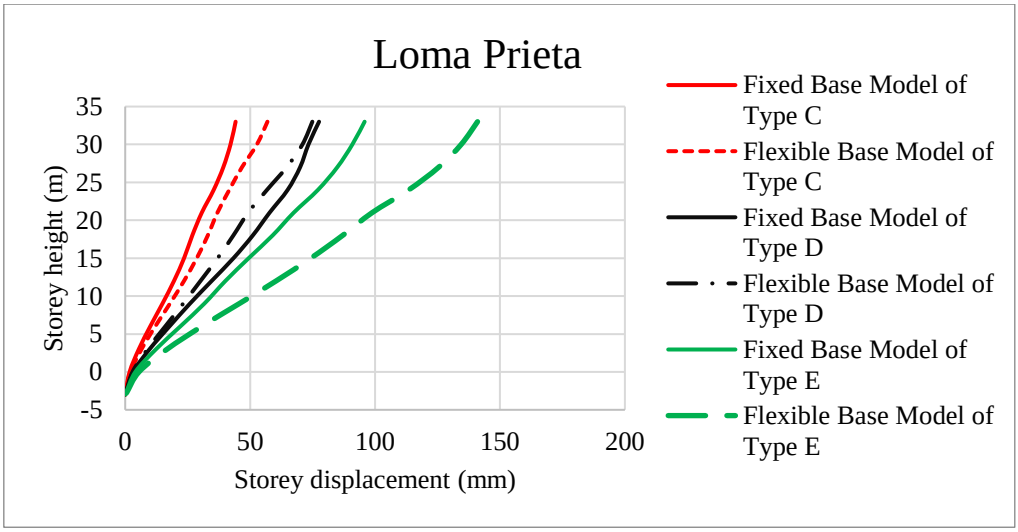

(d)

Figure 6.6: Storey displacement of Model 2 for (b) Chi-Chi_Taiwan 03, (c) Molise-02_ Italy, (d) Loma Prieta

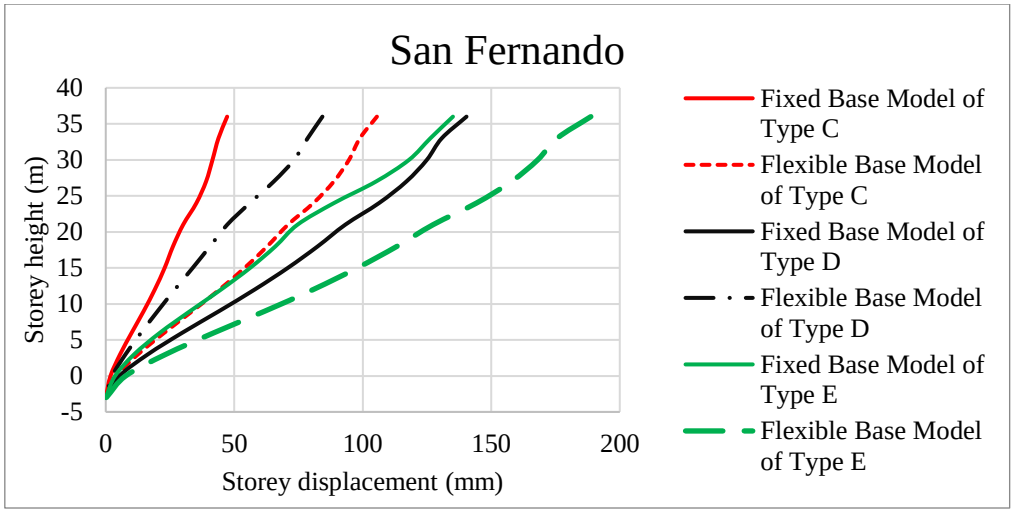

(e)

Figure 6.7: Storey displacement of Model 2 for (e) San Fernando

6.1.3.1.3. Building model 3

In the flexible base model of building model 3, compared to its fixed base counterpart, the storey displacement shows an increase for type C soil when subjected to the Anza-02, Molise-02 Italy, Loma Prieta, and San Fernando earthquakes. However, a decrease is observed during the Chi-Chi Taiwan-03 earthquake. The storey displacement for the flexible base model on type D soil decreases for all earthquakes except Anza-02, while for type E soil, it decreases for all earthquakes except the Loma Prieta earthquake (Figures 6.8 through 6.10).

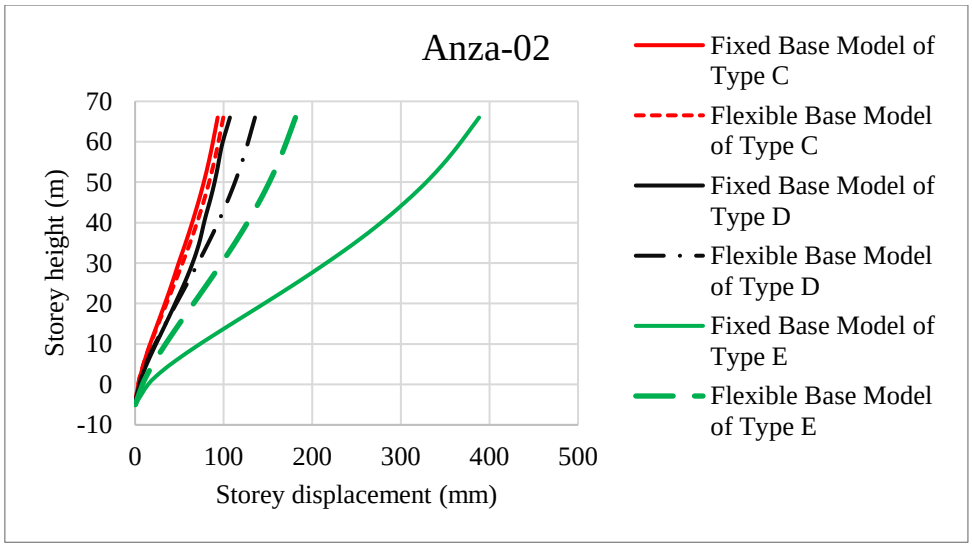

(a)

Figure 6.8: Storey displacement of Model 3 for (a) Anza-02

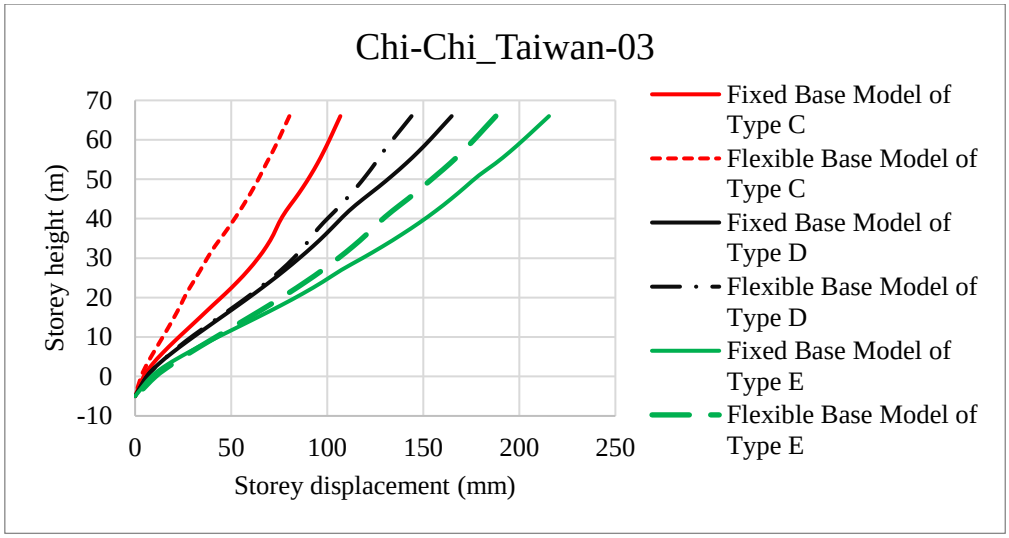

(b)

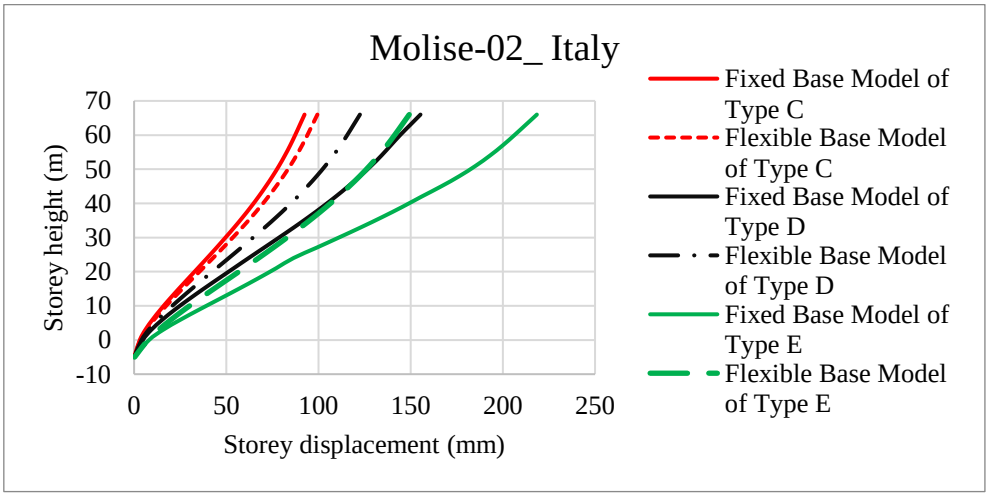

(c)

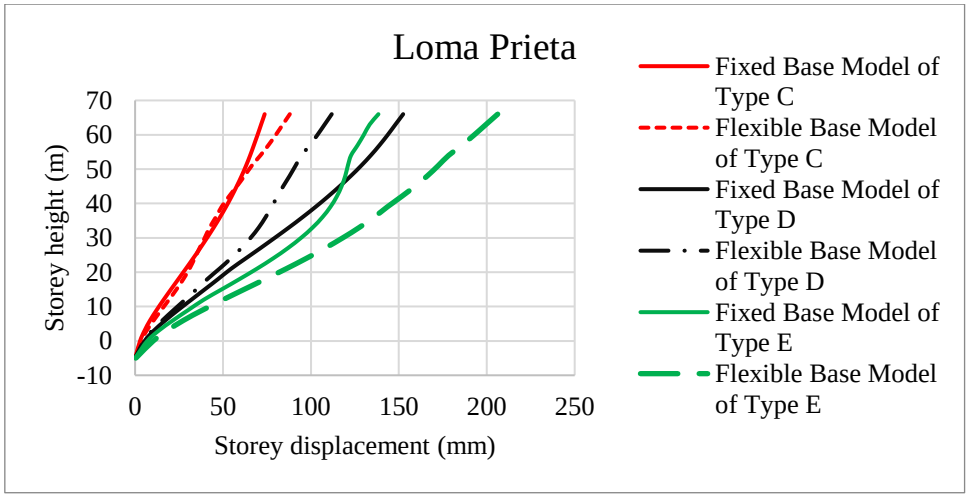

(d)

Figure 6.9: Storey displacement of Model 3 for (b) Chi-Chi_Taiwan 03, (c) Molise-02_ Italy, (d) Loma Prieta

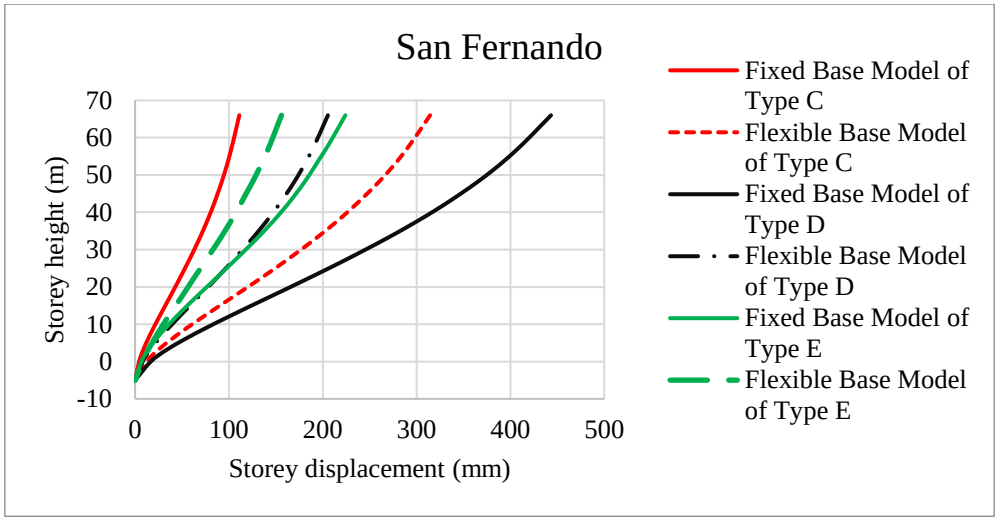

(e)

Figure 6.10: Storey displacement of Model 3 for (e) San Fernando

6.1.3.1.4. Building model 4

When comparing the flexible base model of building model 4 to the fixed base model, the flexible base model shows an increased storey displacement for type C soil under all earthquakes, except for Anza-02 earthquake. For type D soil, the flexible base model results in decreased storey displacement during all earthquakes except Anza-02 and Chi-Chi_Taiwan-03 earthquakes. On the other hand, for type E soil, the flexible base model consistently demonstrates an increased storey displacement across all earthquakes except Anza-02 and Chi-Chi_Taiwan-03 (for higher stories) earthquakes (Figures 6.11 through 6.13).

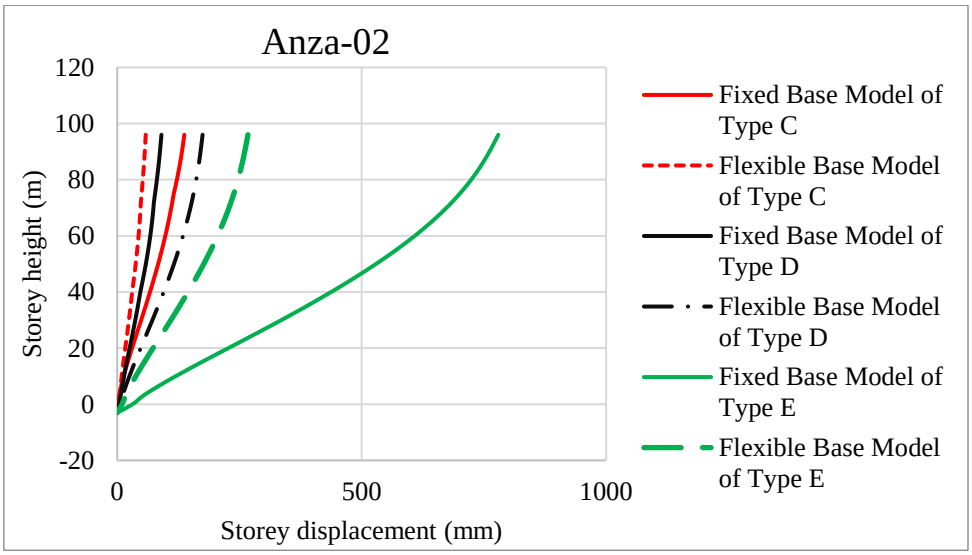

(a)

Figure 6.11: Storey displacement of Model 4 for (a) Anza-02

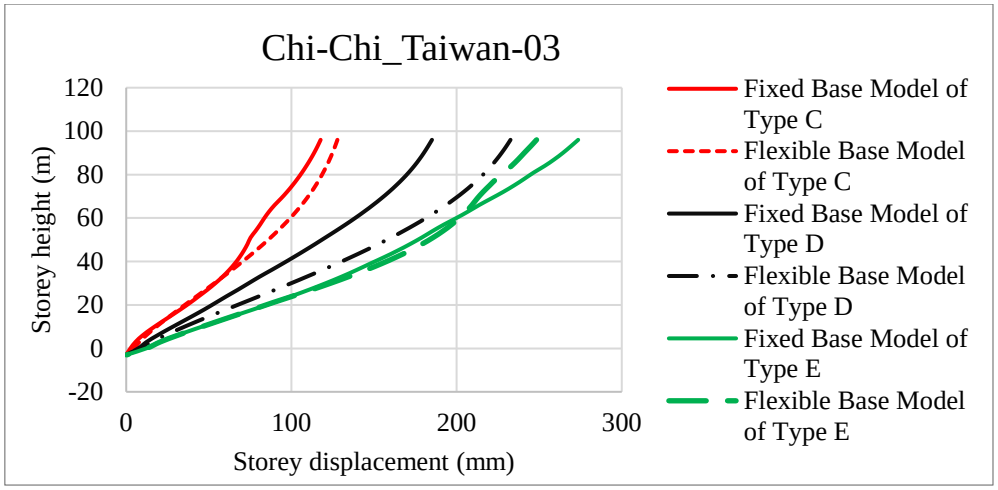

(b)

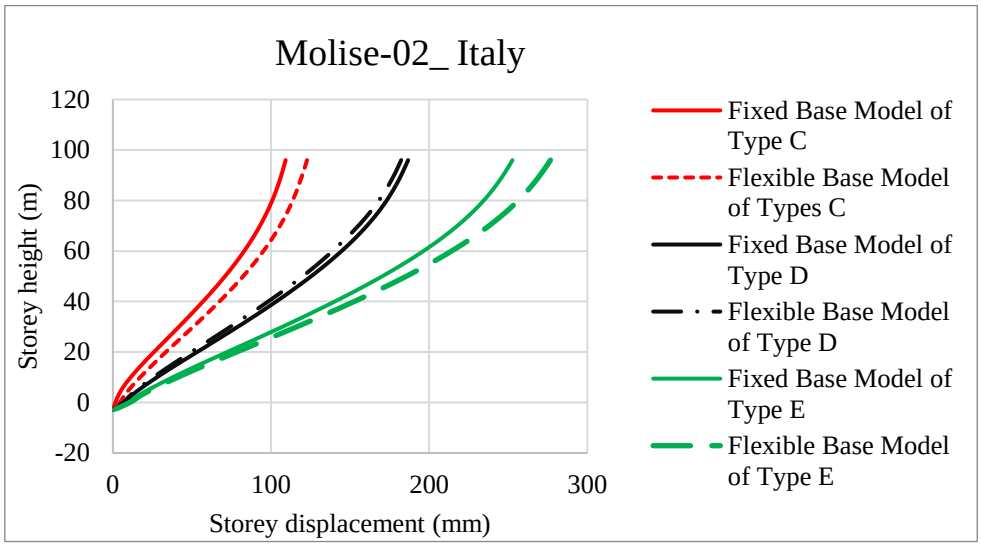

(c)

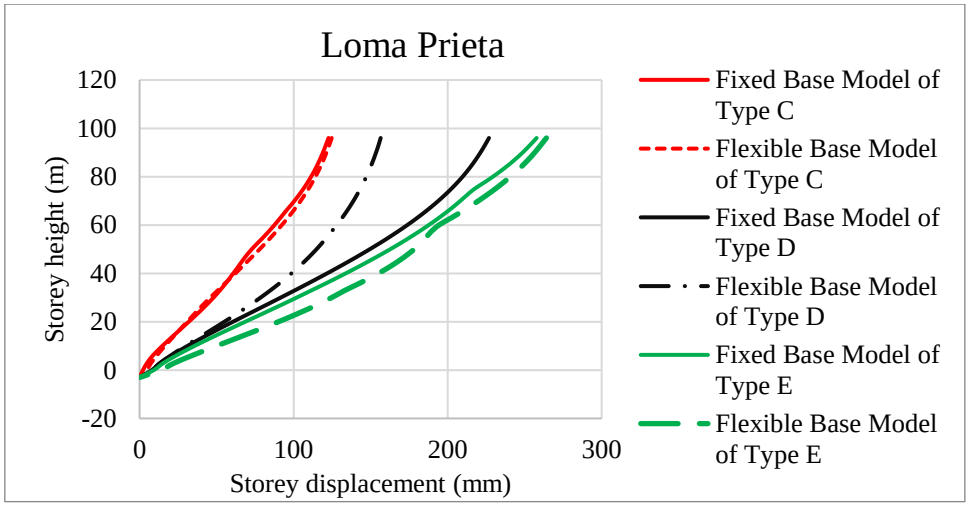

(d)

Figure 6.12: Storey displacement of Model 4 for (b) Chi-Chi_Taiwan 03, (c) Molise-02_ Italy, (d) Loma Prieta

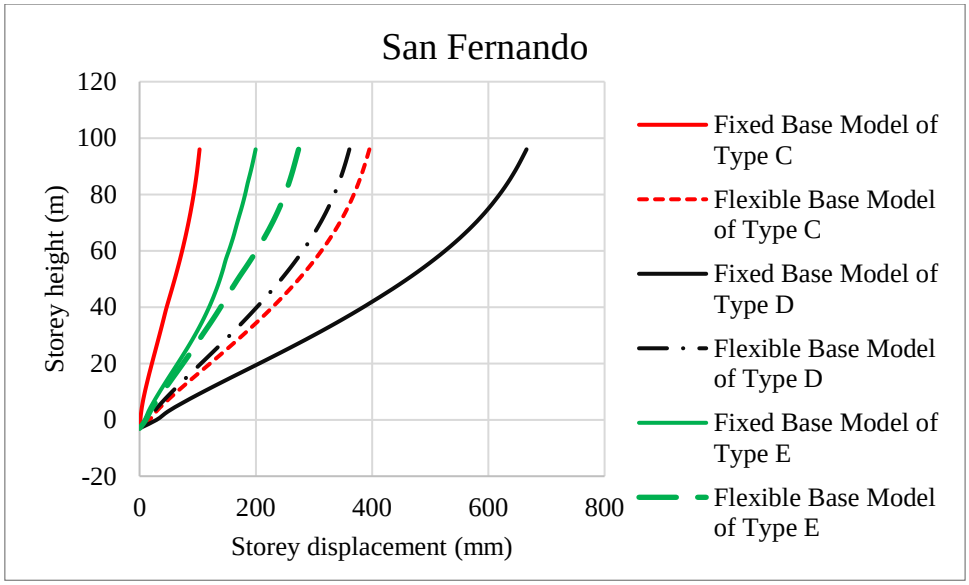

(e)

Figure 6.13: Storey displacement of Model 4 for (e) San Fernando

All building models exhibited different responses to the corresponding earthquake motions. The results did not reveal a clear trend of increasing or decreasing responses for all models.

A significant increase in the flexible base model was observed in Model 1 during the San Fernando earthquake on soil type E. This increase is likely attributed to the model's fundamental period of 0.846 seconds, which is approximately equal to the predominant period of the earthquake motion (Appendix A).

Similar significant increases were also observed in Model 4 (fixed base model) on type E soil during the Anza-02 earthquake. This increment likely occurred because the predominant period of the earthquake was approximately equal to the fundamental period of the structure (Appendix A).

6.1.3.1.5. Comparison between all models

The storey displacement increased as the number of stories increased for all earthquake motions when the models were supported on soil types C, D, and E. The effect of SSI showed a significant change for Model 4 during the Anza-02 and San Fernando earthquakes for soil types C and D. For soil type E, the effect of SSI showed a significant change for Model 4 during the Anza-02 earthquake, and for the San Fernando earthquake, the effect was significant for Models 1 and 4. For other earthquake motions, the effect of SSI increased for shorter buildings when the models were supported on soil types C and E. When the models were supported on soil type D, the SSI effect increased for taller building models (Models 3 and 4) during the Chi-

Chi_Taiwan-03 and Loma Prieta earthquakes. During the Molise earthquake, the effect increased for shorter buildings (see Figures B.1, B.2, C.1, C.2, D.1 and D.2 for further details).

6.1.3.2. Storey drift ratio

Storey drift is the horizontal displacement at the top of the storey relative to the bottom of the storey at a given location.

Storey drift ratio is the storey drift divided by the storey height

$$Drift\ ratio = \frac{d_{i+1} - d_i}{h} \tag{6.11}$$

where d_{i+1} is horizontal displacement at $i + 1$ level, d_i is deflection at (i) level, and h is the height of the storey

6.1.3.2.1. Building model 1

The flexible model of building model 1 compared to fixed base model exhibits a decrease in storey drift ratio for all soil types when subjected to all earthquakes, except for Loma Prieta earthquake on type C and D soil at higher stories and San Fernando earthquake on type E soil (Figures 6.14 through 6.16).

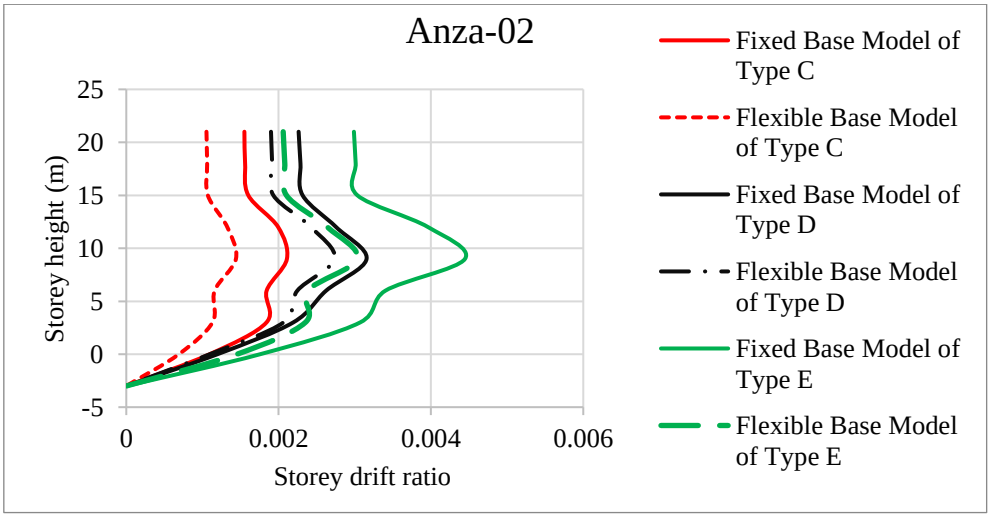

(a)

Figure 6.14: Storey drift ratio of Model 1 for (a) Anza-02

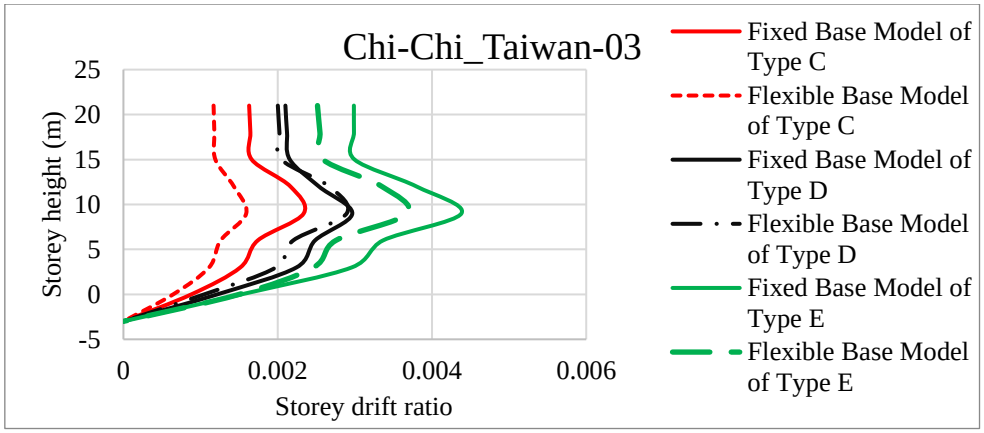

(b)

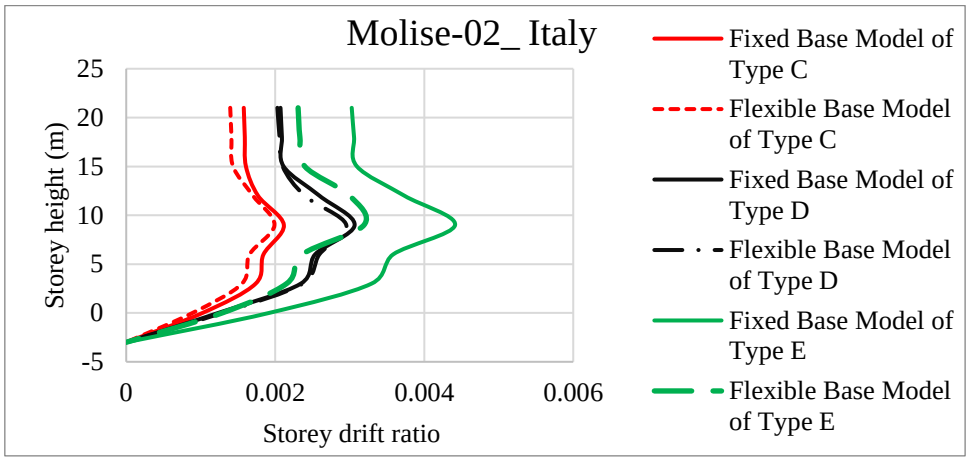

(c)

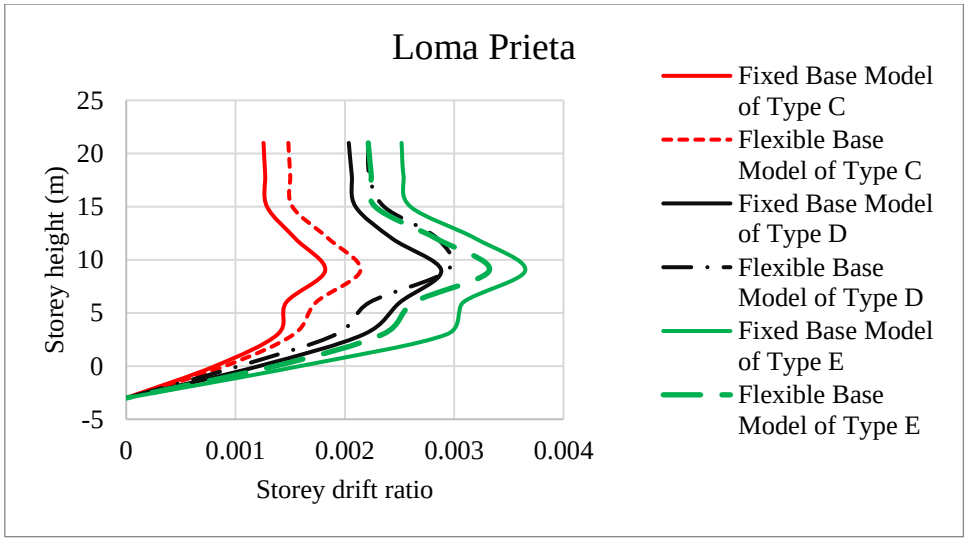

(d)

Figure 6.15: Storey drift ratio of Model 1 for (b) Chi-Chi_Taiwan 03, (c) Molise-02_ Italy, (d) Loma Prieta

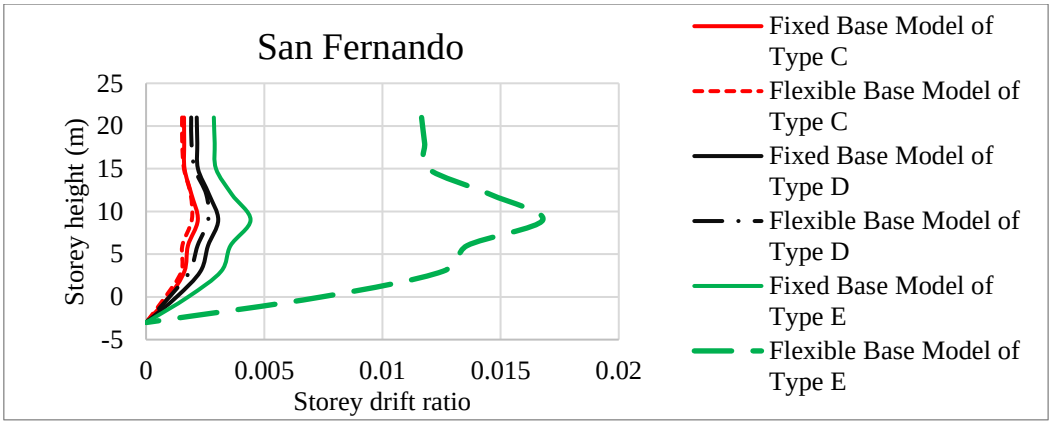

(e)

Figure 6.16: Storey drift ratio of Model 1 for (e) San Fernando

6.1.3.2.2. Building model 2

The flexible base model of building model 2, when compared to the fixed base model, exhibits a decrease in storey drift ratio for type C soil under the Anza-02 (for higher stories), Chi-Chi Taiwan-03, and Molise-02, Italy earthquakes. However, it exhibits an increase in storey drift ratio when subjected to the Loma Prieta and San Fernando earthquakes. For type D soil, the flexible base model shows a decrease in storey drift ratio for all earthquakes except Anza-02 and Loma Prieta (for lower stories). Conversely, with type E soil, the flexible base model exhibits an increase in storey drift ratio for all earthquakes except Anza-02 and Chi-Chi Taiwan-03 (Figures 6.17 through 6.19).

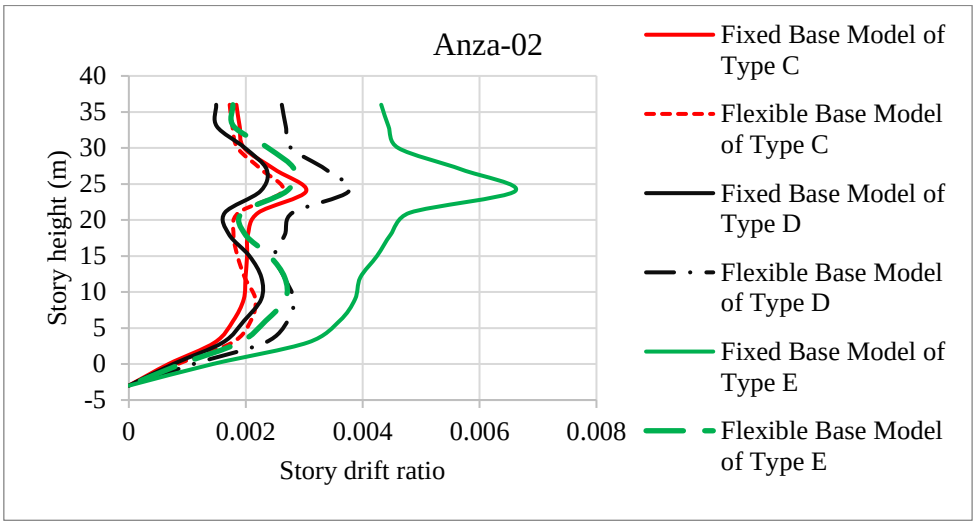

(a)

Figure 6.17: Storey drift ratio of Model 2 for (a) Anza-02

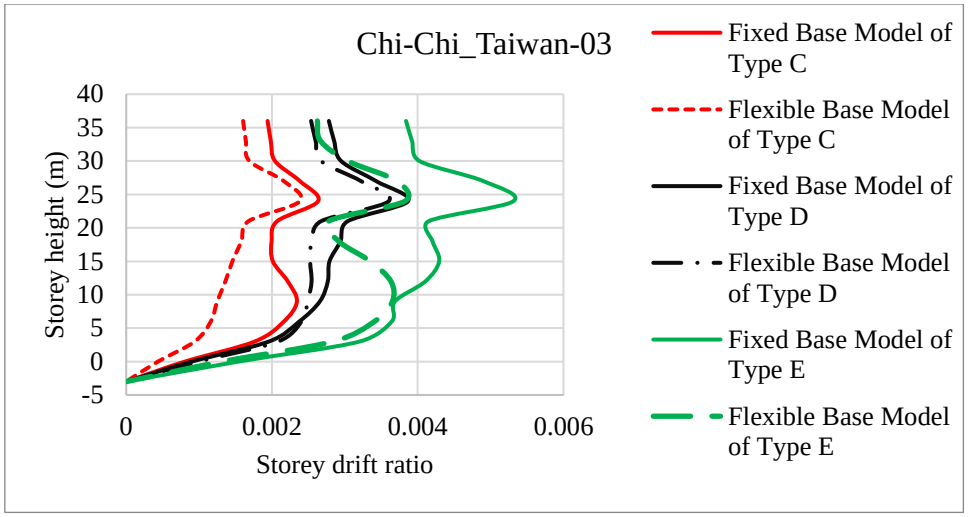

(b)

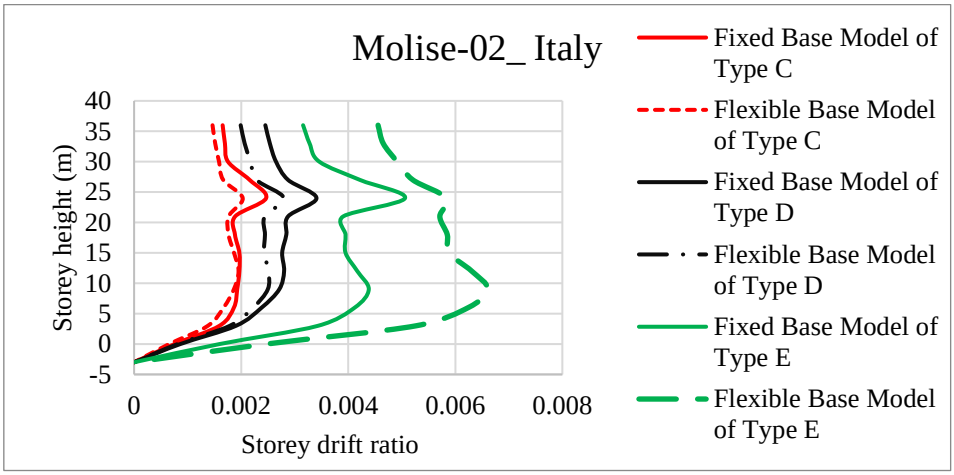

(c)

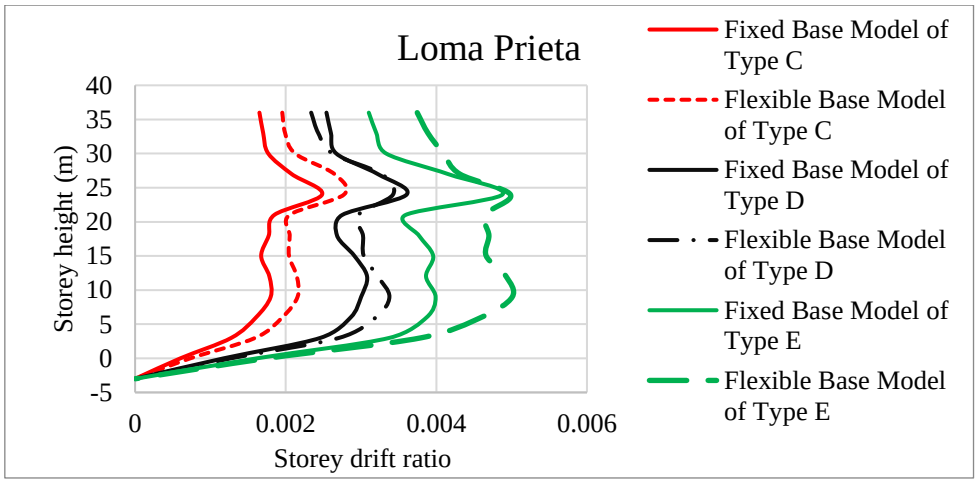

(d)

Figure 6.18: Storey drift ratio of Model 2 for (b) Chi-Chi_Taiwan 03, (c) Molise-02_ Italy, (d) Loma Prieta

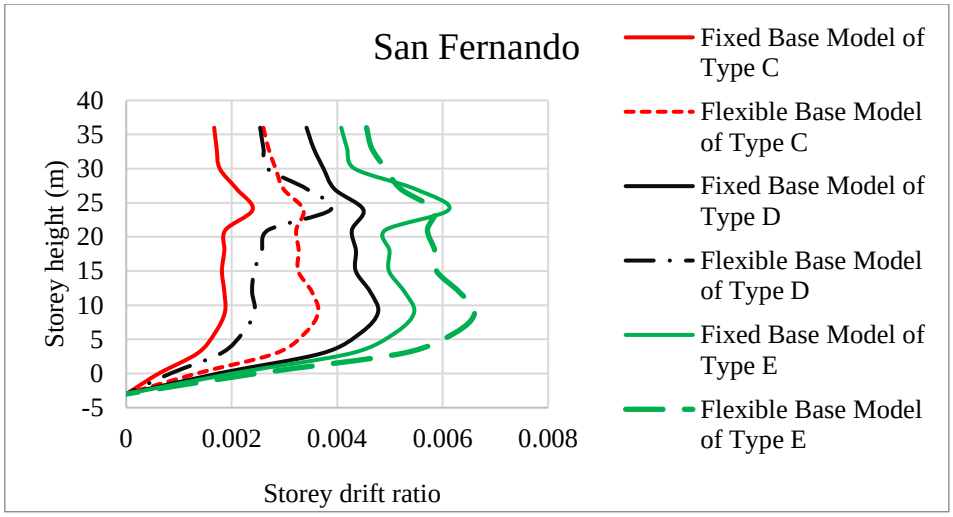

(e)

Figure 6.19: Storey drift ratio of Model 2 for (e) San Fernando

6.1.3.2.3. Building model 3

When comparing the flexible base model of building model 3 to the fixed base model, the flexible base model shows an increased storey drift ratio for type C soil under all earthquakes, except for lower stories during the Anza-02 earthquake and for all stories during Chi-Chi Taiwan-03 earthquake. For type D soil, the flexible base model results in a decreased storey drift ratio during the Anza-02 (for lower stories), Chi-Chi Taiwan-03, and San Fernando earthquakes, but an increased storey drift ratio during the Molise-02, Italy, and Loma Prieta earthquakes. In contrast, for type E soil, the flexible base model consistently demonstrates a decreased storey drift ratio across all earthquakes except Loma Prieta earthquake (Figures 6.20 through 6.22).

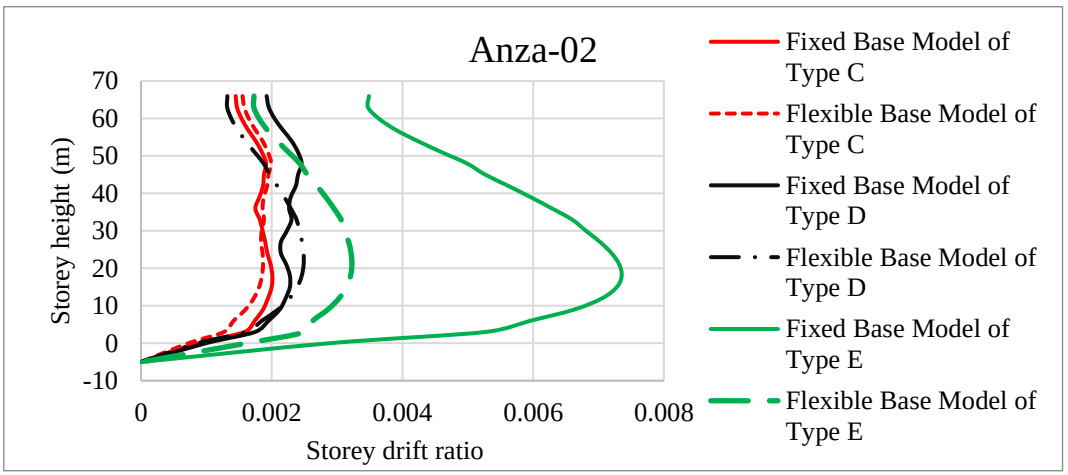

(a)

Figure 6.20: Storey drift ratio of Model 3 for (a) Anza-02

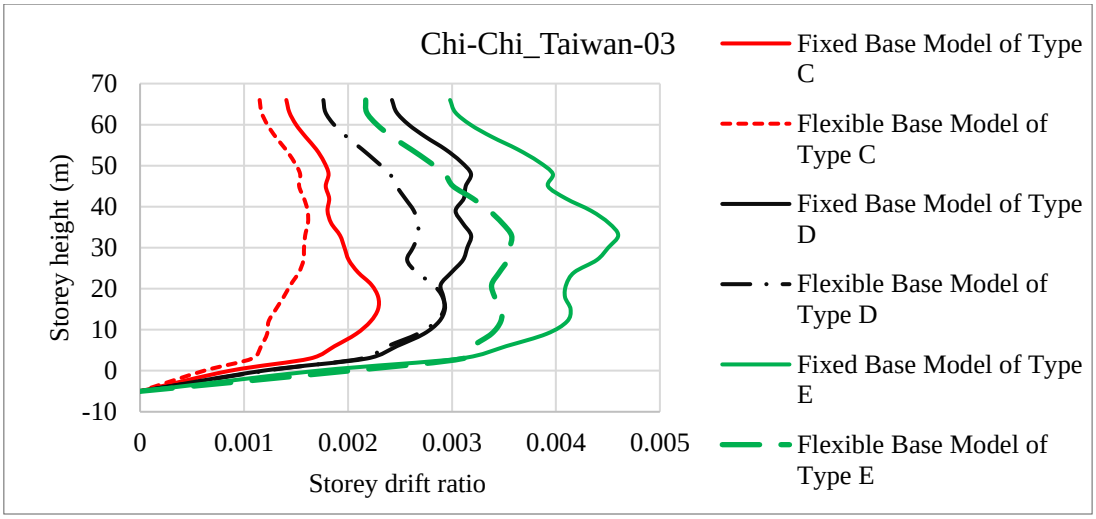

(b)

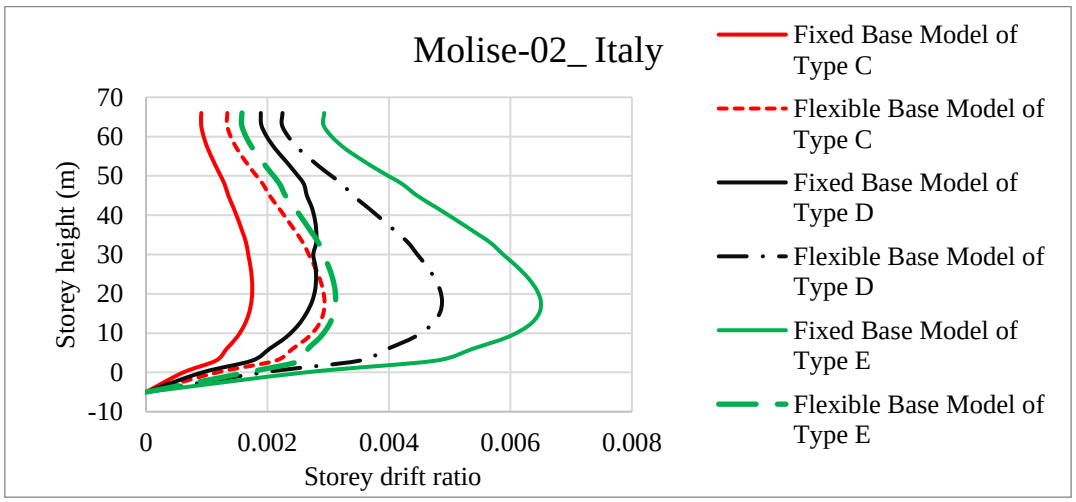

(c)

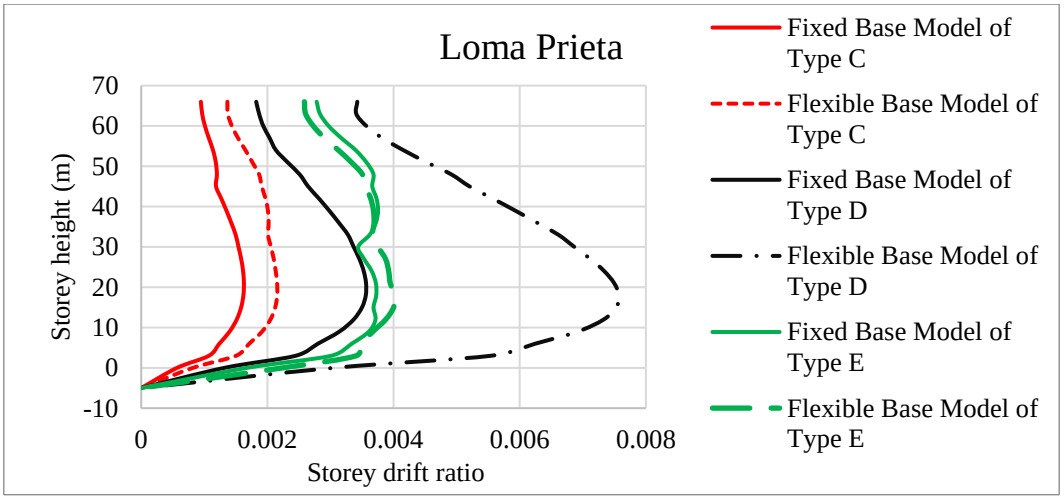

(d)

Figure 6.21: Storey drift ratio of Model 3 for (b) Chi-Chi_Taiwan 03, (c) Molise-02_ Italy, (d) Loma Prieta

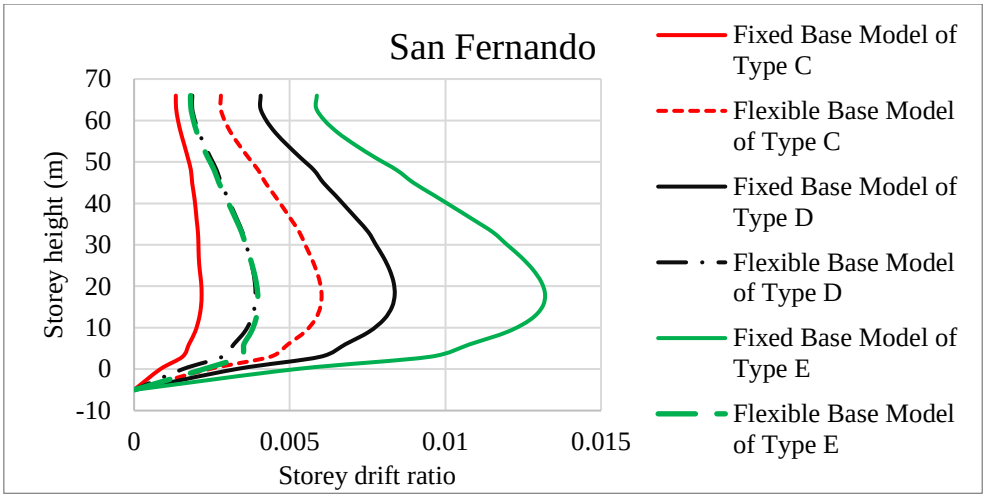

(e)

Figure 6.22: Storey drift ratio of Model 3 for (e) San Fernando

6.1.3.2.4. Building model 4

When comparing the flexible base model of building model 4 to the fixed base model, the flexible base model shows an increased storey drift ratio for type C soil under all earthquakes, except for Anza-02 and Loma Prieta earthquakes. For type D soil, the flexible base model results in increased storey drift ratio during all earthquakes except Chi-Chi_Taiwan-03 (higher stories) and San Fernando earthquakes. On the other hand, for type E soil, the flexible base model consistently demonstrates a decreased storey drift ratio across all earthquakes except Chi-Chi_Taiwan-03 (lower stories) and Loma Prieta earthquakes (Figures 6.23 through 6.25).

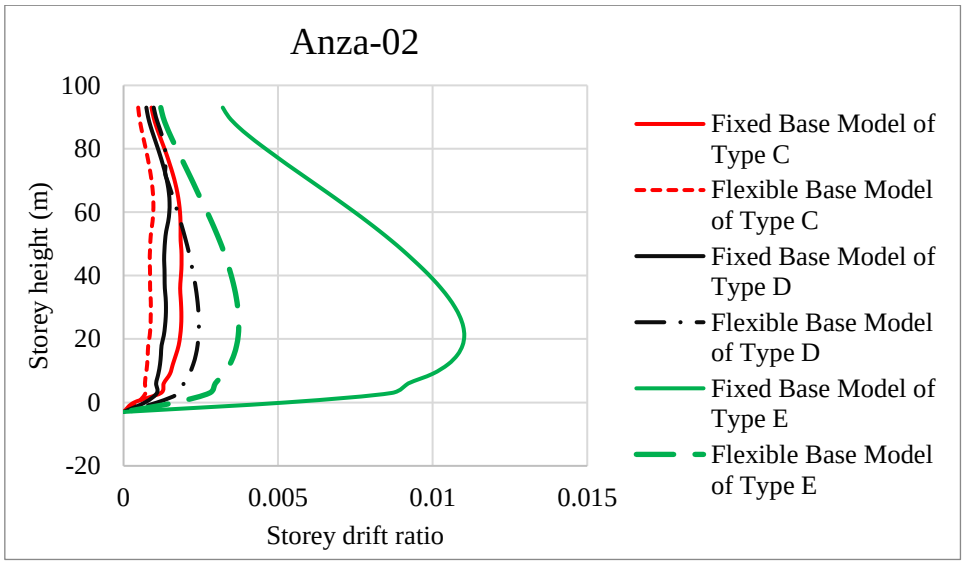

(a)

Figure 6.23: Storey drift ratio of Model 4 for (a) Anza-02

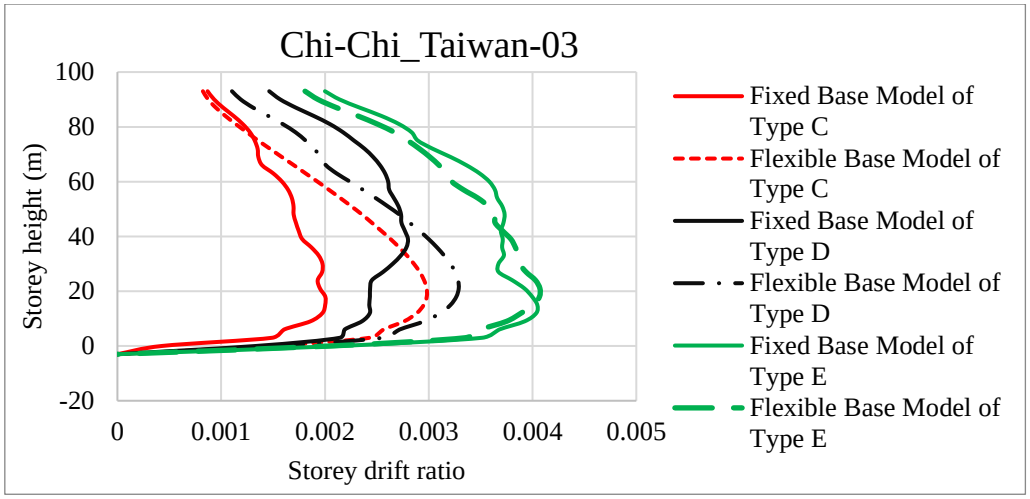

(b)

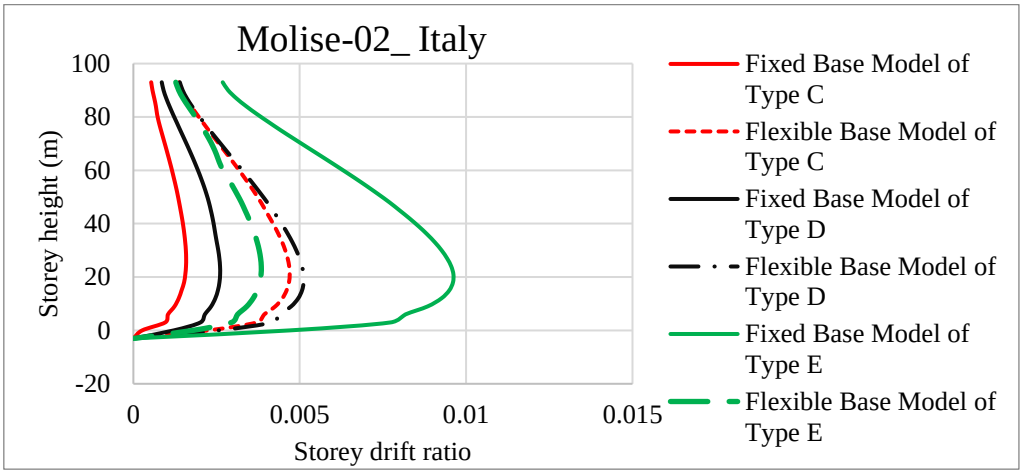

(c)

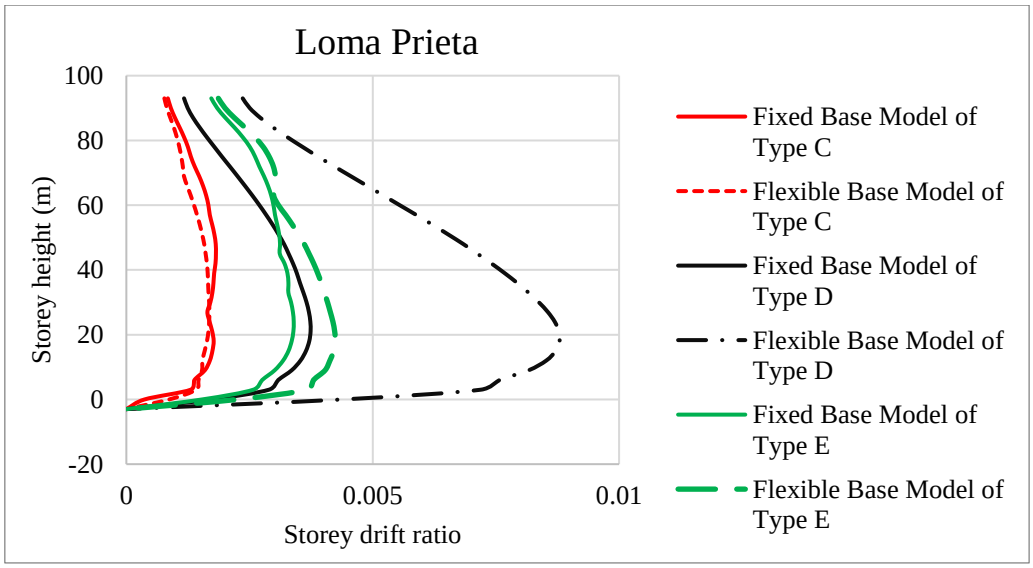

(d)

Figure 6.24: Storey drift ratio of Model 4 for (b) Chi-Chi_Taiwan 03, (c) Molise-02_ Italy, (d) Loma Prieta

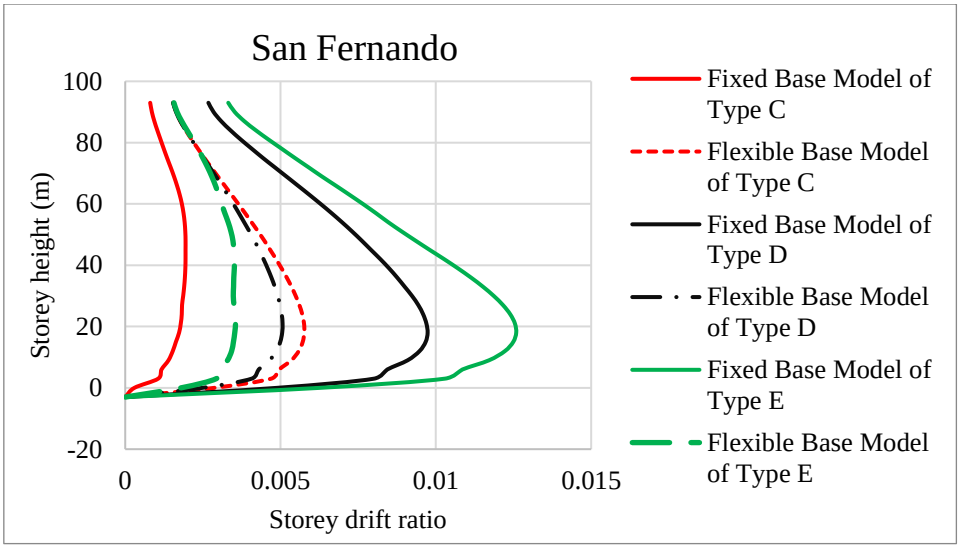

(e)

Figure 6.25: Storey drift ratio of Model 4 for (e) San Fernando

Similar to storey displacement, significant increases in storey drift ratio were shown when the fundamental period of the structure approximated to the predominant period of the corresponding earthquake motions (Appendix A).

6.1.3.2.5. Comparison between all models

The storey drift ratio increased as the number of stories increased, except for the Anza-02 and Loma Prieta earthquakes, which showed a larger drift ratio in Model 2 when the models were supported on soil type C. Additionally, the SSI effect also increased as the number of stories increased, except for the Loma Prieta earthquake (Figures B.3 and B.4).

The storey drift ratio increased as the number of stories increased, except for the Anza-02 and Chi-Chi_Taiwan-03 earthquakes, which showed a larger drift ratio in Model 2 when the models were supported on soil type D. Additionally, the SSI effect also increased as the number of stories increased (Figures C.3, C.4 and C.5).

The storey drift ratio increased as the number of stories increased for the Anza-02 and Molise-02_Italy earthquakes when the models were supported on soil type E. A significant increase was observed for Model 1 during the San Fernando earthquake and for Model 2 during the Chi-Chi_Taiwan-03 and Loma Prieta earthquakes. A large SSI effect was shown for taller building models during the Anza-02, Molise-02_Italy, and Loma Prieta earthquakes (Figures D.3, D.4 and D.5).

6.1.3.3. Storey shear force

The total horizontal force applied to a particular storey of a building as a result of lateral loads like an earthquake or wind is known as the storey shear force.

6.1.3.3.1. Building model 1

Comparing the flexible base model to the fixed base model of building model 1, a decrease in storey shear force is observed for type C soil under all earthquakes with some exceptions under Loma Prieta and San Fernando earthquakes in the lower floors. Conversely, the storey shear force of the flexible base model decreases for Anza-02 (for higher stories), and Chi-Chi Taiwan-03 earthquakes and the rest earthquakes show an increment when considering type D soil. For type E soil, the storey shear force decreases for all earthquakes except San Fernando earthquake in which a significant increase is observed, instead (Figures 6.26 and 6.27).

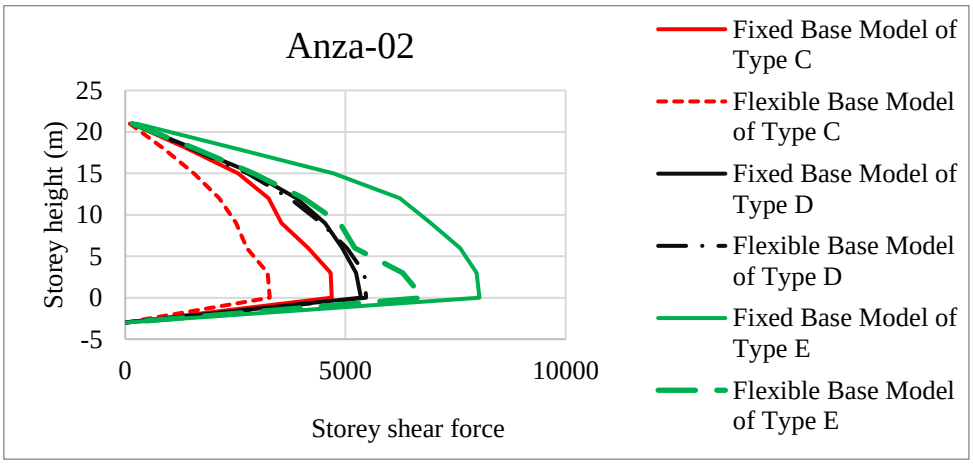

(a)

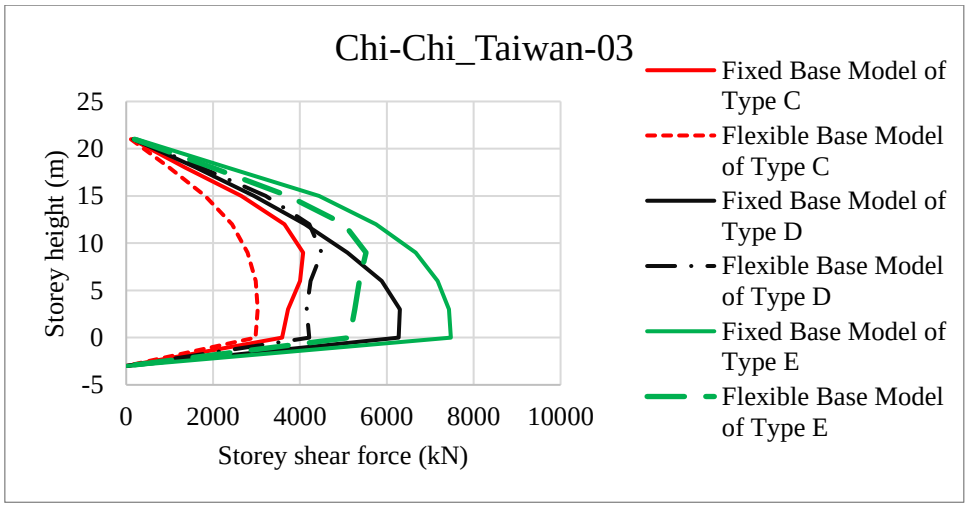

(b)

Figure 6.26: Storey shear force of Model 1 for (a) Anza-02, (b) Chi-Chi_Taiwan 03,

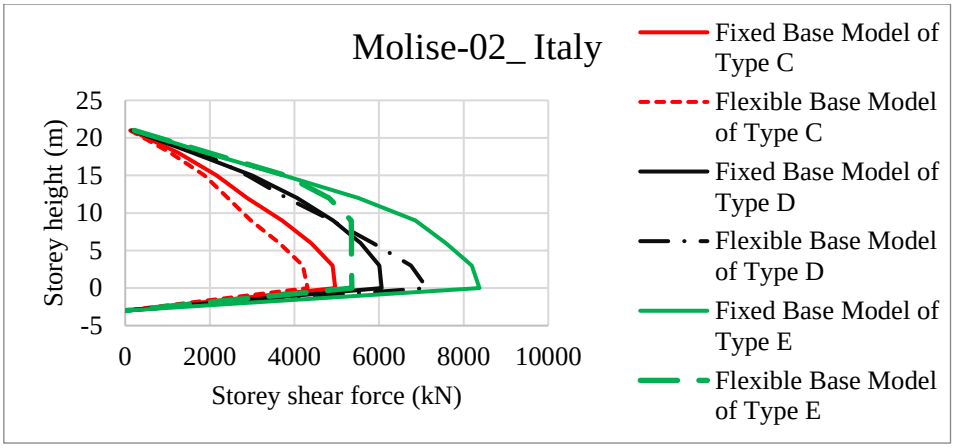

(c)

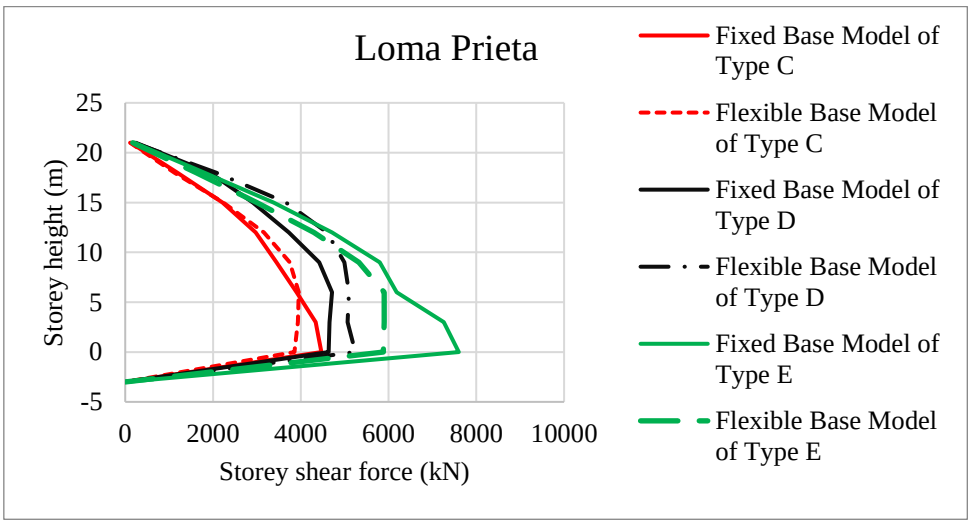

(d)

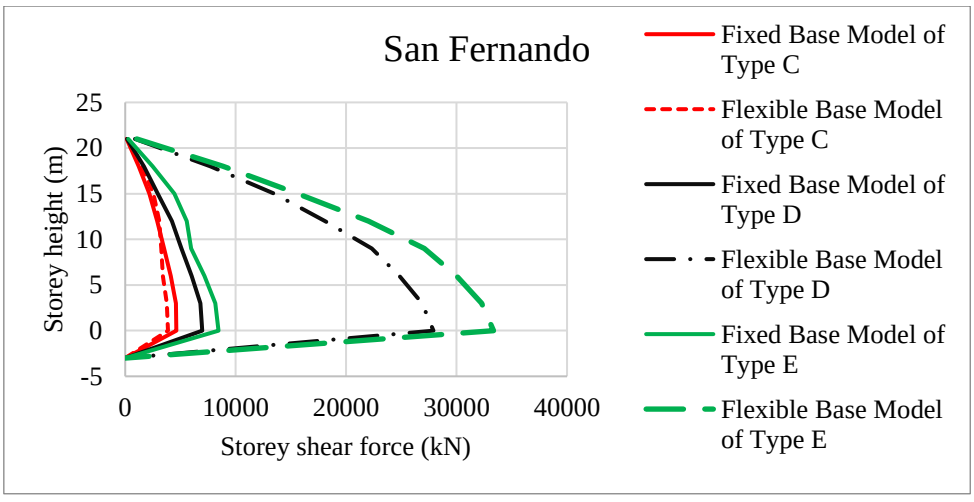

(e)

Figure 6.27: Storey shear force of Model 1 for (a) Anza-02, (b) Chi-Chi_Taiwan 03, (c) Molise-02_ Italy, (d) Loma Prieta, (e) San Fernando

6.1.3.3.2. Building model 2

Comparing the flexible base model to the fixed base model of building model 2, a decrease in storey shear force is observed for type C soil when the model is exposed to the Anza-02 earthquake (higher stories), Chi-Chi Taiwan-03, Molise-02_ Italy, Loma Prieta (higher stories) and San Fernando (higher stories). On the other hand, the storey shear force of the flexible base model increases for all earthquakes except the Molise-02 Italy earthquake and the lower stories during the San Fernando earthquake when considering type D soil. For type E soil, the storey shear force decreases for all earthquakes except the Chi-Chi Taiwan-03 earthquake (for higher stories) (Figures 6.28 and 6.29).

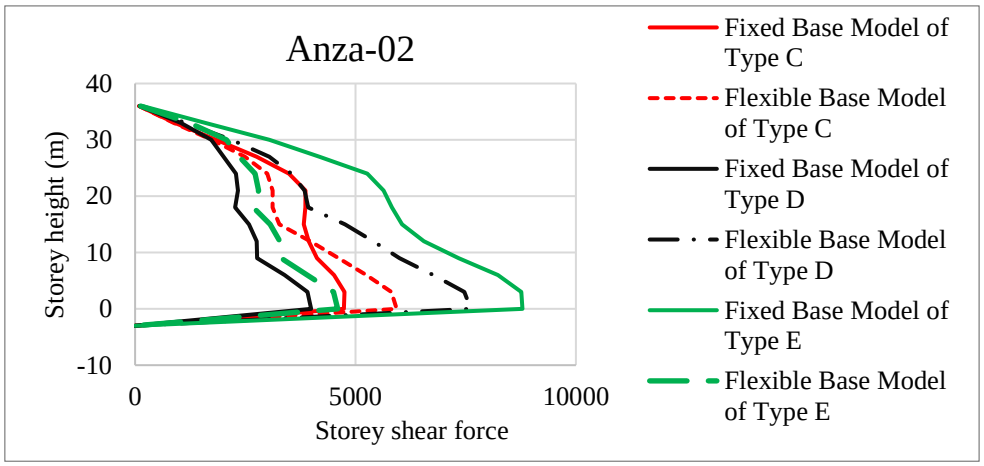

(a)

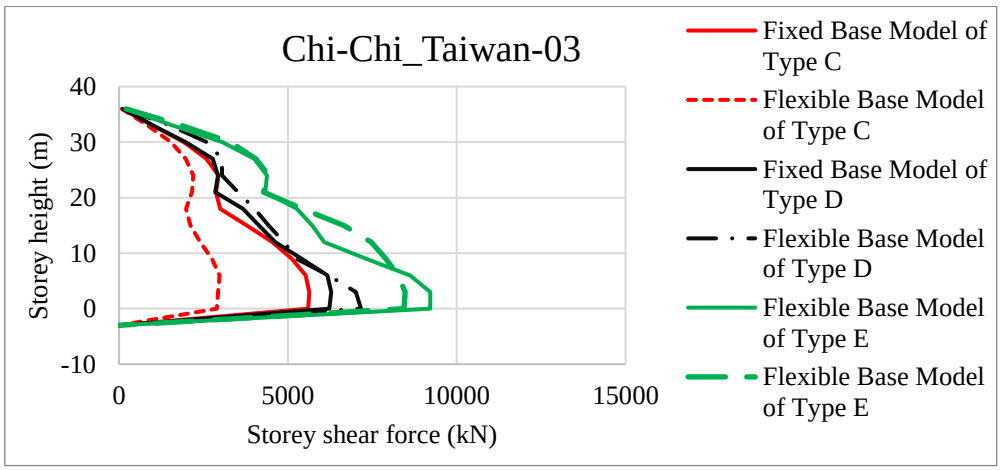

(b)

Figure 6.28: Storey shear force of Model 2 for (a) Anza-02, (b) Chi-Chi_Taiwan 03,

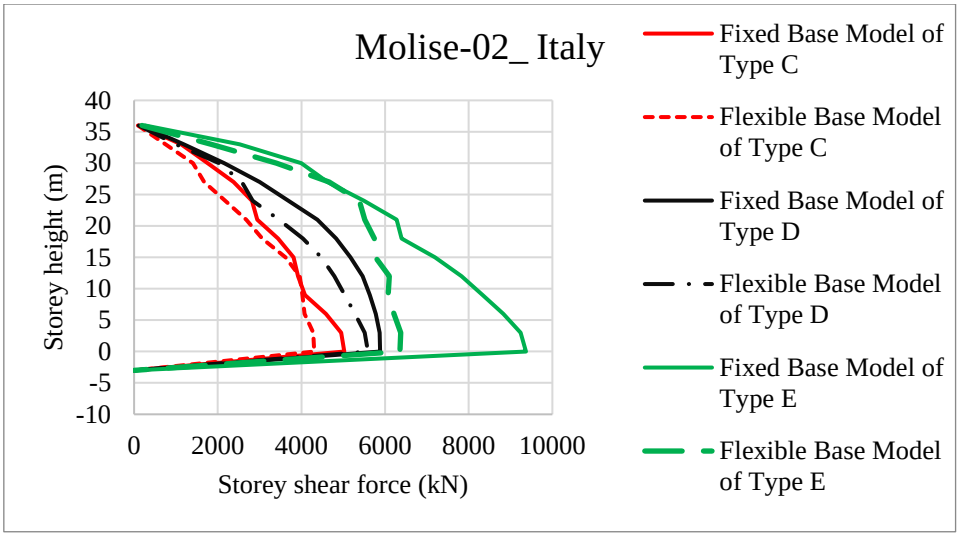

(c)

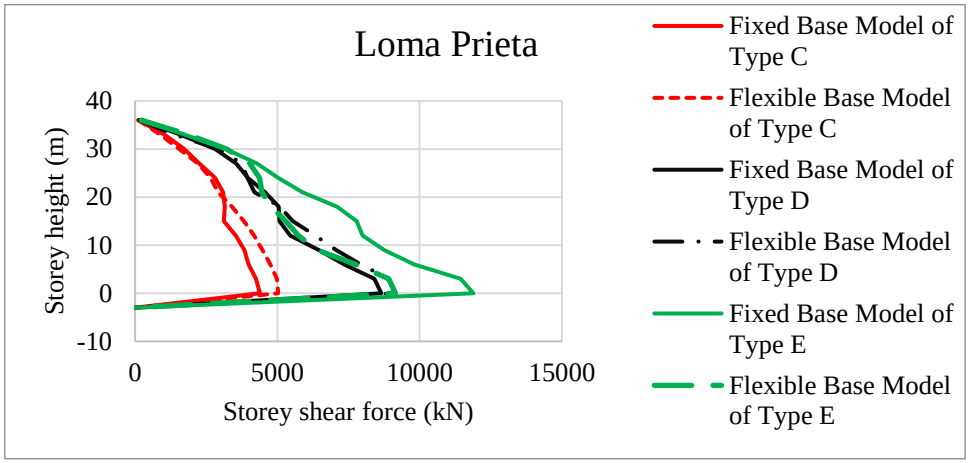

(d)

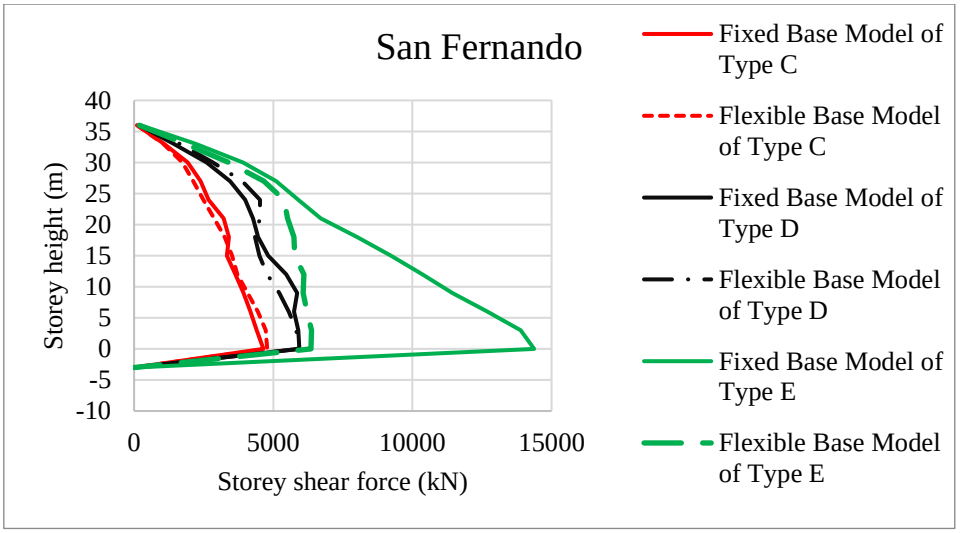

(e)

Figure 6.29: Storey shear force of Model 2 for (c) Molise-02_ Italy, (d) Loma Prieta, (e) San Fernando

6.1.3.3.3. Building model 3

When comparing the flexible base model to the fixed base model of Building Model 3, a decrease in storey shear force is observed for type C and D soils when the model is exposed to the Anza-02, Chi-Chi Taiwan-03 (for lower stories in type C soil), and San Fernando earthquakes. In contrast, the Molise-02 Italy and Loma Prieta earthquakes show an increase in storey shear force. For type E soil, the storey shear force decreases for all earthquakes (Figures 6.30 and 6.31).

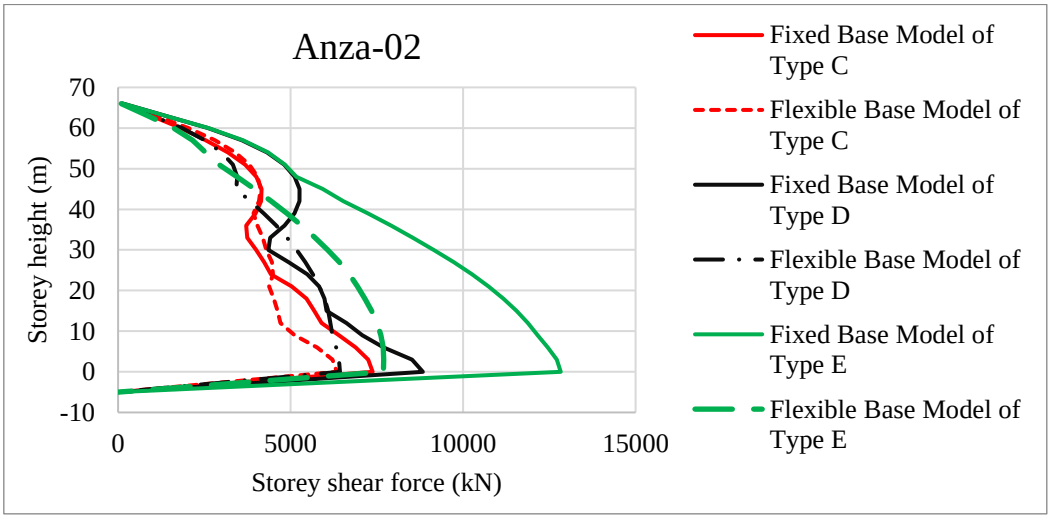

(a)

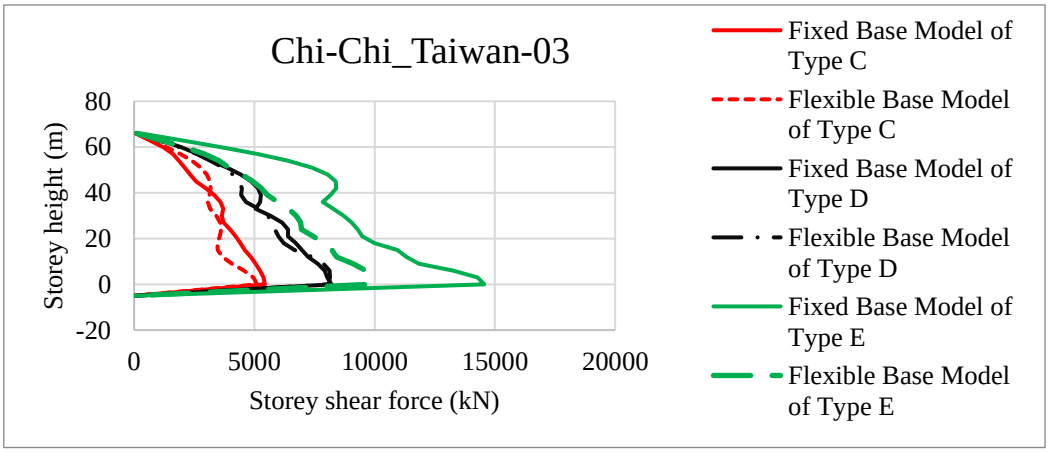

(b)

Figure 6.30: Storey shear force of Model 3 for (a) Anza-02, (b) Chi-Chi_Taiwan 03

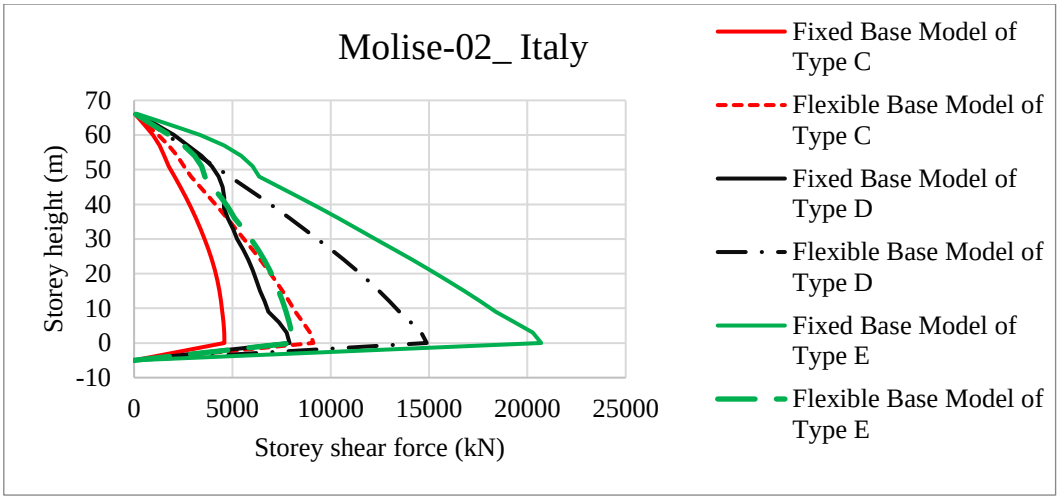

(c)

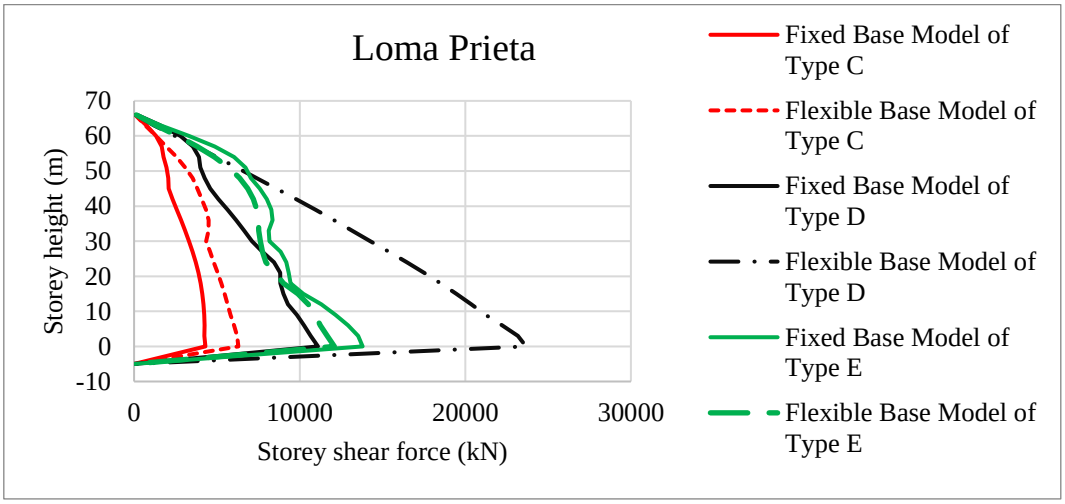

(d)

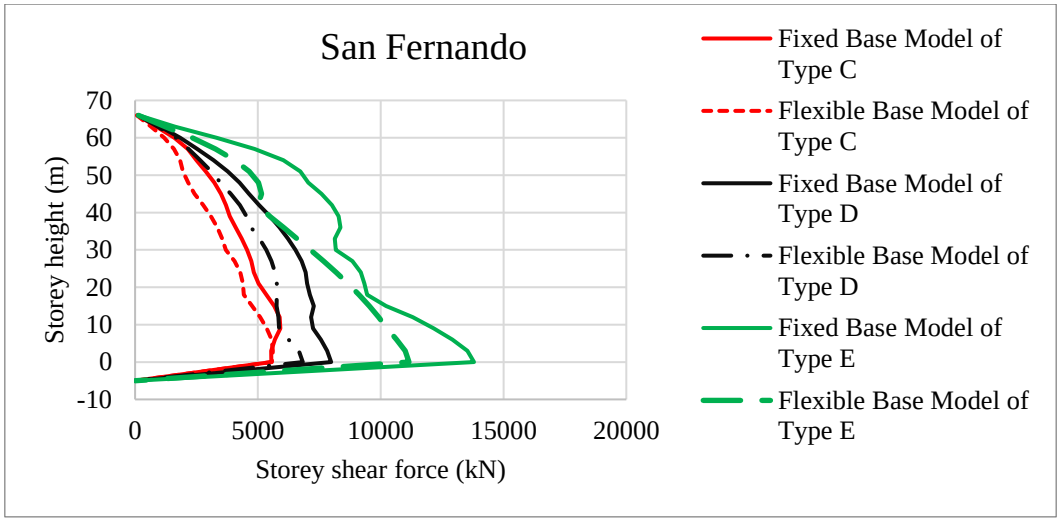

(e)

Figure 6.31: Storey shear force of Model 3 for (c) Molise-02_ Italy, (d) Loma Prieta, (e) San Fernando

6.1.3.3.4. Building model 4

When comparing the flexible base model to the fixed base model of Building Model 4, a decrease in storey shear force is observed for type C soil when the model is exposed to Anza-02, Loma Prieta (for higher stories) and San Fernando (for higher stories) earthquakes. For type D soil, the storey shear force increases for all earthquakes except the Chi-Chi Taiwan-03 and San Fernando (for lower stories) earthquake. For type E soil, the storey shear force decreases for all earthquakes except the Loma Prieta earthquake (Figures 6.32 and 6.33).

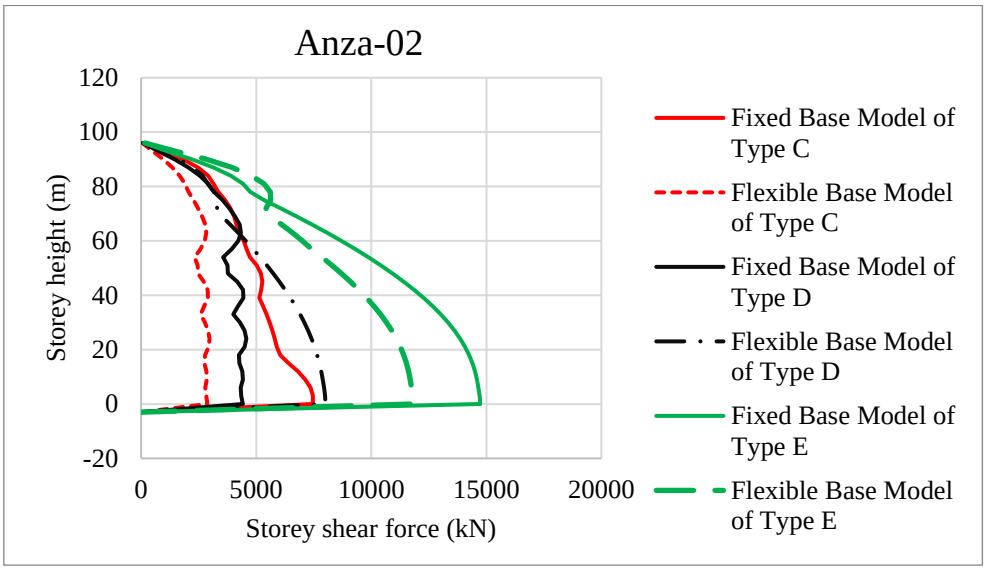

(a)

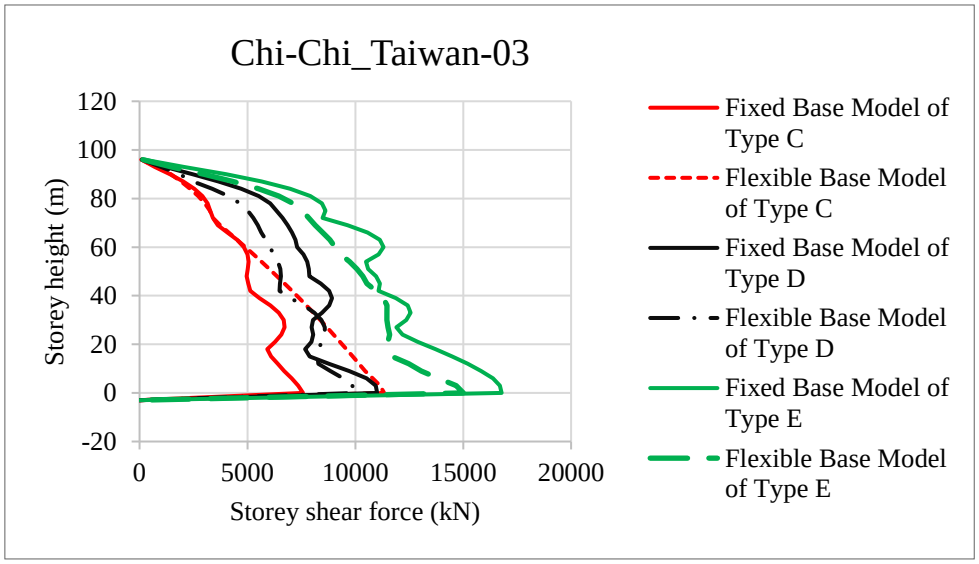

(b)

Figure 6.32: Storey shear force of Model 4 for (a) Anza-02, (b) Chi-Chi_Taiwan 03

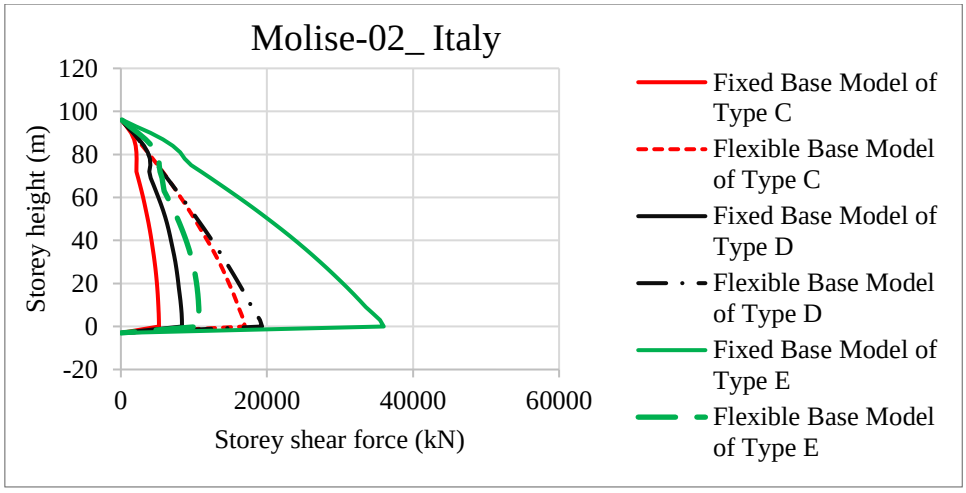

(c)

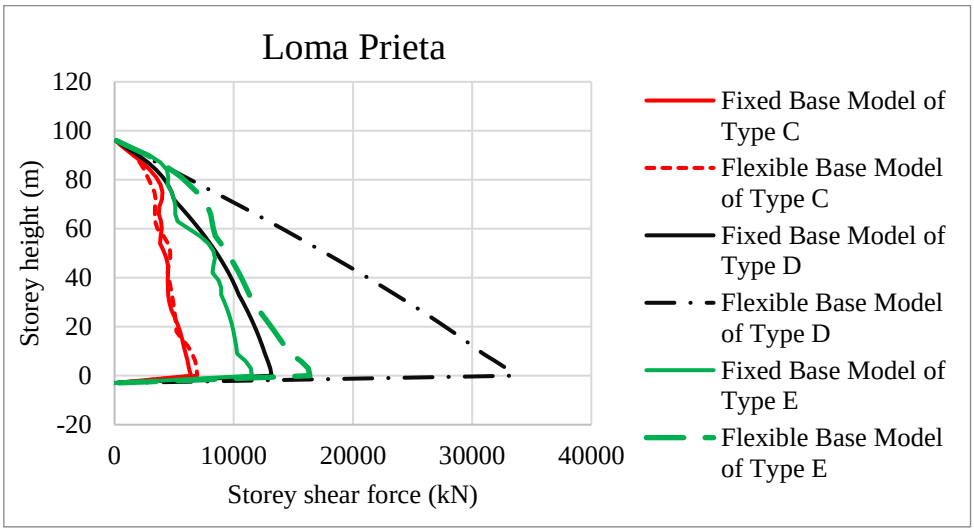

(d)

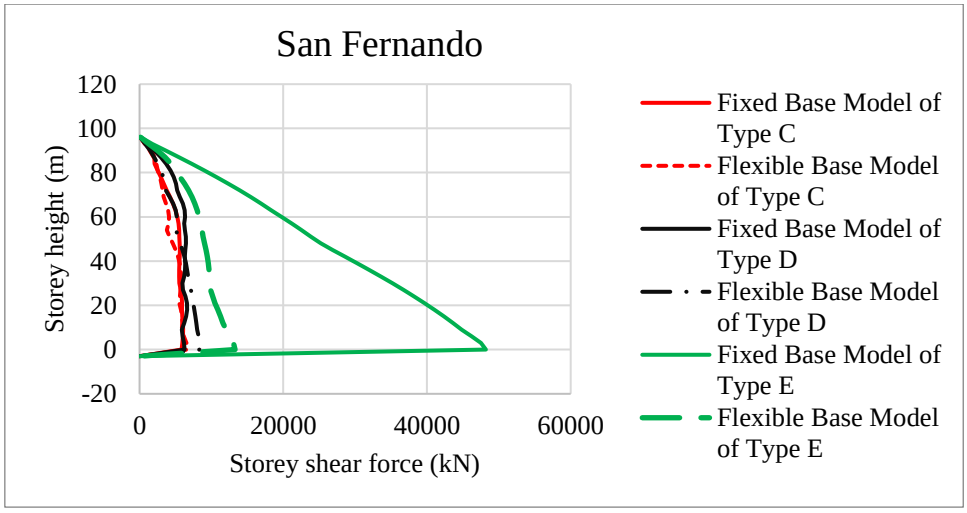

(e)

Figure 6.33: Storey shear force of Model 4 for (c) Molise-02_ Italy, (d) Loma Prieta, (e) San Fernando

A significant increase was observed in the San Fernando earthquake for flexible base model 1 supported on soil types D and E. This occurred when the predominant period of the earthquake motion matched the 7% and 8% damping levels, respectively (Appendix A). These damping levels correspond to fundamental periods of 0.841 seconds for type D and 0.846 seconds for type E soils. Another significant increase was also observed in the San Fernando earthquake for the fixed base model 2 supported on soil type E, in the Anza-02 earthquake for the fixed base model 3 supported on soil type E, in the Loma Prieta earthquake for flexible base models 3 and 4 supported on soil type D, and in the San Fernando earthquake for the fixed base model 4 supported on soil type E.

6.1.3.3.5. Comparison between all models for soil type C

The storey shear force increased as the number of stories increased, except for the Anza-02 earthquake, which showed a larger storey shear force in Model 3 when the models were supported on soil type C. Additionally, the SSI effect also increased as the number of stories increased, except for the Loma Prieta and San Fernando earthquakes (Figures B.5 and B.6).

The storey shear force increased as the number of stories increased, except for the San Fernando earthquake, which showed a significant increase in the flexible base model compared to the fixed base model for Model 1 when the models were supported on soil type D. Additionally, the SSI effect also increased as the number of stories increased (Figures C.6 and C.7).

The storey shear force increased as the number of stories increased during all earthquakes when the models were supported on soil type E. A large SSI effect was observed for taller building models during all earthquakes, except for the San Fernando earthquake, which showed a significant increase in the flexible base model of Model 1 and the fixed base model of Model 4 (Figures D.6 and D.7).

6.1.3.4. Storey overturning moment along X

The storey moments computed during seismic analysis about a structure's horizontal axes are known as overturning moments. These moments occur because the horizontal forces produced by an earthquake can cause a structure to rotate or tip over at its base.

6.1.3.4.1. Building model 1

The flexible base model of model 1 compared to the fixed base model shows a decrement in storey overturning moment for all earthquakes except the Loma Prieta earthquake, which has an increment in the case of type C soil. For type D soil, the flexible base model shows a

decrement in overturning moment for Chi-Chi_Taiwan 03 and Molise-02_ Italy earthquakes. For type E soils subjected to all earthquakes, the flexible base model shows an increment (Figures 6.34 and 6.35).

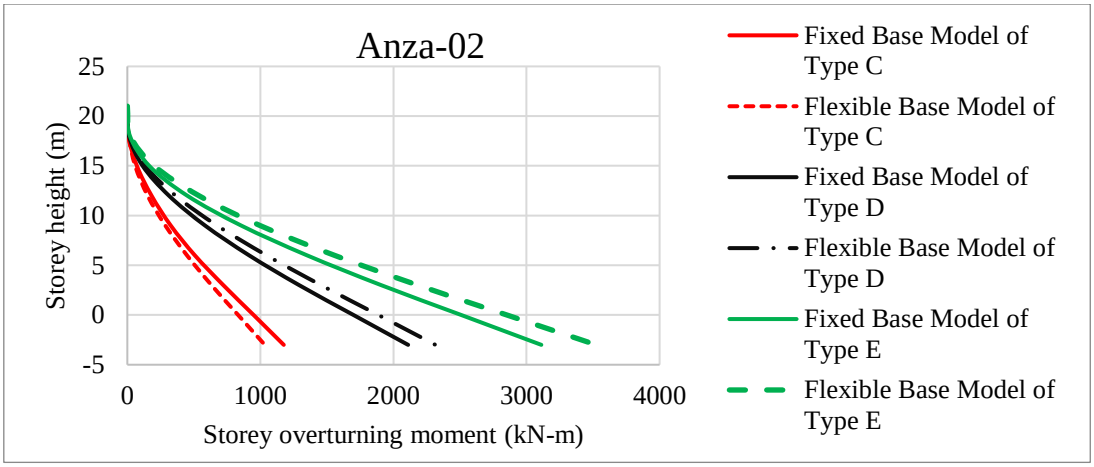

(a)

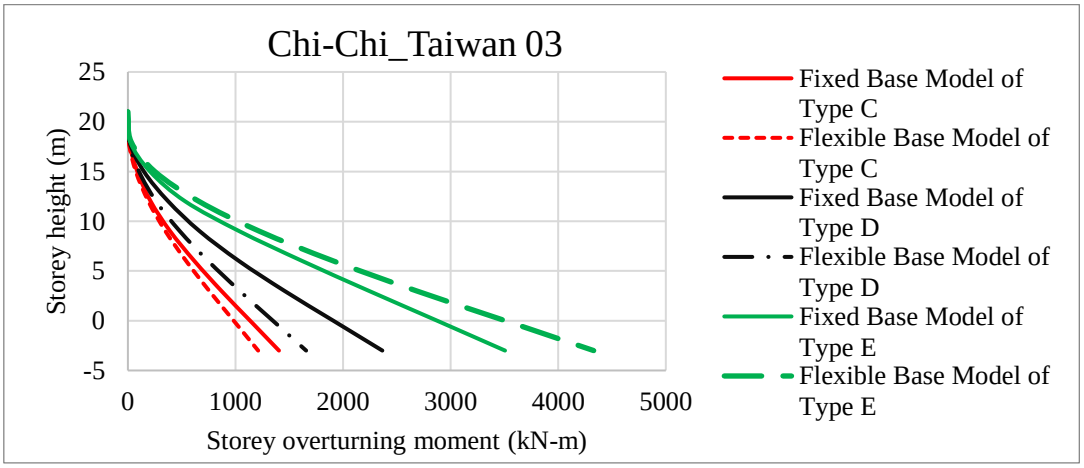

(b)

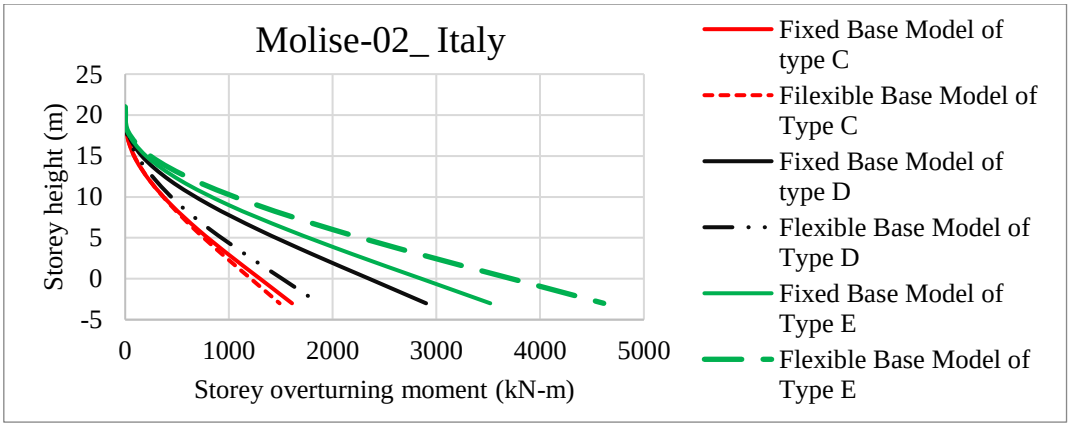

(c)

Figure 6.34: Storey overturning moment of Model 1 for (a) Anza-02, (b) Chi-Chi_Taiwan 03, (c) Molise-02_ Italy

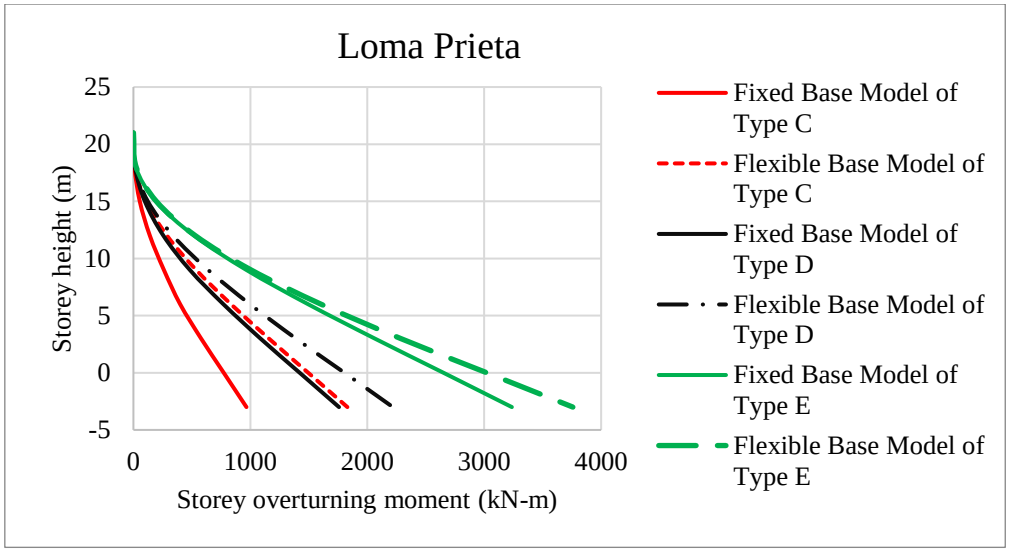

(d)

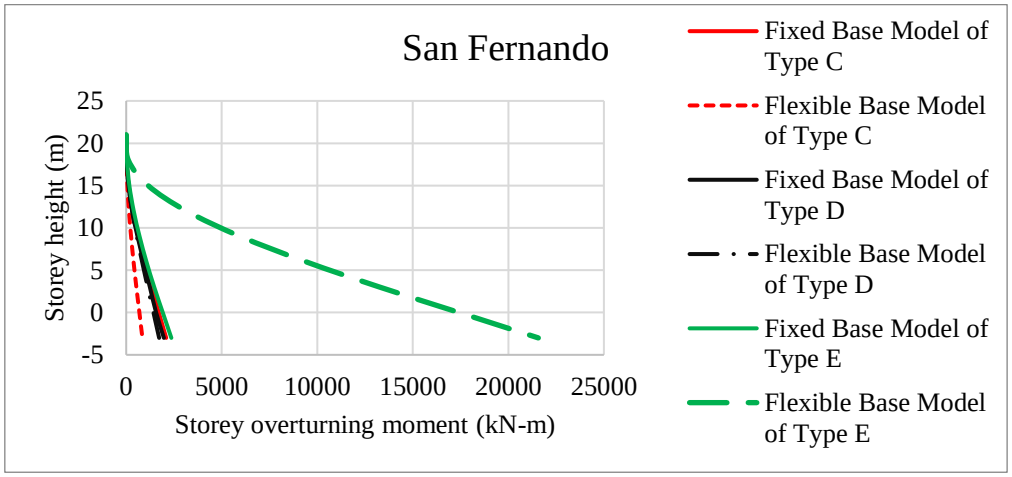

(e)

Figure 6.35: Storey overturning moment of Model 1 for (d) Loma Prieta, (e) San Fernando

6.1.3.4.2. Building model 2

The flexible base model of model 2 compared to the fixed base model shows an increment in storey overturning moment for all earthquakes except the Molise-02_ Italy and Chi-Chi_Taiwan 03 earthquakes, which has a decrement in the case of type C soil. Additionally, for type D soil, the flexible base model shows an increment in overturning moment for all earthquakes except Molise-02_ Italy and Loma Prieta. For type E soils subjected to all earthquakes, the flexible base model shows a decrement for all earthquakes except Loma Prieta (Figures 6.36 and 6.37).

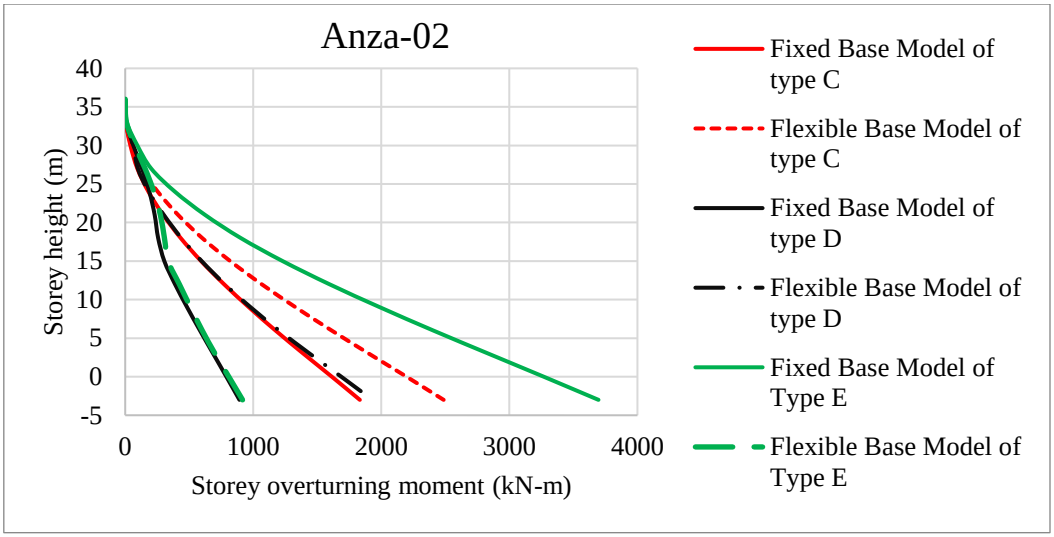

(a)

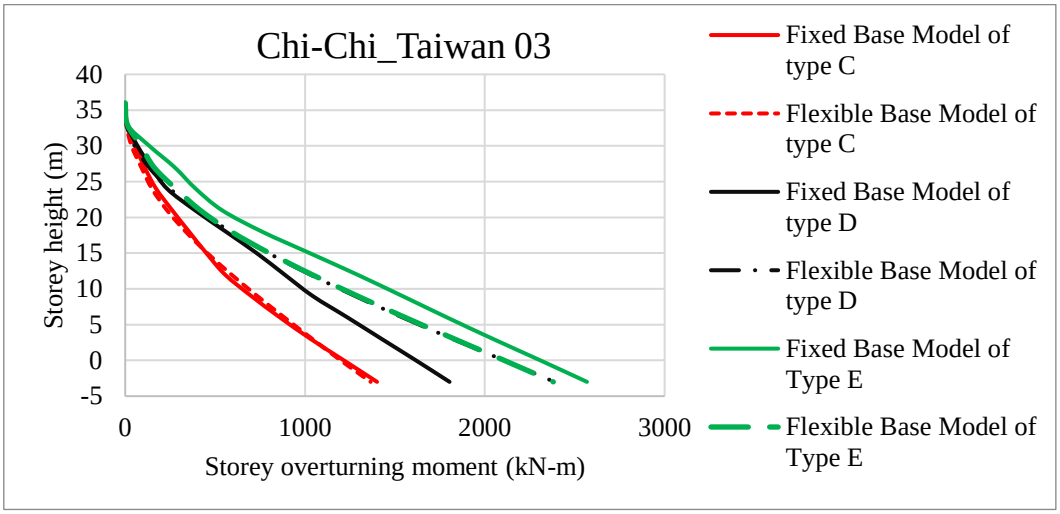

(b)

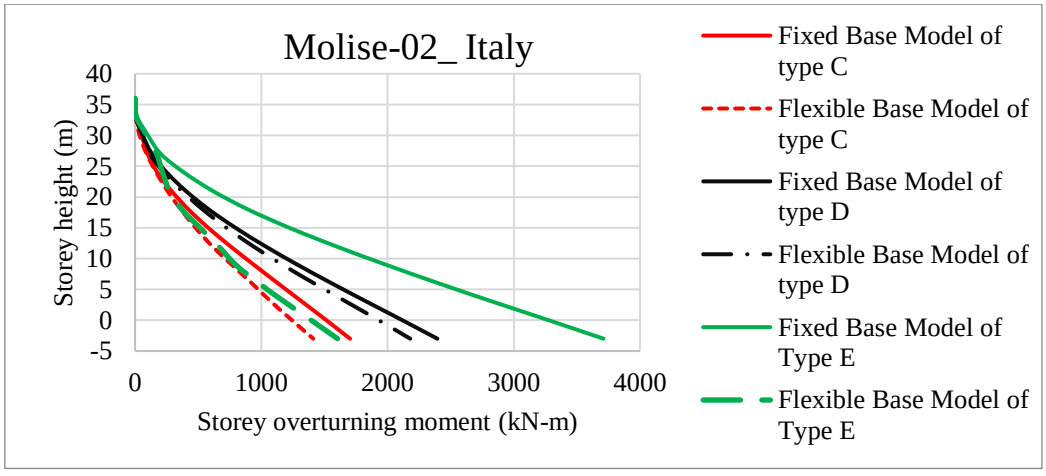

(c)

Figure 6.36: Storey overturning moment of Model 2 for (a) Anza-02, (b) Chi-Chi_Taiwan 03, (c) Molise-02_ Italy

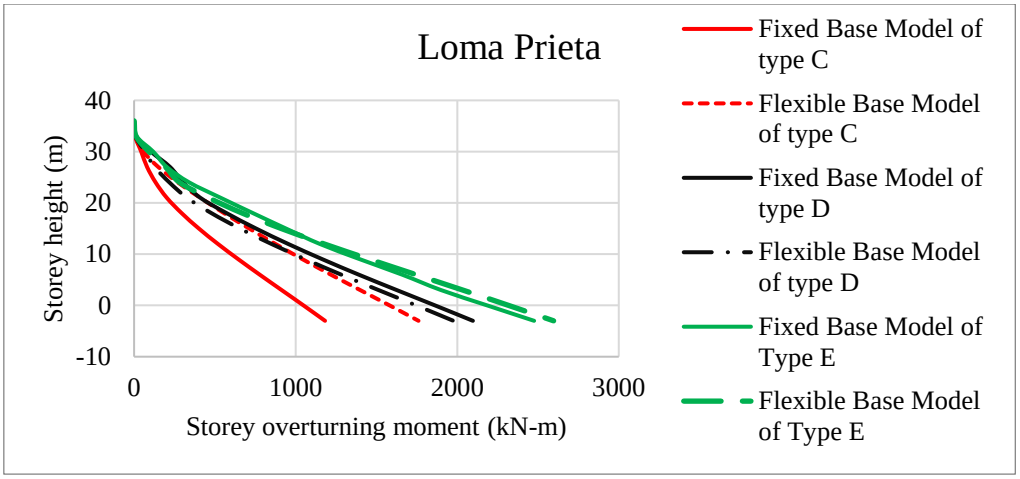

(d)

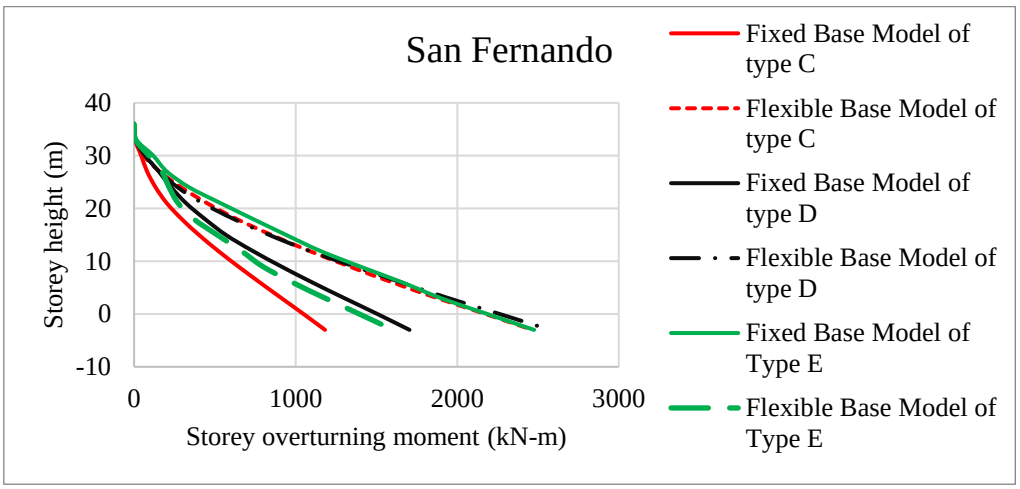

(e)

Figure 6.37: Storey overturning moment of Model 2 for (d) Loma Prieta, (e) San Fernando

6.1.3.4.3. Building model 3

The flexible base model of model 3 compared to the fixed base model shows an increment in storey overturning moment for all earthquakes except Chi-Chi_Taiwan-03 and San Fernando earthquakes, which have a decrement in the case of type C soil. When these models are assigned to type D soil, the following observations are made: a decrement in overturning moment of the flexible base model subjected to all earthquakes except Anza-02 and Loma Prieta earthquakes. For type E soils subjected to all earthquakes, the flexible base model shows a decrement for all earthquakes (Figures 6.38 and 6.39).

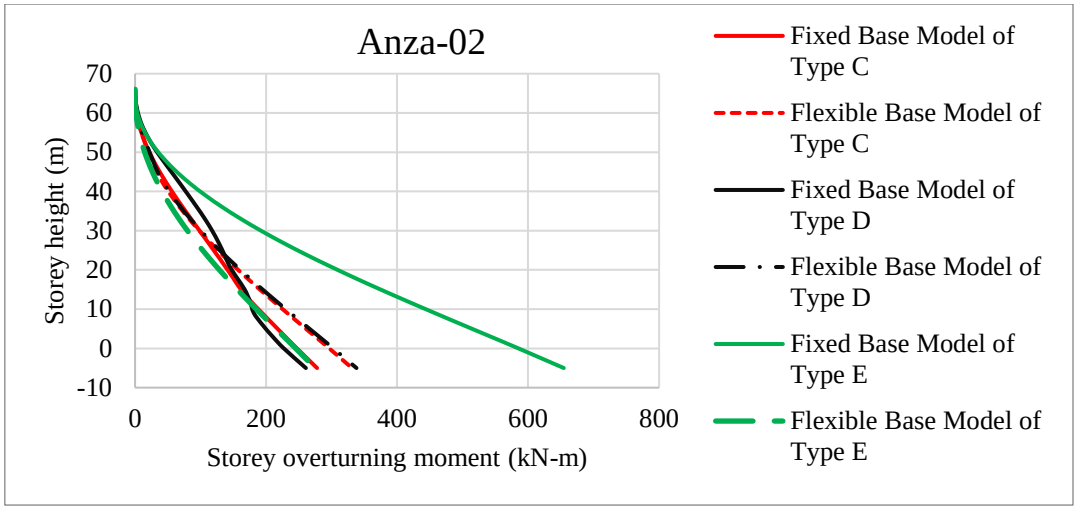

(a)

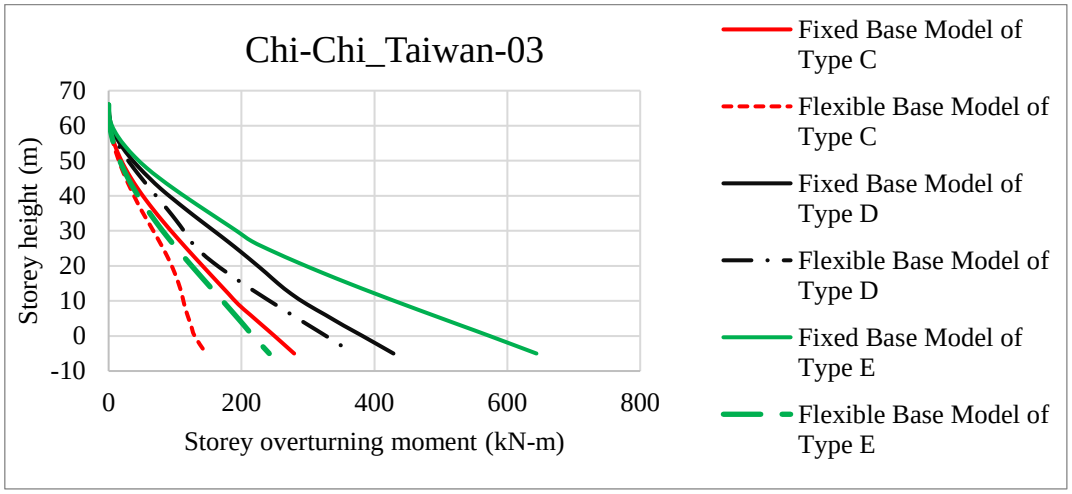

(b)

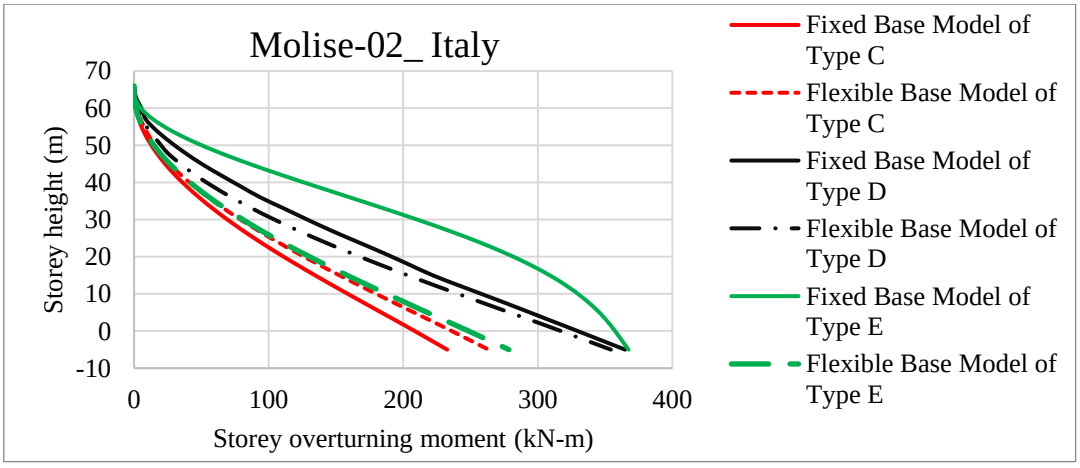

(c)

Figure 6.38: Storey overturning moment of Model 3 for (a) Anza-02, (b) Chi-Chi_Taiwan 03, (c) Molise-02_ Italy

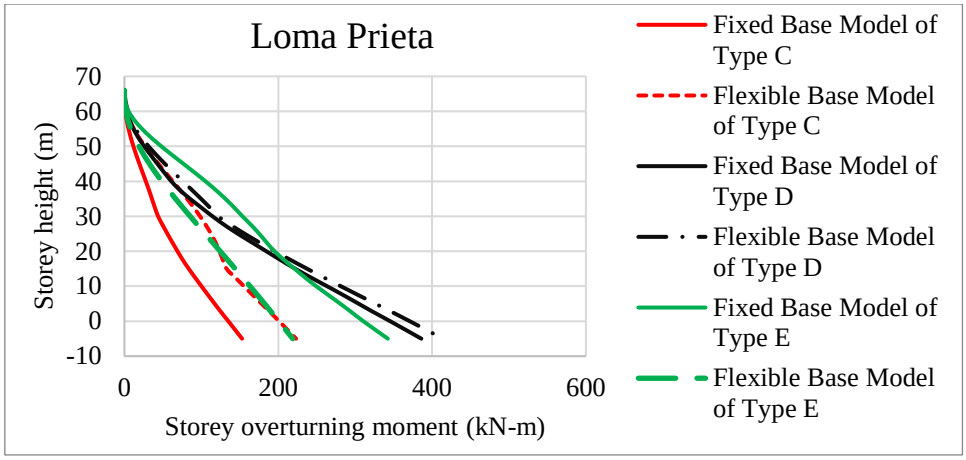

(d)

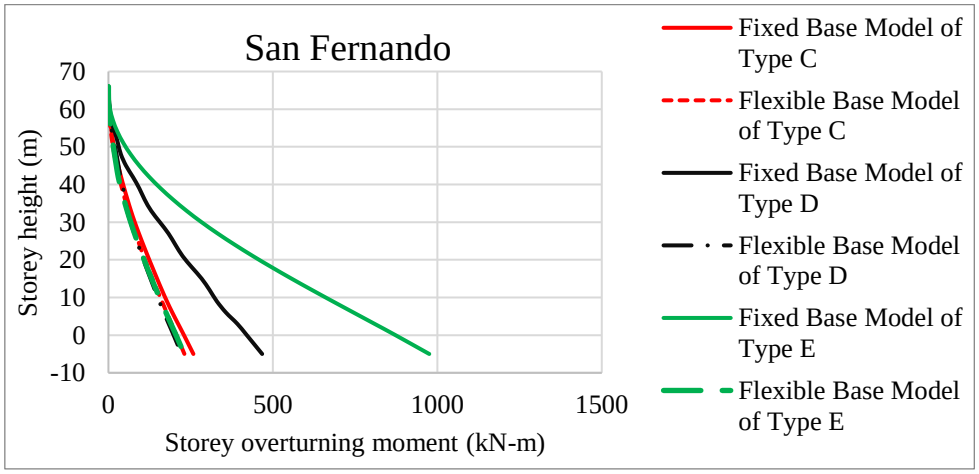

(e)

Figure 6.39: Storey overturning moment of Model 3 for (d) Loma Prieta, (e) San Fernando

6.1.3.4.4. Building model 4

The flexible base model of model 4 compared to the fixed base model shows an increment in storey overturning moment for Chi-Chi_Taiwan-03 (for lower stories), Molise-02_ Italy, Loma Prieta (for lower stories) and San Fernando earthquakes in the case of type C soil. When these models are assigned to type D soil, the following observations are made: a decrement in overturning moment of the flexible base model subjected to all earthquakes except Anza-02 earthquake. For type E soils subjected to all earthquakes, the flexible base model shows a decrement for all earthquakes except for higher stories during San Fernando earthquakes (Figures 6.40 and 6.41).

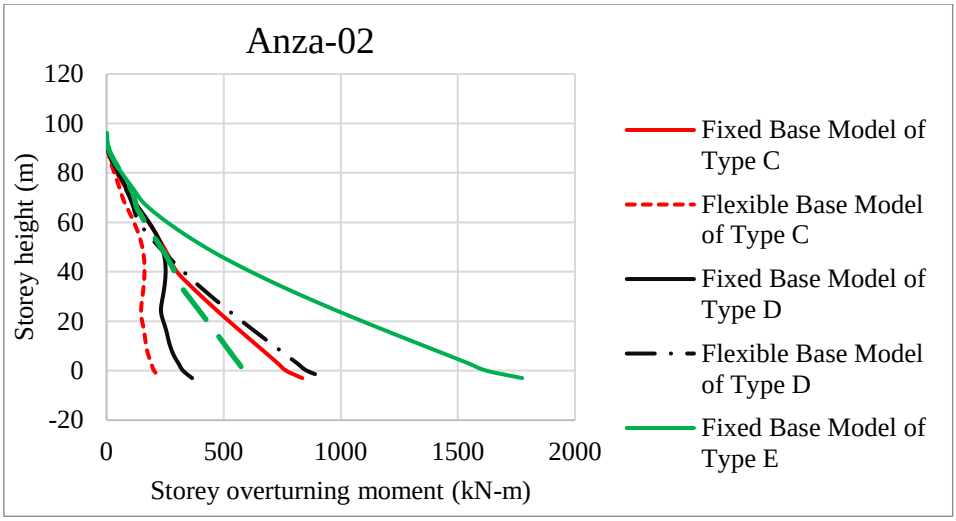

(a)

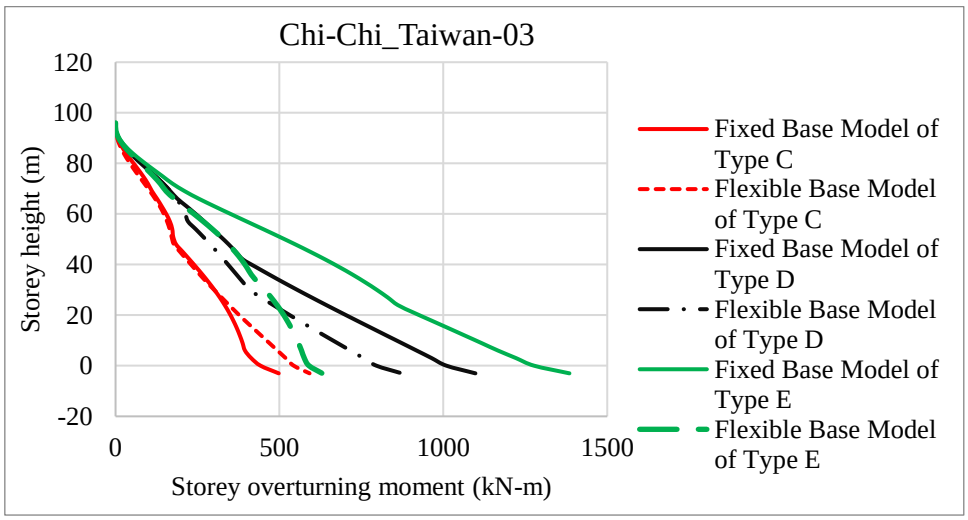

(b)

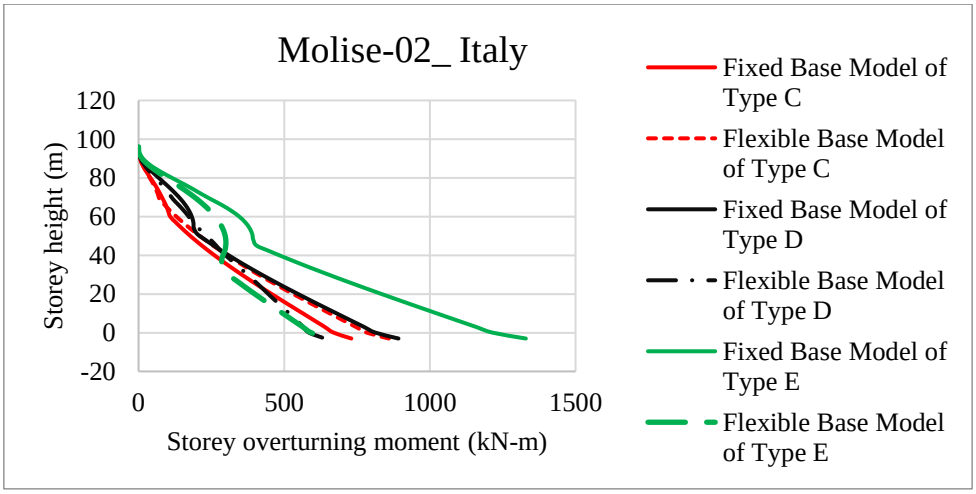

(c)

Figure 6.40: Storey overturning moment of Model 4 for (a) Anza-02, (b) Chi-Chi_Taiwan 03, (c) Molise-02_ Italy

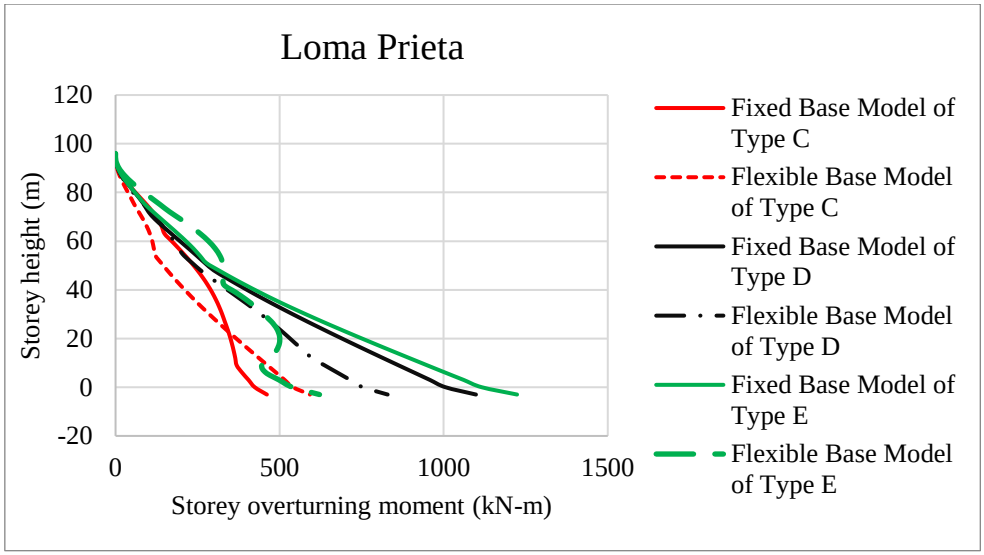

(d)

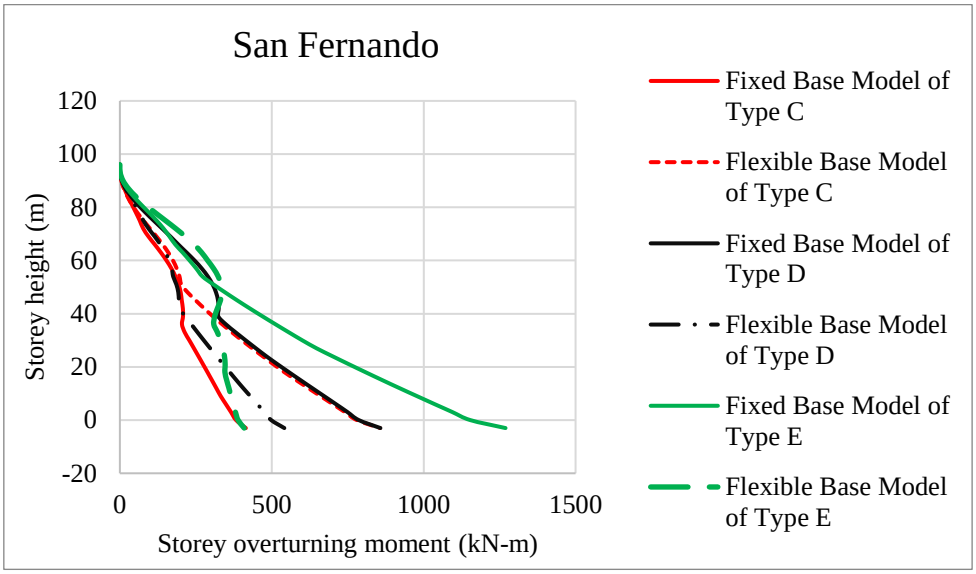

(e)

Figure 6.41: Storey overturning moment of Model 4 for (d) Loma Prieta, (e) San Fernando

Similar to storey displacement, storey drift ratio and storey shear force the storey overturning moment does not have a clear trend of increment and decrement. For the models and earthquake motions that have approximately equal fundamental period and predominant period respectively the response of the structure show a significant increase like flexible base model of type E soil in model 1 during San Fernando earthquake, fixed base model of type E soil in model 3 during Anza-02 earthquake.

6.1.3.4.5. Comparison between all models

A large storey overturning moment is observed in the shorter building models when they are supported on soil types C, D, and E during all earthquake motions. A significant increase is observed for the flexible base model of Model 1 during the San Fernando earthquake. The increased SSI effect is shown in the taller building model (see Figures B.7, B.8, C.8, C.9, D.8, and D.9)

6.1.3.5. Base shear

It is the total design lateral force or shear experienced at the base of a structure during an earthquake.

The base shear and overturning moment for fixed and flexible base models are listed in Table E.1 to E.5

The base shear along X as well as Y axis shows a decrement and an increment for given earthquakes as shown Table 6.4 through 6.7.

For Building Model 1, the base shear along the X-axis shows a decreased value when the flexible base model is compared to the fixed base model on soil types C, D, and E, except during Anza-02 on soil type D, Molise-02_Italy on soil type D, Loma Prieta on soil types C and D, and San Fernando on soil type E (Table 6.4).

For Building Model 2, the base shear along the X-axis shows a decreased value when the flexible base model is compared to the fixed base model on soil types C, D, and E, except during Anza-02 on soil types C and D, Chi-Chi_Taiwan-03 on soil type D, Loma Prieta on soil types C and D, and San Fernando on soil type C (Table 6.5).

For Building Model 3, the base shear along the X-axis shows a decreased value when the flexible base model is compared to the fixed base model on soil types C, D, and E, except during Molise-02_Italy on soil types C and D, and Loma Prieta on soil types C and D (Table 6.6).

For Building Model 4, the base shear along the X-axis shows a decreased value when the flexible base model is compared to the fixed base model on soil types C, D, and E, except during Anza-02 on soil type D, Chi-Chi_Taiwan-03 on soil type C, Molise-02_Italy on soil types C and D, Loma Prieta on soil types C, D, and E, and San Fernando on soil types C and D (Table 6.7).

A more reduced base shear is observed for more flexible soil types, particularly for soil type E, with one exception in Model 1 during the San Fernando earthquake. This exception occurs because the fundamental period of the structure aligns with the predominant period of the San Fernando earthquake (Table 6.4 through 6.7; Appendix A)

Table 6.4: Percentage variation in base shear and total overturning moment for Model 1

Building Models	Earthquake motions	Soil type	Base shear along x axis		Base shear along y axis		Over turning moment along x-axis		Over turning moment along y-axis	
			Increased (%)	Decreased (%)	Increased (%)	Decreased (%)	Increased (%)	Decreased (%)	Increased (%)	Decreased (%)
Model 1	Anza-02	Type C		30.0		5.1		12.1		28.9
		Type D	2.2		11.3		9.7			1.87
		Type E		15.9	19.4		13.3			32.2
	Chi-Chi_Taiwan-03	Type C		13.6		13.8		13.8		22.0
		Type D		32.8		33.4		29.9		21.2
		Type E		31.2	21.2		23.5			23.4
	Molise-02_ Italy	Type C		13.2		6.1		7.4		19.2
		Type D	17.7			32.0		35.5	5.4	
		Type E		36.0	32.6		31.1			23.2
	Loma Prieta	Type C	22.3		69.8		89.4		24.8	
		Type D	13.1		9.0		26.2		17.4	
		Type E		22.6	23.8		16.1			7.9
	San Fernando	Type C		16.3		60.9		59.5		8.4
		Type D		26. 4		21.7		12.6		25.0
		Type E	230.4		791.9		812.9		275.7	

Table 6.5: Percentage variation in base shear and total overturning moment for Model 2

Building Models	Earthquake motions	Soil type	Base shear along x axis		Base shear along y axis		Over turning moment along x-axis		Over turning moment along y-axis	
			Increased (%)	Decreased (%)	Increased (%)	Decreased (%)	Increased (%)	Decreased (%)	Increased (%)	Decreased (%)
Model 2	Anza-02	Type C	25.3		32.2		35.7			3.3
		Type D	90.7		120.8		116.4		114.8	
		Type E		47.7		73.3		75.2		56.9
	Chi-Chi_Taiwan-03	Type C		48.3	0.7			2.5		46.7
		Type D	15.0		44.4		32.3		15.8	
		Type E		8.4		0.3		7.3		0.1
	Molise-02_ Italy	Type C		14.3		14.8		17.1	0.1	
		Type D		4.9		11.6		8.9		14.7
		Type E		32.2		43.5		56.8		26.6
	Loma Prieta	Type C	14.6		70.9		48.9		21.5	
		Type D	5.7			12.4971		5.7	24.1	
		Type E		23.0	6.3		4.8			21.4
	San Fernando	Type C	2.9		94.9		181.8			4.4
		Type D		0.6	52.3		51.0			6.9
		Type E		55.8		25.6		38.1		45.8

Table 6.6: Percentage variation in base shear and total overturning moment for Model 3

Building Models	Earthquake motions	Soil type	Base shear along x axis		Base shear along y axis		Over turning moment along x-axis		Over turning moment along y-axis	
			Increased (%)	Decreased (%)	Increased (%)	Decreased (%)	Increased (%)	Decreased (%)	Increased (%)	Decreased (%)
Model 3	Anza-02	Type C		17.6	8.8		19.2			6.0
		Type D		27.2	0.3		29.6		19.6	
		Type E		40.1		60.4		57.9		35.5
	Chi-Chi_Taiwan-03	Type C		10.7		17.4		47.5		18.5
		Type D		1.5		20.6		13.9		2.3
		Type E		33.1		64.1		62.5		32.6
	Molise-02_ Italy	Type C	103.9		13.8		13.2		73.2	
		Type D	88.2			4.2		2.9	91.6	
		Type E		60.9		50.1		24.2		54.8
	Loma Prieta	Type C	40.8		57.5		45.9		33.6	
		Type D	113.1			11.0	7.3		110.6	
		Type E		12.4		43.5		36.1		5.2
	San Fernando	Type C		0.4		17.2		10.5		15.9
		Type D		14.5		52.7		52.5		18.5
		Type E		72.5		76.7		76.4		71.6

Table 6.7: Percentage variation in base shear and total overturning moment for Model 4

Building Models	Earthquake motions	Soil type	Base shear along x axis		Base shear along y axis		Over turning moment along x-axis		Over turning moment along y-axis	
			Increased (%)	Decreased (%)	Increased (%)	Decreased (%)	Increased (%)	Decreased (%)	Increased (%)	Decreased (%)
Model 4	Anza-02	Type C		61.4		32.3		36.16		72.8
		Type D	81.2		5.5		31.1		156.2	
		Type E		20.0		40.9		69.7		64.2
	Chi-Chi_Taiwan-03	Type C	49.6			24.1		36.5	18.9	
		Type D		9.2		4.5	22.3			20.5
		Type E		10.6		42.3		4.7		54.47
	Molise-02_ Italy	Type C	225.2		25.1		0.3		17.6	
		Type D	131.1			17.1		12.2		28.4
		Type E		70.3		38.6	1.27			51.2
	Loma Prieta	Type C	7.8			8.2		24.2	28.5	
		Type D	153.5			8.2	4.0			24.5
		Type E	42.2		1.8		42.5			49.2
	San Fernando	Type C	13.8		22.9		355.6		106.5	
		Type D	34.6			6.3		50.3		36.9
		Type E		72.4		9.7	12.0			67.8

6.2. Discussion

The study highlights that when a structure is modeled with a flexible base, its fundamental period is longer compared to a model with a fixed base. This elongation of the fundamental period is primarily due to the increased effective damping in the flexible base model. Effective damping refers to the energy dissipation mechanisms that reduce the amplitude of vibrations. In a flexible base model, these mechanisms are more pronounced than in a fixed base model, where only structural damping is considered. This additional damping in the flexible base model helps to absorb more energy, leading to a longer fundamental period.

In general, storey displacements are lower for the flexible base model compared to the fixed base model, although there are some exceptions. Storey displacement and storey drift ratio do not consistently increase or decrease. Regardless of how different motions respond, it is evident that the variation in storey displacement and storey drift ratio becomes more noticeable as the soil becomes more flexible (type C → type D → type E).

SSI allows the soil to absorb and dissipate some of the seismic energy, reducing the amount of energy transferred to the structure. This can lead to lower storey displacement and storey drift ratio. The base shear shown in the study does not always exhibit a uniform increase or decrease when comparing the flexible base model to the fixed base model. Some earthquakes show a reduction, while others show an increase. Overall, the reduction in base shear is more pronounced in lower-storey buildings than in higher-storey buildings, based on the assumed building models for the study (G+5 to G+30). The results depend on the nature of the earthquake. According to NIST GCR 12-917-21 (2012), the correlation between the influence of SSI on base shear and the spectrum is significant. Base shear generally increases when the spectral slope is positive and decreases when it is negative.

Models supported by soil types C, D, and D show different responses when subjected to various ground motions. When the models are exposed to motions with higher amplitudes, their responses become larger, and they also show a significant increase when subjected to ground motions with a predominant period that matches the fundamental period of the structure. This phenomenon is observed for most earthquake motions and different building models (Appendices A, B, C, and D).

The impact of SSI is complicated, as explained by studies such as Razvi et al. (2018) and Kabtamu et al. (2018) and as confirmed by this study. Generally, SSI tends to increase building displacements and decrease base shear, attributed to energy dissipation in the soil. However,

Kabtamu et al. (2018) introduces a counterintuitive dimension by identifying scenarios where specific lower stories may undergo heightened shear forces. The recognition of this potential consequence emphasizes the necessity to move beyond the common assumption of reduced shear forces. These findings by Kabtamu et al. (2018) align with and complement the results of the current study for some earthquake motions, emphasizing the importance of evaluations in understanding the diverse effects of SSI.

The observations from Jha et al. (2015) study on SSI effects highlight instances where the expected outcomes of decreasing shear force and shear stress do not consistently align with common assumptions. Jha et al. (2015) delves into the complexities of SSI effects, particularly concerning the influence of the fundamental period of a structural system. Typically, an increase in the fundamental period is expected to lead to a decrease in a structure's response to ground motion.

However, the findings presented in Jha et al. (2015) reveal that this anticipated decrease does not always hold true. The discrepancy between the expected and observed behavior underscores the complexity of the relationship between SSI effects and the fundamental period of a structural system. In specific cases, the response of a structure under ground motion does not follow the conventional pattern, indicating the involvement of other factors or mechanisms. Some earthquake motions in this study align with the observations made by Jha et al. (2015). This study shows that a significant increase is observed for some earthquakes that have an approximate predominant period similar to the fundamental period of the corresponding model.

In many studies, it was believed that SSI generally reduces the seismic response of a structure by increasing its flexibility and energy dissipation. However, Mylonakis & Gazetas (2000) suggest that this isn't always the case. When a structure's fundamental natural period increases due to SSI, it doesn't necessarily lead to a smaller response. This is also supported by this study, which shows cases with larger responses even though the period is lengthened.

CHAPTER SEVEN
CONCLUSION AND RECOMMENDATION

7.1. Conclusion

Based on the substructure model analysis, the following conclusions are drawn:

- The code-based approach used in the study shows that the common perspective that SSI reduces building response is not always true; in some cases, it can lead to an increased building response, such as higher base shear.
- Energy dissipation can lead to a decrease in storey displacement and drift ratio.
- Decreased storey displacement and storey drift ratio were observed for some models.
- In specific earthquake motions, an increase in fundamental period of flexible base model did not always lead to a decrease in base shear of the corresponding model.
- Increased and decreased storey displacement and drift do not necessarily guarantee reduced shear force when considering SSI. Earthquake characteristics also play a critical role in this relationship.
- A significant increment is shown for specific earthquake motions that have approximate value of predominant period and fundamental period of the structure.
- The increased number of stories, from G+5 to G+30, shows an increased SSI effect for most earthquake motions, in terms of storey displacement, storey drift ratio, and storey overturning moment.
- The effect of SSI shows a reduced base shear for shorter building models and more flexible soil conditions in most earthquake ground motions.
- Flexible base models generally have lower storey displacements than fixed base models, but this trend isn't consistent. As soil flexibility increases (type C → type D → type E), variations in storey displacement and drift ratio become more pronounced.

7.2. Recommendation

Based on observations of the outcomes of this study it is recommended to

- Expand the analysis beyond a single substructure model: The use of a single model from NIST GCR 12-917-21 and Pais and Kausel (1988) limits the scope of the study.

Consider including a wider variety of substructure models representing different structural configurations to account for the diverse responses of structures to earthquake forces.

- While designing structures using the fixed base model is commonly considered standard practice, it does not always ensure safety, particularly in cases involving SSI. This study has shown that SSI can lead to an increase in base shear, which the fixed base model may not capture. Therefore, engineers should integrate SSI analysis into the design process, especially in areas with specific soil conditions, foundation types, or seismic activity that could cause significant interaction between the structure and the soil. Relying solely on the fixed base model may result in inaccurate predictions of structural behavior, potentially compromising safety. A more comprehensive design approach, considering both fixed base and SSI effects, is vital to accurately assess forces like base shear and ensure a safe and stable structure.

REFERENCE

American Society of Civil Engineers. (2010). Minimum design loads for buildings and other structures (ASCE 7-10). Reston, VA: American Society of Civil Engineers.

ASCE/SEI 7-16. (2017). Minimum design loads and associated criteria for buildings and other structures. THE AMERICAN SOCIETY OF CIVIL ENGINEERS, 1–889. https://doi.org/10.1061/9780784414248

ASCE/SEI 7-05. (2006). Minimum Design Loads for Buildings and Other Structures. THE AMERICAN SOCIETY OF CIVIL ENGINEERS, 1–421. https://ascelibrary.org/doi/book/10.1061/9780784408094

ASCE/SEI 41-17. (2017). Seismic Evaluation and Retrofit of Existing Buildings. THE AMERICAN SOCIETY OF CIVIL ENGINEERS, 1–623.

Ayele, A. (2017). Probabilistic seismic hazard analysis (PSHA) for Ethiopia and the neighboring region. Journal of African Earth Sciences, 134, 257-264.

Ayolabi, E. A., Adeoti, L., Oshinlaja, N., Adeosun, I. O., & Idowu, O. I. (2009). Seismic Refraction and Resistivity Studies of part of Igbogbo Township, South-West Nigeria. Journal Sci. Res., 11, 42–61. Lagos, Nigeria. https://www.researchgate.net/publication/268295051

BSSC (Building Seismic Safety Council) 2004. National Earthquake Hazard Reduction Program (NEHRP): Recommended Provisions (and Commentary) for Seismic Regulations for New Buildings and Other Structures. Washington DC: BSSC, FEMA 450-1 and 450–2.

B_Das, & N_Sivakugan. (2019). Principles_of_Foundation_Engineering. Cengage Learning, SI EDITION, 1–884.

Computers & Structures, Inc. (2017). CSI analysis reference manual for SAP2000®, ETABS®, SAFE®, and CSiBridge®. Computers & Structures, Inc.

Bommer, J. J., Stafford, P. J., & Alarcón, J. E. (2009). Empirical equations for the prediction of the significant, bracketed, and uniform duration of earthquake ground motion. Bulletin of the Seismological Society of America, 99(6), 3217–3233. https://doi.org/10.1785/0120080298

EN 1998-1. (2004). Design of structures for earthquake resistance - Part 1: General rules, seismic actions and rules for buildings. CEN, 1–231.

EN 1998-5. (2004). Design of structures for earthquake resistance – Part 5: Foundations, retaining structures and geotechnical aspects. CEN, 1–47.

ES EN 1998-1:2015. (2015). Design of structures for earthquake resistance- part 1: General rules-seismic actions and rules for buildings (A. Zekaria, Ed.). Ministry of Construction. Addis Ababa, Ethiopia.

ES EN 1998-5:2015. (2015). Design of structures for earthquake resistance - Part 5: Foundations, retaining structures and geotechnical aspects. Ministry of Construction. Addis Ababa, Ethiopia.

FEMA 356. (2000). Prestandard And Commentary for The Seismic Rehabilitation of Buildings. American Society of Civil Engineers, 1–518.

FEMA P-2082-1. (2020). NEHRP Recommended Seismic Provisions for New Buildings and Other Structures. BUILDING SEISMIC SAFETY COUNCIL, Vol. I, 1–593.

FEMA P-2091. (2020). A Practical Guide to Soil-Structure Interaction. APPLIED TECHNOLOGY COUNCIL, 1–218. www.ATCouncil.org

Galal, K., & Naimi, M. (2008). Effect of soil conditions on the response of reinforced concrete tall structures to near-fault earthquakes. Structural Design of Tall and Special Buildings, 17(3), 541–562. https://doi.org/10.1002/tal.365

Gashaye, Z. (2018). An Investigation into the Ground Motion Amplification Potential of Selected Sites of Addis Ababa City Addis Ababa University. Addis Ababa, Ethiopia.

Gazetas, G. (1991). Foundations Vibrations. Foundation Engineering Handbook 2nd Edition, H.Y.Fang, Ed., Van Nostrand Reinhold, 2nd EDITION, 1–42.

George Mylonakis & George Gazetas (2000) Seismic Soil-Structure Interaction: Beneficial Or Detrimental?, Journal of Earthquake Engineering, 4:3, 277-301, DOI: 10.1080/13632460009350372

Getu, B. (2023). Nonlinear Ground Response Analysis of Selected Sites of Addis Ababa using Geotechnical and Seismic data. Addis Ababa University. Addis Ababa, Ethiopia.

Getu, B., & Worku, A. (2024). The influence of soils of selected sites of Addis Ababa on predicted earthquake ground motions. Journal of African Earth Sciences, 215, 105260.

Giardini, D., Grunthal, G., Shedlock, K. M., & Zhang, P. (1999). The_GSHAP_Global_Seismic_Hazard_Map. ANNALI DI GEOFISICA, 42, 1–6.

Hanna Razvi, A. J., Kumar, V. R., Yashaswini R.K, & Arun A.C. (2018). Effect of Soil Structure Interaction on High Rise Building using ETABS. International Journal of Civil and Structural Engineering Research, 6, 165–172. www.researchpublish.com

John P. Wolf. (1985). Dynamic Soil-Structure Interaction. Prentice-Hall International Series in Civil Engineering and Engineering Mechanics. New Jersey 07632.

Jha, A. K., Utkarsh, K., & Kumar, R. (2015). Effects of soil-structure interaction on multi storey buildings on mat foundation. In Advances in Structural Engineering: Mechanics, Volume One (pp. 703–715). Springer India. https://doi.org/10.1007/978-81-322-2190-6_56

Kabtamu, H. G., Peng, G., & Chen, D. (2018). Dynamic Analysis of Soil Structure Interaction Effect on Multi Story RC Frame. Open Journal of Civil Engineering, 08(04), 426–446. https://doi.org/10.4236/ojce.2018.84030

Kebede, F., & van Eck, T. (1997). Probabilistic seismic hazard assessment for the Horn of Africa based on seismotectonic regionalisation. Tectonophysics, 270, 221–237.

Kramer, S. L. (1996). Geotechnical Earthquake Engineering. Prentice-Hall, Inc.Upper Saddle River.

Luna, R., & Jadi, H. (2000). Determination of Dynamic Soil Properties Using Geophysical Methods. First International Conference on the Application of Geophysical and NDT Methodologies to Transportation Facilities and Infrastructure, St. Louis, MO, 1–15.

Mammo, T. (2005). Site-specific ground motion simulation and seismic response analysis at the proposed bridge sites within the city of Addis Ababa, Ethiopia. Engineering Geology, 79(3–4), 127–150. https://doi.org/10.1016/j.enggeo.2005.01.005

Mylonakis, G., & Gazetas, G. (2000). Seismic soil-structure interaction: Beneficial or detrimental? Journal of Earthquake Engineering, 4(3), 277–301. https://doi.org/10.1080/13632460009350372

NIST GCR 12-917-21. (2012). Soil-Structure Interaction for Building Structures. NEHRP Consultants Joint Venture, 1–292.

Pais, A., and Kausel, E., 1988, Approximate formulas for dynamic stiffnesses of rigid foundations, Soil Dynamics and Earthquake Engineering, Vol. 7, No. 4, pp. 213-227.

Salmon, M. W., Short, S. A., & Kennedy, R. P. (1992). Strong motion duration and earthquake magnitude relationships. U.S. Department of Energy by Lawrence Livemore National Laboratory. Livermore, California.

Stewart, J. P., Afshari, K., & Hashash, Y. M. A. (2014). Guidelines for performing hazard-consistent one-dimensional ground response analysis for ground motion prediction. University of California, Los Angeles. https://www.researchgate.net/publication/308052147

Villaverde, Roberto. (2009). Fundamental concepts of earthquake engineering. Taylor & Francis Group, LLC, 1–990.

Williams, F.M. (2016). Understanding Ethiopia. In *GeoGuide*. Springer International Publishing Switzerland. DOI: 10.1007/978-3-319-02180-5_24.

Appendix A

A.1. Fourier Amplitude of input ground motions matched to ground type C with 7% damping

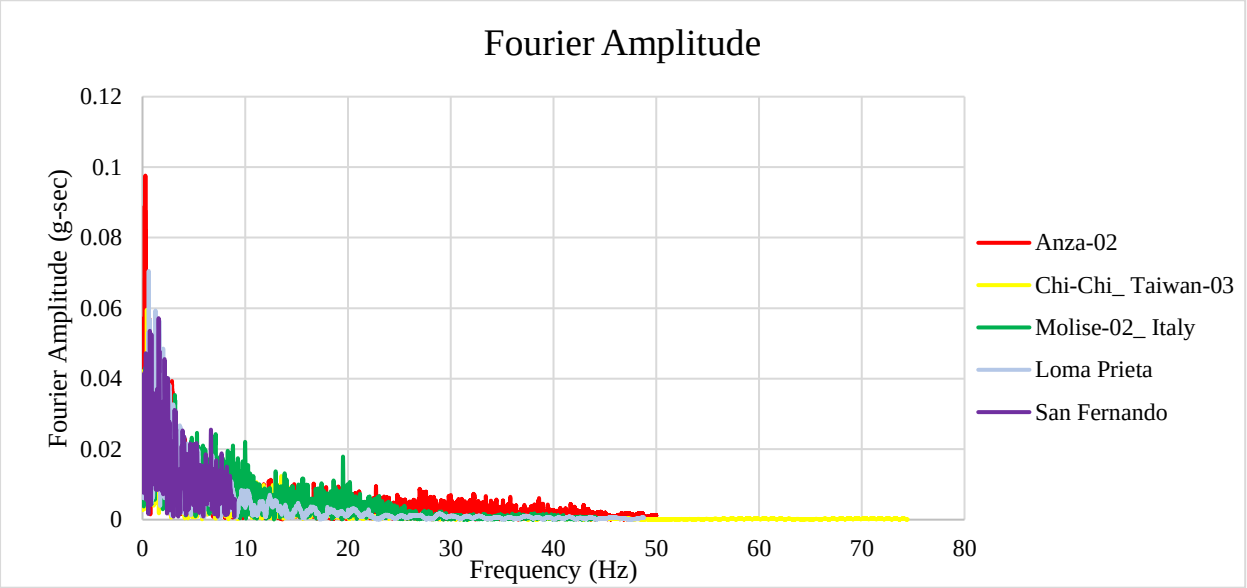

Figure A.1: Fourier Amplitude of input ground motions matched to ground type C with 7% damping for all earthquakes

A.2. Fourier Amplitude of input ground motions matched to ground type D with 5% damping

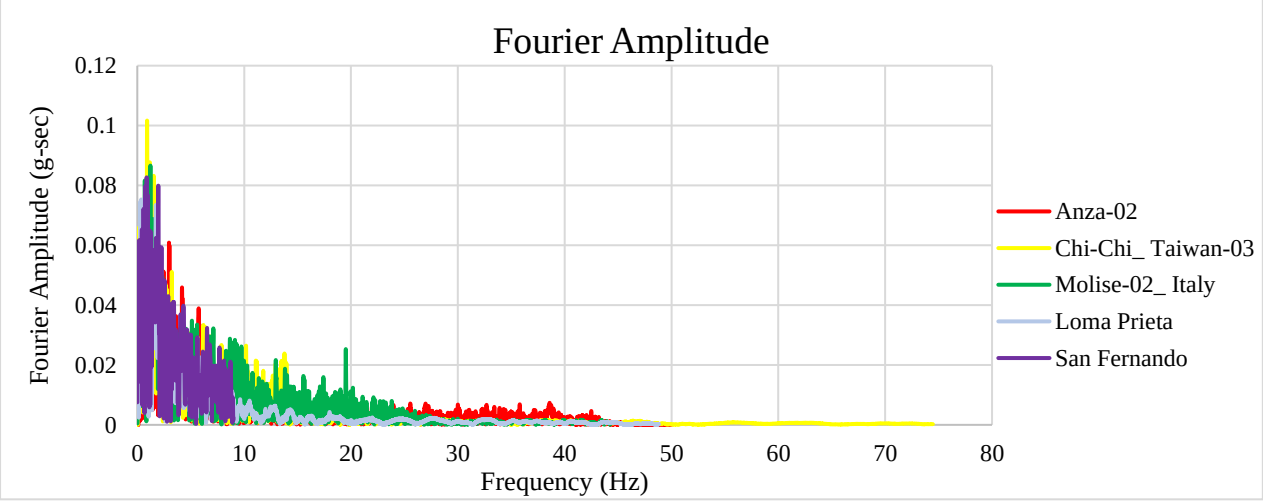

Figure A.2: Fourier Amplitude of input ground motions matched to ground type D with 5% damping for all earthquakes

A.3. Fourier Amplitude of input ground motions matched to ground type D with 7% damping

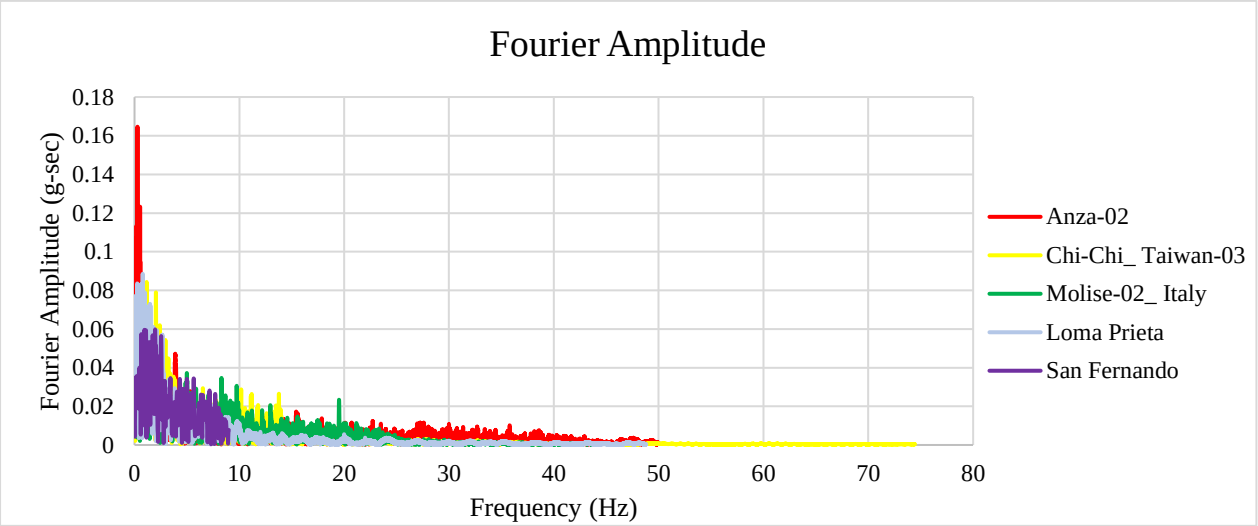

Figure A.3: Fourier Amplitude of input ground motions matched to ground type D with 7% damping for all earthquakes

A.4. Fourier Amplitude of input ground motions matched to ground type E with 5% damping

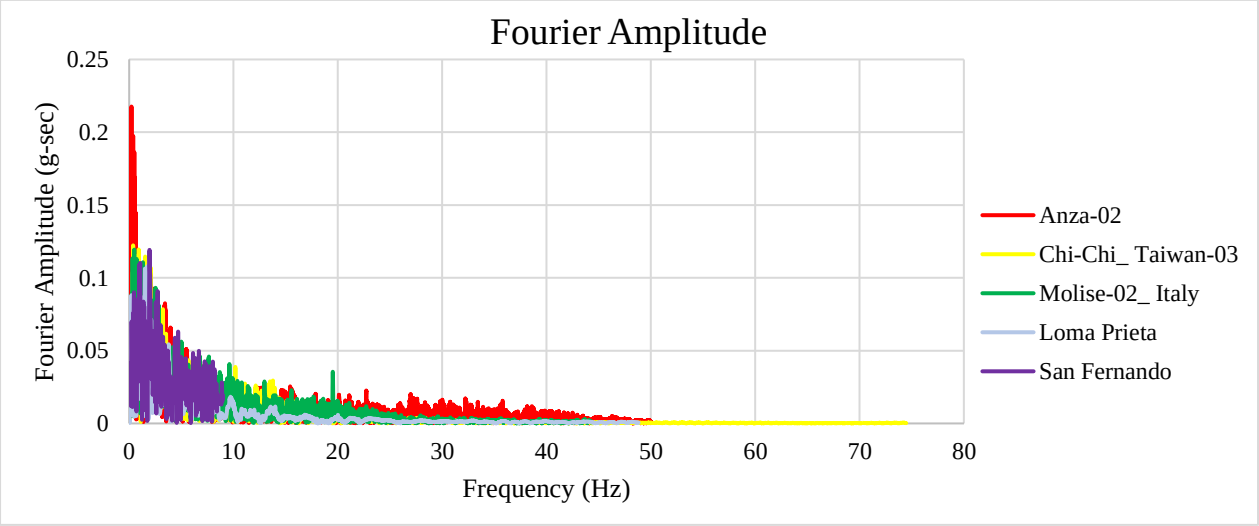

Figure A.4: Fourier Amplitude of input ground motions matched to ground type E with 5% damping for all earthquakes

A.5. Fourier Amplitude of input ground motions matched to ground type E with 6% damping

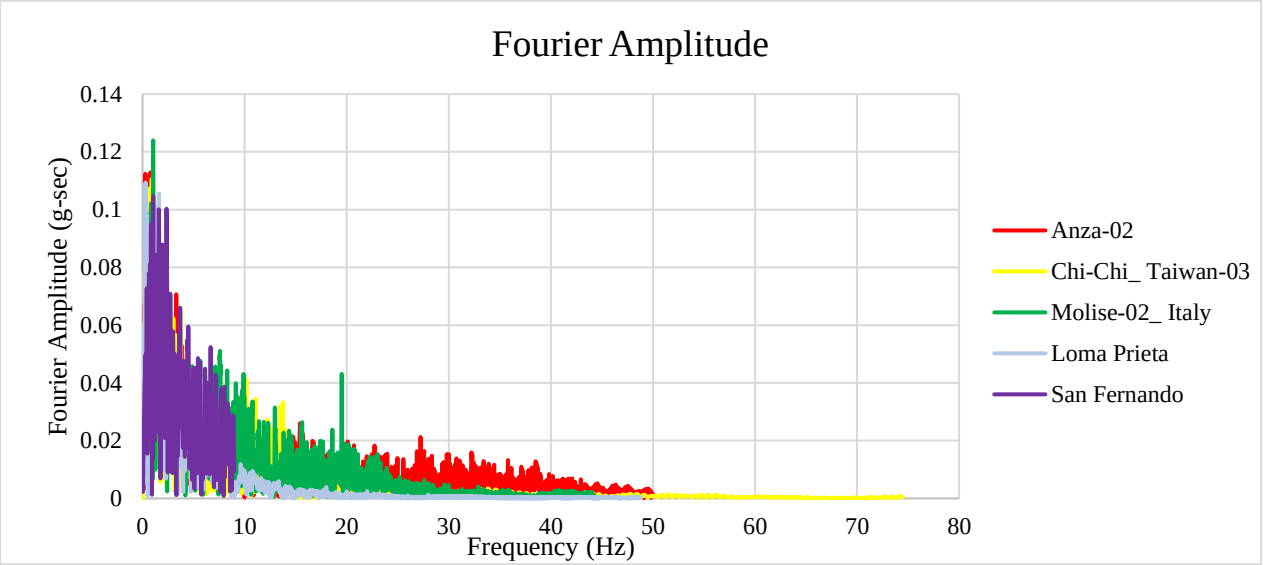

Figure A.5: Fourier Amplitude of input ground motions matched to ground type E with 6% damping for all earthquakes

A.6. Fourier Amplitude of input ground motions matched to ground type E with 8% damping

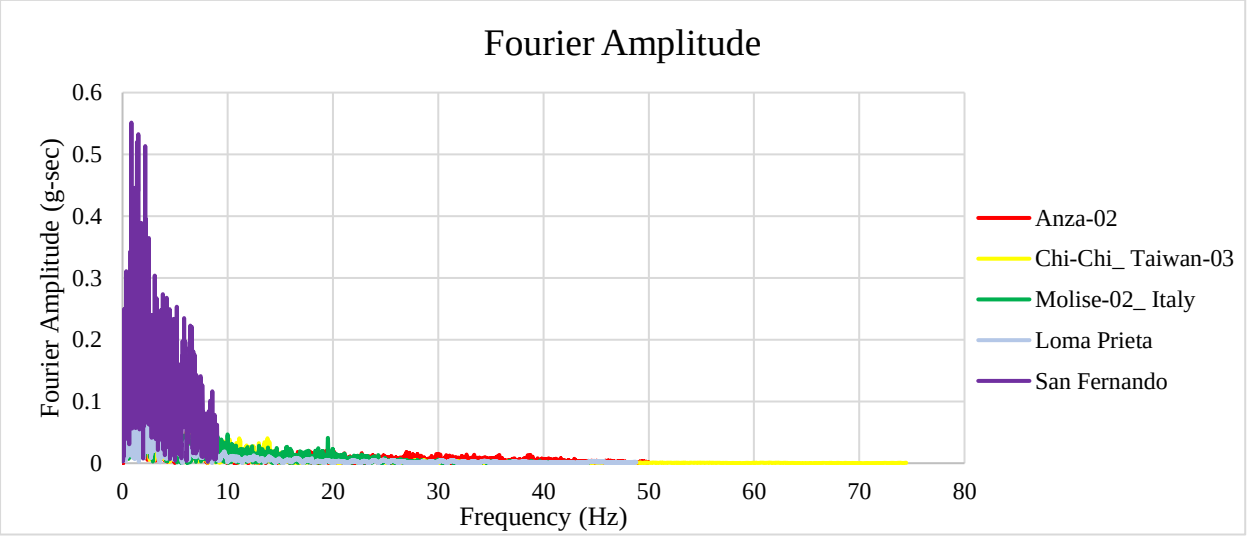

Figure A.6: Fourier Amplitude of input ground motions matched to ground type E with 8% damping for all earthquakes

A.7. Fourier Amplitude of input ground motions matched to ground type E with 10% damping

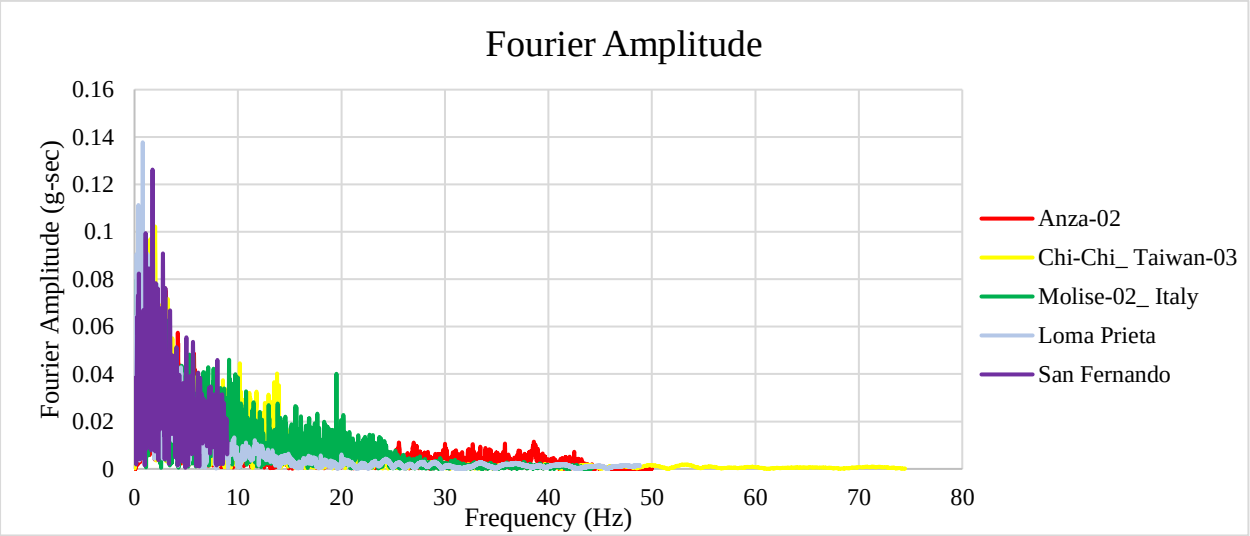

Figure A.7: Fourier Amplitude of input ground motions matched to ground type E with 10% damping for all earthquakes

Appendix B

Comparison between all models for soil type C

B.1. Storey displacement

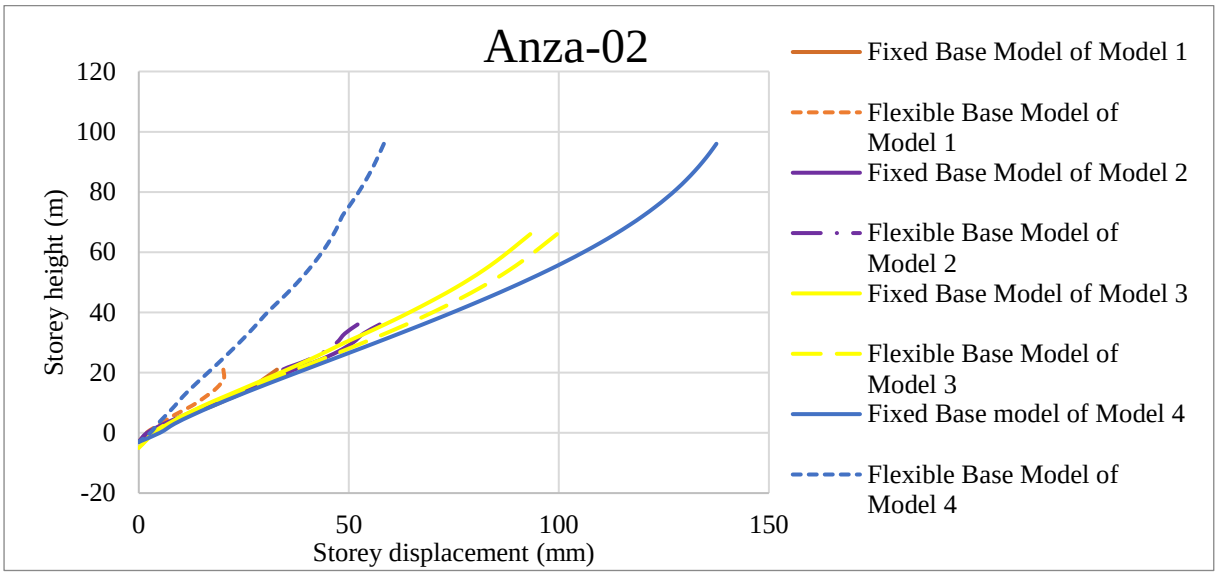

(a)

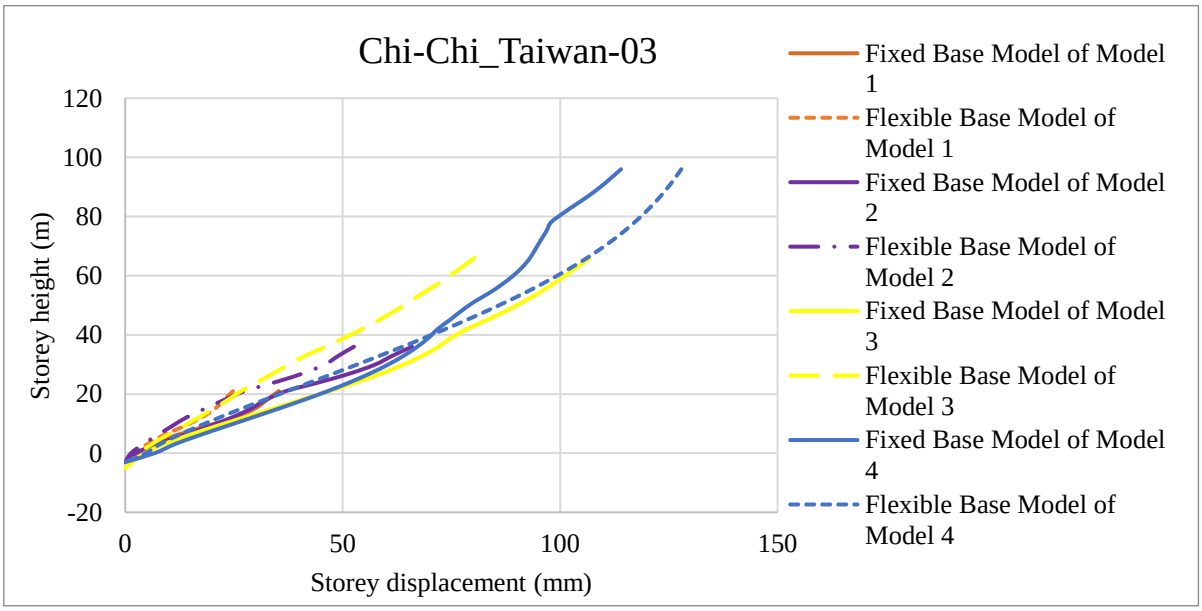

(b)

Figure B.1: Storey displacement of all models on soil type C for (a) Anza-02, (b) Chi-Chi_Taiwan 03

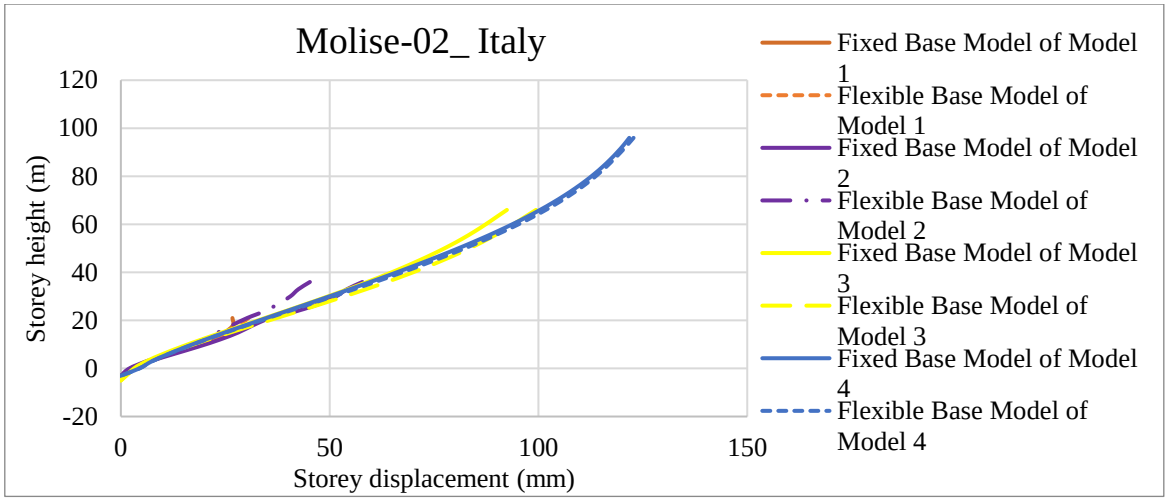

(c)

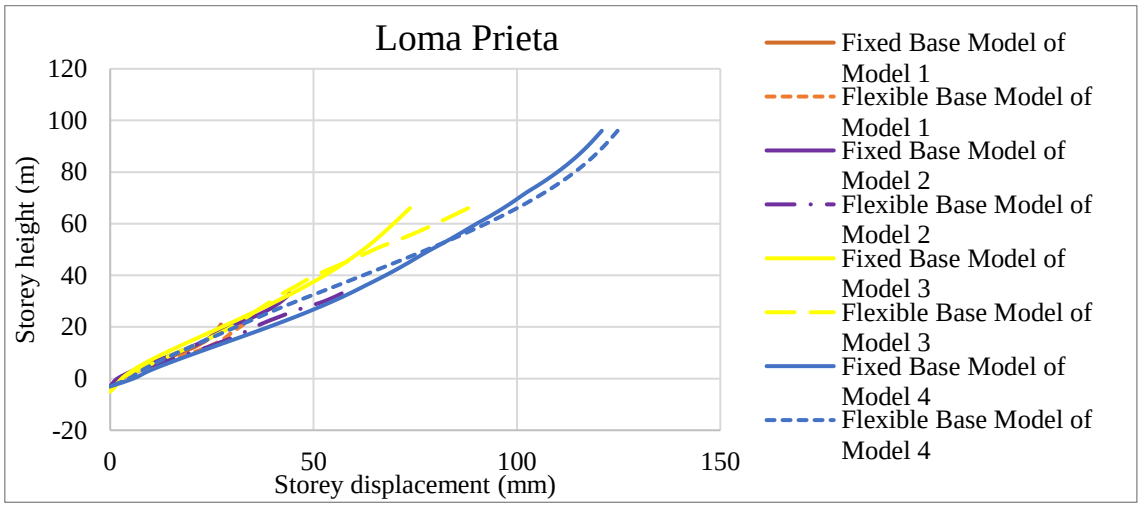

(d)

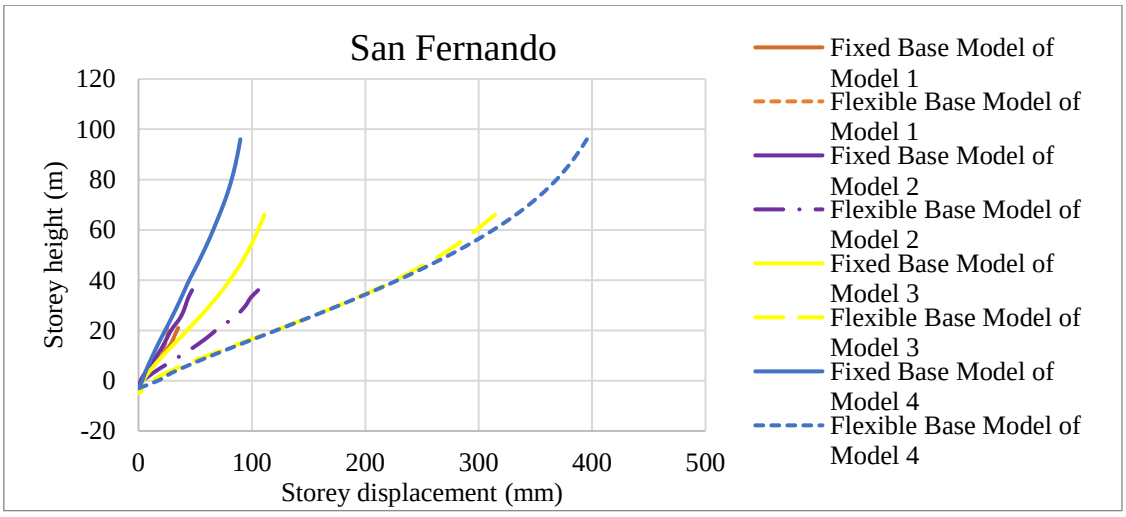

(e)

Figure B.2: Storey displacement of all models on soil type C for, (c) Molise-02_ Italy, (d) Loma Prieta, (e) San Fernando

B.2. Storey drift ratio

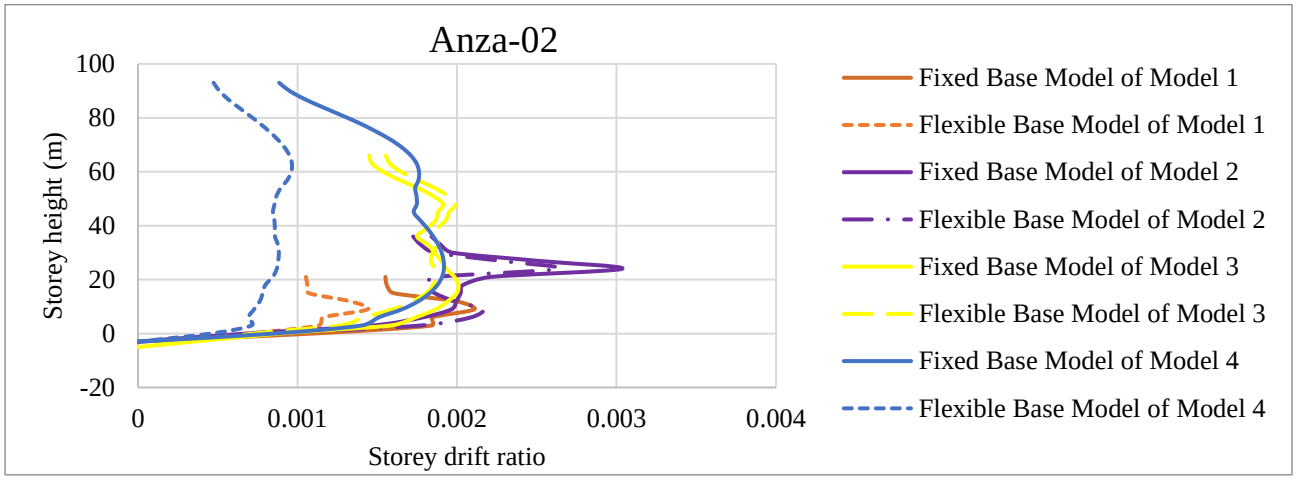

(a)

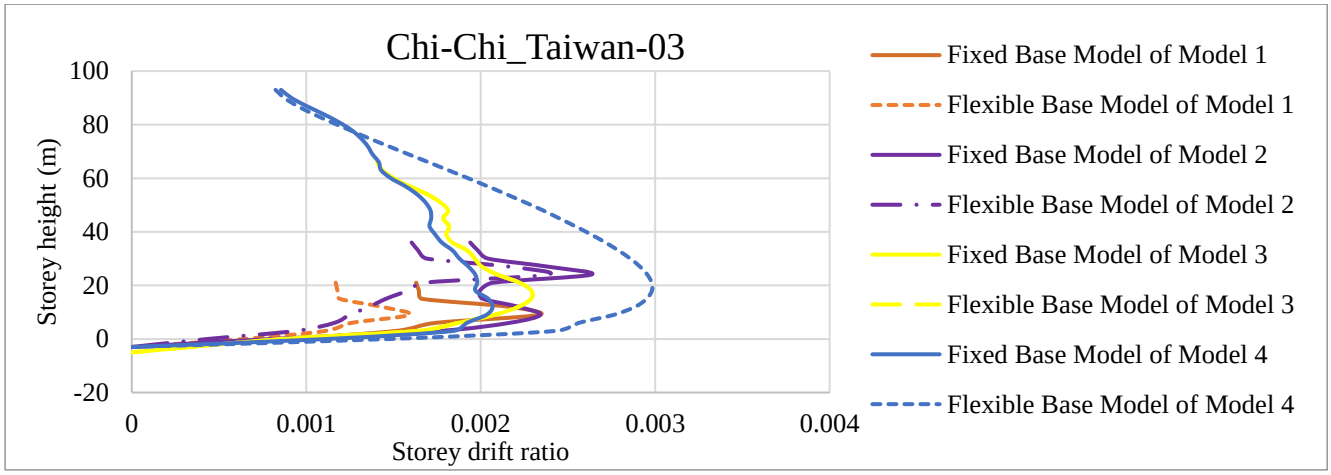

(b)

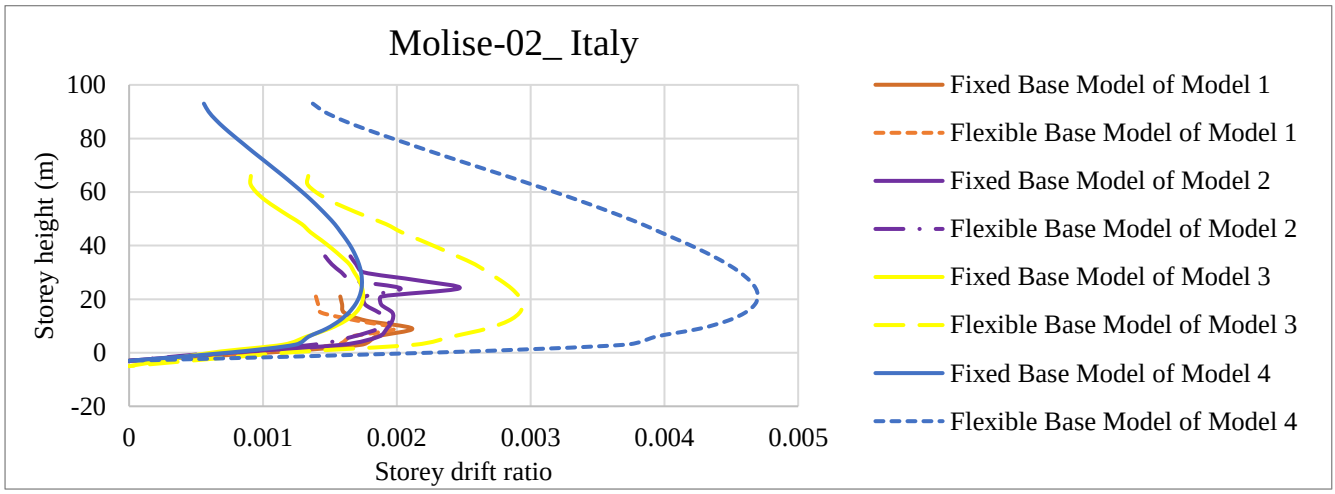

(c)

Figure B.3: Storey drift ratio of all models on soil type C for (a) Anza-02, (b) Chi-Chi_Taiwan-03, (c) Molise-02_ Italy

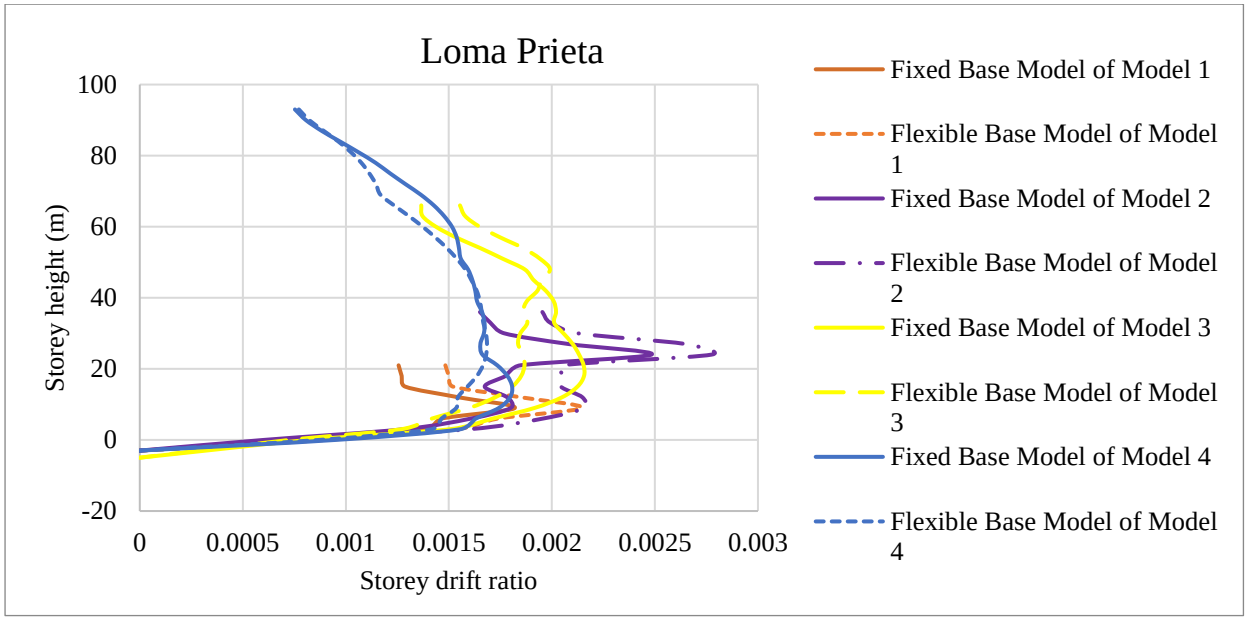

(d)

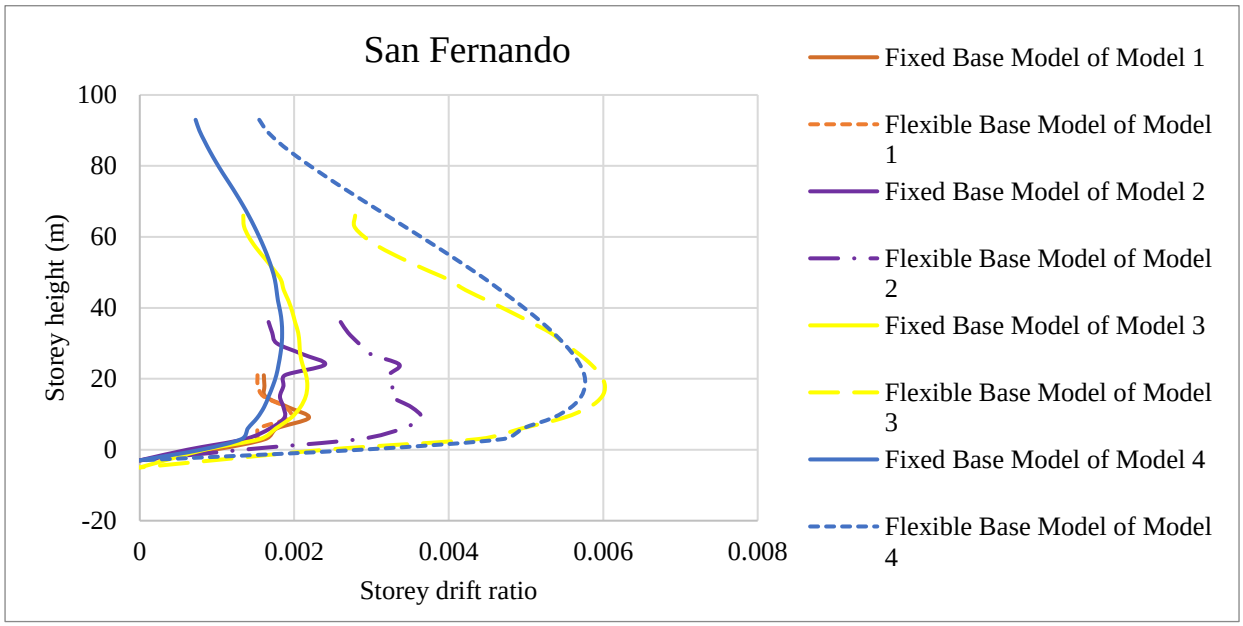

(e)

Figure B.4: Storey drift ratio of all models on soil type C for (c) Molise-02_ Italy, (d) Loma Prieta, (e) San Fernando

B.3. Storey shear force

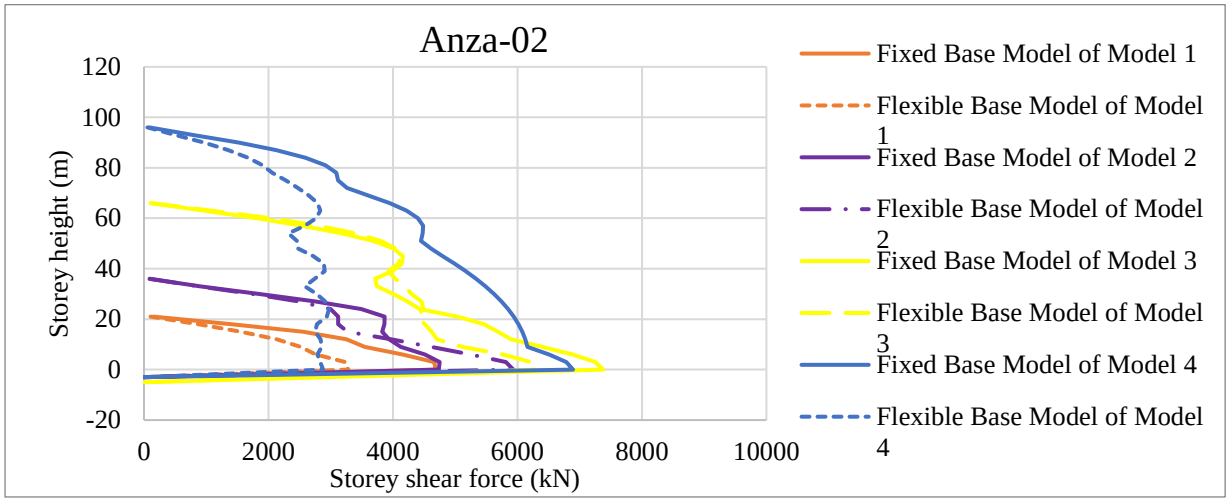

(a)

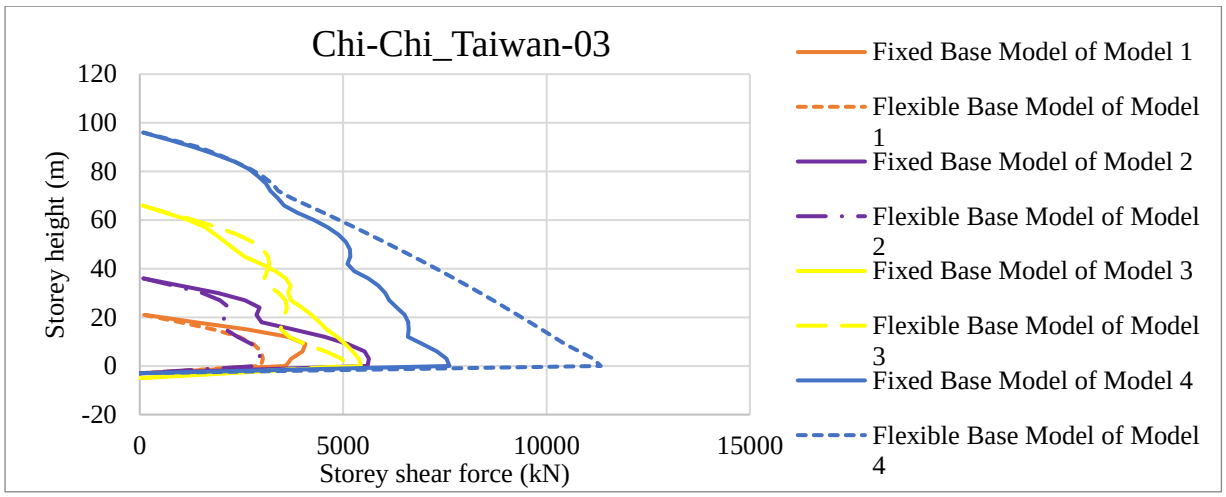

(b)

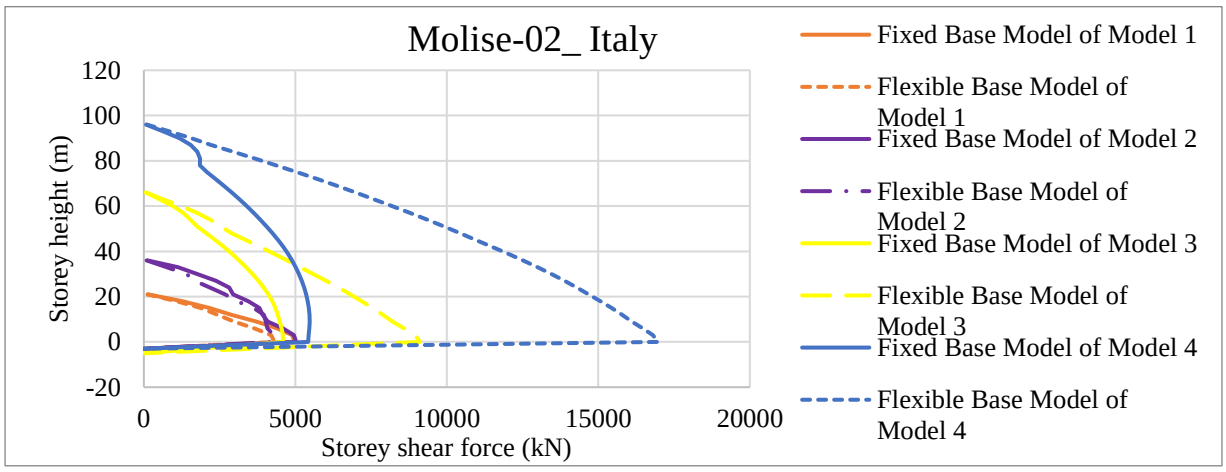

(c)

Figure B.5: Storey shear force of all models on soil type C for (a) Anza-02, (b) Chi-Chi_Taiwan-03, (c) Molise-02_ Italy,

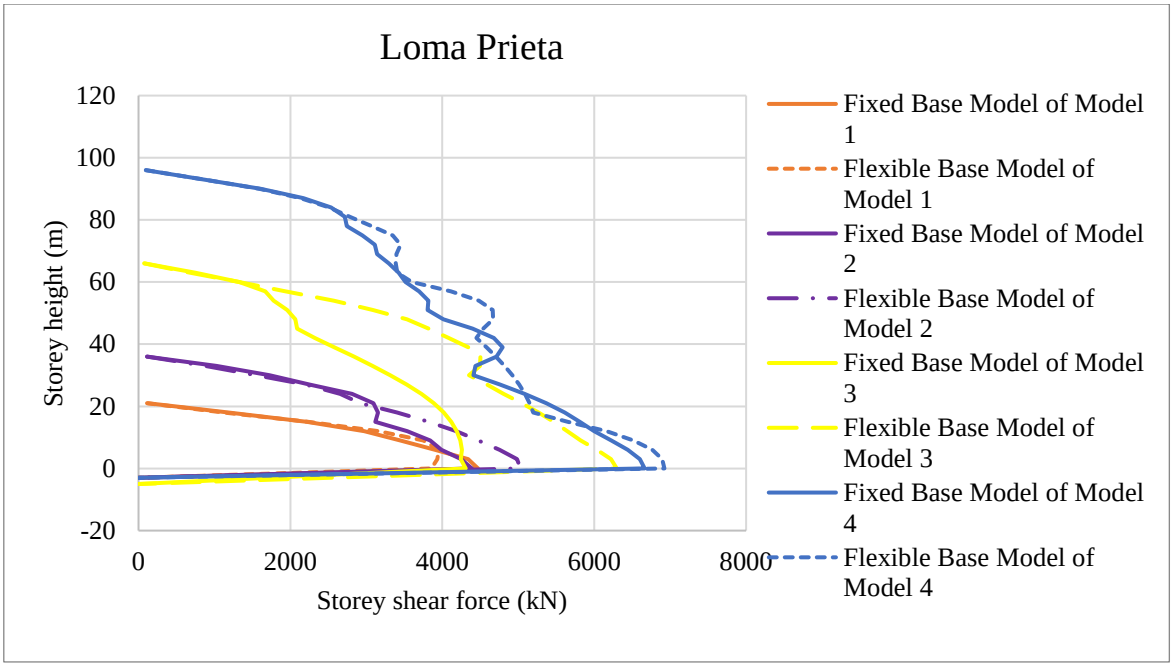

(d)

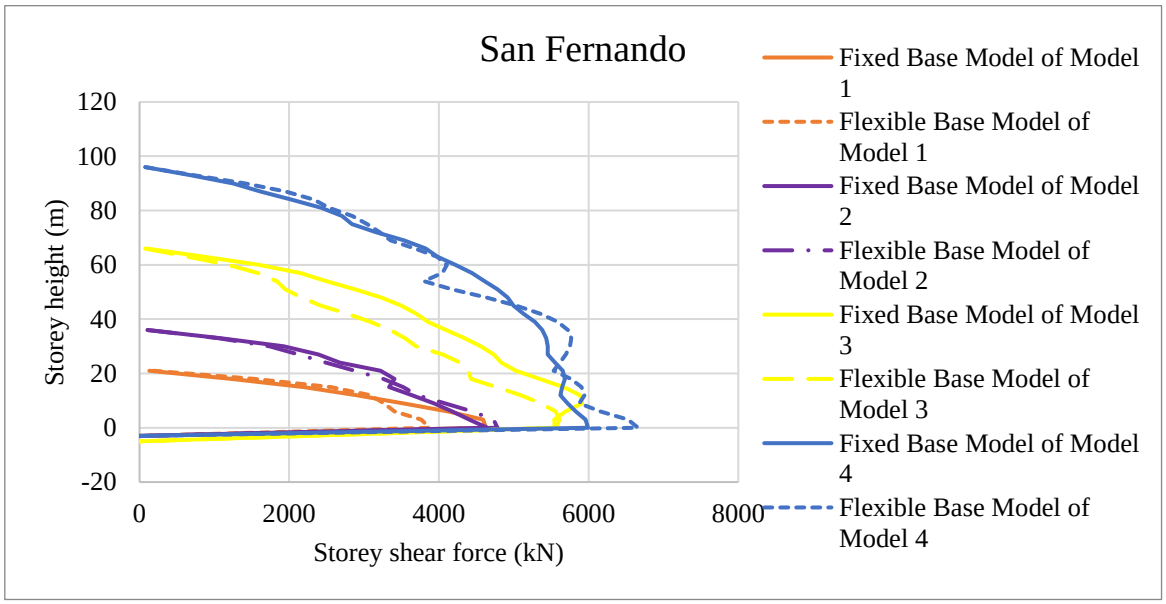

(e)

Figure B.6:Story shear force of all models on soil type C for (d) Loma Prieta, (e) San Fernando

B.4. Storey overturning moment

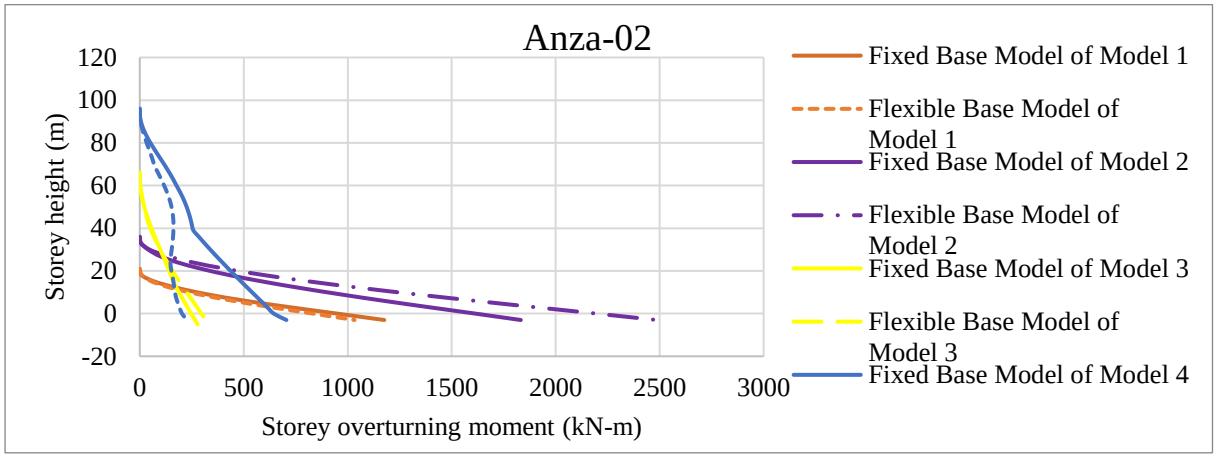

(a)

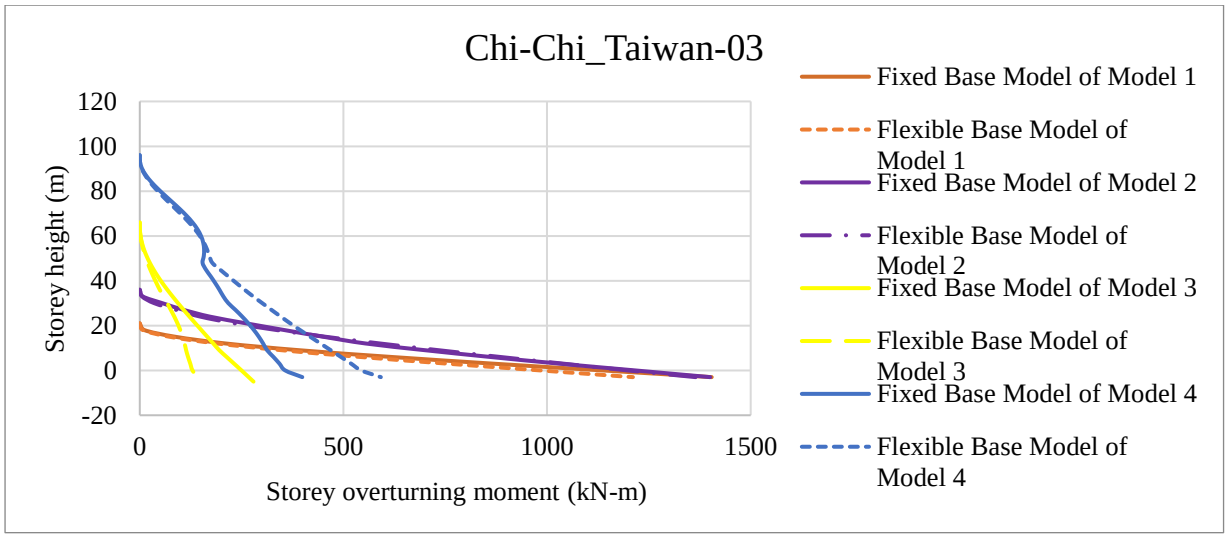

(b)

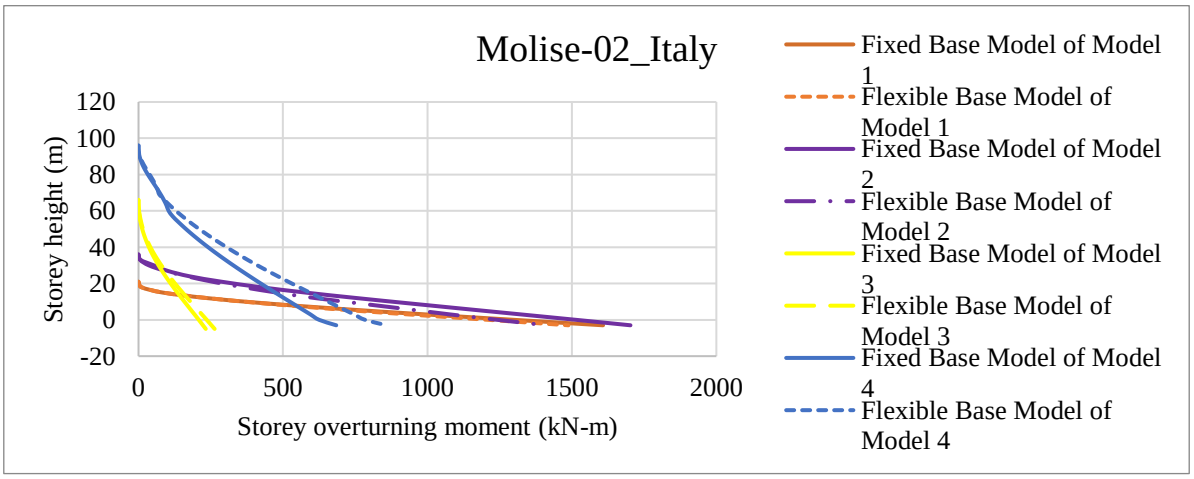

(c)

Figure B.7: Story overturning moment of all models on soil type C for (a) Anza-02, (b) Chi-Chi_Taiwan-03, (c) Molise-02_ Italy

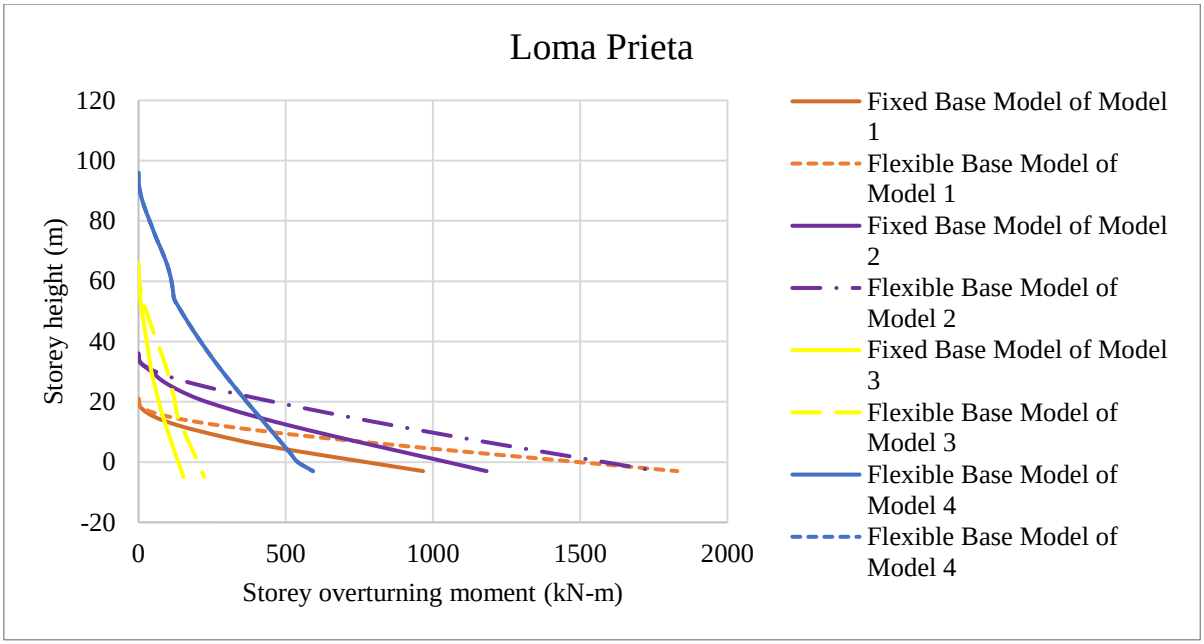

(d)

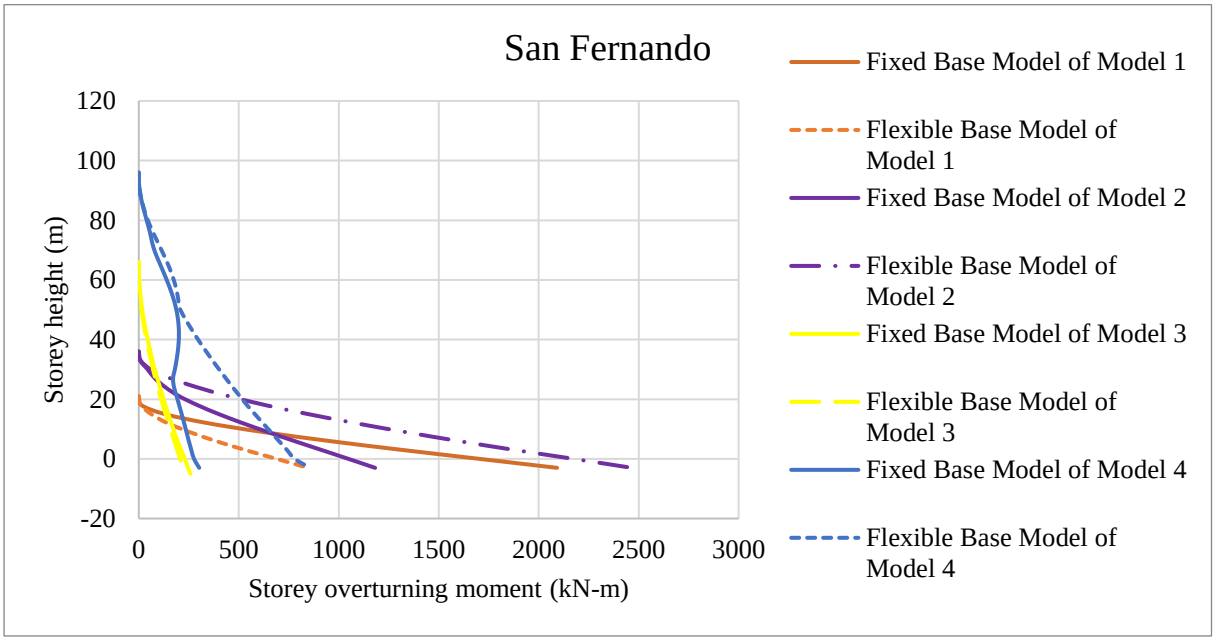

(e)

Figure B.8: Story overturning moment of all models on soil type C for (d) Loma Prieta, (e) San Fernando

Appendix C

Comparison between all models for soil type D

C.1. Story displacement

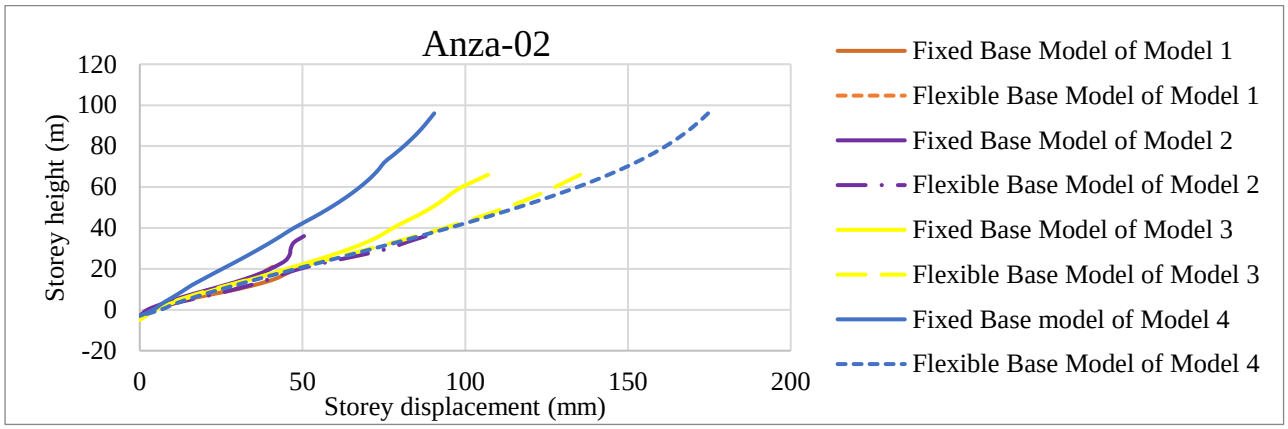

(a)

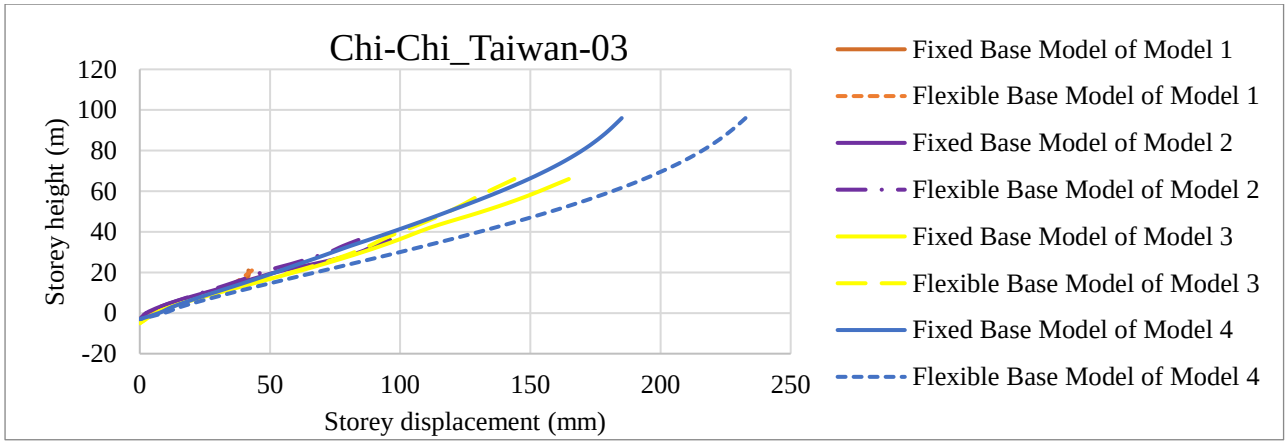

(b)

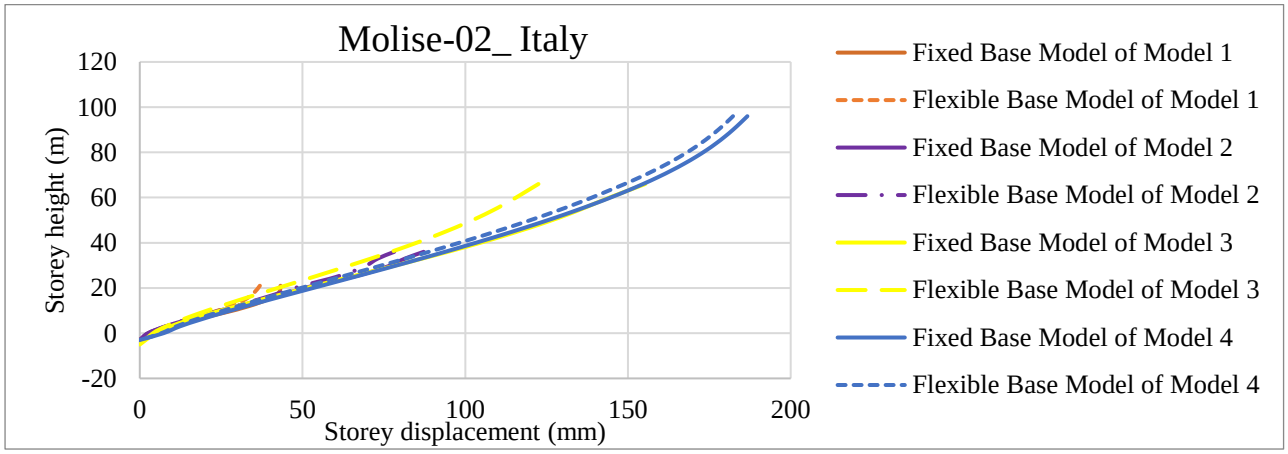

(c)

Figure C.1: Story displacement of all models on soil type D for (a) Anza-02, (b) Chi-Chi_Taiwan-03, (c) Molise-02_ Italy

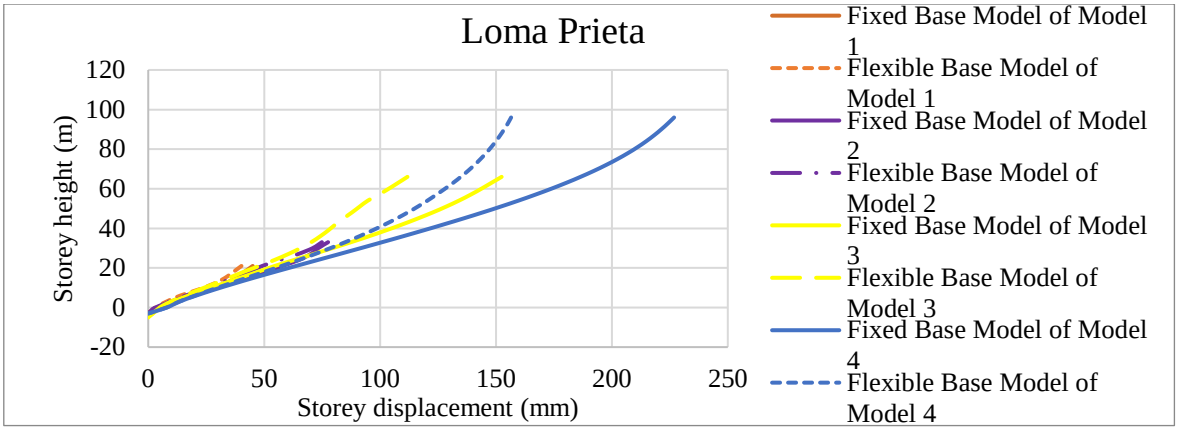

(d)

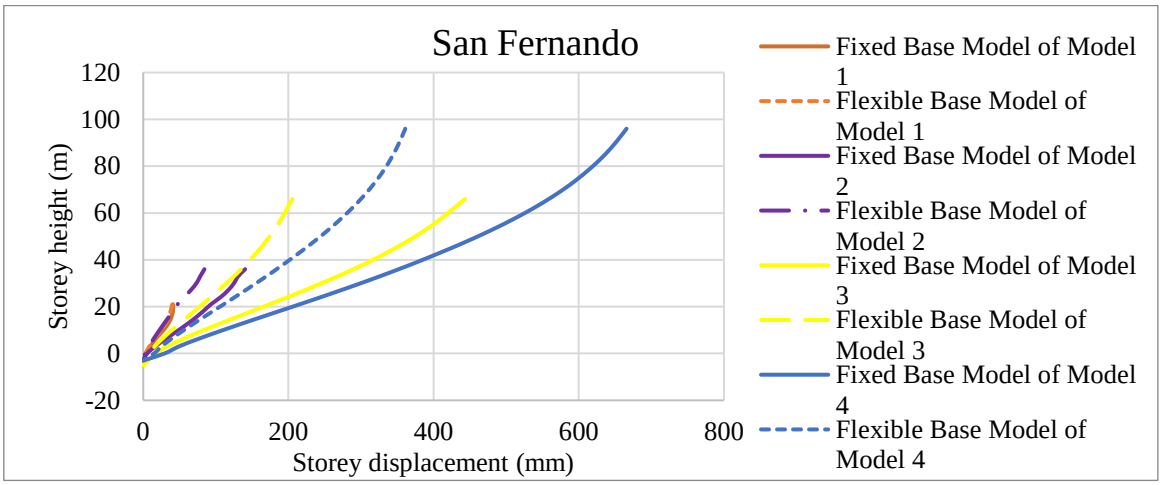

(e)

Figure C.2: Story displacement of all models on soil type D for (d) Loma Prieta, (e) San Fernando

C.2. Story drift ratio

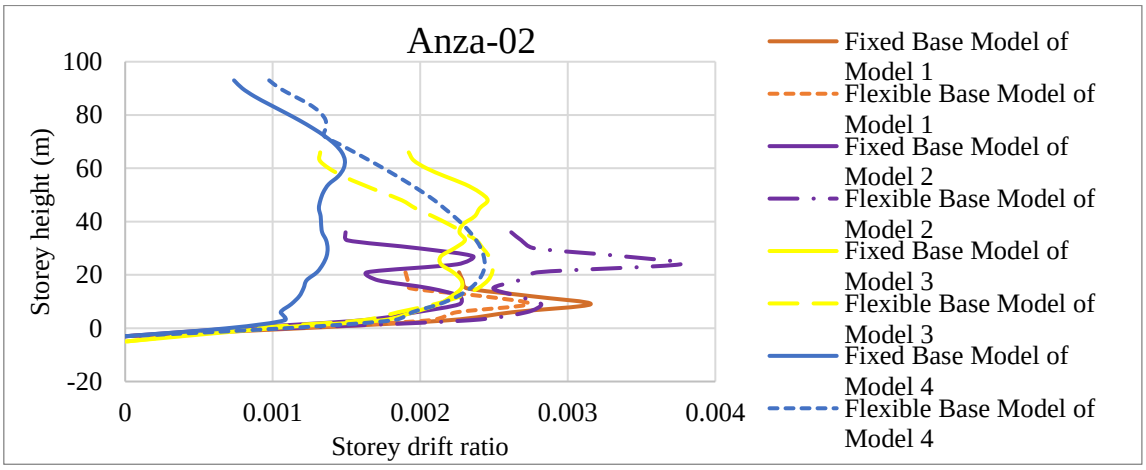

(a)

Figure C.3: Story drift ratio of all models on soil type D for (a) Anza-02

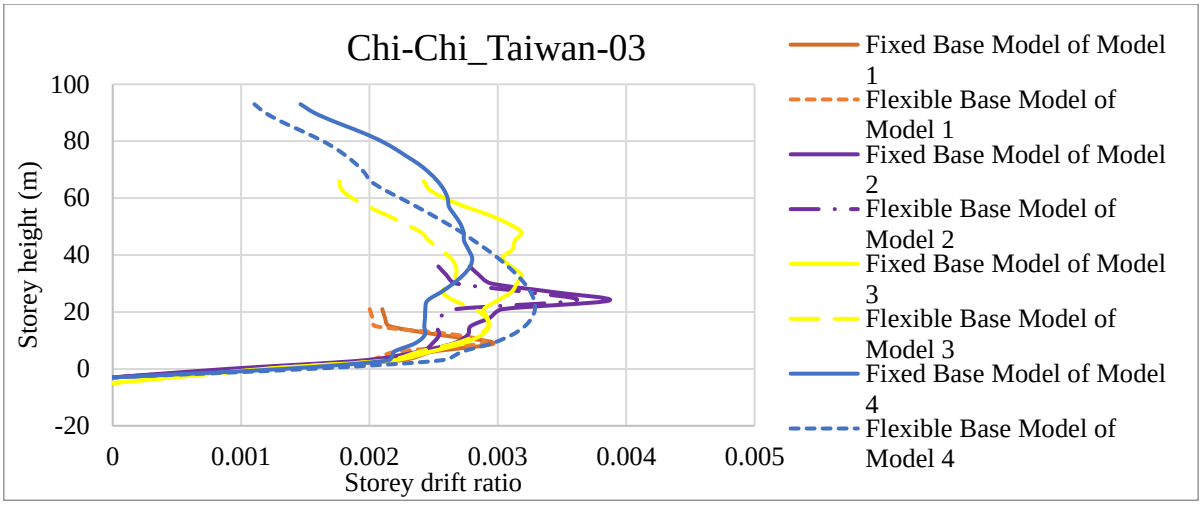

(b)

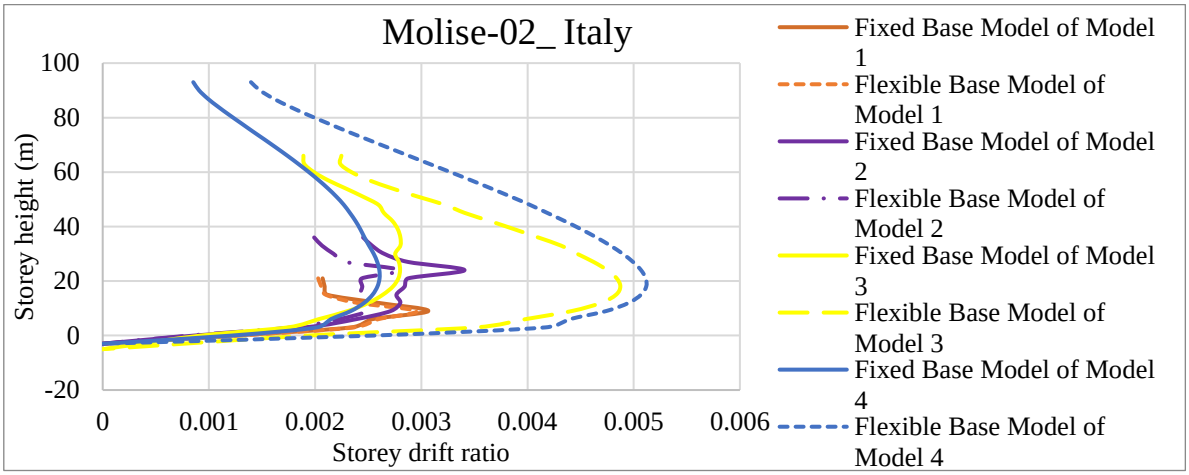

(c)

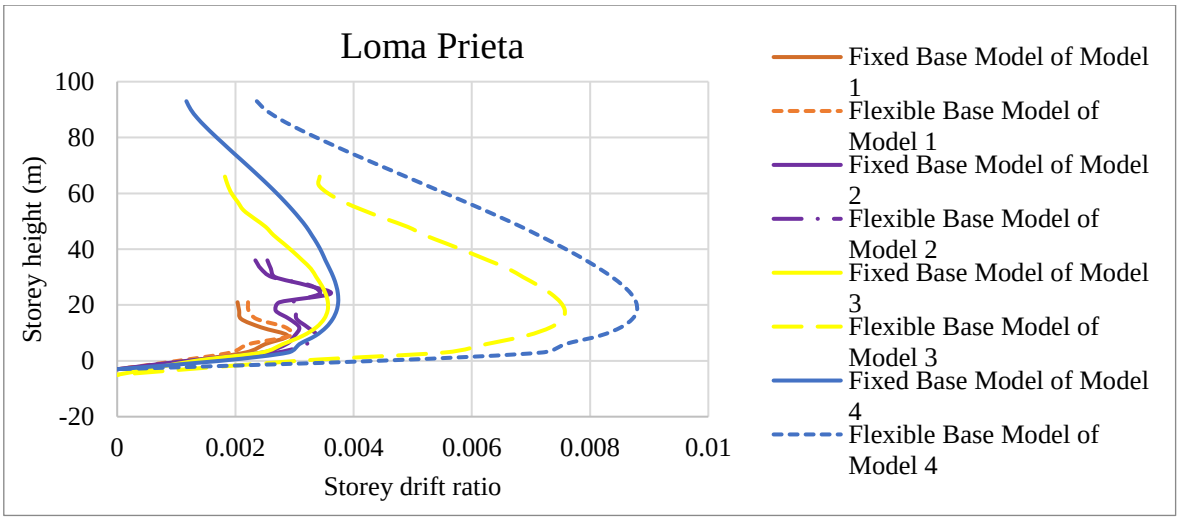

(d)

Figure C.4: Story drift ratio of all models on soil type D for (b) Chi-Chi_Taiwan-03, c) Molise-02_ Italy, (d) Loma Prieta,

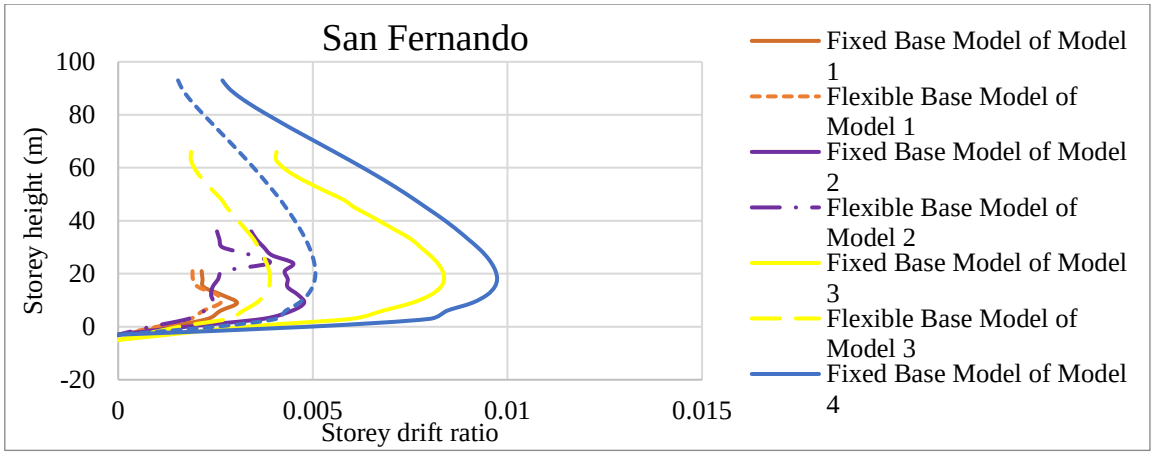

(e)

Figure C.5: Story drift ratio of all models on soil type D for (e) San Fernando

C.3. Story shear force

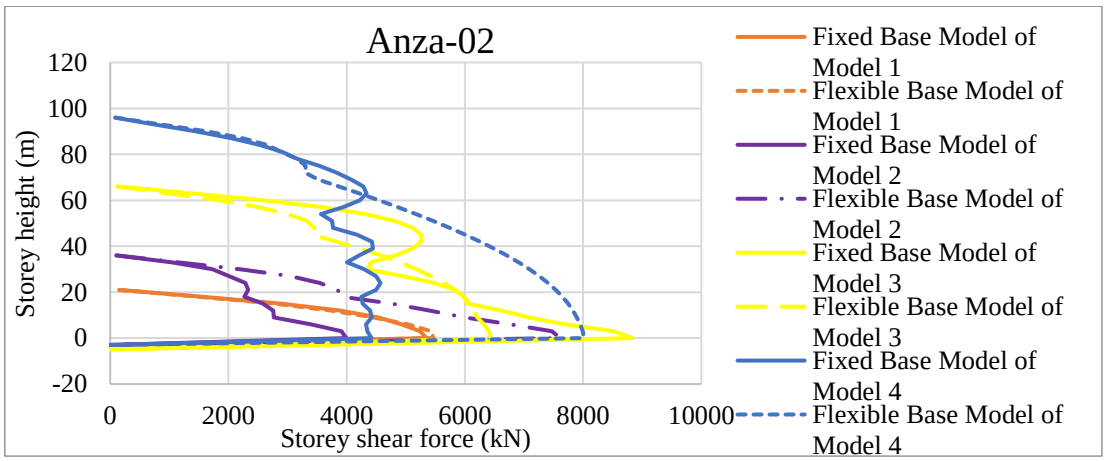

(a)

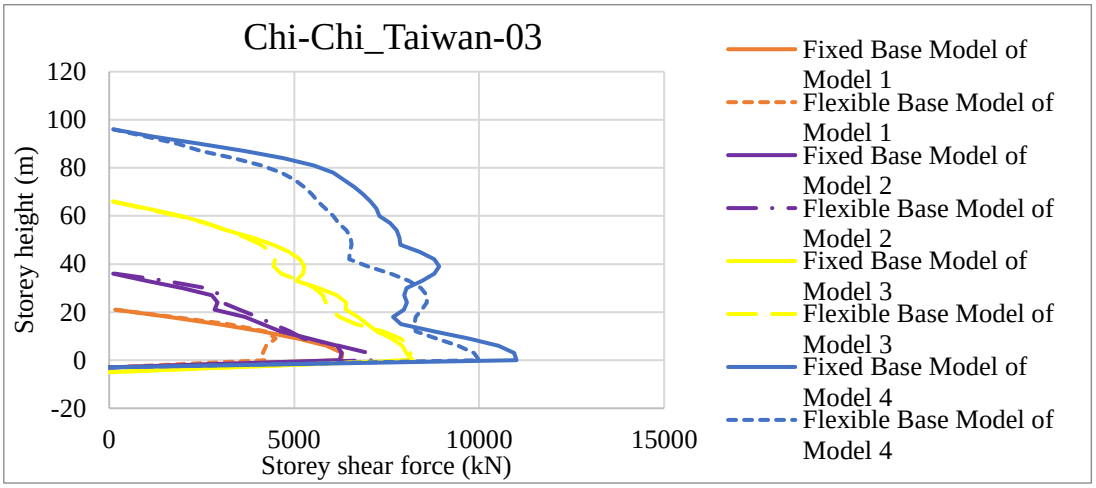

(b)

Figure C.6: Story shear force of all models on soil type D for (a) Anza-02, (b) Chi-Chi_Taiwan-03

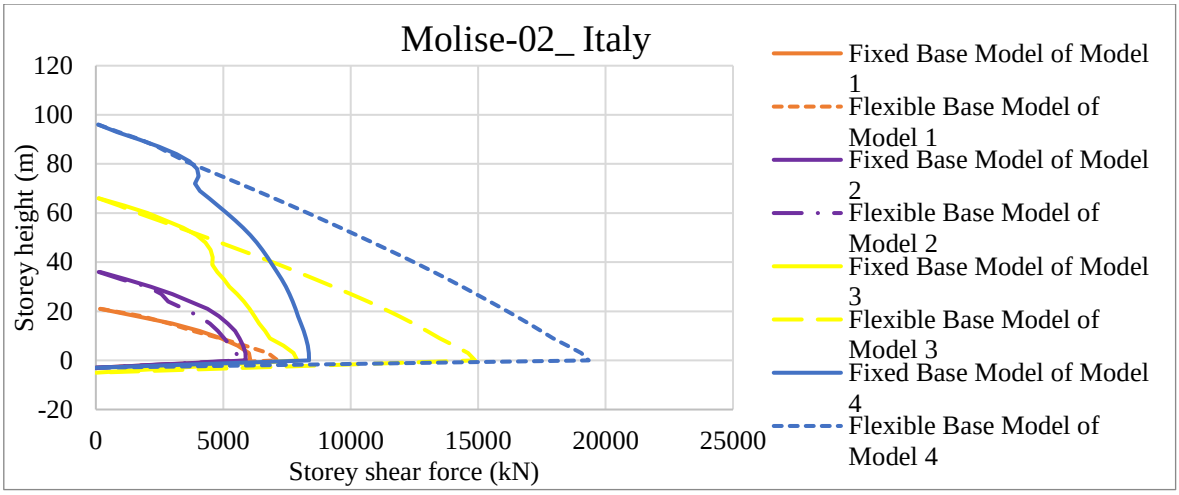

(c)

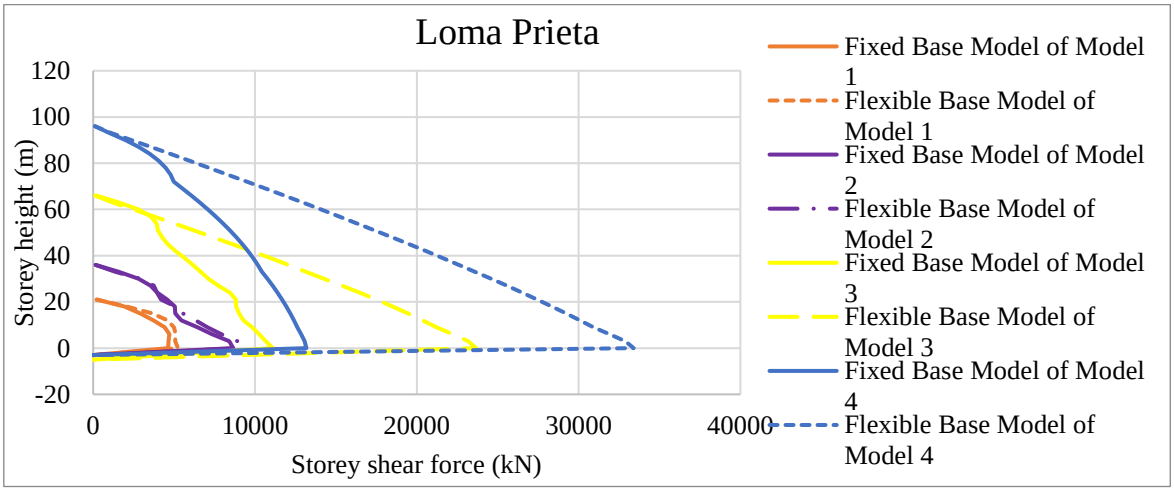

(d)

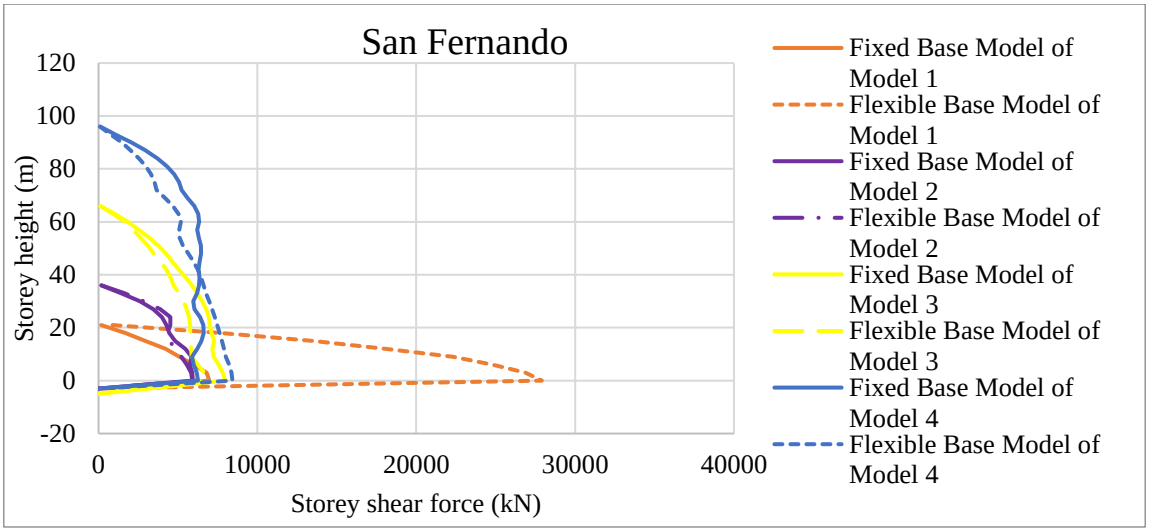

(e)

Figure C.7: Story shear force of all models on soil type D for (c) Molise-02_ Italy, (d) Loma Prieta, (e) San Fernando

C.4. Story overturning moment

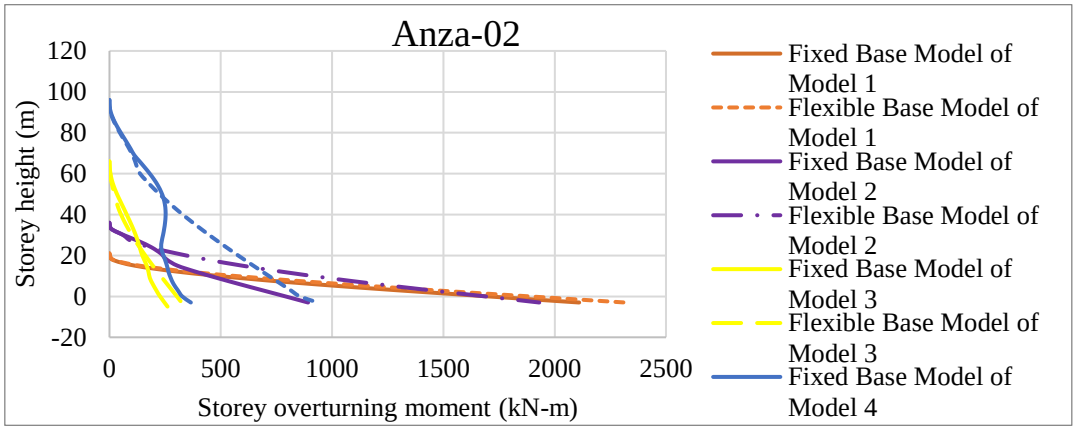

(a)

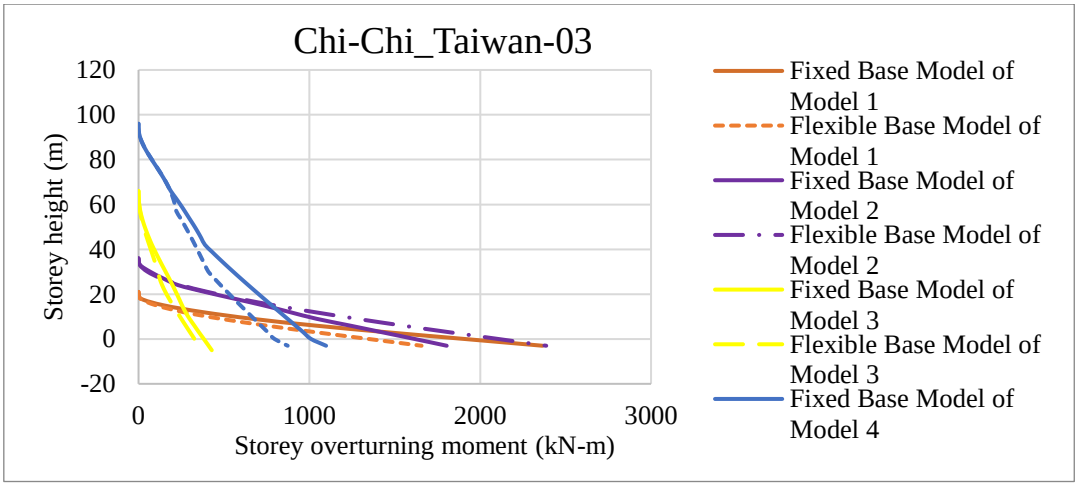

(b)

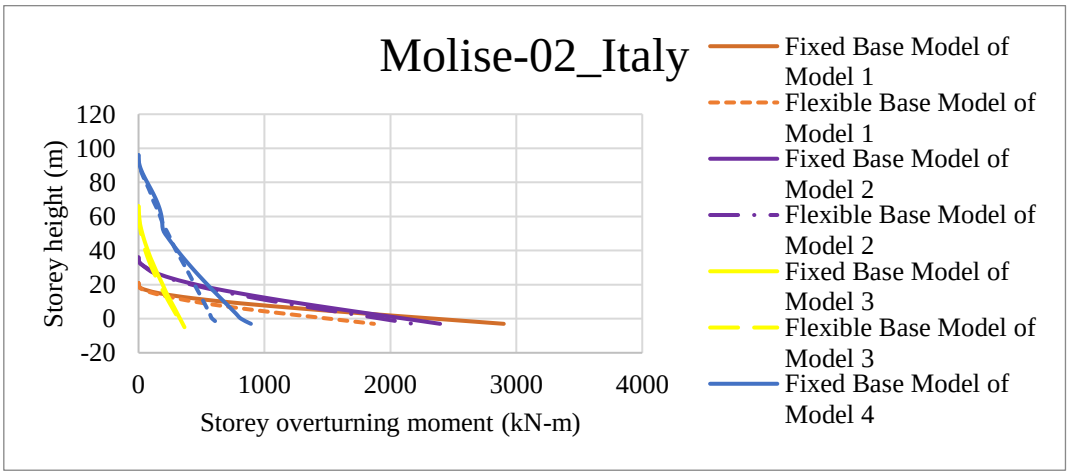

(c)

Figure C.8: Story overturning moment of all models on soil type D for (a) Anza-02, (b) Chi-Chi_Taiwan-03, (c) Molise-02_ Italy

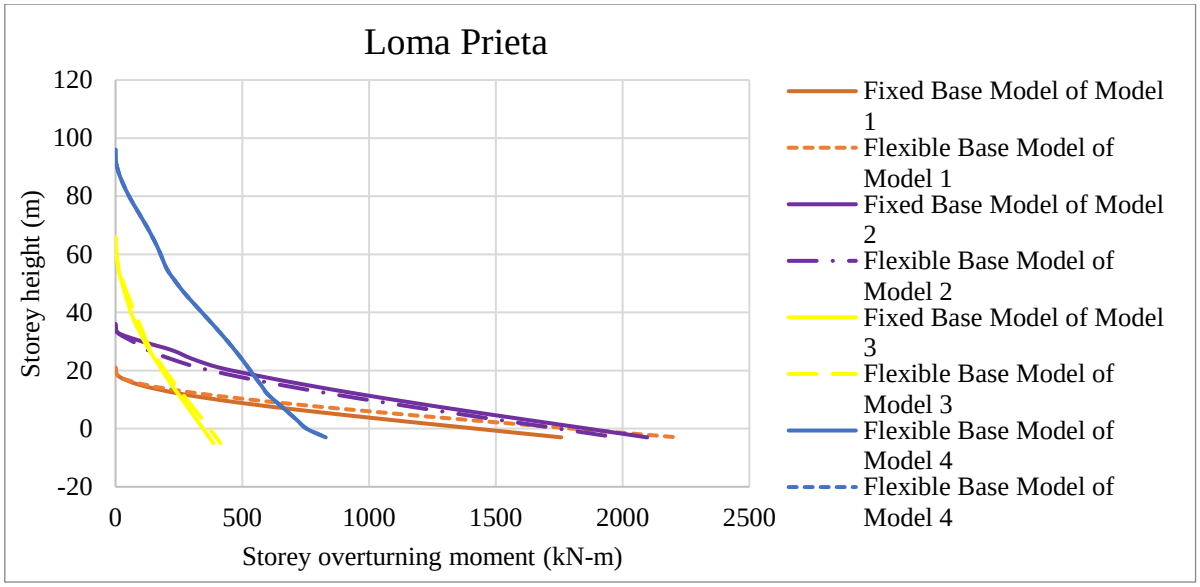

(d)

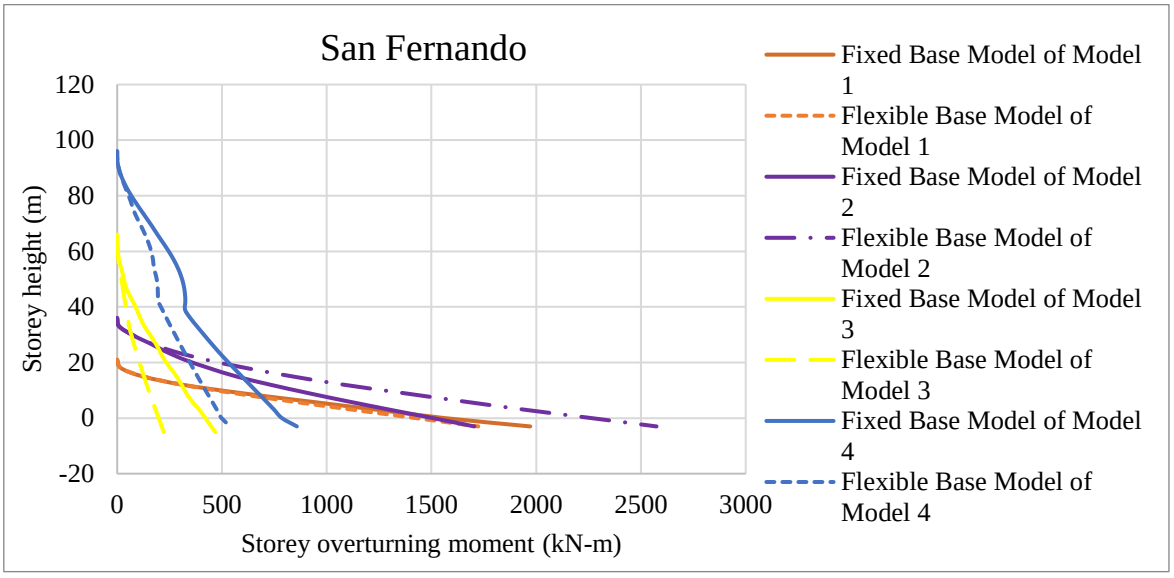

(e)

Figure C.9: Story overturning moment of all models on soil type D for (d) Loma Prieta, (e) San Fernando

Appendix D

Comparison between all models for soil type E

D.1. Story displacement

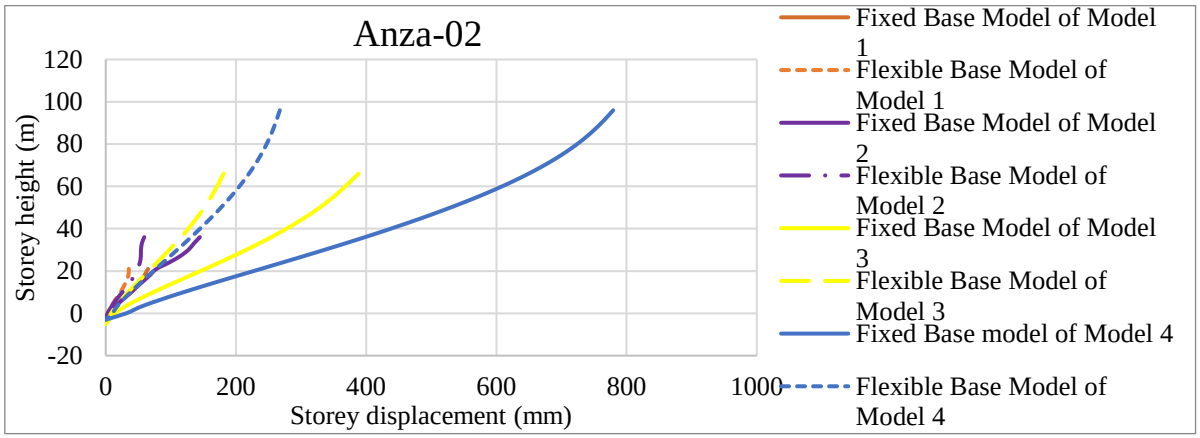

(a)

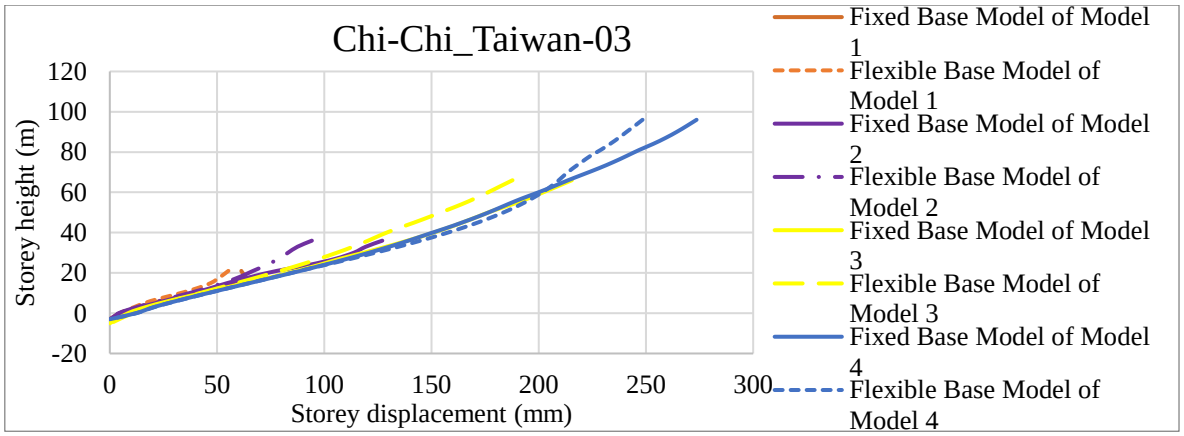

(b)

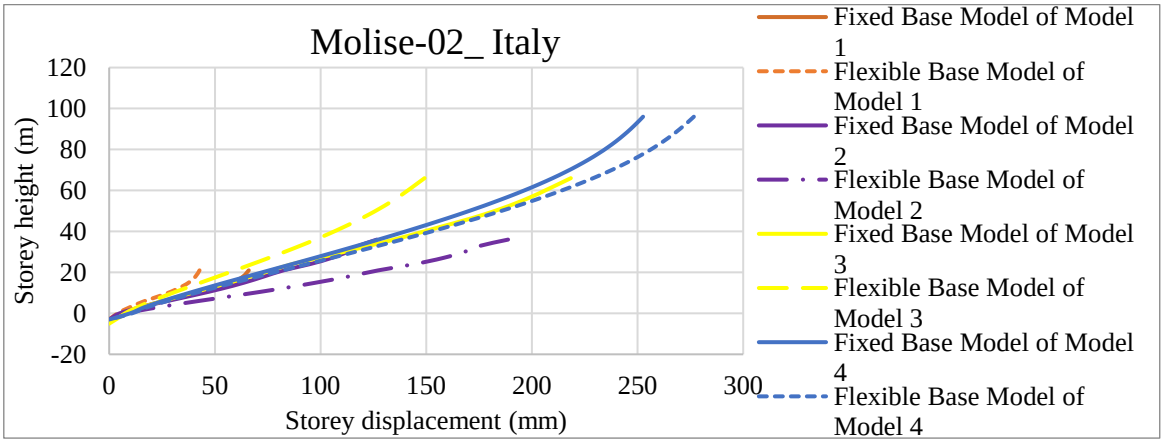

(c)

Figure D.1: Story displacement of all models on soil type E for (a) Anza-02, (b) Chi-Chi_Taiwan-03, (c) Molise-02_ Italy

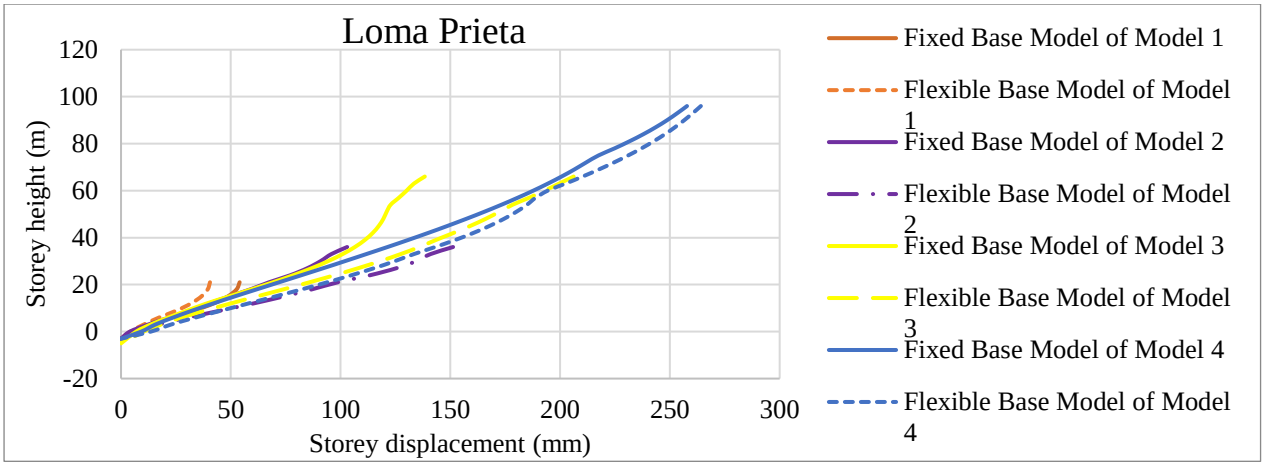

(d)

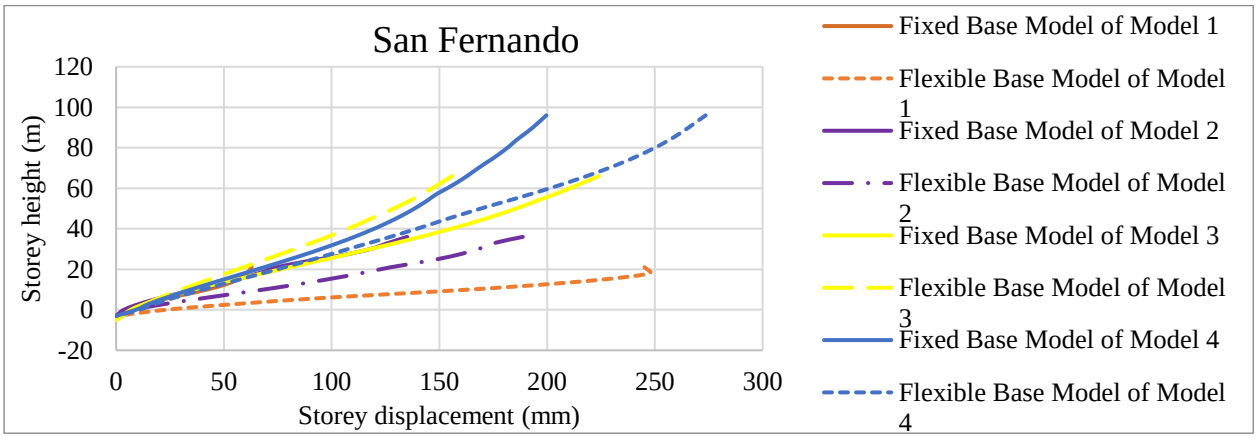

(e)

Figure D.2: Story displacement of all models on soil type E for (d) Loma Prieta, (e) San Fernando

D.2. Story drift ratio

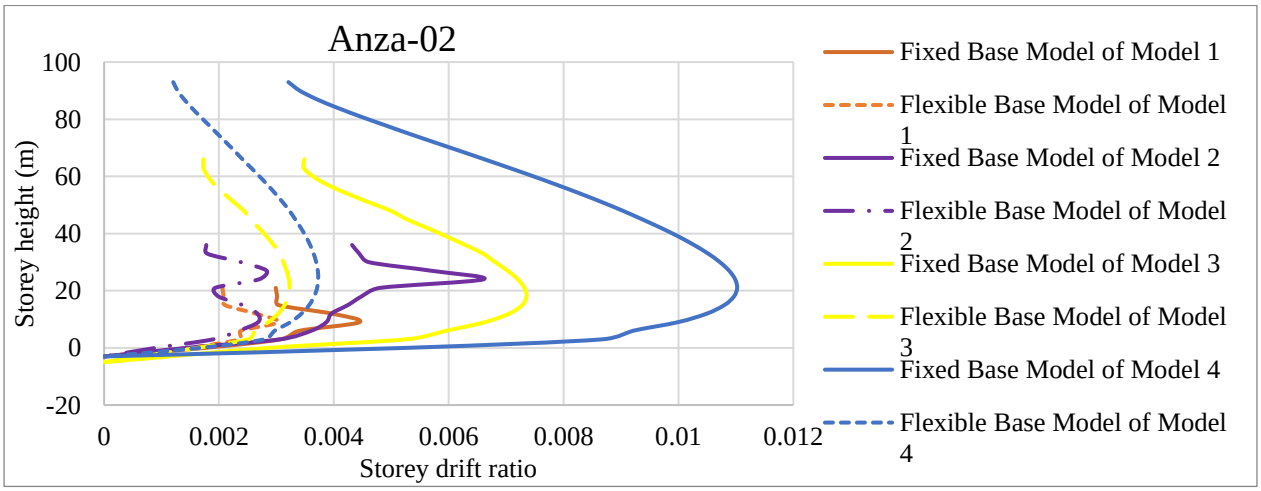

(a)

Figure D.3: Story drift ratio of all models on soil type E for (a) Anza-02

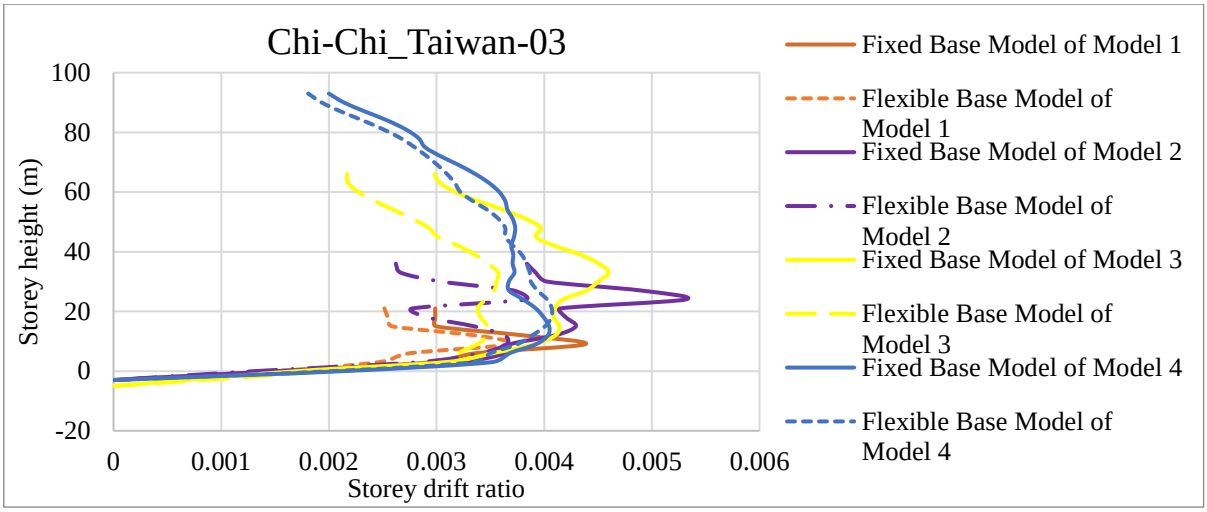

(b)

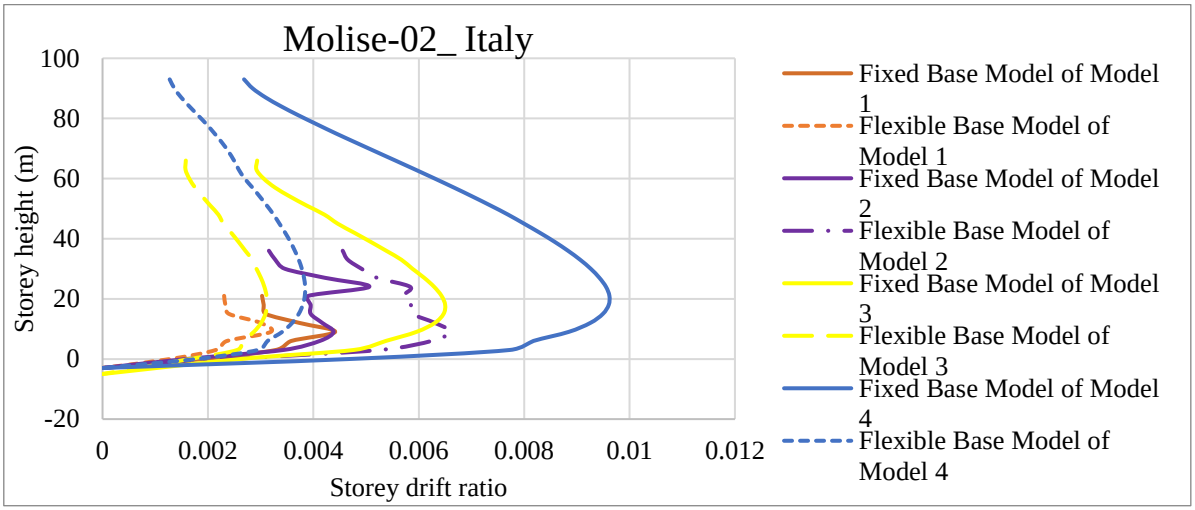

(c)

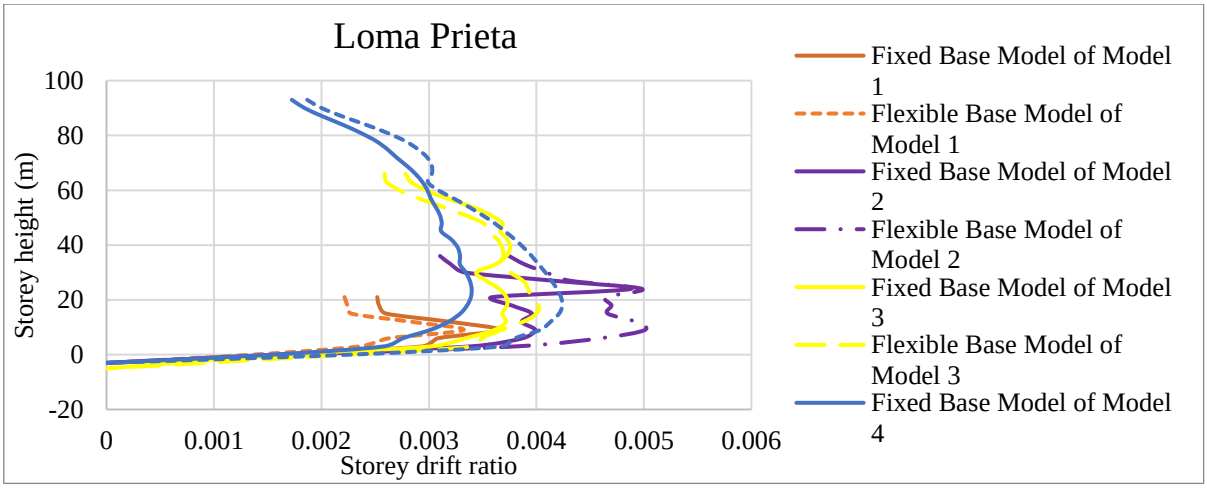

(d)

Figure D.4: Story drift ratio of all models on soil type E for (b) Chi-Chi_Taiwan-03, (c) Molise-02_ Italy, (d) Loma Prieta

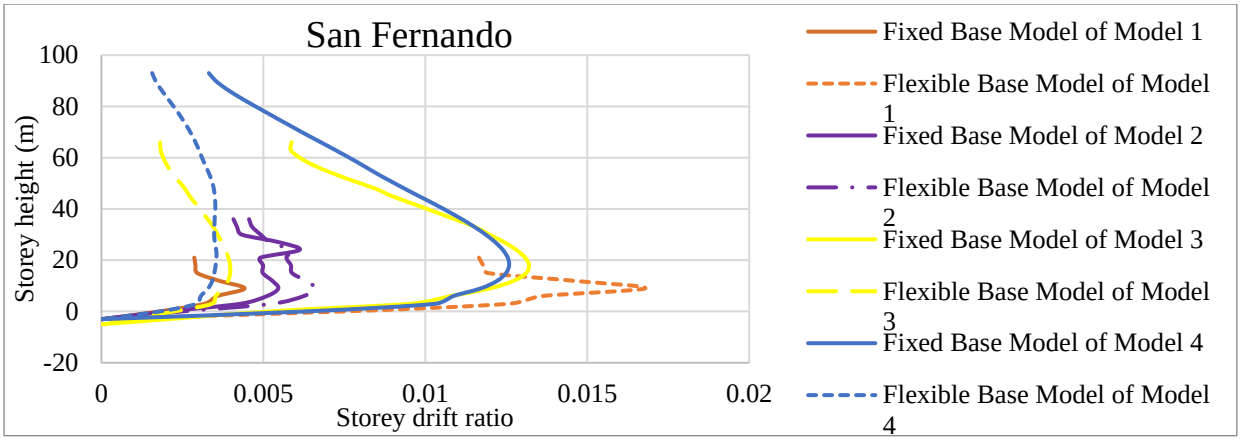

(e)

Figure D.5: Story drift ratio of all models on soil type E for (c) Molise-02_ Italy, (d) Loma Prieta, (e) San Fernando

D.3. Story shear force

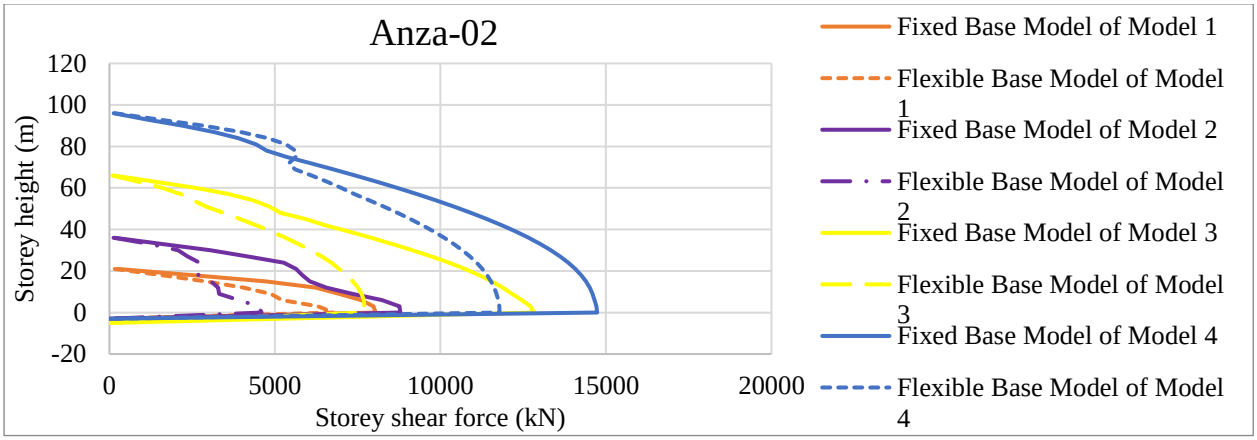

(a)

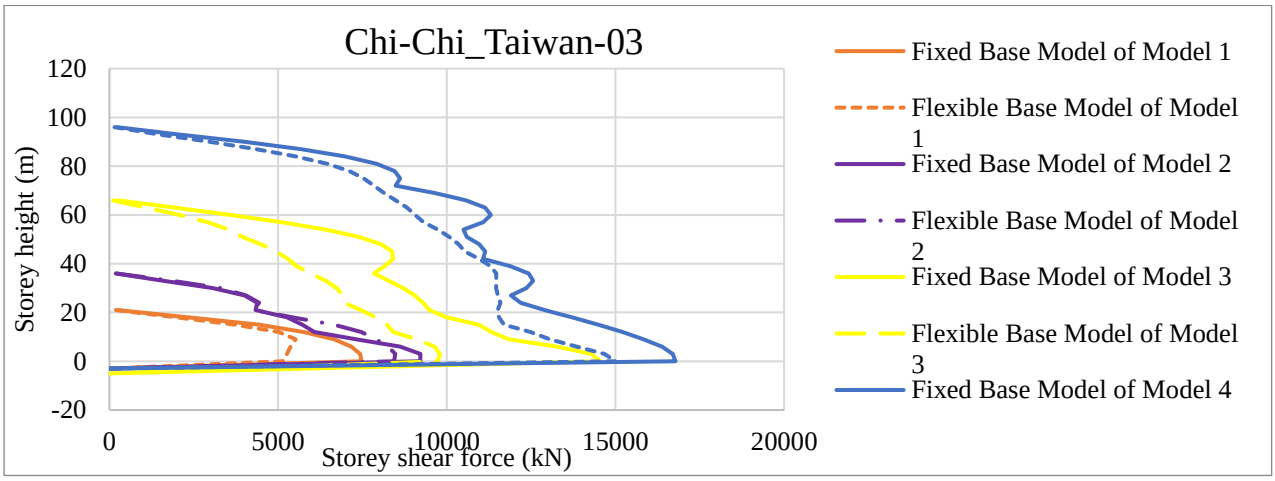

(b)

Figure D.6: Story shear force of all models on soil type E for (a) Anza-02, (b) Chi-Chi_Taiwan-03

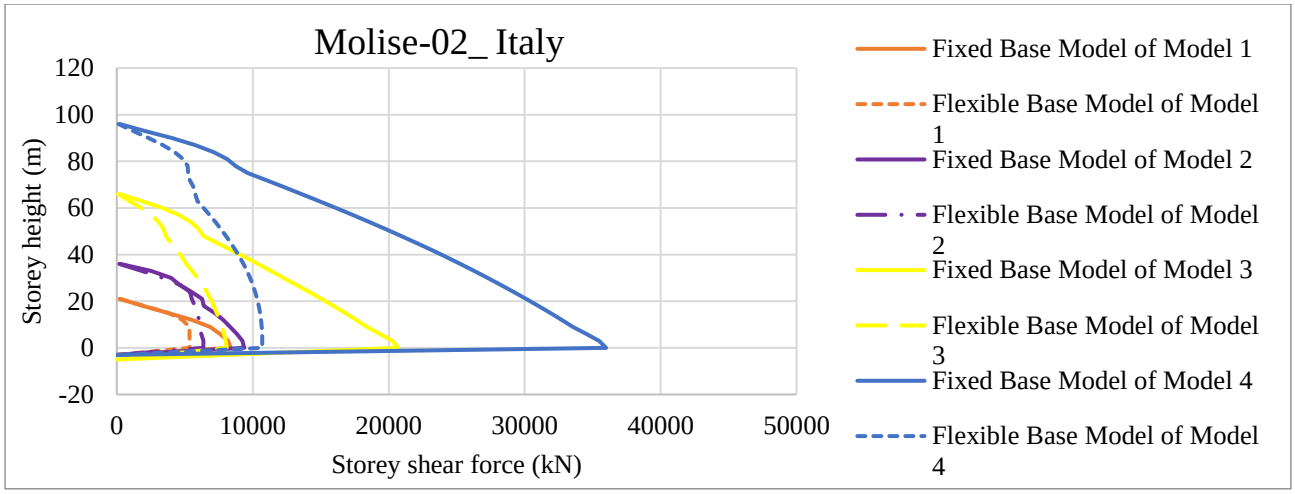

(c)

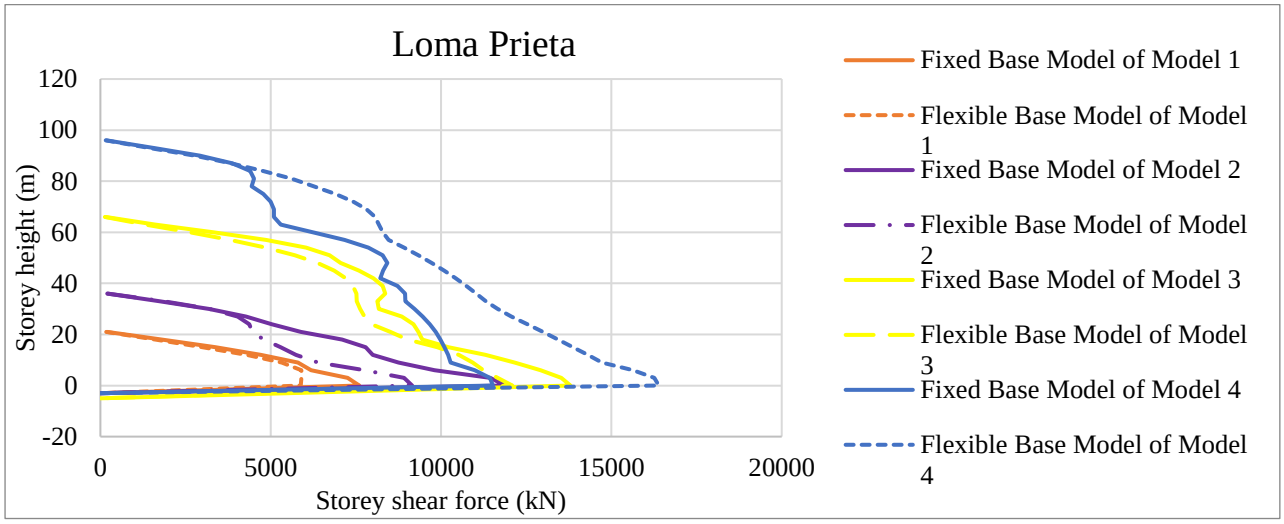

(d)

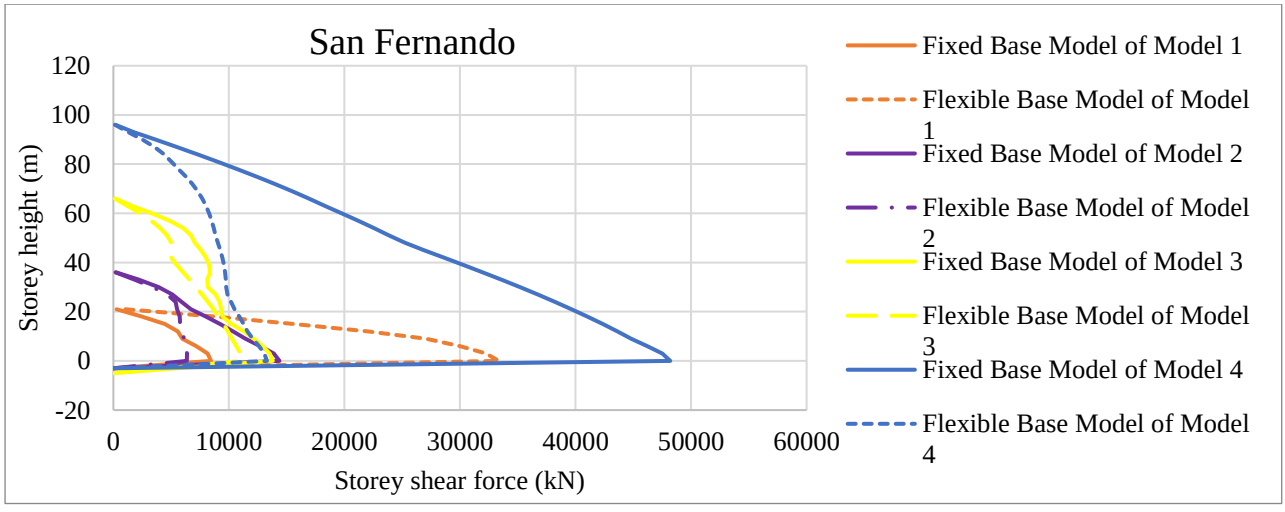

(e)

Figure D.7: Story shear force of all models on soil type E for (c) Molise-02_ Italy, (d) Loma Prieta, (e) San Fernando

D.4. Story overturning moment

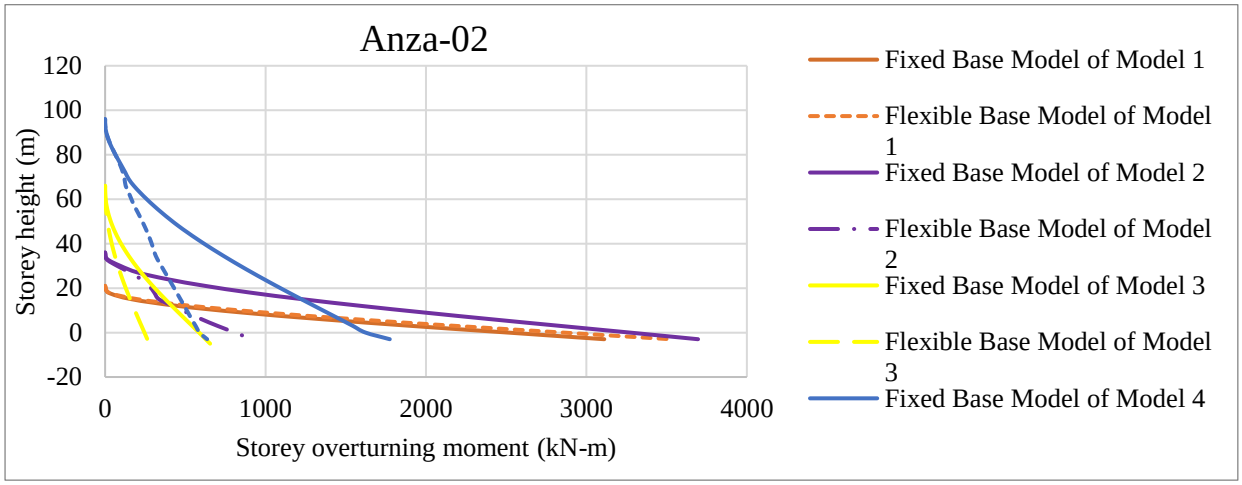

(a)

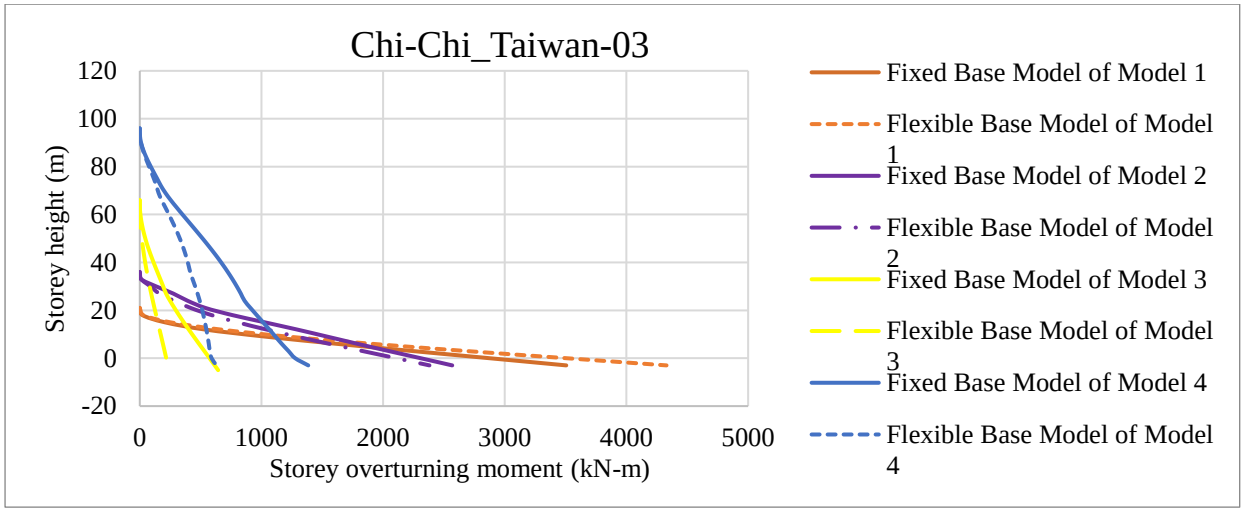

(b)

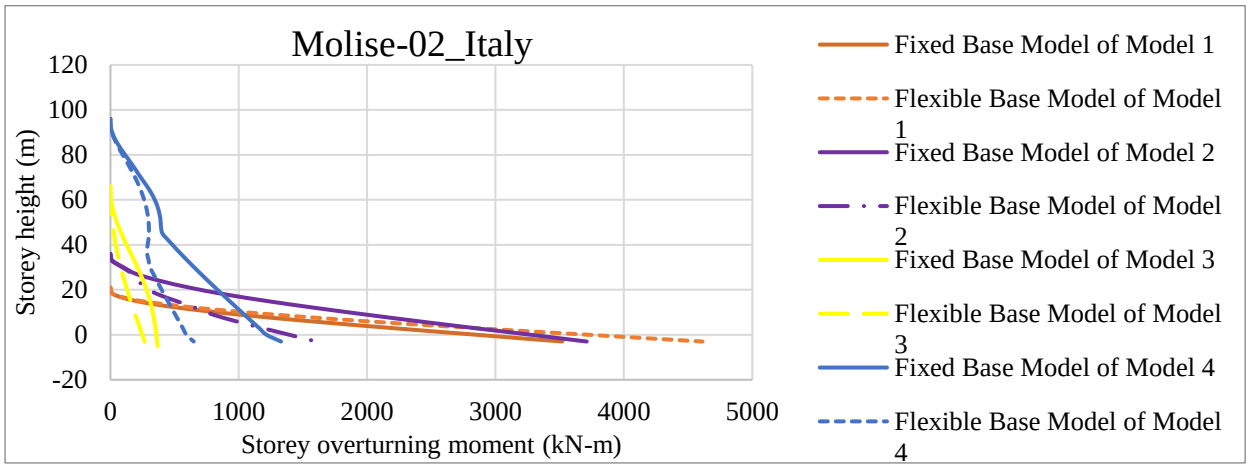

(c)

Figure D.8: Story overturning moment of all models on soil type E for (a) Anza-02, (b) Chi-Chi_Taiwan-03, (c) Molise-02_ Italy

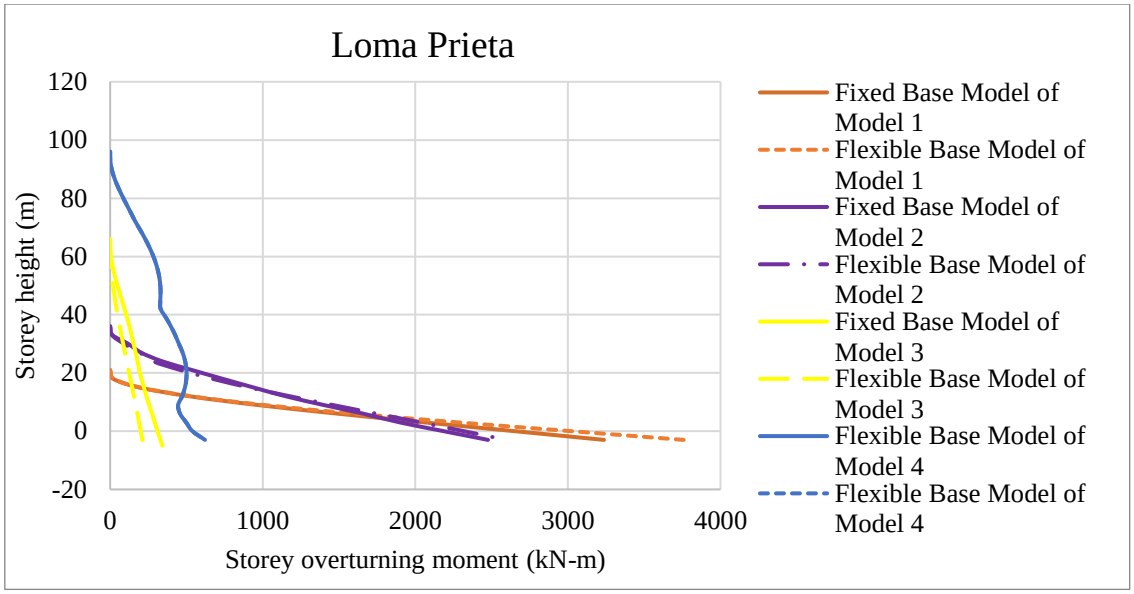

(d)

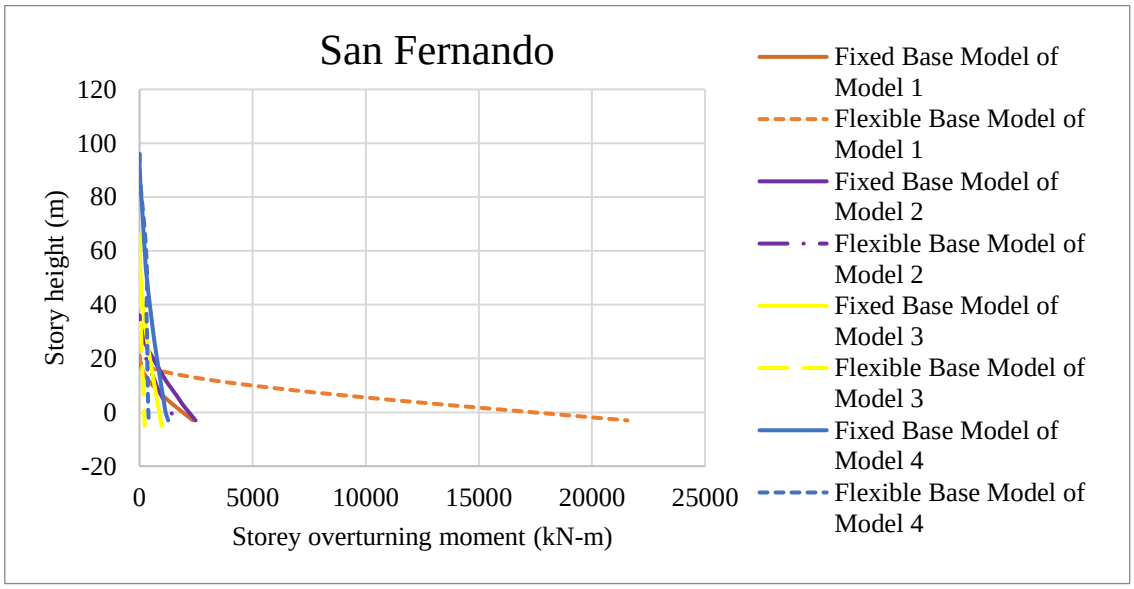

(e)

Figure D.9: Story overturning moment of all models on soil type E for (d) Loma Prieta, (e) San Fernando

Appendix E

Table E.1: Base shear and overturning moment for Anza-02 earthquake

Building model	Soil type	Model type	Base shear along x-axis	Base shear along y-axis	Over turning moment along x-axis	Over turning moment along y-axis
Model 1	Type C	Fixed base	4689.3	70.9	1175.6	67501.5
		Flexible base	3282.0	67.3	1032.9	47971.3
	Type D	Fixed base	5352.3	128.7	2110.0	87499.3
		Flexible base	5470.0	143.3	2315.3	85859.6
	Type E	Fixed base	8041.6	197.1	3111.3	130857.2
		Flexible base	6762.7	235.3	3524.0	88744.8
Model 2	Type C	Fixed base	4736.4	71.3	1832.3	114169.9
		Flexible base	5933.4	94.3	2486.7	110432.6
	Type D	Fixed base	3993.5	37.2	892.1	71264.3
		Flexible base	7615.5	82.1	1930.7	153086.5
	Type E	Fixed base	8787.4	141.7	3695.6	195892.7
		Flexible base	4596.0	37.8	916.4	84382.9
Model 3	Type C	Fixed base	7378.9	6.1	277.8	255895.5
		Flexible base	6079.4	6.6	331.1	240435.9
	Type D	Fixed base	8834.4	6.8	260.7	270739.2
		Flexible base	6431.7	6.9	338.0	323822.4
	Type E	Fixed base	12830.2	13.2	654.4	601286.3
		Flexible base	7691.2	5.2	274.9	388059.9
Model 4	Type C	Fixed base	7459.9	11.8	835.6	448796.8
		Flexible base	2877.6	7.9	227.5	189270.1
	Type D	Fixed base	4420.0	12.2	365.4	292671.9
		Flexible base	8010.7	12.9	936.1	575471.3
	Type E	Fixed base	14733.7	23.3	1774.3	1081117.2
		Flexible base	11784.8	13.6	635.9	865476.8

Table E.2: Base shear and overturning moment for Chi-Chi_Taiwan-03

Building model	Soil type	Model type	Base shear along x-axis	Base shear along y-axis	Over turning moment along x-axis	Over turning moment along y-axis
Model 1	Type C	Fixed base	3445.1	88.7	1404.3	67386.0
		Flexible base	2976.1	76.3	1210.8	52538.2
	Type D	Fixed base	6272.0	150.2	2364.9	99276.0
		Flexible base	4214.4	100.1	1656.7	78195.8
	Type E	Fixed base	7474.4	217.4	3505.2	124819.7
		Flexible base	5141.1	263.5	4329.4	95656.9
Model 2	Type C	Fixed base	5599.6	58.8	1400.4	116997.4
		Flexible base	2893.4	59.2	1364.9	62358.2
	Type D	Fixed base	6227.9	64.9	1803.8	126756.5
		Flexible base	7164.3	93.6	2386.5	146825.8
	Type E	Fixed base	9215.9	92.4	2568.1	181751.4
		Flexible base	8439.3	92.1	2380.8	181695.4
Model 3	Type C	Fixed base	5436.8	5.6	279.2	231057.2
		Flexible base	4855.6	4.7	146.7	188183.6
	Type D	Fixed base	8204.6	10.3	428.7	324950.5
		Flexible base	8080.4	8.2	368.8	317456.3
	Type E	Fixed base	14559.9	13.8	643.9	548710.4
		Flexible base	9733.3	5.0	241.8	369977.8
Model 4	Type C	Fixed base	7575.7	10.5	497.8	463492.6
		Flexible base	11333.9	7.9	591.9	693802.4
	Type D	Fixed base	11011.5	16.3	1097.8	634810.7
		Flexible base	9999.0	15.6	873.1	555219.7
	Type E	Fixed base	16779.7	26.8	1384.6	879950.8
		Flexible base	15005.3	15.5	630.3	844318.2

Table E.3: Base shear and overturning moment for Molise-02_ Italy

Building model	Soil type	Model type	Base shear along x-axis	Base shear along y-axis	Over turning moment along x-axis	Over turning moment along y-axis
Model 1	Type C	Fixed base	4964.9	99.8	1607.9	74857.5
		Flexible base	4310.4	93.7	1488.1	60502.0
	Type D	Fixed base	6061.5	179.3	2900.3	94582.0
		Flexible base	7134.8	121.9	1869.3	99692.0
	Type E	Fixed base	8374.0	219.1	3518.8	128267.5
		Flexible base	5358.4	290.4	4612.8	98525.1
Model 2	Type C	Fixed base	5025.2	63.5	1702.7	107662.2
		Flexible base	4305.4	54.1	1411.7	107749.3
	Type D	Fixed base	5881.5	90.8	2394.6	166177.1
		Flexible base	5590.9	80.3	2179.7	141660.4
	Type E	Fixed base	9368.6	140.6	3710.2	232088.3
		Flexible base	6356.0	79.3	1603.6	170162.8
Model 3	Type C	Fixed base	4592.6	4.8	232.7	230078.0
		Flexible base	9365.9	5.4	263.4	398504.7
	Type D	Fixed base	7906.5	7.4	364.9	333415.0
		Flexible base	14881.6	7.1	354.3	638788.4
	Type E	Fixed base	20703.8	11.0	367.4	855866.1
		Flexible base	8084.9	5.5	278.5	386794.5
Model 4	Type C	Fixed base	5219.3	9.9	730.4	371857.4
		Flexible base	16972.7	12.5	859.2	1095164.8
	Type D	Fixed base	8366.4	13.0	892.2	603763.2
		Flexible base	19337.8	10.8	639.1	1182254.1
	Type E	Fixed base	35991.9	18.4	1329.2	2243487.8
		Flexible base	10693.3	11.3	648.9	794024.2

Table E.4: Base shear and overturning moment for Loma Prieta

Building model	Soil type	Model type	Base shear along x-axis	Base shear along y-axis	Over turning moment along x-axis	Over turning moment along y-axis
Model 1	Type C	Fixed base	3153.1	64.9	966.4	54340.3
		Flexible base	3855.9	110.2	1829.9	67809.8
	Type D	Fixed base	4634.9	122.5	1758.1	80169.6
		Flexible base	5242.8	133.5	2218.8	94097.4
	Type E	Fixed base	7600.2	201.9	3236.4	106428.1
		Flexible base	5881.2	250.0	3758.3	97964.6
Model 2	Type C	Fixed base	4387.7	46.2	1181.9	102925.3
		Flexible base	5028.4	78.9	1760.4	125075.5
	Type D	Fixed base	8654.4	85.8	2097.1	155706.3
		Flexible base	9145.9	75.0	1976.4	193284.1
	Type E	Fixed base	11887.6	91.1	2476.0	208030.9
		Flexible base	9150.8	96.8	2596.7	163408.9
Model 3	Type C	Fixed base	4307.7	3.3	152.9	209876.9
		Flexible base	6064.1	5.1	223.2	280437.0
	Type D	Fixed base	11104.1	9.1	386.0	470424.7
		Flexible base	23668.8	8.1	414.2	990949.4
	Type E	Fixed base	13799.1	8.4	342.5	462997.4
		Flexible base	12091.9	4.7	218.8	438890.9
Model 4	Type C	Fixed base	6421.9	10.0	461.1	318092.3
		Flexible base	6924.0	9.2	592.5	407396.8
	Type D	Fixed base	13177.8	14.6	1098.3	879601.3
		Flexible base	33405.9	13.4	829.1	2018209.4
	Type E	Fixed base	11523.7	17.7	1223.6	728344.8
		Flexible base	16391.1	17.9	621.6	984381.6

Table E.5: Base shear and overturning moment for San Fernando

Building model	Soil type	Model type	Base shear along x-axis	Base shear along y-axis	Over turning moment along x-axis	Over turning moment along y-axis
Model 1	Type C	Fixed base	4628.2	134.9	2091.9	67068.6
		Flexible base	3872.2	52.7	847.2	61463.3
	Type D	Fixed base	6973.7	133.1	1971.5	103323.1
		Flexible base	5133.2	104.2	1723.6	77450.1
	Type E	Fixed base	8446.7	154.5	2362.4	112885.0
		Flexible base	27904.6	1378.4	21567.8	424139.0
Model 2	Type C	Fixed base	4646.6	48.4	875.0	111728.6
		Flexible base	4782.2	94.4	2466.0	106806.0
	Type D	Fixed base	5938.1	64.4	1704.6	149550.0
		Flexible base	5903.6	98.1	2574.2	139204.7
	Type E	Fixed base	14374.5	106.7	2590.6	314028.4
		Flexible base	6356.0	79.3	1603.6	170162.8
Model 3	Type C	Fixed base	5547.4	5.6	258.3	274144.9
		Flexible base	5523.5	4.6	231.1	230346.5
	Type D	Fixed base	7982.7	10.3	467.4	390590.5
		Flexible base	6828.2	4.9	222.2	318358.0
	Type E	Fixed base	40523.4	20.2	975.5	1723924.0
		Flexible base	11150.9	4.7	230.5	489344.2
Model 4	Type C	Fixed base	5853.2	9.9	414.6	474892.4
		Flexible base	6660.5	12.1	856.1	361696.1
	Type D	Fixed base	6261.9	13.5	857.6	435640.7
		Flexible base	8428.4	12.6	541.3	553592.1
	Type E	Fixed base	48198.4	18.6	1269.4	2831248.4
		Flexible base	13291.3	16.8	409.2	850836.8